Experimental Simulation of the Natural Shoulder Joint

Sophie Elizabeth Hutchinson

Submitted in accordance with the requirements for the degree of Doctor of Philosophy

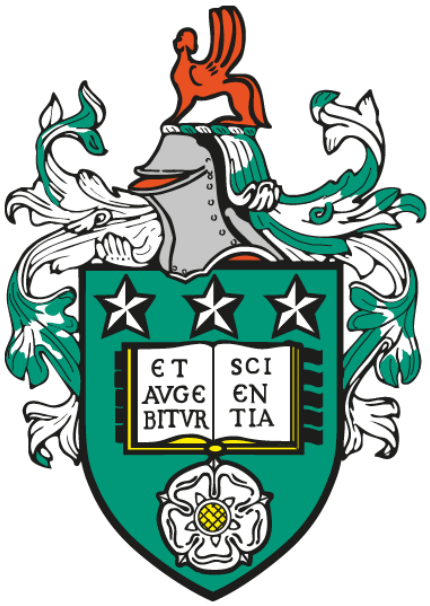

The University of Leeds

Institute of Medical and Biological Engineering

School of Mechanical Engineering

August 2024

The candidate confirms that the work submitted is her own and that appropriate credit has been given where reference has been made to the work of others.

Acknowledgements

Firstly I would like to acknowledge and thank EPSRC for financially supporting this project through a DTP studentship. I am extremely grateful to the donors and their families who selflessly donated their bodies to scientific research which enabled me to complete this research.

I would like to thank my primary supervisor, Professor Sophie Williams for this opportunity and for her continuous guidance, expertise and compassion throughout my project. Thank you for allowing me to join the 'hip' research group which has been a source of great friendship, support and knowledge through my PhD and particularly during the Covid-19 pandemic.

I would also like to thank Professor Pete Culmer and Professor Claire Brockett for your kindness and support through challenging times of my project. Also thank you to Mr Dan Henderson and Mr Paul Cowling for coming over to anatomy countless times to dissect my samples and providing expert guidance on the clinical aspects of my project.

In addition, I am very grateful to Sarah Wilson and Charlotte Coleman from the Division of Anatomy for enabling my testing with such flexibility and generosity – without you I would not have completed the human tissue aspect of the project. Thanks also to all the technical staff involved in my work including Phil Wood, Matt Broadbent and Andrew Stockdale. It was your know-how that got me through the many challenges.

A massive thankyou also to my wonderful colleagues from iMBE, in particular Taiyibah, Mackenzie, Meg, Saudah and Tanya - I truly could not have done this without you. Our lunch breaks, cake Wednesdays and walks have helped to keep me laughing through hard office days. Thanks also to my housemates Lara, Sasha and Ailsa for providing a welcome distraction from work.

Finally, I'd like to thank my family and friends. To Genevieve Pounds and Beth Lowe, thank you for your amazing friendship and kindness and for showing me it's possible to finish a PhD! Thanks also to my hockey team and my brownies who have provided me with a great distraction every week. A special thanks goes to my parents and brothers, Sam and Jake for their unending support which I am forever grateful for.

Abstract

The rotator cuff muscles surround the glenohumeral joint of the shoulder and compress the humeral head into the glenoid fossa to prevent dislocation and allow for movement at the joint. Tears of the rotator cuff are common, if conservative treatment of these fail then surgical repair is on occasion possible. However, such repairs often lead to unsatisfactory results. The development of surgical repair methods and new treatments are limited by a lack of appropriate functional pre-clinical assessment, especially over extended motion cycles. The aim of this thesis was to develop a novel experimental human shoulder simulator capable of producing repeatable controlled movements over extended motion cycles to assess the biomechanics of the rotator cuff in an intact, torn and repaired state.

During the method development process, surrogate animal tissue was evaluated as an alternative to human tissue, however, this had significant limitations and the use of animal tissue was not pursued. The premise of the developed simulator was to actuate rotator cuff muscles of a cadaveric human shoulder. This was firstly assessed in a computational model and then in an experimental simulator. The cadaveric human shoulder simulator applied controlled displacements to tendons to produce cyclic abduction and flexion motions representative of normal shoulder function. The resultant force applied to each tendon during the cycles was measured. Braided polyethylene thread was secured to tendon ends (supraspinatus, infraspinatus, subscapularis, teres minor, anterior and middle deltoid) using a modified finger trap suture. Eyelet screws were attached to the scapula to act as pulleys and maintain the line of action of the muscles. Forces applied by the stepper motors were measured using a custom load measurement platform and a compression load cell.

The human shoulder simulator was used to assess three cadaveric shoulder samples, studies investigated the repeatability of the human shoulder simulator and the effect of a surgical double row repair on the biomechanics of the joint. Successful cyclic testing of cadaveric shoulder samples was achieved using the novel shoulder simulator to obtain repeatable force data through abduction and flexion motions. It was observed that the supraspinatus muscle initiated the abduction motion followed by the deltoid muscles. When the supraspinatus tendon was torn, the force in the anterior deltoid muscle increased to compensate for the reduction in force in the supraspinatus tendon. The total magnitude of force within all the muscles increased when the supraspinatus was torn suggesting a higher level of joint instability. After a double row repair of the tendon, the force in the supraspinatus increased and surpassed the magnitude observed during the intact condition tests.

Table of Contents

List of Tables

List of Figures

Chapter 1 - Introduction

1.1 General Introduction

The shoulder joint is capable of the widest range of motion of any joint in the body however to achieve this it is also the most unstable joint (Rockwood and Matsen, 1998a). The rotator cuff muscles surround the large glenohumeral joint of the shoulder and compress the humeral head into the glenoid fossa of the scapula preventing dislocation (Hess, 2000). Half of all major shoulder injuries are tears of the rotator cuff tendons. Over 62% of adults over the age of 80 years have a rotator cuff tear (May and Garmel, 2020). Tears of the rotator cuff are often initially managed conservatively however in over 40% of cases continuing pain leads to the requirement for surgical intervention (Greenall et al., 2018). The age, tendon quality and size of tear impact the success of surgical repair with failure rates between 25-50% at 12-months post-surgery (Greenall et al., 2018). Simulator models enable the surgical repair methods to be tested through appropriate loading cycles and ranges of motion.

The anatomy and biomechanics of the shoulder will be discussed followed by the causes of rotator cuff injuries and the surgical repair approaches. Computational simulation methods and the application of these to the shoulder joint and in particular the rotator cuff will be considered. Current cadaveric rotator cuff studies will be assessed followed by the suitability of porcine tissue to represent the human shoulder. Finally natural joint simulators will be discussed for the hip and knee joints leading on to the natural shoulder simulators including their advantages and limitations.

1.2 The Shoulder

1.2.1 Anatomy

The shoulder complex consists of three bones, four joints and 30 muscles which create a joint capable of the widest range of motion of any joint in the human body (Martini et al., 2017). However, to permit this range of motion the shoulder joint is also the most unstable joint in the body (Rockwood and Matsen, 1998a).

The scapula, clavicle and the humerus are the three bones which directly participate in shoulder motion. Other bones such as the spine and sternum are important for muscle attachment however do not interact directly at the shoulder joint (Rockwood and Matsen, 1998a). The bones of the shoulder are shown in Figure 1.1.

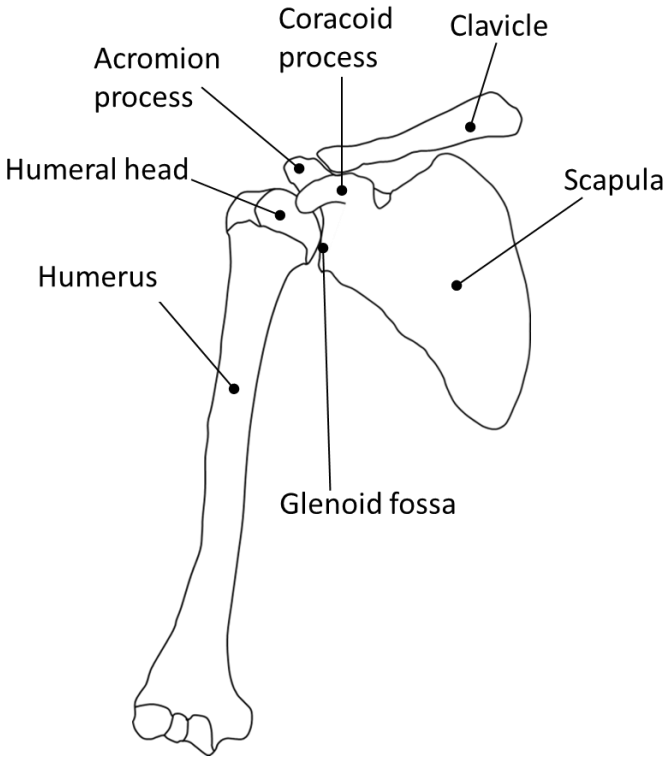

Figure 1.1 – Anterior view of the bones of the shoulder joint; humerus, scapula and clavicle. The bony landmarks of the acromion process and the corocoid process of the scapula are also indicated.

The longest bone in the upper limb is the humerus. At the proximal end of the bone there is a half spherical articulating surface called the humeral head (Tortora and Nielson, 2012). Relative to the shaft of the humerus, the head is inclined by an angle of between 130° and 150° (Terry and Chopp, 2000). The scapula is a large, triangular bone that lies posterior to the thorax (Plausinis et al., 2006). The scapula 'floats' on top of the rib cage, unconnected to the spine and ribs other than through muscle attachments. The main function of the scapula is muscle attachment with 17 muscles attached to or originating on the scapula. The acromion and the corocoid process are bony struts projecting off the superior portion of the scapula as shown in Figure 1.1. The main function of the acromion is for muscle attachment and it also acts to increase the lever arm of the deltoid muscle. The coracoid process serves as the origin site for several ligaments of the shoulder (Terry and Chopp, 2000). The glenoid cavity lies inferior to the acromion and articulates with the humeral head (Tortora and Nielson, 2012). The clavicle lies horizontally at the base of the neck, anterior to the scapula. It is an "s" shaped strut which connects the upper limb to the axial skeleton (Plausinis et al., 2006).

Movement at the three anatomical joints allow for the wide range of motion possible at the shoulder joint (Plausinis et al., 2006). The acromioclavicular joint is a diarthrodial joint between the acromion of the scapula and the lateral portion of the clavicle (Felstead and

Ricketts, 2017). At the other end of the clavicle, the sternoclavicular joint links the medial portion of the clavicle to the sternum. This joint provides the only skeletal articulation between the axial skeleton and the upper limb (Rockwood and Matsen, 1998a). The acromioclavicular and sternoclavicular joints combine to allow the scapula to 'glide' over the posterior portion of the ribcage which is often referred to as the scapulothoracic joint. The final joint is the glenohumeral joint between the humeral head and the glenoid fossa of the scapula. The large radial mismatch between the humeral head and the glenoid fossa allows for the large mobility at the joint (Terry and Chopp, 2000). The joints of the shoulder complex are shown in Figure 1.2.

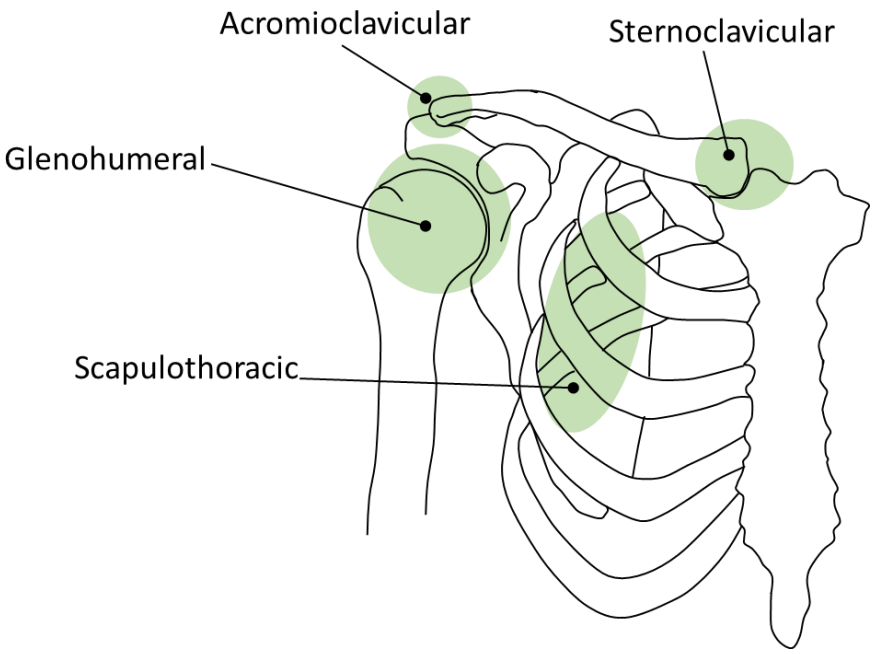

Figure 1.2 - Joints of the shoulder complex. The sternoclavicular, acromioclavicular, glenohumeral and scapulothoracic joints are highlighted in green.

At any one time only approximately 25% to 30% of the humeral head is in contact with the glenoid fossa in the glenohumeral joint. Therefore, to prevent dislocations of this joint and to allow for the wide range of movement, several passive and active stabilisers act in the shoulder (Terry and Chopp, 2000). The articular cartilage in the glenoid fossa is thicker in the peripheral than in the central region in order to mitigate the shallow nature of the glenoid fossa (Funk, 2005). Alongside this, the glenoid labrum also acts to increase the contact area within the joint (Clavert, 2015). Consequently, the conformity in the joint is increased such that a negative pressure exists within the joint. The pressure within the joint is lower than atmospheric pressure resulting in a vacuum effect which helps to hold the humeral head into the joint (Rau et al., 2000). However the impact of the negative pressure on the joint stability is limited during daily life as maximum stabilisation forces occur when a net pulling force acts on

the joint which is rare during normal use (Veeger and van der Helm, 2007). The final static stabilisers are ligaments. Two main groups of ligaments contribute to the stability at the joint. The glenohumeral ligaments connect the humeral head to the rim of the glenoid which helps to prevent anterior translation and hence dislocation of the joint (Rau et al., 2000). The coracohumeral ligament originates on the coracoid process of the scapula and inserts onto the tubercles of the humerus. This ligament works to stabilise the joint particularly during the motions of forward flexion, adduction and internal rotation (Terry and Chopp, 2000).

The main dynamic stabiliser of the shoulder is the rotator cuff. This comprises of four muscles: the supraspinatus, infraspinatus, teres minor and the subscapularis (Terry and Chopp, 2000). The primary role of the rotator cuff muscles is to compress the humeral head into the glenoid, particularly during the middle range of shoulder movement (Hess, 2000). The muscles of the rotator cuff are shown in Figure 1.3. The subscapularis is the most powerful rotator cuff muscle contributing 53% of the total cuff power. The supraspinatus contributes 14%, 22% from the infraspinatus and the remaining 10% from the teres minor muscle (Keating et al., 1992; Goetti et al., 2020).

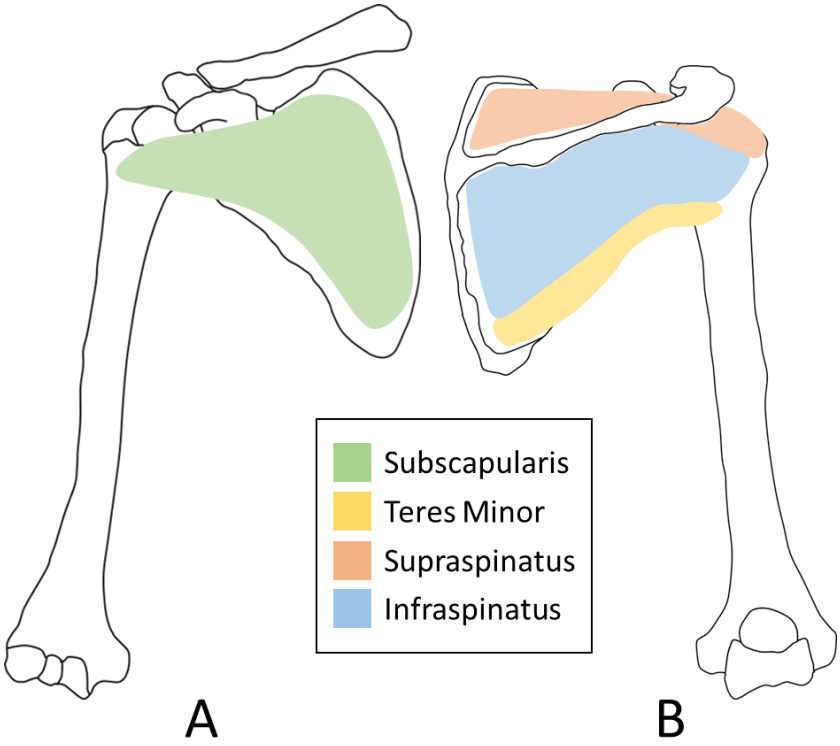

Figure 1.3 - The rotator cuff muscles of the shoulder: subscapularis, supraspinatus, infraspinatus and teres minor. A: anterior view. B: Posterior view.

Other dynamic stabilisers include the biceps tendon which sits over the top of the humeral head depressing it into the glenoid cavity. The deltoid muscle is the primary abductor of the

shoulder. It also provides a superior force to the humeral head which is counteracted by the force of the rotator cuff muscles. Finally, the position of the scapula throughout the range of motion also contributes to the stability at the shoulder (Felstead and Ricketts, 2017).

1.2.2 Biomechanics

A wide range of movements are achievable at the shoulder joint. The shoulder joint has six degrees of freedom however very little translation can occur in the joint without causing dislocation leaving the three main rotational degrees of freedom (Veeger and van der Helm, 2007). Flexion, extension, abduction, adduction, internal and external rotation can all be achieved at the shoulder joint. These motions of the shoulder are shown in Figure 1.4. The average value of the range of each of these motions that can be achieved at the joint are provided in Table 1.1.

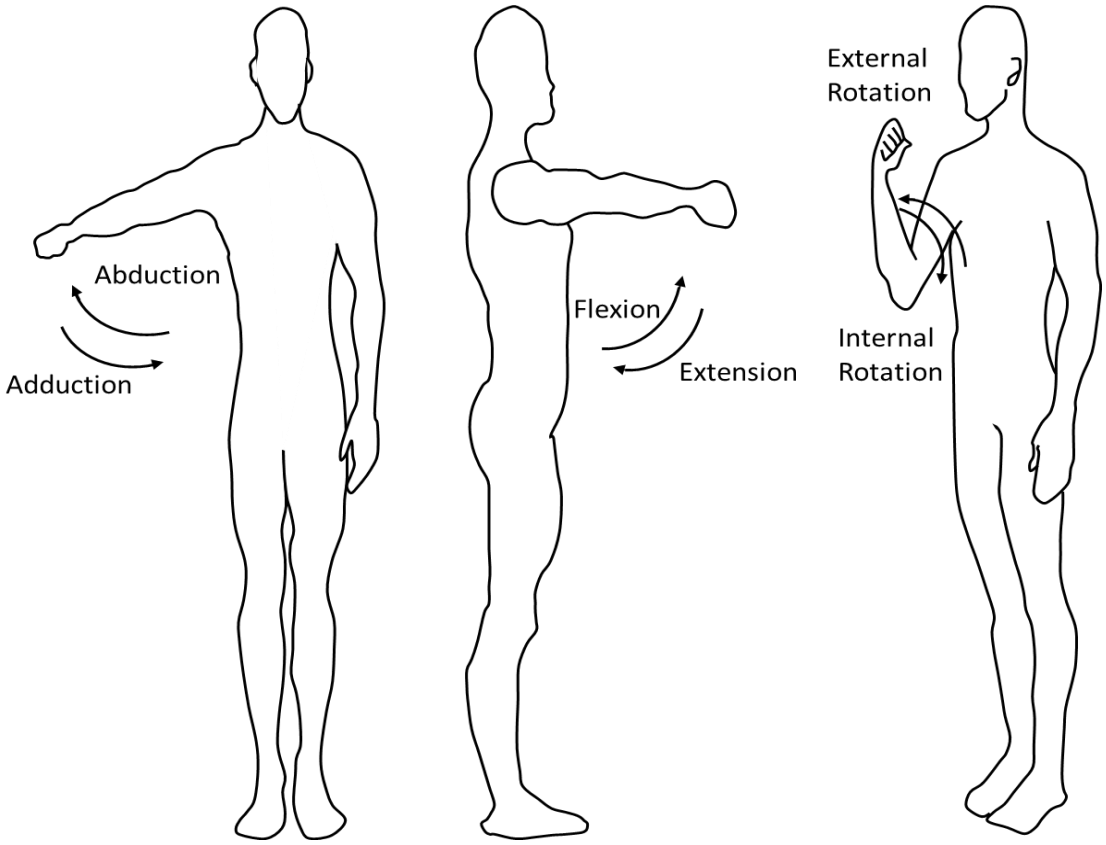

Figure 1.4 - The motions achievable at the shoulder; flexion/extension, abduction/adduction and internal/external rotation.

Table 1.1 - Range of motion at the shoulder joint at a mean of 23 and 71 years for male subjects (Dempster, 1955; Doriot and Wang, 2006)

Motion	Range of Motion	
	Age 23 ± 5 years	Age 71 ± 4 years
Flexion	193°	75°
Extension	63°	45°
Abduction	132°	122°
Adduction	51°	1°
Internal Rotation	96°	120°
External Rotation	31°	7°

The values shown in Table 1.1 were taken from two studies, one focusing on young male participants and another focusing on elderly male subjects. Age is shown to have an important role in the range of motion achievable at the joint. Flexion, extension, abduction, adduction and external rotation were shown to decrease with age however the value for internal rotation increases with age (Barnes et al., 2001). The motions shown in Table 1.1 are achievable only due to the combined motion of all the joints within the shoulder. Primarily the motion occurs within the glenohumeral and scapulothoracic joints however at the extreme positions, movement in the sternoclavicular and acromioclavicular joints is also required (Rockwood and Matsen, 1998a).

Scapulohumeral rhythm refers to the coordinated motion in the glenohumeral and scapulothoracic joints (Lugo et al., 2008a). The rotation of the scapula has three key functions. Firstly, the rotation ensures that there is maximum contact between the humeral head and the glenoid fossa throughout the motion cycle (Felstead and Ricketts, 2017). Secondly impingement of the humeral head on the coracoid process of the scapula is prevented (Rockwood and Matsen, 1998a). Finally scapula rotation allows the acromion (deltoid origin point) to move away from the deltoid insertion point on the humerus. This ensures that the length of the deltoid is maintained which hence maintains the power output of the deltoid (Lucas, 1973).

During the first 30° of abduction and 60° of flexion, little scapulothoracic motion is required (Felstead and Ricketts, 2017). Beyond this point, scapulohumeral rhythm performs an increasingly important role. The normal rhythm is often quoted as 2° of glenohumeral motion for every 1° of scapulothoracic motion (Flores-hernandez et al., 2019). The humerus must also externally rotate in order to reach maximum elevation. This prevents impingement whilst also

loosening the inferior glenohumeral ligaments (Rockwood and Matsen, 1998a). The clavicle also moves upward to allow for maximum abduction and flexion of the shoulder. Up to 90° abduction, there is approximately 4° of elevation of the clavicle per 10° elevation of the humerus. Beyond 90° there is negligible elevation of the clavicle. The clavicle elevation occurs due to rotation at both the acromioclavicular joint and the sternoclavicular joint (Lucas, 1973).

Activities of daily living (ADLs) are a collection of activities used to determine a patient's ability to live independently. They are key to establishing the need for surgical or non-surgical intervention when a patient has an injury (Edemekong et al., 2020). The activities of daily living can be separated into five categories: eating, bathing, dressing, mobility and toileting (Anspach, 2020). The shoulder joint plays a key role in many of these activities with a loss in its function proving detrimental to the independence of a patient.

The range of motion required to do a selection of key activities of daily living are provided in Table 1.2.

Table 1.2 - Range of motion required for activities of daily living (Oosterwijk et al., 2018).

Activity	**Flexion**	**Extension**	**Abduction**	**Adduction**
Reach shelf above shoulder height	142°	-	34°	-
Combing hair	139°	-	125°	-
Washing opposite armpit	95°	-	-	25°
Reaching back pocket	-	50°	5°	-
Eating with a fork	35°	-	44°	-

It can be seen from Table 1.2 that a large functional range of motion is required in the shoulder to be able to complete activities of daily living and remain independent.

Bergmann et al., used an instrumented shoulder replacement to record the glenohumeral contact force in the glenohumeral joint throughout a range of activities of daily living (Bergmann et al., 2007). The forces recorded during a selection of these ADLs are provided in Table 1.3.

Table 1.3 - Forces required for activities of daily living given as a percentage body weight and the resultant force for a male of average weight (Bergmann et al., 2007).

Activity	Resultant force (% body weight)	Resultant force for an average 80 kg male (N)
75° abduction without weight	85	667
120° flexion without weight	121	950
Lifting 1.4kg jug	103	808
Driving	42	330
Walking with 2 crutches	118	926
Putting 2.5 Kg onto a shelf 60 cm in front	69	542
Combing hair	65	510

There is a large range in the force values reported in the literature. Particularly in the case where analytical shoulder models were used to predict the glenohumeral contact forces. Due to the limited anatomical landmarks on the scapula, optical tracking systems to determine scapula motion produce variable results. When these are then applied to dynamic computer simulations the contact forces vary across studies (Bergmann et al., 2007). Despite providing more repeatable force values, the study by Bergmann et al used an instrumented shoulder replacement and hence not a natural shoulder environment potentially altering the glenohumeral contact forces.

1.2.3 Rotator Cuff Injuries

Over 50% of major shoulder injuries are due to tears of the rotator cuff muscles (Murrell and Walton, 2001). Tears can either be acute, due to a traumatic injury such as a fall, or chronic. The differentiation between acute and chronic tears can be difficult due to the additional sub-category of acute on chronic tear which involves an acute tear on an already degenerated rotator cuff (Abdelwahab et al., 2021; Paul et al., 2022). Purely acute tears of the rotator cuff are rare accounting for approximately 8% of all rotator cuff tears and are predominantly seen in younger patients (Abdelwahab et al., 2021).

There are several factors which can lead to chronic rotator cuff tears. Firstly, repetitive motions such as sports or overhead activities can stress the muscles and tendons. Due to ageing, the blood supply to the tendons decreases which reduces the ability of the tendon to heal. Bone spurs can also form on the inferior portion of the acromion as a patient ages. This causes impingement of the acromion on the supraspinatus tendon. These three factors all

increase the likelihood of a rotator cuff tear as a patient ages (Athwal and Armstrong, 2017). A tear that involves more than one of the rotator cuff muscles is termed a massive rotator cuff tear. These are particularly common in the elderly and account for 10-40% of all tears (Manske, 2018).

Any of the four rotator cuff muscles can be affected by a rotator cuff tear, however the majority of tears occur in the supraspinatus muscle due to the impingement of the acromion (Sward et al., 1992). Tears of the subscapularis tendon along with the supraspinatus were seen in 31% of cases however an isolated tear of the subscapularis tendon only occurred in 4. 9% of rotator cuff tears (Lafosse et al., 2010). The infraspinatus tendon was torn alongside the supraspinatus tendon in 18.2% but occurred on its own in only 0.1% of cases (Minagawa et al., 2013).

Rotator cuff tears are also categorised as being partial or full thickness tears. A partial tear does not sever the tendon as the tear extends only partially through the thickness. A full thickness tear however separates the bone from the tendon leading to a hole forming (Athwal and Armstrong, 2017a). The severity of the rotator cuff tear impacts on the outcome for the patient and the time required to return to full use of the shoulder joint (Kessel and Bayley, 1986). Acute tears often stem from high energy mechanisms which result in full thickness tears however, chronic tears are more likely to originate as partial thickness tears which then progress to full thickness tears (Abdelwahab et al., 2021).

Patients with rotator cuff tears often present with stiffness, weakness and instability in the shoulder (Rockwood and Matsen, 1998b). The impact on the range of motion at the joint is dependent on the severity of the tear and the muscles which are torn. Often elevation and external rotation of the arm are impacted leading to difficulties in completing many of the activities of daily living (Sward et al., 1992). A massive rotator cuff tear or one involving the supraspinatus muscle can cause the humeral head to translate superiorly on the glenoid surface as seen in Figure 1.5. This is because the force opposing the deltoid has been reduced. The superior shear force can then cause structural damage to the glenohumeral joint surface and can lead to cuff tear arthropathy (Sharkey et al., 1994).

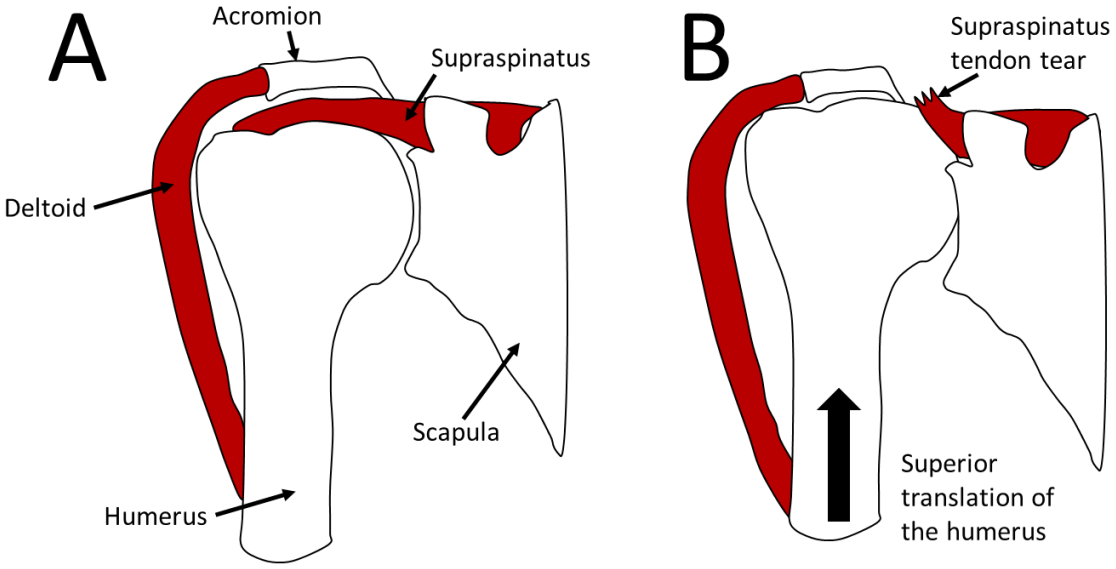

Figure 1.5 - Superior translations of the humeral head due to a tear of the supraspinatus tendon. A: Shoulder joint with an intact supraspinatus. B: Shoulder with a supraspinatus tendon tear showing superior translation of the humerus.

1.2.4 Rotator Cuff Treatment

Rotator cuff tears (both acute and chronic) are treated either surgically or through conservative non-surgical management. Acute tears of the rotator cuff in young patients, where identified early, are usually repaired surgically since tendons are often of good quality allowing for a successful and more stable repair (Manske, 2018). Partial thickness chronic tears can heal or become smaller through non-operative techniques. Around 28% of partial thickness tears propagate to become a full thickness tear, causing increased pain and weakness in the affected shoulder (Pandey and Jaap Willems, 2015). Treatment of most chronic tears begins with conservative methods. However, 40% of patients will require surgical intervention due to continuing pain despite non-operative management (Greenall et al., 2018).

Regardless of if the rotator cuff tear was due to an acute event or a degenerative tear the factors for a surgical decision are the same. Surgery is usually recommended for patients younger than 70 years of age due to the increased muscle and tendon quality required to yield a satisfactory repair result (Williams et al., 2004; Tashjian, 2012; Sambandam et al., 2015). The activity level which the patient expects to return to also impacts the decision for surgery along with the level of retraction of the torn muscle and the presence of muscle atrophy and fatty infiltration which would limit the ability of the tendon to heal (Williams et al., 2004; Paul et al., 2022).

Non operative treatment involves a combination of physical therapy, rest and steroid injections (Rockwood and Matsen, 1998b). The main benefit of non-operative treatment is that the patient avoids the risks associated with a surgical procedure. However, risks of this approach include extension of the tear and arthritis due to cuff tear arthropathy and migration of the humeral head as shown in Figure 1.5 (Sambandam et al., 2015).

Surgical repair of a tear can be performed either using open or arthroscopic techniques. Open surgery requires a larger incision which allows for greater access enabling bone spurs to be removed or additional reconstruction to be completed if required. Arthroscopic surgery requires smaller incisions hence reducing the healing time and the chance of infection (Athwal and Armstrong, 2017a). The choice between performing the procedure in an open or arthroscopic manner depends mainly on surgeon preference and experience.

There are three main surgical techniques for the arthroscopic repair of rotator cuff muscles: single row, double row and transosseous equivalent (Pandey and Jaap Willems, 2015). The three arthroscopic surgical techniques are shown in Figure 1.6.

The single row technique is the simplest repair technique allowing for quicker surgery times and easier revision surgeries. The double row technique uses both a medial and lateral row of sutures in order to increase the contact area of the repair. This improves the initial strength of the repair however the operative time, procedure complexity and cost are all increased (Pandey and Jaap Willems, 2015). The transosseous equivalent technique uses two rows of anchors but, unlike the double row technique, does not pass an anchor through the lateral stump of the tendon (McCormick et al., 2014). This technique can improve the vascularity of the repaired tendon whilst having comparable complexity, cost and operative time to the double row technique (Pandey and Jaap Willems, 2015).

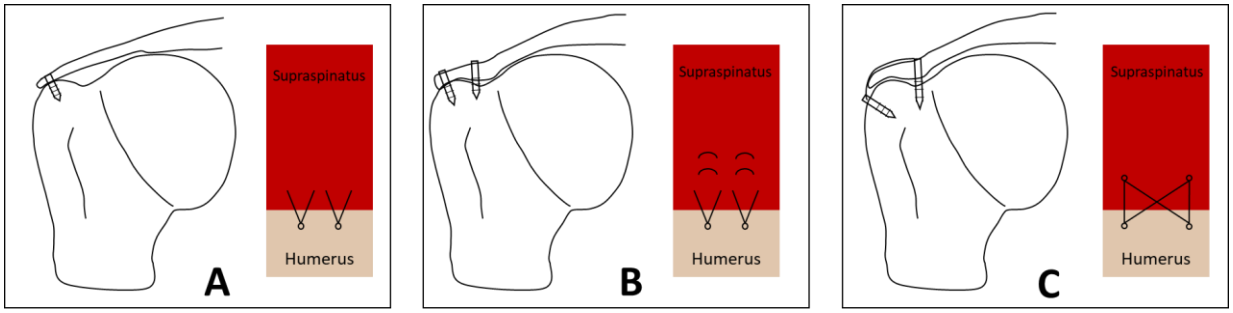

Figure 1.6 - Surgical techniques for the arthroscopic repair of the rotator cuff. A - Single row repair. B - Double row repair. C - Transosseous equivalent technique

Age, tendon quality and the size of the original tear are factors that have the highest impact on the success rate of a tendon repair (Athwal and Armstrong, 2017a). Small tears which are

surgically repaired early have the lowest failure rates however, large or massive tears frequently re-rupture after surgery. This is due to the degenerative changes in the tendon tissue. Greenall et al found failure rates of 25-50% at 12 months post-surgery (Greenall et al., 2018). The double row and transosseous equivalent repair techniques offer the best outcomes for large tears as they increase the contact of the tendon edge to the greater tuberosity whilst also improving the vascularity of the repair (Matthews et al., 2006). A systematic review conducted by Longo et al., found that the double row repair method had lower retear rates compared to the single row repair based upon 18 studies. The average retear rate was found to be 12.7% for double row repair patients, 14.5% for patients who underwent a single row repair and 23.6% for patients who underwent a transosseous re pair (Longo et al., 2021). This would suggest that the transosseous repair technique was biomechanically inferior however, the transosseous repair is more likely to be used in the case of a large tear with poorer quality tendon which would be less likely to heal surgically (Pandey and Jaap Willems, 2015).

1.3 Computer Simulation Methods

1.3.1 Biomechanical Simulation Methods

Computational models of the human body allow for a deeper understanding of how joints and muscles work together to produce motion. Computational models are used to determine what muscles are involved with certain movements and the reaction forces involved in a movement (Veeger et al., 1991). Gait analysis was initially used to gain quantitative data on the dynamics and movements of the human body by using high precision cameras to track positional changes of body segments. Gait analysis however could not provide any insight into forces in the muscles or accelerations of body segments (Pandy, 2001). Computer modelling allows simulations to be used to predict how muscles interact with one another (Maurel et al., 1996).

There are two different methods of analysis used to calculate or measure muscle force: inverse and forward dynamics. Inverse dynamics takes the motion and external l oads as inputs to the system and calculates the internal muscle forces (Rasmussen, 2003). Forward dynamics however, uses inputs of muscle activity and external forces in order to calculate the motion of the body (Pandy, 2001). The musculoskeletal system as a whole is mechanically redundant meaning that there are a greater number of muscles in the body than are necessary to create most motions (Rasmussen, 2003). In the human body, the central nervous system instantly selects muscles to perform each motion however a computational model must use optimisation theory to make the same decision (Pandy, 2001). Optimisation theory uses a combination of linear and quadratic programs in order to select the muscles which minimise the muscle fatigue caused by the motion (Rasmussen et al., 2002). The main difference

between the forwards and inverse dynamics methods is that during inverse dynamics, the optimisation problem is solved at every point throughout the motion whereas in inverse dynamics, the optimisation is solved once, after the complete simulation. Consequently, forward dynamics problems can take longer to run. Inverse dynamics methods produce results which are very dependent on the accuracy of the input values, in this case the position, velocity and acceleration of body segments. This information can be very difficult to obtain accurately leading to significant errors building up within the computational model (Pandy, 2001). Most musculoskeletal modelling systems use an inverse dynamic approach as this allows the unknown internal muscle forces to be calculated from prescribed motions (Bolsterlee et al., 2013).

Another challenge with computer modelling of musculoskeletal systems is the modelling of muscles. They are commonly modelled using either a '*straight line'* or '*centroid line'* method. The straight line method assumes that the muscle forms a straight line between the origin and insertion points. This assumption means that the muscle is simple to implement but the quality of the results generated is compromised as the lengths of the muscles are not representative. The centroid line method constructs the muscle using cross sectional centroids of the muscle. A line then joins several centroids providing a much better representation of the muscle geometry. However, this method can prove very hard to implement due to a lack of literature surrounding the cross sectional centroids and how these change through motion. Therefore, via points are often used to enhance the representation provided by the straight line method. Via points allow the straight line to 'root' to several points between its origin and insertion points in order to improve the definition of the length of the muscle (Pandy, 2001).

The AnyBody modelling system uses inverse dynamics and numerical methods which estimate the internal muscle forces based on inputted motions and movements (Lemieux et al., 2012). A Hill model is used in order to allow the maximal force to be exerted by a muscle when it is at its optimum length. The optimisation theory used in the AnyBody software is referred to as the min/max criterion which aims to minimise the energy expenditure of the system to reflect the natural synergism of the muscular system (Lemieux et al., 2012).

Other commercial software enables the modelling of the musculoskeletal system. OpenSim is an open source modelling system, allowing analysis of reactions between the human body and the environment (Delp et al., 2007). Whereas the AnyBody system runs the inverse dynamics and optimisation equations in parallel, OpenSim completes these in two steps. This means that the AnyBody software is more efficient at solving the closed systems and also allows for greater control over individual parameters of the model (Cadova, 2013). Other programs such as Siemens Jack, allow for integration of modelling software such as AnyBody with CAD

systems. Digital human modelling systems such as Jack and Human Builder create visual representations of anthropometric and kinematic data to aid engineering design. This type of model are most commonly used in order to determine human and environment compatibility (Paul, 2011).

1.3.2 Models of the Shoulder Complex

The Delft shoulder model uses inverse dynamics to model the shoulder joint on a computer program called SPACAR which is a finite element software designed specifically for mechanisms with multiple degrees of freedom such as the shoulder joint. Bones are represented as single elements with multiple nodes and the Delft shoulder model comprises of seven segments: thorax, clavicle, scapula, humerus, ulna, radius and hand. The model also contains 17 muscles which control the motion at the shoulder and elbow joints (van der Helm, 1997). A cadaveric study was used to provide the information regarding optimal muscle fibre length and muscle structures. This information along with external forces were the inputs to the model providing internal muscle forces as the outputs (Nikooyan et al., 2011). Applications of this model include a study looking at glenohumeral arthrodesis conducted by van der Helm and Pronk (1994), manual wheelchair propulsion and analysis of a glenohumeral prosthetic design (van der Helm, 1997).

The AnyBody shoulder model was created based upon data and assumptions from the Dutch Shoulder Group. The model represents an average male of 75 Kg and 1.8 m in height (Lemieux et al., 2012). There are 118 muscle-tendon units that represent the muscles and tendons of the shoulder joint. The only ligaments included on the model are the coracoacromial and conoid ligaments for stability (Lemieux et al., 2013).

1.3.3 Rotator Cuff Models

Several in-silico studies have been completed to determine the effect of rotator cuff injuries and repair mechanisms on the shoulder joint. A study conducted by Steenbrink et al (2009) used the Delft shoulder and elbow model to assess the impact of rotator cuff tears. Thirty-one muscles were used. To simulate a rotator cuff tear the affected muscle was removed from the model. The study found that a tear of the rotator cuff caused instability and increased forces in the alternative abducting muscles (Steenbrink et al., 2009). Only one motion, abduction, was assessed during this study and so the effects of a rotator cuff tear on other motions were not analysed.

Holscher et al (2016) used the basic human model from the AnyBody repository to simulate a rotator cuff tear. The joint reaction force in the shoulder was restricted to the glenoid cavity in order to mimic a rotator cuff tear. The study indicated that the deltoid and te res major

muscles compensated most for the reduced forces produced in the torn rotator cuff. Again only one motion, elevation, was considered (Weber et al., 2016).

AnyBody was used in another study by Haering et al (2015) to assess the risk of failure of repairs to the rotator cuff muscles during passive motion. In this study different sized tears were simulated by reducing the size of the muscles within the model and hence reducing the forces produced. Healthy participants with no history of shoulder pai n were used to obtain kinematic data for each of the passive rehabilitation exercises being modelled.

1.4 Experimental Simulation Methods

1.4.1 Cadaveric Rotator Cuff Models

Cadaveric studies have been undertaken to assess the strength of the repair methods in vitro. The mechanical properties and boundary conditions do not have to be estimated when using cadaveric tissue leading to an advantage of cadaveric studies over purely computational models (Kim et al., 2006). Several cadaveric studies have assessed the effect of the different surgical rotator cuff repair methods on the strength and outcomes of the repair. Limitations remain in cadaveric studies in comparison to in vivo clinical tests. Some general limitations include the quality of the rotator cuff tissue, the duration of the studies and the loads and motions applied to the joint. Often the tissue used in these studies are from specimens with no previous rotator cuff injuries rather than those with rotator cuff tears which often have poor tendon quality due to the degeneration of the tendons (Kim et al., 2006). The cadaveric tissue will start to degrade in quality once it has been removed from the body and so the duration of any tests are limited to ensure that the mechanical properties of the tissue remains relevant (Cartner et al., 2011). Also the freeze/thaw cycles that the tissue undergoes during dissection, preparation and storage prior to the studies commencing has been demonstrated to reduce the Youngs modulus of the tendons. Consequently, the results from these studies cannot be directly translated to in vivo outcomes. However, the comparisons between different repair methods can still be made as the effect applies to all the tissue used equally (Smith et al., 2006). Finally, the loads and motions that are simulated in the studies in literature are simplifications of the motions experienced in vivo (Kim et al., 2006).

Waltrip et al. (2003) and Kim et al. (2006) removed all the soft tissue in the shoulder joint except the supraspinatus tendon which was cut in order to simulate a rotator cuff tear. The supraspinatus tendon in the most commonly injured of all the rotator cuff muscles due to the proximity to the acromion process of the scapula (Athwal and Armstrong, 2017a) hence why this tendon tear was chosen to be simulated. Smith et al. (2006) also simulated a supraspinatus tear however the remaining rotator cuff muscles were left intact surrounding

the joint. Oh et al. (2012) was the only study to simulate a massive rotator cuff tear where both the supraspinatus and the infraspinatus tendons were torn. The remaining rotator cuff muscles, along with the deltoid, pectoralis major and latissimus dorsi muscles were replaced with wires from their intact insertion points. To replicate the wide origins, and multiple lines of action of these muscles, several wires represented a single muscle. The amount of static loading applied to each wire was determined from the physiological muscle cross-sectional area (PCSA) ratios of the corresponding muscles (Oh et al., 2012). The PCSA is directly proportional to the maximum force that can be produced by the muscle (Rockwood and Matsen, 1998a).

Oh et al. (2012) and Smith et al. (2006) applied purely static loads to the tendons hence why other soft tissues were left in situ in order to maintain some stability within the joint. As mentioned, Oh et al. (2012) applied loads relative to the cross sectional area (PCSA) of the muscles. Smith et al. (2006) on the other hand applied forces obtained from literature to the four tendons of the rotator cuff muscles. Smith et al. (2006) left the static loads on the cadaveric shoulders for 60 minutes whilst the shoulder was abducted to 30°; the angle of a sling following rotator cuff surgery. Oh et al. (2012) applied the static loads at 0°, 30° and 60° of shoulder abduction including a 2:1 ratio of glenohumeral to scapulothoracic abduction. In both cases the distance from a static reference point on the humerus to a reference point on the repair was measured in order to determine the fixation strength of the different repair methods.

Waltrip et al. (2003), Kim et al. (2006) and Smith et al. (2006) performed cyclic tests using a universal material testing machine. All these studies fixed the humerus to the base of the machine and then used a variety of clamping methods to fix the tendon to the crosshead of the testing machine. The angle of abduction of the shoulder within the testing machine was selected to try and replicate the line of action of the supraspinatus tendon as the testing machine could rigidly only apply this force in one direction. Smith et al. (2006) attached the humerus at an angle of 30° abduction, Kim et al. (2006) at 45° abduction and Waltrip et al. (2003) at an abduction angle of 100°. Both Waltrip et al. (2003) and Kim et al. (2006) performed cyclic tests up to a load of 180 N whereas Smith et al. (2006) performed these tests up to a value of 100 N. Once the specified number of cycles had been conducted, in all cases, the maximum load was then increased incrementally until failure occurred. The fixation method of the tendon end to the crosshead of the testing machine was crucial in order to obtain accurate results instead of the tendon pulling out of the clamp system leading to premature failure. Kim et al. (2006) used a soft tissue clamp with additional fine sand paper to clamp the tendon. A cryoclamp was used in the study conducted by Smith et al. (2006) which

maintained the temperature of the tendon end between -20°C and +2°C to maximise the grip on the tendon. The connection method between the tendon and an artificial material is important to ensure that the results from any test were accurate and not impacted by a connection failure. Consequently in order to allow for active actuation of the rotator cuff muscles as outlined in the project objectives in Section 1.6, preliminary testing regarding suitable connection techniques would have to be conducted.

1.4.2 Animal Models of the Shoulder

The use of a surrogate model of the human shoulder joint allows for biomechanical testing to be completed using a more available source of tissue. Suitable anatomy of the surrogate shoulder joint is required to enable biomechanical testing. Common animal models such as the dog, pig, sheep, cow, rat and rabbit do not have a true rotator cuff where the tendons of the supraspinatus, infraspinatus, teres minor and subscapularis muscles insert together to form a single cuff surrounding the glenohumeral joint. Primates and a tree kangaroo were found by Sonnabend and Young (2009) to be the only animals whose rotator cuff anatomy relevant to the human anatomy due to the function of their upper limbs. However, costs, accessibility and ethical concerns would prevent widespread use of these animals as biomechanical models of the shoulder (Sonnabend and Young, 2009).

Tissue from the food chain results in tissue with less variability compared to human cadaveric tissue due to the consistent age of the tissue (Cone et al., 2017; Jimenez-Cruz et al., 2022). The most widely available biomechanical animal models (excluding live animal models) are the porcine model and the ovine model (Sonnabend and Young, 2009).

1.4.2.1 Porcine Models of the Shoulder

Quadrupeds such as the pig, use the forelimb in a largely different capacity to humans. The forelimb and hence shoulder joint is a weight-bearing joint undergoing much greater forces (Hast et al., 2014). Anatomically, the main difference between the pig and the human shoulder is the clavicle. Most quadrupeds do not have a clavicle but instead have a clavicular tendon within the brachiocephalicus muscle (Frandson et al., 2009). The skeletal anatomy of the pig forelimb is shown in Figure 1.7.

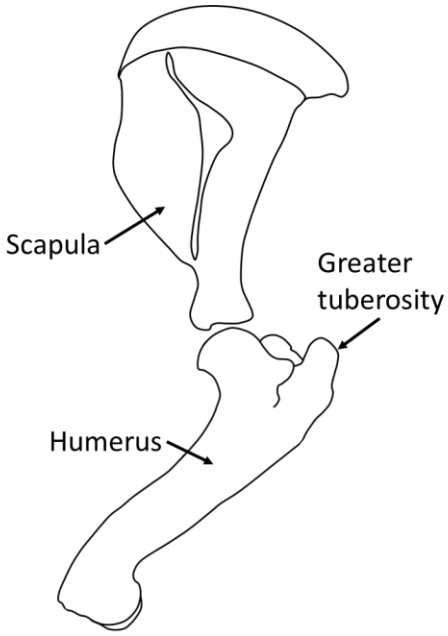

Figure 1.7 - Skeletal anatomy of the porcine forelimb. The scapula and humerus bones are labelled as well as the greater tuberosity of the humerus.

The greater tuberosity of the pig humerus extends much further than that of the human such that it extends past the humeral head. The additional height of the tuberosity increases the lever arm of the muscles which insert onto this region (Frandson et al., 2009).

The forelimb muscles of a pig are expected to be larger than those of a human of a similar mass due to the weight-bearing nature of the joint. This is particularly the case with the rotator cuff muscles. In the human, the rotator cuff muscles are particularly crucial in retaining the stability in the joint during the full range of motion. The range of motion is much less for a quadruped and hence the weight bearing function is of much more importance. Whereas the subscapularis muscle is the dominant rotator cuff muscle in humans, primates and small quadrupeds, larger quadrupeds are infraspinatus dominant (Mathewson et al., 2014). The difference in the mass and the physiological cross sectional area (PCSA) of the rotator cuff muscles between humans and pigs is provided in Figure 1.8. The PCSA is directly proportional to the maximum force that can be produced by the muscle (Rockwood and Matsen, 1998a).

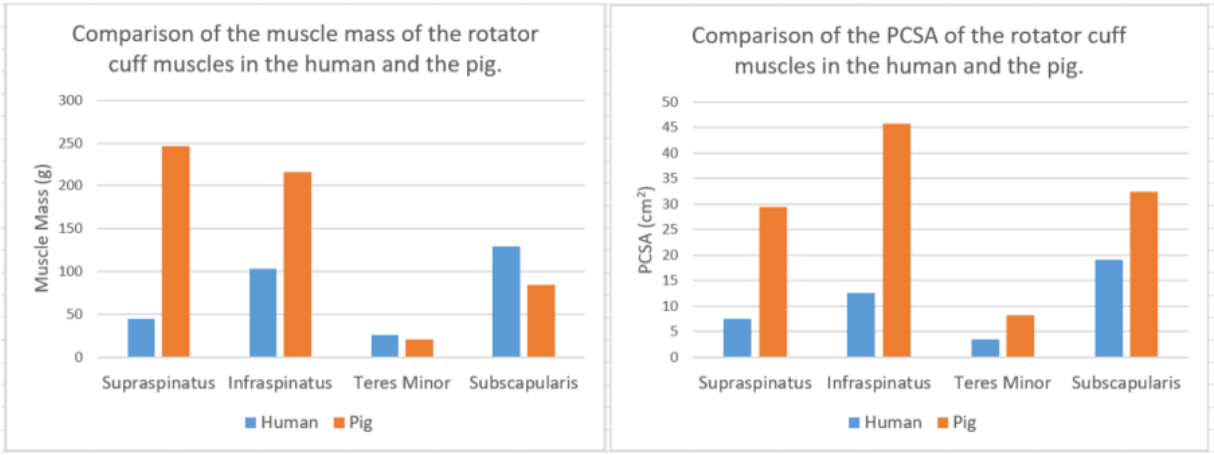

Figure 1.8 - Mass and physiological cross sectional area (PCSA) of the rotator cuff muscles in the pig and the human (Mathewson et al., 2014).

It can be seen from Figure 1.8 that the mass of both the supraspinatus and infraspinatus muscles are considerably greater in the pig. Alongside this, the PCSA is greater in the pig for all the muscles. This is due to the much increased forces passing through the joint. During normal walking, the maximum force through the porcine shoulder was shown to be 550% body weight (Thorup et al., 2007) whereas the maximum force reported to pass through the human shoulder was 118% body weight when walking with two crutches (Bergmann et al., 2007).

Despite all these differences porcine shoulders have been used to conduct tests on rotator cuff repair methods. Milano et al (2008) used 50 fresh porcine shoulders to assess the difference between the single-row and double-row repair techniques. A full thickness tear of the infraspinatus was replicated and then repaired. The proximal humerus was then loaded to the base of a universal testing machine with the tendon fixed to the crosshead. A cyclic load was then applied to the tendon repair. The main limitation that was observed was that the tested repairs produced much greater fixation than that observed clinically. This was related to the difference in bone density between a young pig and a typically older patient who would require the surgery (Milano et al., 2008).

1.4.2.2 Ovine Models of the Shoulder

The anatomy of the sheep shoulder joint is very similar to that of a pig because they are both quadrupeds. Neither animal has a true rotator cuff which is defined as the joining of the rotator cuff to form a common insertion. The tendons of the pig and sheep supraspinatus, infraspinatus and teres minor insert separately onto the greater tuberosity of the humeral head (Sonnabend and Young, 2009). The role of the rotator cuff in a quadruped is considerably different to the role played in an animal which raises their forelimb above the head. The rotator cuff is purely used to swing the limb in the sagittal plane creating a pendulum motion

(Ahmad et al., 2020). Consequently the supraspinatus muscle which is predominantly used in the human joint to abduct the shoulder and maintain stability is of less importance in a quadrupeds joint which undergoes less abduction and is inherently more stable (Mathewson et al., 2014).

The ovine infraspinatus is the largest muscle of the rotator cuff and has similarity to the human supraspinatus tendon (Turner, 2007). The shape and anatomy of the ovine infraspinatus is similar to the human supraspinatus tendon but also the thickness and direction of muscle fibres are similar to the human anatomy (Bisbinas et al., 2013). Ovine tendon fibres have a more parallel arrangement than in humans. However, as human tendons degenerate their fibres lose some orientation and hence become more parallel, similar to the ovine model (Smith et al., 2017).

1.4.3 Natural Joint Simulators

1.4.3.1 Lower Limb Joints

Experimental simulator models enable whole joints to be tested through a consistent range of motion and loading cycles (Pallan, 2016). Commercial joint simulators predominantly focus on the preclinical assessment of replacement joints. These can provide three-dimensional forces and motions to evaluate a wide range of artificial joints including hips, knees, ankles, fingers, spines and shoulders (Dowson and Unsworth, 2016). Wear rate and total wear of the components are the most commonly measured outcomes but geometry, materials, loading and motion profiles can also be considered (Shen et al., 2019).

Testing of natural tissue within a mechanical simulator means that estimations of material properties and boundary conditions do not have to be taken. Limitations of using natural tissue primarily focus on the length of time that tests can run for. Over time, after the tissue is removed from the body, the mechanical properties of the tissue changes as it decays (Pallan, 2016). Groves (2015) used a simulator to apply a dynamic load to a whole natural hip joint during motion. The dynamic load and motion regime ran for over 2 hours however the motion was limited to a single flexion/extension plane (Groves, 2015).

Pallan (2016) conducted testing of the natural hip joint throughout the whole gait cycle. An ISO standard gait cycle was applied to the natural tissue using a single-station anatomical hip simulator. Porcine tissue was used due to the availability of the tissue in the food chain and was fixed into the simulator with the use of Polymethymethacrylate (PMMA) bone cement (Pallan, 2016). The tissue can be dissected to just reveal the joint geometry which can be mounted into the simulator. Due to the high conforming nature of the hip joint no soft tissue is required to maintain the stability during motion within the simulator.

Knee simulators often are designed to study the tribology of total knee replacements rather than soft tissue conditions such as cartilage or meniscal repair techniques. A porcine knee model was used within a knee simulator to assess the biomechanical properties of the cartilage. Stabilising tissue such as ligaments surrounding the knee were replicated using springs to ensure that the knee was stable throughout the testing (Liu et al., 2015). Several knee simulators have been made which use natural tissue alongside natural soft tissue such as muscles and ligaments. In most cases however, very low forces are passed through the soft tissue leading to poor physiological conditions within the knee (Schall et al., 2019). The Munich knee rig, shown in Figure 1.9, powers the quadriceps and hamstring muscles via pneumatic actuators. Although these muscles are powered, the simulator initiates the motion and the soft tissue is purely used to maintain stability in the joint throughout the motion hence the true forces within the joint are not represented (Heinrichs et al., 2018).

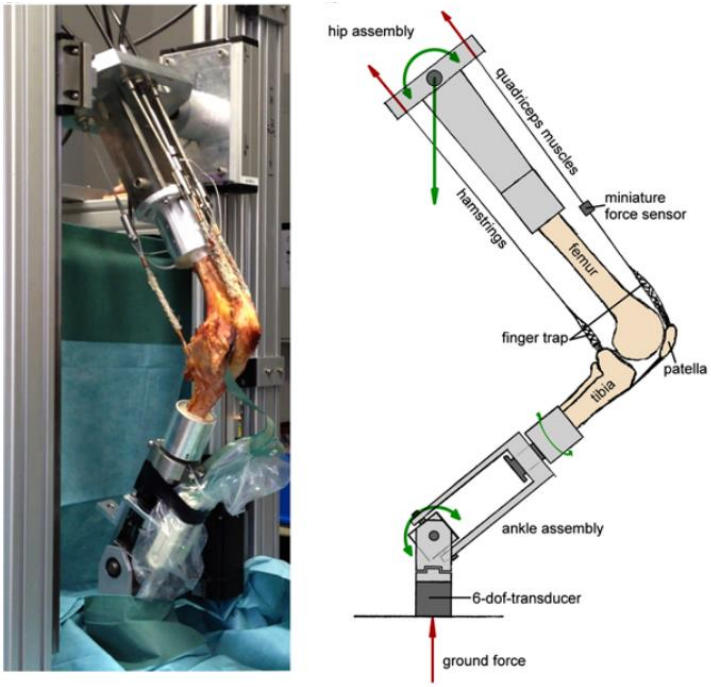

Figure 1.9 - The Munich knee rig which uses pneumatic actuators to power the quadriceps and hamstring muscles (Steinbrück et al., 2013). *Image reproduced under the creative commons attribution license.*

1.4.3.2 Natural Shoulder Simulators

Natural shoulder simulators are required to demonstrate the natural unstable shoulder environment whilst simulating some of the wide range of motion achievable at the joint. Due to the complexity of the joint, most current simulators use the static joint to evaluate shoulder biomechanics as demonstrated in Section 1.4.1. In order for a simulator to be truly representative of the shoulder environment, the muscles must be actively powered in order to

produce motion. Passive motion occurs when the simulator moves the humerus directly instead of powering the muscles to produce the motion. Passive motion produces less muscle forces and reduces the contact force within the glenohumeral joint which result in outputs that are less well aligned to the natural shoulder case (Verjans et al., 2016).

The Aachen shoulder simulator is shown in Figure 1.10. A cadaveric shoulder was used along with six pneumatic muscles which could perform active motion. UHMWPE ropes and ball bearing pulleys were used to connect the pneumatic actuators to the equivalent muscle tendon (Verjans et al., 2016).

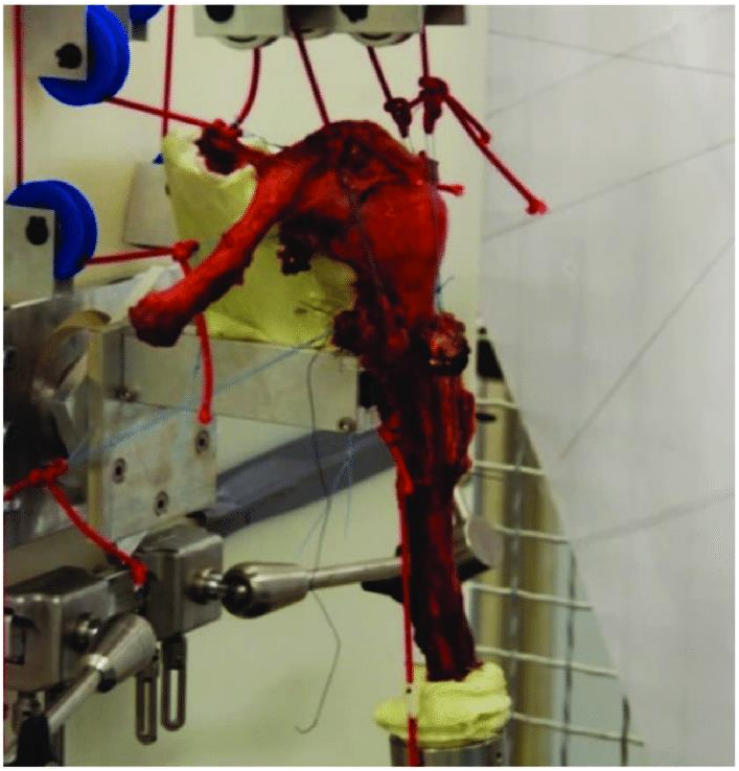

Figure 1.10 – The Aachen shoulder simulator. Six pneumatic muscles provide active motion of a cadaveric shoulder (Verjans et al., 2016). *Image reproduced under the creative commons attribution license.*

Active motion was achieved by the use of a teach-in process. The user was required to move the humerus in the desired motion to determine the length of muscles and hence actuation that was required to perform these motions (Verjans et al., 2016). Although this provided more realistic results than passive motion, there was no control over the distribution of motion between the over-constrained system of muscles. The teach-in method did however, allow for a wide range of motions to be studied using the simulator including: abduction/adduction, internal/external rotation and flexion/extension.

Kedgley et al (2007) used a cadaveric shoulder simulator to assess the repeatability of the motions when different muscle inputs were used. The simulator used is shown in Figure 1.11 and uses a similar set-up to the Aachen simulator. A cadaveric shoulder is powered by a series of pneumatic actuators, pulley and ropes which are attached to muscle tendons (Kedgley et al., 2007).

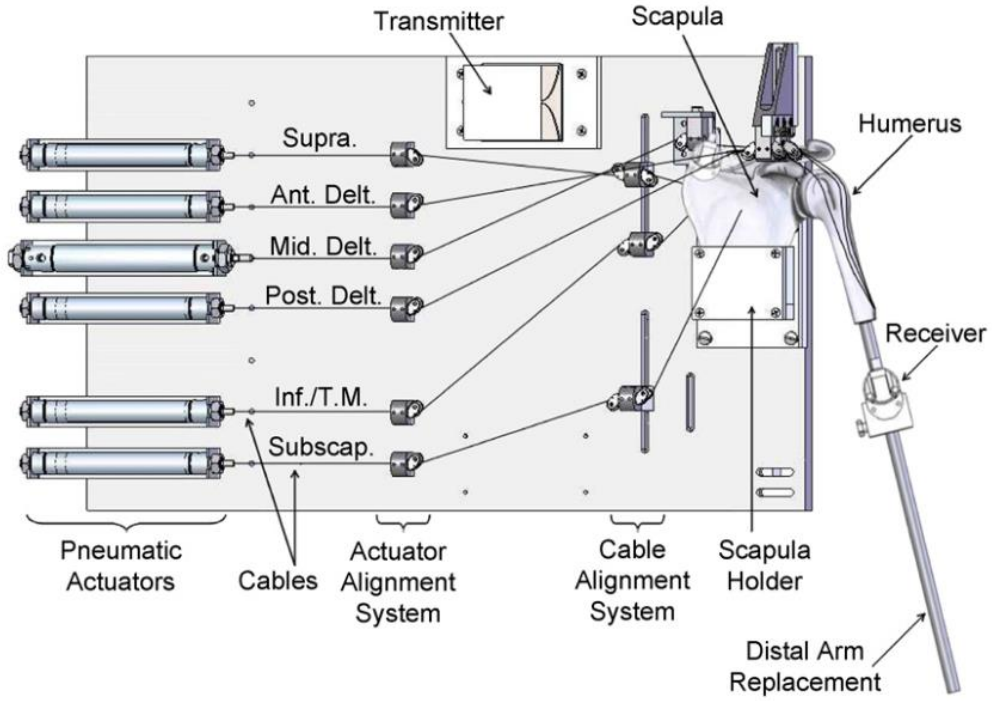

Figure 1.11 - Cadaveric shoulder simulator created by Kedgley et al (2007). A series of pneumatic actuators, pulleys and wire power a cadaveric shoulder. Image reproduced with permission.

The pulleys were required in the system to allow for the changing lines of action of the musdes throughout the motion cycle. Four regimes of muscle loading were tested alongside a passive system: (1) loads applied to each muscle were equal, (2) loads applied to each muscle were relative to the PCSA of the muscle, (3) loads from an EMG study constant throughout the motion, and (4) loads from an EMG study which changed as a function of abduction angle. It was concluded that none of these regimes gave a true representation of physiological loading due to the assumptions made in each method. In particular the likelihood of the PCSA to change in relation to the changing length of the muscles and the difficulty in obtaining accurate EMG data for the rotator cuff muscles was noted. Despite this, all the active muscle controlled methods provided much more repeatable motion than passive motion indicating that active motion should be used for natural shoulder simulation (Kedgley et al., 2007).

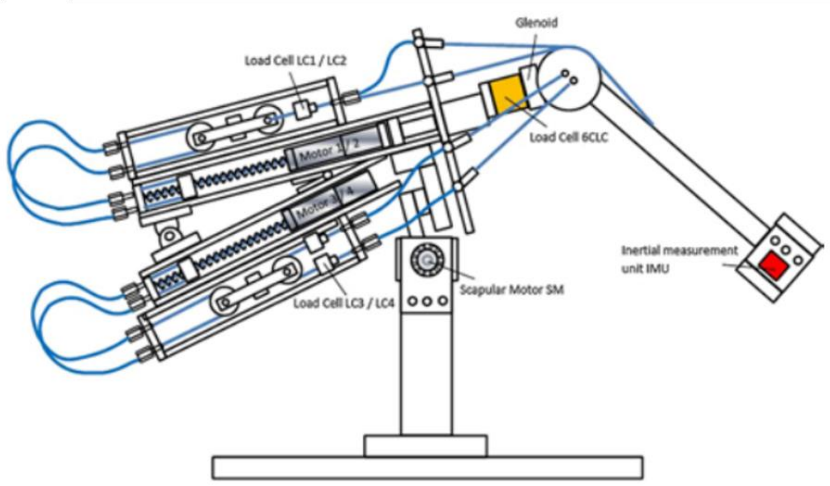

Figure 1.12 - Shoulder replacement simulator by Baumgartner et al (2014). Pneumatic actuators replicate the forces provided by the rotator cuff muscles. Image reproduced with permission.

A shoulder replacement simulator created by Baumgartner et al (2014) is shown in Figure 1.12. A shoulder replacement was used in place of the natural joint and a series of electroactuators were used to power four muscles including the rotator cuff. This simulator also incorporates the scapulohumeral rhythm by rotating the scapula using a stepper motor. Cyclic motions could also be performed with the simulator to represent repetitive loading tasks and determine the forces within the replacement throughout its lifetime (Baumgartner et al., 2014).

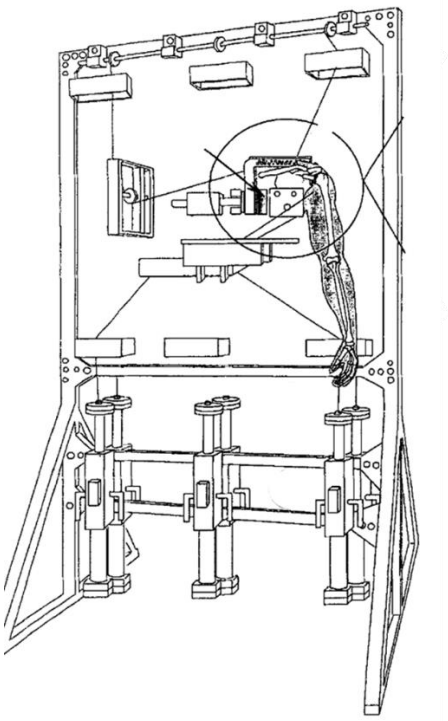

Figure 1.13 - Shoulder simulator by Debski et al (1995). Image reproduced with permission.

The Debski shoulder simulator is shown in Figure 1.13 which uses hydraulic cylinders in order to apply load to the four rotator cuff tendons and the middle deltoid. The model only simulated abduction of the shoulder and no scapulothoracic motion was included in the model hence the abduction motion was limited to 60°. The same force was applied to all the actuated muscles and was increased until the desired motion was achieved (Debski et al., 1995).

Guo et al (2023) made a natural shoulder simulator which used active control of the supraspinatus, subscapularis, infraspinatus and deltoid muscles to perform three cycles of flexion, abduction and internal and external rotation. The force required in each muscle during the motions was recorded using load cells. The scapulothoracic motion was not modelled and so the range of abduction motion was limited to 60°. The input data required for these motions was obtained through cross-sectional area and EMG data from literature (Guo et al., 2023).

Comparisons between the key features of the five simulators above are detailed in Table 1.4.

Table 1.4 - Comparisons between key features of the Aachen simulator, the Kedgley et al (2207) simulator, the Baumgartner et al (2014) simulator, the Debski et al (1995) simulator and the Guo et al (2023) simulator. A/A: Abduction/Adduction, F/E: Flexion/Extension, IR/ER: Internal/External rotation.

Requirements	Aachen Simulator	Kedgley Simulator	Baumgartner Simulator	Debski Simulator	Guo Simulator
Natural Joint	✓	✓		✓	✓
Active Motion	✓	✓	✓	✓	✓
Scapulo-thoracic motion			✓		
Cyclic Motion			✓		
RoM	A/A, IR/ER, F/E	A/A	A/A	A/A	A/A, F/E, IR

It can be seen that none of the natural simulators provide the capability to represent the scapulohumeral rhythm. Accurately measuring the motion of the scapula in-vivo can be difficult and often requires invasive methods such as bone pins to get accurate results. Non-invasive methods such as skin marker tracking systems are less accurate due to limited bony landmarks on the skin (Flores-hernandez et al., 2019). As the Aachen simulator, the Kedgley simulator and the Guo simulator performed abduction to an angle less than 120°,

impingement of the humeral head onto the scapula did not occur even when the scapulohumeral rhythm was ignored. However a computational study using the AnyBody modelling system concluded that the scapulohumeral rhythm had a significant impact on the forces within the glenohumeral joint. The changing angle of the scapula lead to the moment arms and muscle lengths of the key shoulder muscles changing throughout the motion impacting the internal muscle forces (Flores-hernandez et al., 2019). The change in length muscles during the rotation of the scapula varies across the shoulder muscles dependant on the origin and insertion locations of the muscle. The supraspinatus muscle has a very small change in length through the abduction motion due to its position on the superior portion of the scapula as seen in Figure 1.3. Contrastingly, the muscles which enable to rotation of the scapula such as the latissimus dorsi and pectoralis major muscles undergo large length changes through the motion of abduction (van der Helm, 1994b).

To simulate the performance of a rotator cuff repair method throughout its lifetime, cyclic motions must be achievable in a shoulder simulator. In the lower limb, common repetitive motion can be characterised using the gait cycle. The approximate number of cycles that the lower limb undergoes each year can then be defined providing a testing standard. However the shoulder joint rarely undergoes similar repetitive motion on a daily basis. Consequently, defining a cycle of shoulder motions to encompass the whole range of motion required becomes more difficult in the non-weight-bearing joint (Langohr, 2015). A study using inertial sensors that were worn by healthy subjects for a portion of the day provided data regarding the daily use of the shoulder. The majority of the day (96%) shoulder motion was below 100° of abduction and there were on average 19 instances of abduction above 100° every hour (Coley et al., 2008).

The current gap in the literature was identified to be a natural tissue shoulder simulator which used active motion of the joint to produce cyclic motions. Increasing the number of motion cycles performed by the simulator would allow for a wider understanding regarding the natural joint biomechanics through repeated motions and the effect of time on the muscle forces. The Baumgartner simulator, which used a replacement shoulder joint, was the only identified previous study to look at the effect of longer cycles on the shoulder biomechanics. Active motion must also be achieved by the simulator due to the importance of the soft tissue structures on the stability and movement of the shoulder. Consequently, combining an active natural shoulder simulator with cyclic motion cycles would allow for a deeper understanding to be made regarding the biomechanics of the shoulder and the effect of rotator cuff tears and repairs on the joint biomechanics.

1.5 Summary

This literature review has discussed the anatomy and biomechanics of the natural shoulder along with rotator cuff tears and the surgical approaches to repairs. Following from this both computational and experimental methods of shoulder simulation have been investigated. Finally current natural shoulder simulators have been discussed with the assumptions that these simulators have used. It was made clear from completing the literature review that the shoulder joint is a very complex mechanism creating difficulties in accurate in vitro simulations.

Rotator cuff tears are common injuries however the success of surgical repair methods can be low. This can partially be attributed to the lack of appropriate pre-clinical testing and the limited cycles and range of motion that are experimentally tested. Computational models of the shoulder complex have been created which provide insight into the effect of a rotator cuff tear on the remainder of the muscles in the joint. Limitations with the computational models include a lack of motions modelled and the assumptions required to create the models. Employing natural joint simulation removes the need for certain assumptions such as material properties, geometry and boundary conditions. Physical shoulder simulators have demonstrated an ability to represent physical phenomena, and could be used to allow rotator cuff repair methods to be tested under cyclic physiological loads over a range of motion that is usually experienced within the shoulder joint. An inverse dynamics computational simulation could be used to provide the forces required within the muscles to produce certain motions required for activities of daily living. Natural shoulder simulators that have previously been made do not allow the joint to be tested throughout a cycle for a period of time. This would not provide enough information in order to assess the functional competence of the intervention throughout its lifetime.

1.6 Project Aims and Objectives

1.6.1 Aims

The overall aim was to develop an experimental simulator which will enable testing of a cadaveric shoulder joint through a wide range of repeatable cyclic motions with appropriate loading applied to the muscles of the shoulder joint. The force in each muscle required to perform the desired motion will be measured in order for the biomechanics to be assessed and different rotator cuff tears and repairs to be assessed.

1.6.2 Objectives

The objectives were:

- To develop a specification for an experimental natural shoulder simulator to identify the important parameters in clinical function that must be mimicked in an in-vitro simulator.
- Use a multi-body modelling system to define the constraints and degrees of freedom needed in the experimental simulation. This will determine the experimental constraints that will be used and how these will impact the joint.
- Determine if a suitable surrogate animal model could meet the defined specification.
- Develop a natural shoulder simulator which can simulate the environment of the natural shoulder joint through a series of cyclic shoulder motions. This will include the translation from a surrogate model to a human cadaveric model.
- Use the natural shoulder simulator to experimentally assess different surgical repair strategies for the rotator cuff.

The objectives are shown in the flow chart in Figure 1.14 indicating how each objective will feed into the subsequent objective and therefore meet the overall aim of the project.

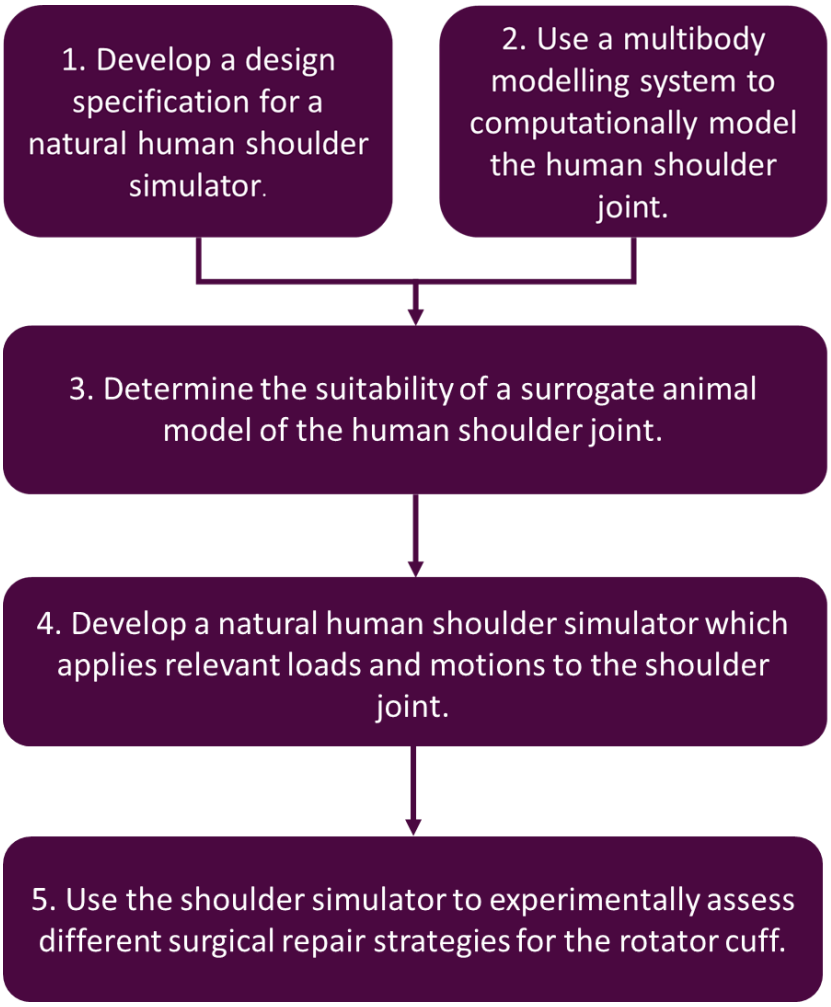

Figure 1.14 - Flowchart of the objectives of the overall project showing how each objective will feed into the overall aim of the project.

Chapter 2 – Evaluation of Surrogate Tissues for the Experimental Simulation of the Human Shoulder Joint

2.1 Introduction

The use of human tissue within research and particularly during the development of methodologies is costly and requires additional ethical consideration. The use of a surrogate model allows for the method development stage to be completed using a more available source of tissue. A model using tissue from the food chain means that the tissue has less variability compared to human cadaveric tissue due to the consistent age of the tissue (Cone et al., 2017; Jimenez-Cruz et al., 2022).

Rotator cuff repair strategies have been widely investigated using animal shoulder models however limited models were found to be capable of reproducing all the features of the human shoulder joint (Hast et al., 2014). For an animal model to be a suitable surrogate model for the human shoulder the following features must be present; (1) anatomically similar (soft tissue and bony) to the human joint, (2) used in a similar functional way to the human joint, (3) a tendon size and shape similar to the human to allow for surgical procedures (Derwin et al., 2010; Hast et al., 2014). The porcine joint has been widely used for a variety of musculoskeletal studies including in the hip, knee, ankle and temporomandibular joints as well as bone, cartilage and ligament studies (Cone et al., 2017). Consequently, due to the wide use of porcine tissue and the availability of the tissue within the food chain the porcine joint was selected for investigation within this chapter.

Through the analysis of previously developed shoulder simulators in Section 1.4.3.2, it was determined that the active control of the muscles was required in order for the simulator to produce relevant shoulder motions. Therefore the surrogate model selected must allow for the active actuation of the tendons of the rotator cuff and a suitable method for the secure attachment of wire to the tendon ends must be determined.

The main objectives for this chapter of work are:

- To determine the suitability of the porcine shoulder as a surrogate model for the human shoulder joint for use within the shoulder simulator.
- To determine the most appropriate method of loading the tendons of the porcine joint for the application of force within the simulator.

2.2 Dissection of a Porcine Shoulder

2.2.1 Methodology for the Dissection of a Porcine Shoulder

Porcine tissue (forelimb and shoulder) was obtained, within 24 hours of slaughter, from a local abattoir (John Penny and Sons, Leeds) from animals of approximately six months of age. The age was determined due to the availability within the food chain and all the pigs were slaughtered for human consumption. The shoulder joints were dissected fresh or stored at -20°C for dissection within 7 days.

The forelimbs were dissected initially to obtain the whole shoulder joint including the scapula, humerus, the four rotator cuff muscles, tendon of the long head of the biceps and the short head of the biceps. Further dissections could then be undertaken depending on the work required with the specific sample. All other skin, muscles, bones and fat were removed in order to allow for easier access to the desired components. The porcine forelimbs were obtained from the abattoir as shown in Figure 2.1Aand B. The spine, ribcage and surrounding tissue were dissected from the medial side to reveal the underlying scapula as shown in Figure 2.1C. On the lateral side, large overlying muscles such as the latissimus dorsi were removed as shown in Figure 2.1D until the scapula spine was visible. The fascia surrounding each muscle was followed using a finger in order to separate each muscle from its neighbouring muscles prior to removal. This ensured that the muscles which were removed from the samples were identified and not the required muscles.

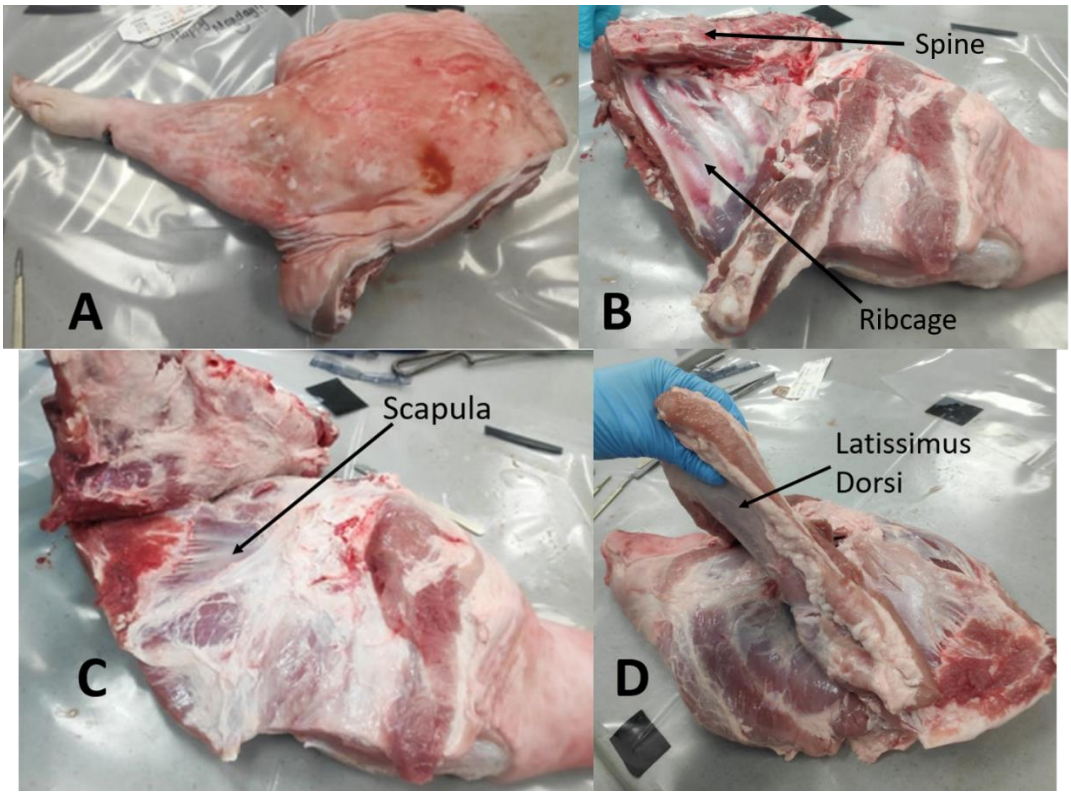

Figure 2.1 - Dissection of the porcine forelimb. A: Lateral view of the porcine forelimb. B: Medial view of the porcine forelimb. C: Removal of the spine, ribcage and tissue to reveal the scapula. D: Removal of soft tissue on the lateral side.

All overlying muscle and tissue was then removed to leave the rotator cuff muscles alongside the short and long heads of the biceps. The medial and lateral views of the resulting samples are shown in Figure 2.2 with the muscles labelled.

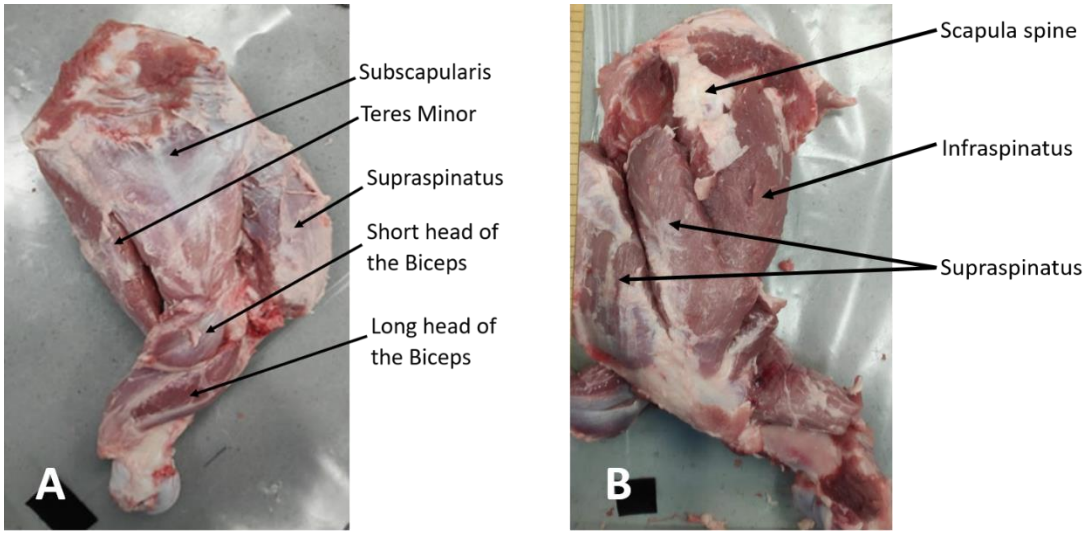

Figure 2.2 - Fully dissected porcine shoulder with the four rotator cuff muscles (supraspinatus, infraspinatus, teres minor and subscapularis) and the long and short head of the biceps labelled. A: Medial view. B: Lateral view.

2.2.2 Discussion

The dissections also allowed for the anatomy and functionality of the porcine shoulder to be analysed to determine the suitability of the porcine model to mimic the human shoulder joint.

Porcine tissue has the major advantage over human tissue of being cost effective and readily available in the food chain which would allow for greater opportunity in developmental testing of the shoulder simulator. The forelimb is used in a very different manner by quadrupeds such as pigs compared to humans, especially since the shoulder joint is a weight bearing joint in a porcine. Hence, there are several anatomical differences between the two shoulder joints. Firstly, pigs have restricted forward movement of the forelimb, therefore they do not have a clavicle but instead a clavicular tendon within the brachiocephalicus muscle (Frandson et al., 2003). It was noted during the dissection of the porcine forelimbs described in Section 2.2.1, that the greater tuberosity of the pig humerus extends much further than that of the human such that it reaches past the proximal edge of the humeral head, as shown in the schematic in Figure 2.3. The lever arms of the muscles which insert onto this region are increased by the additional height of the tuberosity (Frandson et al., 2003). However, the extension of the greater tuberosity led to the impingement of the humerus on the scapula at very small values of abduction (<5°). Several of the rotator cuff muscles insert onto the greater tuberosity and therefore this cannot be removed whilst keeping the rotator cuff muscles intact. Consequently, abduction beyond 5° was not possible with a porcine shoulder. During activities of daily living, abduction of the human shoulder reaches angles of 125° when combing hair (Oosterwijk et al., 2018). Therefore, it can be seen that the porcine model would severely limit the range of activities that a natural shoulder simulator would be able to perform.

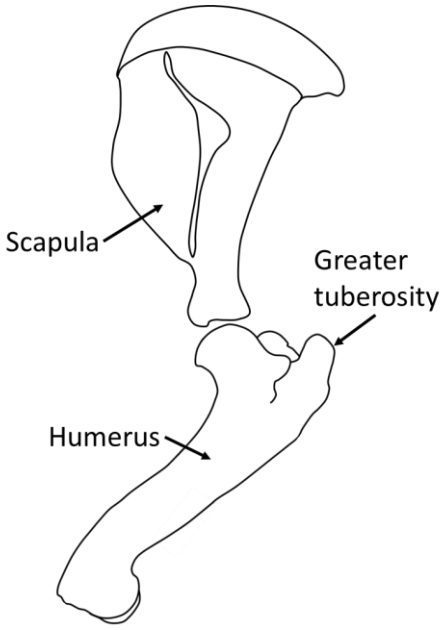

Figure 2.3 - Schematic showing the bones of the porcine shoulder. The humerus and scapula bones are labelled along with the greater tuberosity feature of the humerus.

In humans, the tendon of the supraspinatus muscle must pass through a small gap between the humeral head and the acromion process of the scapula. Due to the small gap, the supraspinatus tendon is a long and thin shape. Impingement of this tendon on the acromion is one of the leading causes of degenerative rotator cuff tears in humans. The porcine shoulder however, does not have an acromion process due to the different orientation of the scapula. Hence, the tendon does not have to pass through a gap and as such is short and wide. The tendon was found during dissection to be so short that it would not be suitable to replicate the repair that can be performed on a human supraspinatus. The only rotator cuff tendon in the porcine model that was deemed by two consultant shoulder surgeons, to be suitable for a tear repair to be simulated on was the subscapularis tendon. This tendon is much more rarely torn in humans, with isolated tears of the subscapularis accounting for only 4.9% of all rotator cuff tears (Lafosse et al., 2010). The porcine model would not be able to be used to simulate the most common supraspinatus tears, however, would be able to be used to simulate the less common subscapularis tendon tear.

The three criteria for a successful surrogate model of the shoulder given in Section 2.1 were (1) anatomically similar to the human joint in both the soft tissue and bony anatomy, (2) functionally similar to the human joint, and (3) a tendon size and shape similar to the human to allow for surgical procedures (Derwin et al., 2010). Firstly, the anatomical differences have been discussed, including the difference in bony structure where the porcine joint had a more prominent greater tuberosity of the humerus which limited the movement of the joint. The

range of motion achievable at the porcine joint was considerably limited due to this anatomical difference, particularly during the abduction motion. The soft tissues surrounding the porcine joint were also found to be incomparable to the human, particularly the supraspinatus tendon which did not pass through the small gap between the humeral head and the acromion of the scapula. Due to these differences between the joints, the porcine joint would not be a suitable surrogate model for the human joint. However, the method development process would be completed with the more accessible porcine tissue before being translated to the human shoulder.

2.3 Fixation of Muscle Ends to Allow for Actuation of Rotator Cuff Muscles

2.3.1 Introduction and Aims

Muscles of the rotator cuff had to be loaded throughout the experimental simulation in order to maintain the stability of the naturally unstable shoulder. In order to load these muscles within a simulator environment, the muscle ends distal to the joint were securely connected to a pulley and actuation system.

In order to produce force in the muscles of the shoulder during simulation, an actuation system was connected to the muscle ends. The aim of the study was to experimentally determine the optimum attachment method according to a criteria determined to be key to the success of the simulator.

2.3.2 Study Approach and Success Criteria

The requirements for a suitable fixation method between the muscle and the actuation method are detailed in Table 2.1.

Table 2.1 - Requirements for the fixation method

Requirement	Reason
Lightweight	Fixation method must not interfere with the actuation of the muscles.
Small and compact	Fixation must not interfere with the method of actuation.
Strong	The fixation method must be able to withstand the loads of 450 N applied to the shoulder muscles.
Non-elastic	The fixation method must not stretch when load is applied.
Repeatable	The fixation method will be required several times per sample and so a repeatable method of fixation must be developed.

The loads applied to the shoulder muscles were determined using a computational model of the human shoulder joint detailed in Chapter 3. The model performed a flexion of the shoulder to 100° where a load of 350 N was applied to the deltoid muscle, hence a minimum load to be withstood by the fixation method was selected to be 450 N to allow for error and to prevent the system from breaking within the test. The value of 450 N was based upon the human shoulder, as detailed in Section 2.2 the structure of the porcine shoulder differs from the structure of a human shoulder. Hence, it may not be possible to achieve a value of 450 N and so the highest possible force that can be achieved by a connection method will be taken into account.

2.3.3 Previously Used Attachment Methods

The application of force to a muscle or tendon requires a secure connection method between the soft tissue and a mechanical actuation system. Many fixation methods have been developed and demonstrated throughout literature. A range of pneumatic, hydraulic and electrical actuators have been used to simulate muscle activity however the secure connection of these systems to the soft tissues has remained challenging (Sharkey et al., 1995).

During surgical repair of soft tissues, such as tendons, a variety of suture methods are used to secure the soft tissue. Consequently, many previous studies have used suturing methods to connect soft tissue to actuation systems for use in natural joint simulators (Kedgley et al., 2007; Ferreira et al., 2010; Giles et al., 2011; Giles et al., 2014; Verjans et al., 2016; Dyrna et al., 2018). The use of suture methods within a simulator environment ensures that the connection method remains small and light enough to not interfere with the actuation of the muscle elements (Jiang et al., 2020).

In order to distribute the applied load over a greater surface area of the tendon Steinbrück et al (2013) used a metallic finger trap which was then sutured to the tendon in order to secure the finger trap into position (Steinbrück et al., 2013).

Clamps have also been very commonly used but were often adapted in order to maximise the strength of the connection. Clamp modifications can be split into three types: (i) altering the surface geometry of the clamp-tissue interface, (ii) inclusion of additional materials or adhesives and (iii) modifying the mechanical properties of the tissue in the clamped region. Increasing the contact area and friction of the tissue-clamp junction was achieved through the use of serrated clamps. Despite the ease of use and inexpensive nature of this modification, these clamps can increase the stress concentration leading to failure at the clamped edge. Materials such as sandpaper or adhesive have also be applied to the clamp surface, however

the water content of natural tissue can hinder the application of adhesive to the tissue surface (Jiang et al., 2020).

Muscle tissue is composed of bundles of parallel muscle fibres called fascicles (Rockwood and Matsen, 1998a). Therefore, thicker specimens are composed of many layers of fibres and fascicles. When the surface of the muscle is clamped, the slippage of the outer fibres is prevented, however shear can occur between internal and outer muscle fibres resulting in failure of the tissue (Jiang et al., 2020). Consequently, the technique of altering the mechanical properties of the tissue prior to clamping can prevent internal shear from occurring. The current gold standard method for clamping soft tissue is often deemed to be by freezing the tissue within the area to be clamped, using cryogenic clamps. Freezing the tissue means that the shear between the inner fibres can be neglected because the clamped portion has become a solid sample. However, in order to maintain the strength of the junction throughout testing, the clamped specimen must remain frozen throughout the test which can be difficult to achieve (Jiang et al., 2020).

Dehydration of the clamped portion of the tissue sample may also be performed in order to alter the mechanical properties to aid clamping. However, a suitable drying method must be developed in order to reduce the flexibility of the clamped region whilst maintaining the hydration and hence the mechanical properties of the test region (Jiang et al., 2020).

2.3.4 Pilot Study to Determine Fixation Methods

A pilot study was conducted to perform initial assessments of tendon attachment methods in order to select the most appropriate technique to adopt within the shoulder simulator. Mechanical testing of the different techniques was conducted in order to aid this decision.

2.3.4.1 Study Design

It was important for the successful attachment method to be easily repeatable and compact in order to fit within the simulator area as stated in Table 2.1. Therefore two simple surgical suture techniques were selected initially to determine if a more complicated attachment process was required.

The porcine forelimb was used throughout all preliminary tests due to the advantages of being cost effective and freely available in the food chain. The porcine shoulder was dissected as described in Section 2.2.

The long and short heads of the biceps, supraspinatus, infraspinatus and teres minor muscles were removed. The origin of the subscapularis muscle on the scapula was severed leaving the insertion on the humeral head in place. Removing these tissues allowed the capsule

surrounding the glenohumeral joint to be dissected, enabling the scapula to be removed. The resulting sample is shown in Figure 2.4. The subscapularis tendon was selected for these tests due to the length of the tendon available for suturing. The subscapularis tendon is the longest of all the porcine rotator cuff tendons and hence the tendon best suited for suturing. The bone-tendon sample was stored at -20°C prior to biomechanical testing.

Figure 2.4 - The resulting bone-tendon sample consisting of the porcine humerus and the subscapularis muscle.

Dorisea extreme braid fishing line (Dorisea Fishing, UK) was selected for use as the suture material. A common suture material used for tendon repair is Arthrex Fibrewire (Arthrex, Munich), the properties of Arthrex Fibrewire and Dorisea extreme braid fishing line are provided in Table 2.2. From the values presented in Table 2.2, it can be seen that the Arthrex Fibrewire and the Dorisea fishing line are both made from braided UHMWPE with a very similar diameter. The maximum load to failure of the Dorisea fishing line also exceeded the value for the Arthrex suture material. Therefore, due to the much reduced cost and the easier accessibility, the Dorisea extreme braid fishing line was selected for use during this study.

Table 2.2 - Properties of Arthrex Fibrewire and Dorisea extreme braid fishing line (Najibi et al., 2010; Dorisea, 2017).

Property	**Arthrex Fibrewire**	**Dorisea Extreme Braid Fishing Line**
Material	UHMWPE core with braided jacket of polyester and UHMWPE	8 strands of braided UHMWPE
Diameter (mm)	0.98	1
Max load to failure (N)	620	1334
Price per meter	£12.70	£0.079

The suture methods selected to be tested were the Krackow whip stitch and the modified finger trap method. The Krackow whip stitch was considered as the gold standard for securing the suture-tendon interface during soft tissue fixation (Sherman, 2018). The Krackow whip stitch was performed on the tendon of the short head of the biceps using the Dorisea extreme braid fishing line and is shown in Figure 2.5.

Figure 2.5 - The Krackow whip stitch on a porcine tendon of the short head of the biceps using the Dorisea extreme braid fishing line.

The modified finger trap stitch (MFT) was developed to prevent the need for multiple passes through the tendon with a needle, hence reducing the damage to the integrity of the tendon tissue (Su et al., 2012). The suture material was crisscrossed and tied around the tendon with a rolling-hitch knot to prevent slippage of the stitch. The modified finger trap stitch was

performed on the tendon of the long head of the biceps using the Dorisea extreme braid fishing line and is shown in Figure 2.6.

Figure 2.6 - The modified finger trap stitch on a porcine tendon of the long head of the biceps using Dorisea extreme braid fishing line.

A fixture was designed to ensure that the natural angle of 110° between the subscapularis tendon and the humerus was maintained throughout testing. The resulting fixture is shown in Figure 2.7 and the technical drawings are provided in Appendix 1. A collection of slots on the base of the fixture allowed for it to be clamped in different positions ensuring that the force on the humeral head was always vertical regardless of the size of the porcine humerus tested.

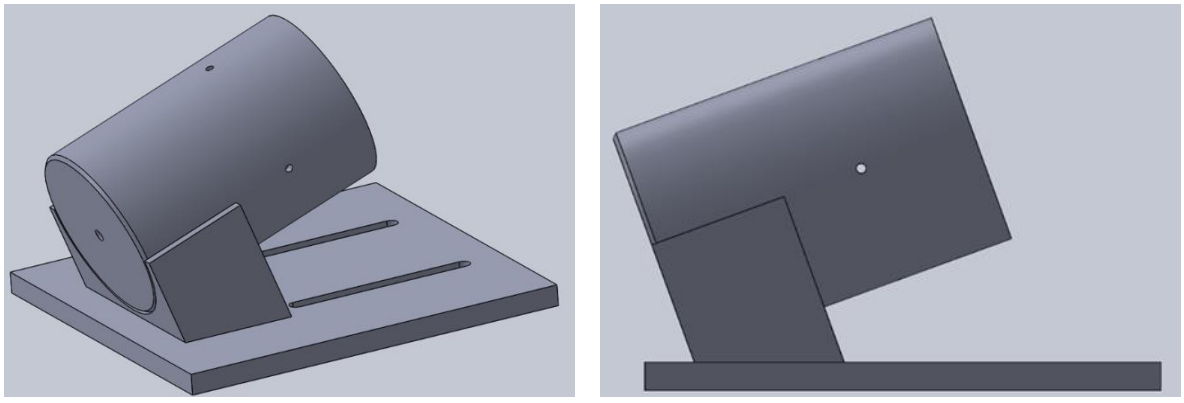

Figure 2.7 - The fixture designed to ensure that the natural angle of 110° between the subscapularis tendon and the humerus was maintained throughout testing.

2.3.4.2 Sample Preparation

The bone-tendon samples were thawed at room temperature for 24 hours prior to the mechanical testing. Once the samples had reached room temperature, the subscapularis muscle was cut to size determined by a template. The use of a template when cutting the muscle ensured that the subscapularis muscle was always the same size regardless of the variability of porcine tissue.

The relevant suture method (Krackow whip stitch or modified finger trap) was then performed on the subscapularis muscle. The two suture techniques were initially practiced to ensure that they could be performed consistently. Each suture method was performed on three independent samples.

The humerus was fixated into the custom designed holder using non-sterile Polymethylmethacrylate (PMMA) bone cement (WHW plastics, Hull, UK). The alignment of the sample within the cement pot was achieved by attaching the suture material to a clamp directly above the fixture, to ensure that the subscapularis tendon was vertical. The muscle was also aligned with a vertical notch that was cut into the fixture. Three pointed screws were inserted into the fixture until they gripped the humerus, securing it into place.

PMMA bone cement required the mixing of liquid and powder components during which an exothermic reaction occurs as the viscosity of the cement increased. The cement was used immediately, whilst in a liquid state, to ensure that the humerus was securely held within the pot. The samples were wrapped in a phosphate buffered saline (PBS) soaked tissue whilst undergoing the cementing process to maintain the hydration of the tissue through the exothermic curing process.

2.3.4.3 Mechanical Testing Protocol

The humerus fixture was clamped into place on the base of the Instron E10000 (Instron, High Wycombe UK) machine. The slots in the base of the fixture, shown in Figure 2.7, allowed for the fixture to be positioned such that the humeral head was vertically beneath the top loading bar of the Instron machine. The suture material was then tied securely to a bar at the top of the Instron using alternating half hitch knots. The samples were loaded at a ramp rate of 120mm/min in accordance with previous studies, to a maximum value of 450 N (Mathewson et al., 2014). Three independent samples for each type of attachment method were assessed. All mechanical tests were conducted at room temperature with PBS being sprayed regularly throughout the study to maintain the hydration of the tissue. Extension of the samples, failure mechanisms and failure loads were recorded and photographs were taken at regular intervals throughout the study.

2.3.4.4 Results and Discussion

The results from the three samples tested using the modified finger trap stitch are shown in Figure 2.8 on a force-displacement graph. The results from the three samples with the Krackow whip stitch are shown in force-displacement graphs in Figure 2.9.

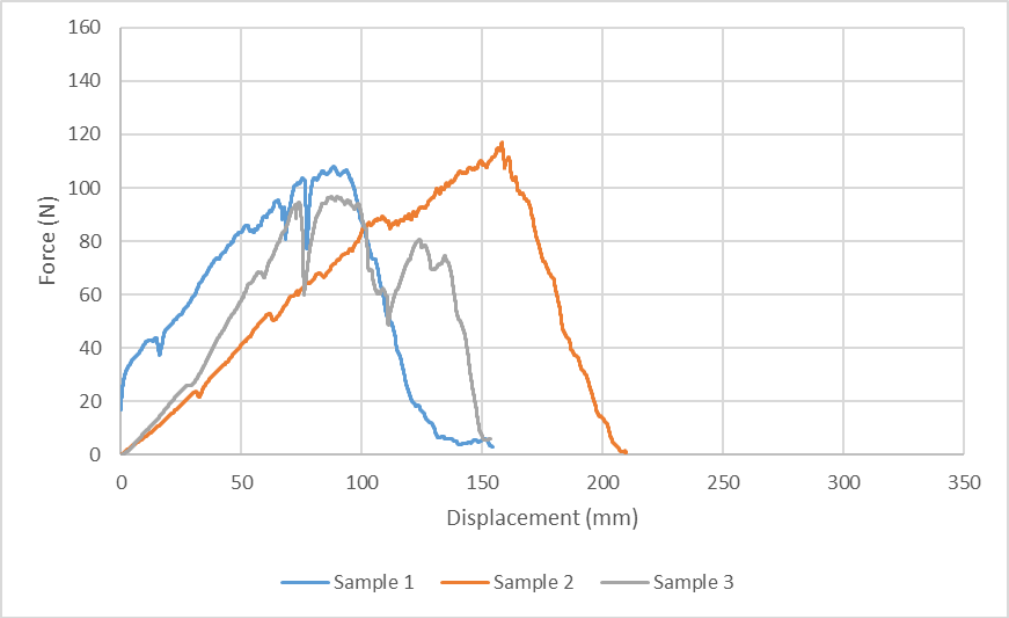

Figure 2.8 - Force-displacement graph for the three samples using the modified finger trap stitch.

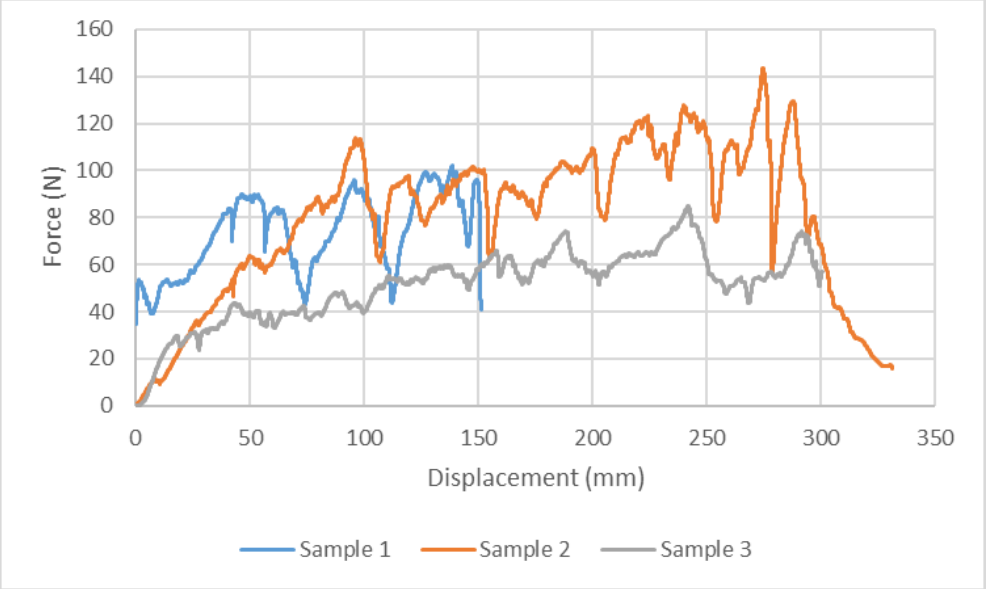

Figure 2.9 – Force-displacement graph for the three samples using the Krackow whip stitch.

The peak loads for the modified finger trap samples in Figure 2.8 were 96.9 N, 108.1 N and 117.0 N and for the Krackow whip stitch in Figure 2.9 were 102.1 N, 143.3 N and 85 N. The displacement of the tissue prior to failure for the Krackow whip stitch was higher than the displacement to failure for the modified finger trap stitch. The failure of the Krackow whip stitch method was gradual and underwent high displacement as each stitch pulled through the tissue as shown in Figure 2.10A-D. The pre-test sample is shown in Figure 2.10A, the subsequent images show the stitches pulling through the tissue, the corresponding peaks and troughs on the force-displacement graph for sample 2 are indicated.

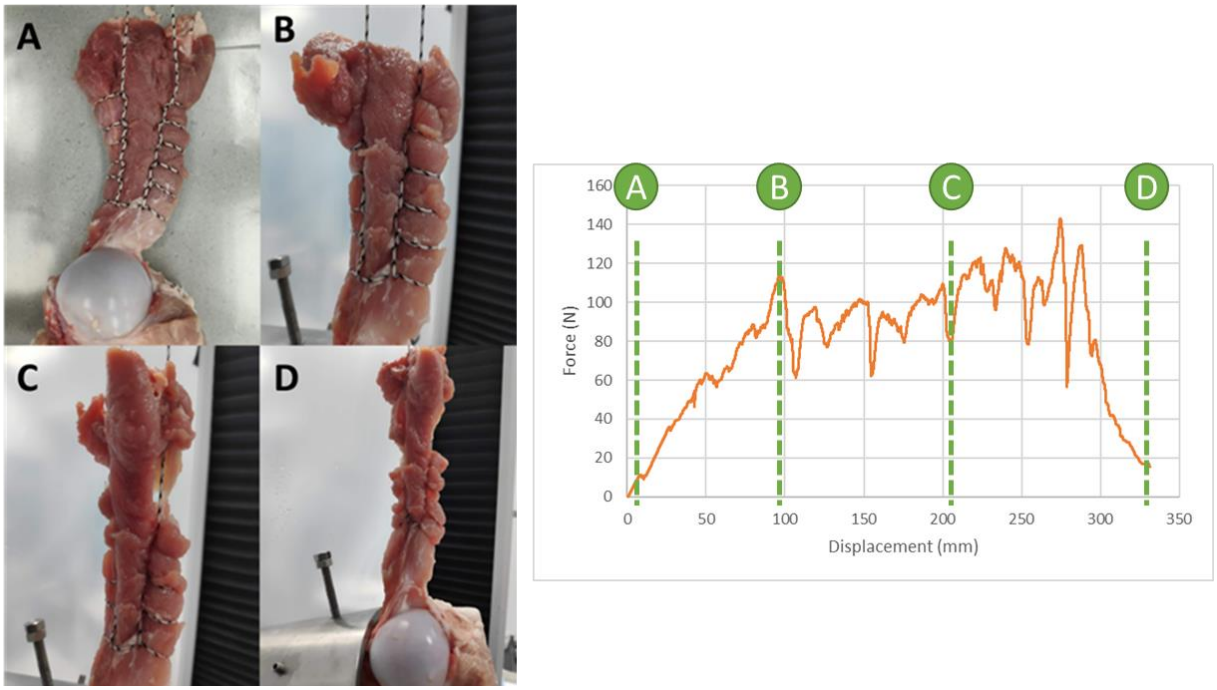

Figure 2.10 - The failure process of the Krackow whip stitch on sample 2. A: Pre-test sample prepared with the Krackow whip stitch. B: Tightening of the top stitches as force is applied. C: Progressive rupture of the tissue surrounding each stitch. D: Failure of the tissue. The displacement-force graph for sample 2 with the appropriate locations of images A-D is provided.

The failure process for the modified finger trap stitch was a faster event that occurred with less displacement when the suture material cut through the tissue leading to failure. The pre-test and post-test samples are shown in Figure 2.11.

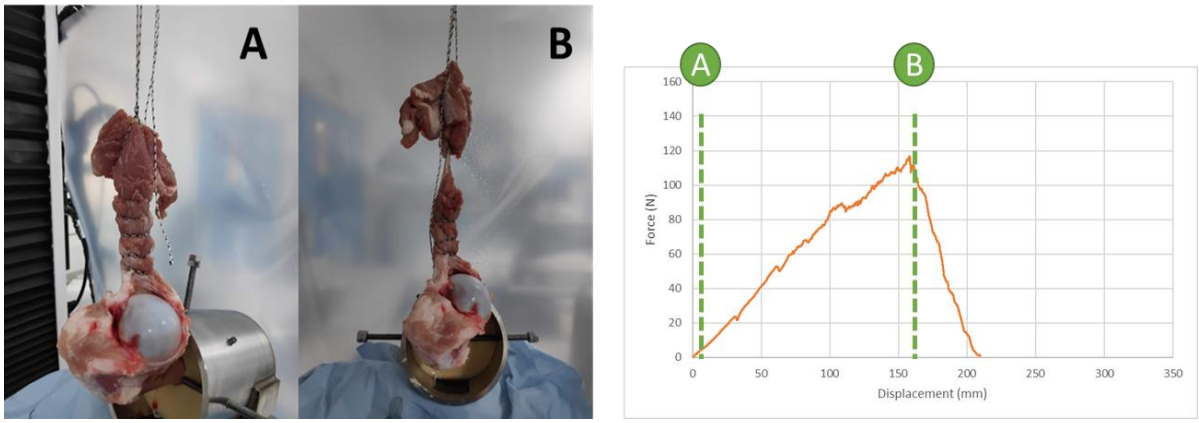

Figure 2.11 - The failure process for the modified finger trap stitch on sample 2. A: Pre-test sample, B: Sample at failure. The location on the force-displacement graph where the images were taken are indicated.

In both cases the tissue failed due to the concentrated load applied by the suture slicing through the muscle tissue. Therefore, it was determined that a method to increase the surface area of the gripping method would prevent the suture material from slicing the tissue and hence increase the maximum force able to be applied to the sample.

2.3.5 Further Method Development for Tendon Attachment

Following the results from the previous section where surgical suture techniques of the modified finger trap stitch and the Krackow whip stitch were used for tendon attachment, it was determined that a technique involving increasing the surface area of the gripping method may improve the success of the method. A wrapping technique using synthetic woven bandages and a finger trap technique were tested.

2.3.5.1 Wrapping Technique

In order to distribute the applied load over a larger surface area of the tendon and hence prevent the suture slicing through the tissue, a wrapping techniques was developed. Suture material was weaved through woven bandages as demonstrated in Figure 2.12A. This was then wrapped tightly around the muscle end and secured in place with alternating half hitch knots as shown in Figure 2.12B.

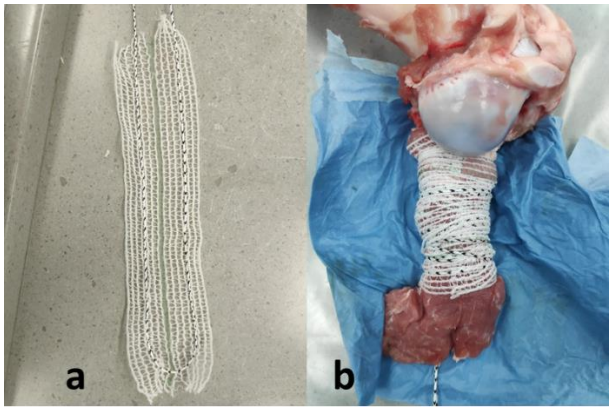

Figure 2.12 - Wrapping technique. A: Suture material weaved through woven material. B: The material and suture material wrapped tightly around the muscle end and secured with alternating half hitch knots.

The loose ends of the suture material were attached to the top bar of the Instron machine using alternating half hitches as described in Section 2.3.4.3. The samples were loaded at a ramp rate of 120 mm/min in accordance to previous studies, to a maximum of 450 N or failure (Mathewson et al., 2014). All mechanical tests were conducted at room temperature with PBS being sprayed onto the tissue regularly throughout the study to maintain the hydration of the tissue. Extension of the samples, failure mechanisms and failure loads were recorded and photographs were taken at regular intervals throughout the study.

Four samples were prepared and tested using the above method. The results from the four samples were plotted onto the same force-displacement graph as shown in Figure 2.13.

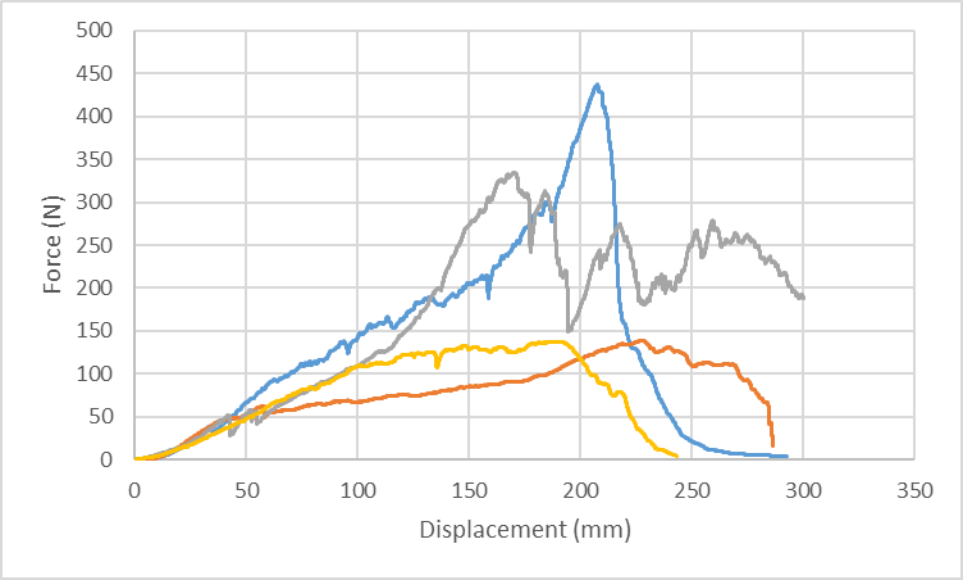

Figure 2.13 - Force-displacement graph for the four wrapped samples

It can be seen from Figure 2.13 that none of the samples reached the desired load of 450 N, with the maximum load reached by any of the samples being 440 N. The peak load reached was 436.9 N however there was a variation of 300 N between the maximum loads of the different samples.

The results from this study confirmed that by increasing the surface area to which the load was applied, the maximum load that could be applied to the tissue was increased as the maximum load achieved using this technique was 440 N however only a load of 143 N was achieved with the surgical techniques. A consistent and repeatable method for the application of a bandage wrap to the tissue was found to be very difficult due to the natural tissue variations despite the same muscle being used each time. These inconsistencies caused the wide range of results seen in Figure 2.13. A more consistent method which still enables the force to be spread over a larger surface area of the tissue was required.

2.3.5.2 Finger Trap Technique

Steinbrück et al (2013) used a metallic Chinese finger trap sutured to tendons of the knee muscles (Steinbrück et al., 2013). Therefore, this method was explored in order to provide a more repeatable method of distributing the applied load over a greater surface area of the tissue.

The samples were prepared as described in Section 2.3.4. The tissue ends were then fed into a finger trap and secured with suture material as shown in Figure 2.14.

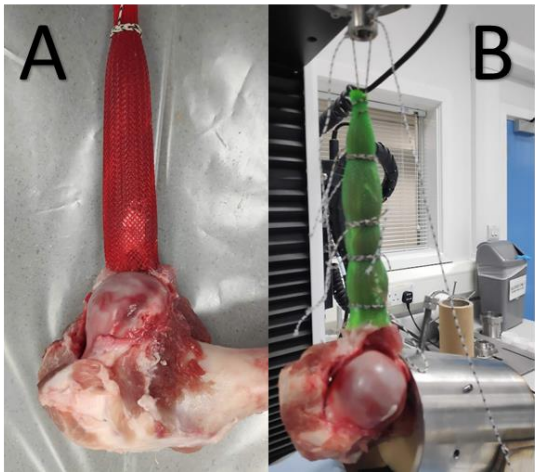

Figure 2.14 - Finger trap secured to the muscle end using sutures. (A) A finger trap tightly positioned over the tendon end. (B) The finger trap tightly positioned over the tendon end with the inclusion of four additional suture supports.

The loose ends of the suture material were attached to the top bar of the Instron machine using alternating half hitches as described in Section 2.3.4. The loading procedure was conducted as described in Section 2.3.4.3. Two samples were prepared as shown in Figure 2.14. Sample 1 shown in Figure 2.14A consisted of a finger trap tightly positioned over the muscle end. A single suture was placed at the tip of the muscle in order to secure the finger trap and allow for the connection to the top bar of the Instron. Sample 2, shown in Figure 2.14B, was prepared in the same way as sample 1 with the added inclusion of four additional suture supports. These suture supports were included in order to prevent the finger trap from slipping off the end of the tendon. The results from the two samples are plotted in Figure 2.15 on the same force-displacement graph.

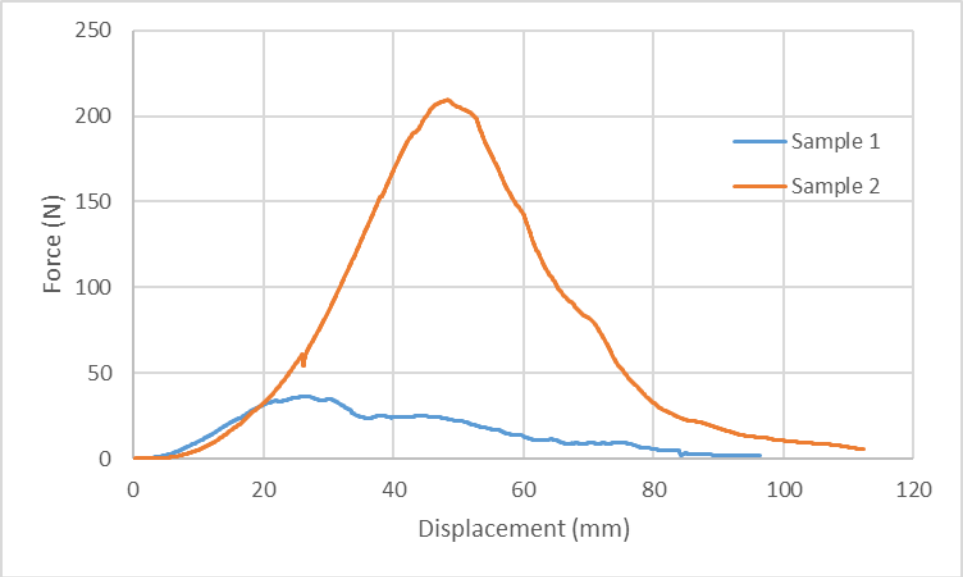

Figure 2.15 - The force-displacement graph for the two samples using finger traps.

The maximum force reached by the second sample was considerably higher than for the first sample: an increase of 180 N. In both cases the failure mechanism was the slippage of the finger trap against the moist surface of the muscle ends. The moisture content of the tissue was so high that when load was applied to the finger trap, the compression caused the moisture to collect on the tissue surface. The increased surface moisture content led to a decrease in friction between the two surfaces and hence the finger trap slipped off the tendon.

2.3.6 Dehydration Technique

Freezing the tissue within the area to be clamped is often deemed to be the gold standard method for clamping soft tissue as the shear between the inner and outer fibres is greatly reduced and so the tissue can be treated as a solid sample. In order to maintain the strength of the connection throughout testing, the sample must remain in a frozen state at all times (Jiang et al., 2020). Within a simulator environment, prolonged freezing of the tissue would be very difficult to achieve due to the space constraints and extended testing. Therefore an alternative method of dehydrating the tissue within the clamp was tested to determine if the same effect could be achieved.

The porcine tissue was prepared in line with the other experiments following the procedure described in Section 2.3.4. Calcium chloride ($CaCl_2$) powder was selected as the drying agent due to its availability and success during preliminary investigations. The calcium chloride powder was ground using a pestle and mortar to a fine powder. This powder was then spread evenly on all sides of the top 5 cm of the subscapularis tendon. The end of the tissue was then wrapped tightly in clingfilm. The remaining portion of the subscapularis tendon was wrapped in a tissue soaked with PBS solution and then wrapped in clingfilm. Three samples were

prepared following this procedure and were then placed into a cold room at 4°C for 24, 36 and 48 hours. The three time periods were selected in order to give a range of tissue dehydration in order to determine the optimum time for dehydration and if dehydration was a viable option.

A clamp, shown in Figure 2.16, was used in order to grip the dehydrated surface of the tissue. The securing screws were placed both sides of the serrated gripping surface in order to keep the gripping surfaces parallel to each other and to ensure the grip could be tightened evenly. The clamp was attached to the top of the Instron machine and the loading procedure was conducted as described in Section 2.3.4.

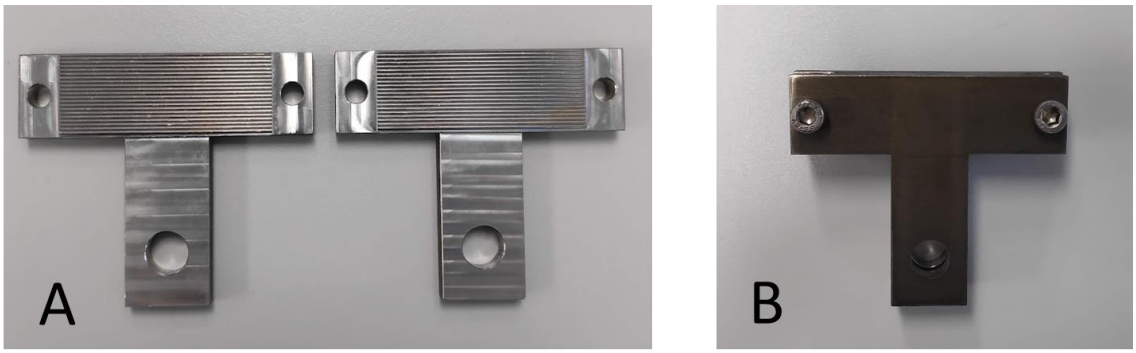

Figure 2.16 - The clamp used to grip the dehydrated surface of the porcine subscapularis tissue. (A) Ridged inner surface of the clamp. (B) Clamp assembled.

In all cases the tissue tore at the interface between the dry and wet tissue as indicated in Figure 2.17. The maximum force applied to the tissue before this rupture occurred in the sample that was dried for 24 hours and was 120 N. The samples dried for 36 and 48 hours reached lower loads of 87 N and 62 N respectively.

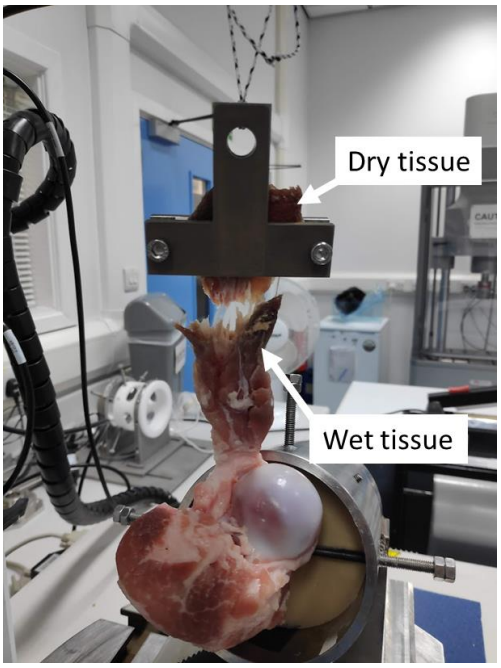

Figure 2.17 - The failure of the tissue occurred in the region between the dry and wet portions of the tissue in all three samples

The dehydration method was found to introduce a weakness into the tissue at the junction between the wet and the dry portions of tissue. When cryoclamps are used on tissue there is a gradual temperature gradient within the tissue from the frozen tissue at the clamps to a natural temperature. However, the change was much more abrupt with the dehydration technique due to the importance of keeping the main body of the tendon hydrated in order to maintain the mechanical properties during testing. Alongside this, the length of time that was required in order for the tissue to undergo the dehydration process would complicate the set up procedure for the testing using the natural tissue simulator. Therefore, due to the se two reasons, it was concluded that the dehydration of the tissue was unnecessary and did not improve the clamping of the tissue.

2.3.7 Discussion

Based upon the list of requirements detailed in Table 2.1, the original suturing technique was deemed to be the most suitable attachment method. None of the methods tested were able to withstand the loads of 450 N originally required. These loads were determined based upon a computational model of the human shoulder joint during the motion of flexion to an angle of 100°. The structure of the rotator cuff muscles and tendons vary largely between the porcine and the human shoulder joint as detailed in Section 2.2. A significant limitation of this testing was that assessing an attachment method on the porcine rotator cuff did not provide for accurate translations to the human set up due to these differences in tissue structure. The suture techniques, particularly the modified finger trap, were lightweight, small and compact

which would provide little interference with the tissues during simulation of the joint. The modified finger trap stitch was also the most repeatable of all the attachment methods and would be able to be performed on all the actuated tendons of the shoulder regardless of size or shape. Therefore it was selected that the modified finger trap suture technique would be used during the experimental simulation and additional measures may be included if it did not meet the requirements once tested on the human shoulder tissue.

2.4 Summary

The suitability of the porcine joint as a surrogate model for the human shoulder was assessed through the dissection of a joint and a visual inspection of the anatomical differences. It was determined that despite the advantages of being freely available within the food chain, the anatomical differences between the porcine and human joint meant that the porcine joint could not be used as a direct surrogate for the human joint. The lack of a suitable supraspinatus tendon and the extended greater tuberosity of the porcine humerus resulted in a considerably limited range of motion achievable at the joint and a limited ability to perform clinically relevant tests with the porcine joint. Consequently, the method development process would be undertook with the porcine joint before being translated to human tissue.

The second objective of this study was to determine an appropriate method of loading tendons of the porcine joint to allow for application of force within the simulator. The modified finger trap suture technique was concluded to be the most appropriate technique as it was lightweight and compact providing little interference to the natural tissues during simulation. It was also a repeatable attachment method which could be performed on tendons of all shapes and sizes. None of the techniques were able to withstand the loads of 450 N which were obtained through a computational model of the human joint and were considerably higher than forces that these muscles would undergo in the porcine shoulder. The structural differences between the human and porcine joint were not accounted for in these calculations and hence it was decided to go forward with the most reliable method, the modified finger trap stitch to test with the human joint.

Chapter 3 – The Development of a Musculoskeletal Computational Model of the Human and Porcine Shoulder Joint.

3.1 Introduction and Aims

An experimental natural joint simulator enables the whole natural joint to be tested through a consistent range of motion and loading cycles. For a simulator to be truly representative of the unstable natural shoulder environment, the muscles of the shoulder must be loaded to replicate the loads seen in vivo during shoulder motion. To produce these loading cycles for the shoulder muscles, the internal muscle forces for the primary muscles associated with shoulder motion must be determined. A computational model of the shoulder joint will be created to calculate the internal muscle forces of the muscles of the shoulder complex during a range of common motions of the shoulder. The force values obtained through this study will then be used to determine the forces required in a natural shoulder simulator to replicate the force experienced in the in vivo rotator cuff muscles. The objectives of the computational model study are outlined below.

1. To develop a multibody model of the human shoulder complex that can simulate the motions of abduction, flexion and internal rotation.

2. To identify the significant muscles that must be included in a natural shoulder simulator, and the corresponding forces required to perform each motion.

3. To assess the effect of simplifying the complex shoulder joint in order to produce a physical natural shoulder joint simulator.

4. To develop a similar multibody model of the porcine shoulder joint to enable the development of a preliminary porcine shoulder joint simulator

3.2 Methods

3.2.1 Overview

The AnyBody modelling system (AnyBody 7.4, Denmark) was used to model the natural human shoulder joint. The AnyBody modelling system uses an inverse dynamics approach, with inputs of desired motion and external forces used to calculate the internal muscle forces. The musculoskeletal system as a whole is mechanically redundant; meaning that there are a greater number of muscles in the body than are necessary to perform most motions (Rasmussen, 2003). Hence in the human body, the central nervous system instantly selects the

required muscle to perform each motion to limit the overall energy required (Pandy, 2001). The AnyBody modelling system includes optimisation theory which uses a combination of linear and quadratic equations to select the muscles which minimise the muscle fatigue caused by the motion (Rasmussen, 2003) as discussed in Section 1.3.

3.2.2 Repository Model

The AnyBody Managed Model Repository (AMMR) is an open-source collection of generic human body models which can be adapted to perform specific motions (AnyBody, 2024). The generic shoulder model was assessed as an option to be adapted for use within the project. With adaptions, the model was able to complete the abduction motion cycle (0° - 90°), however the results that were provided by the model were unexpected in relation to the literature. Lam and Bordoni (2021) state that the supraspinatus muscle is required for the initiation of abduction from 0° to 15°, the deltoid muscle then takes over as primary mover until 90° abduction (Lam and Bordoni, 2021). The results from the adapted repository model, given in Figure 3.1, did not align with the literature as the supraspinatus muscle did not take a key part in the abduction of the shoulder. The supraspinatus muscle (indicated by the light orange line in Figure 3.1) produces a maximum of 32.5N at an angle of 47° however according to literature the supraspinatus muscle is most important during the early stages of abduction from 0° to 15°.

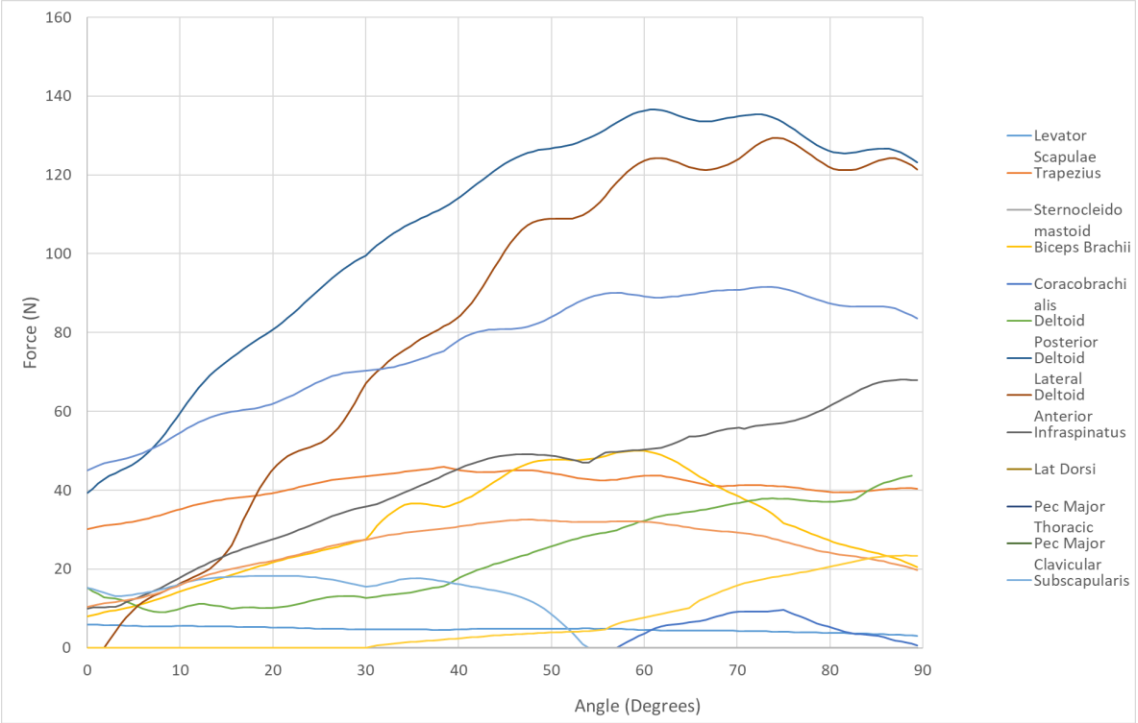

Figure 3.1 - Force results from the adapted repository AnyBody model with the motion of 0° - 90° abduction. The muscles with the largest magnitude of force are the lateral and anterior deltoid and the trapezius muscles.

The repository models have inputs and constraints that are specific to a single use of the model and hence do not provide universally accurate results. It was decided that a test-specific model would be developed to represent the desired shoulder simulator model to ensure that the results for the motion cycles to be used within the simulator correspond to literature.

3.2.3 Input Parameters

A novel model was created containing rigid body segments to represent four of the bones of the shoulder complex: the humerus, scapula, clavicle and spine. The inputs required to construct these segments were mass, position and the moment of inertia of the corresponding bone. Available anthropometric data, including the mass and moment of inertia for the individual bones, was limited (Veeger et al., 1991). Many studies recorded the mass and moment of inertia for large segments of the body such as the trunk and upper arm, however there was found to be a lack of literature that split the trunk into its constituent bones. Maurel et al (1996) provided mass and moment of inertia data of the humerus for a range of cadavers with a mean age of 80 years (data shown in Table 3.1). Due to the high ages of the subjects, the mass of the segments is likely to be less than that of a population with a lower mean age as the density of the bones decreases with increasing age, particularly over the age of 50 (Wishart

et al., 1995). However, due to the limitations in the literature, anthropometric data for a lower age range was not available.

Table 3.1 – Anthropometric data for the humerus (Maurel et al., 1996). *I_{xx} = Moment of inertia in the x direction, I_{yy} = Moment of inertia in the y direction and I_{zz} = Moment of inertia along the z direction.*

Mass (Kg)	1.8
I_{xx}(Kg.m^2)	0.0023
I_{yy}(Kg.m^2)	0.011
I_{zz}(Kg.m^2)	0.011

The anthropometric data was used to construct the humerus in the modelling software. The moment of inertia was approximated for the other segments such that the segment sizes and shape were in line with those for the humerus.

Four joints were created to allow for motion of the computational shoulder joint. Two static joints ensured that the mechanism was held stationary to the origin during the simulation. The glenohumeral joint and scapulothoracic joint had the same centre of rotation being at the superior end of the humerus and the lateral portion of the scapula. The resultant model is shown in Figure 3.2 with the four bones labelled.

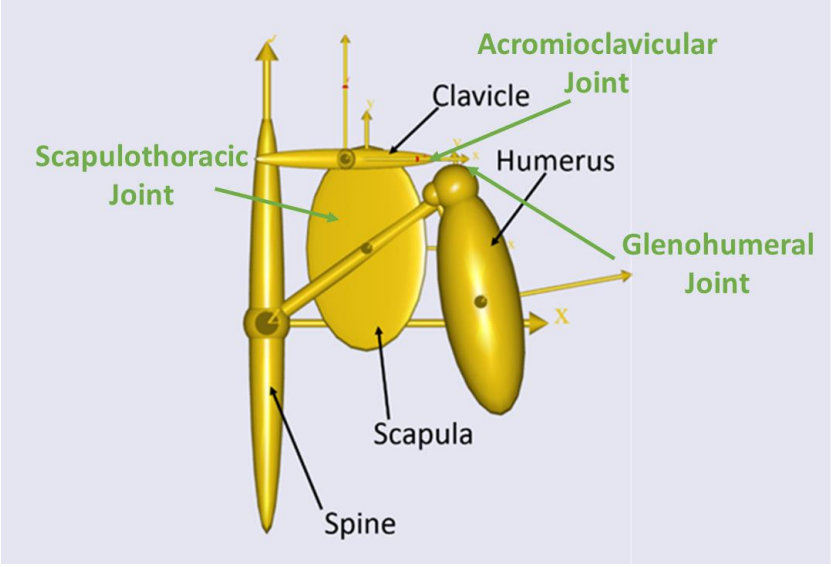

Figure 3.2 - AnyBody model of the four bones of the left shoulder joint. The humerus, clavicle, scapula and spine are labelled in black. The joints of the shoulder model are labelled in green.

Muscles were then added to the model to create the model shown in Figure 3.3. Most muscles of the shoulder complex originate over a large area, tapering towards a single insertion point.

In order for this to be modelled within the AnyBody software, several muscle strands are created with the same insertion points but several origins as seen in Figure 3.3. Consequently, a total of 59 muscle strands were created to represent twelve muscles of the shoulder joint. Each strand acts as an independent muscle and therefore simultaneous activation of all strands of a given muscle was unlikely to occur through the inputted motions. This was similar to the way the central nervous system activates a specific portion of the larger muscles required for motion (Lumen Learning, 2024).

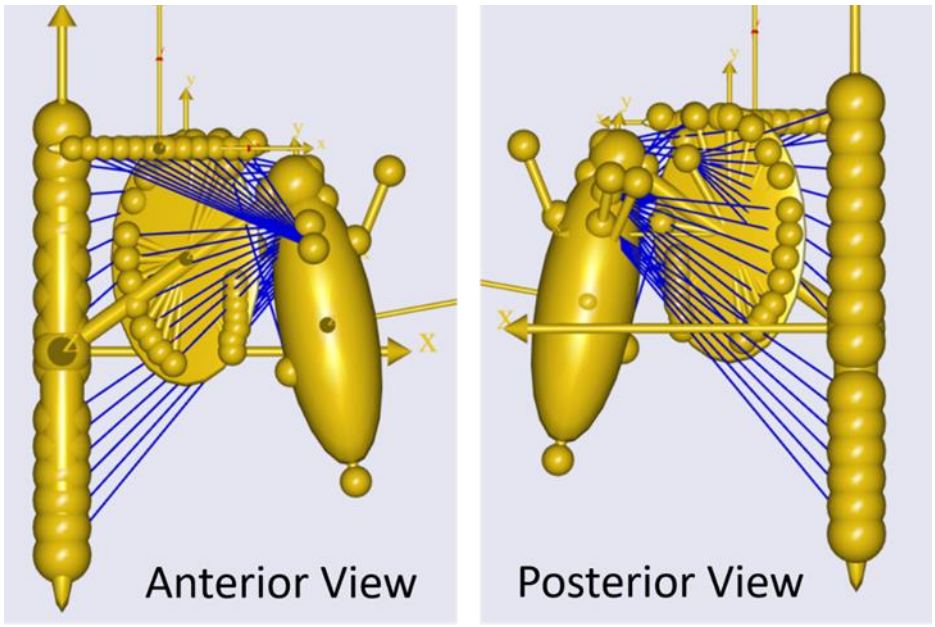

Figure 3.3 - Anterior and posterior views of a model of the human shoulder in the AnyBody modelling system.

The inputs required to model the muscles of the shoulder joint were the maximum force output of the muscle (F0), length of a muscle fibre (Lf0) and the volume of the muscle fibres (Vol0). Equations 3.1 and 3.2 show the relationship between these values and the physiological cross sectional area (PCSA) and a constant K (AnyBody Technology, 2021).

$$PCSA = \frac{Vol0}{Lf0} \quad [3.1]$$

$$F0 = k \times PCSA \quad [3.2]$$

The relationship between PCSA and maximum force in the shoulder muscles was determined to be 0.7 MNm^{-2} (Favre et al., 2005). Peterson and Rayan (2011) measured the cross-sectional area and fibre length of the shoulder muscles from five cadavers with an average age of 73 years. Where more than one muscle strand is used in the model to represent a single muscle unit, the maximum output force and the volume was divided by the number of individual muscle strands. The inputs to the muscles within the model are detailed in Table 3.2.

Table 3.2 - Muscle inputs to the shoulder model (Peterson and Rayan, 2011). *Physiological cross sectional area (PCSA), rest length of muscle fibre (Lf0), rest muscle volume (Vol0) and maximum muscle force (F0).*

Muscle	PCSA (m^2)	Lf0 (m)	Vol0 (m^2)	F0 (N)	Number of muscle strands	Vol0 (m^2) per muscle strand	F0 (N) per musde strand
Supraspinatus	0.000248	0.117	$2.902x10^{-5}$	173.6	4	$7.26x10^{-6}$	43.4
Infraspinatus	0.000589	0.124	$7.31x10^{-5}$	412.3	8	$9.14x10^{-6}$	51.5
Teres Minor	0.000126	0.085	$1.07x10^{-5}$	88.2	4	$2.68x10^{-6}$	22.1
Pectoralis Major	0.000405	0.193	$7.82x10^{-5}$	283.5	5	$1.56x10^{-5}$	56.7
Latissimus Dorsi	0.000399	0.255	$1.02x10^{-4}$	279.3	6	$1.7x10^{-5}$	46.6
Teres Major	0.000298	0.126	$3.75x10^{-5}$	208.6	3	$1.17x10^{-5}$	69.5
Anterior Deltoid	0.000254	0.144	$3.66x10^{-5}$	177.8	1	$3.66x10^{-5}$	177.8
Middle Deltoid	0.001118	0.055	$6.15x10^{-5}$	782.6	1	$6.15x10^{-5}$	782.6
Posterior Deltoid	0.000273	0.178	$4.86x10^{-5}$	191.1	1	$4.86x10^{-5}$	191.1
Biceps	0.000349	0.125	$4.36x10^{-5}$	244.3	1	$4.36x10^{-5}$	244.3
Triceps	0.00156	0.0827	$1.29x10^{-4}$	1092	1	$1.29x10^{-4}$	1092
Coracobrachialis	0.000241	0.0600	$1.45x10^{-5}$	168.7	1	$1.45x10^{-5}$	168.7

The AnyBody modelling software does not restrict the muscles from penetrating the rigid body segments meaning that the muscles take the shortest path from the origin to the insertion points. A series of rigid cylinders were therefore created throughout the segments of the model to create solid structures which the muscles could not penetrate and hence had to slide over (AnyBody Technology, 2024). This ensured that the muscles were appropriate lengths and the lines of action of the muscles were more representative of the physiology of the human shoulder. The cylinders of the humerus, which are not normally visible in the model, are shown in Figure 3.4.

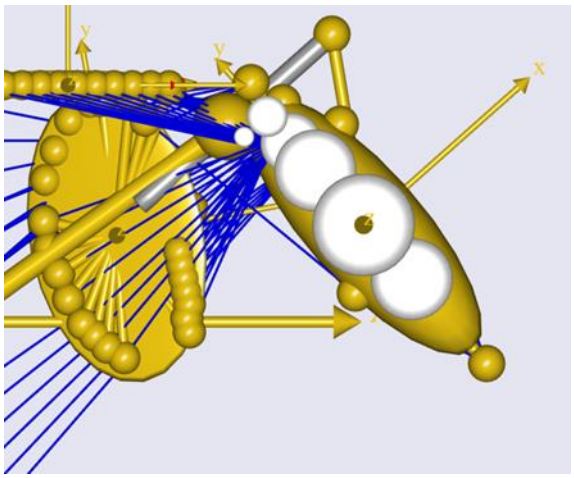

Figure 3.4 - AnyBody model showing the cylinders located within the humerus to ensure that the muscles do not penetrate the bone (anterior view).

The origin and insertion point of the muscles were approximated based upon anatomical diagrams of the location of these points in the human shoulder joint. The limited inputs available to create the bone segments lead to a large disparity between the geometrical shapes of the solid segments produced in the model and the geometry of the bones in anatomical diagrams. Hence, approximations had to be made regarding the location of the origin and insertion points of the muscles within the model.

3.2.4 Motion

Activities of daily living are a collection of activities such as eating, bathing, dressing and mobility activities that are used to determine a patient's ability to live independently. The shoulder joint plays a key role in many of these activities with a loss in its function proving detrimental to the independence of a patient (Edemekong et al., 2020). Abduction, flexion and internal rotation are the most commonly used motions required for the activities of daily living as described in Section 1.2.2.

The AnyBody model was used to simulate the abduction of the arm from 0° to 150°. During the first 30° of abduction the majority of the motion occurred in the glenohumeral joint. Following this the ratio between motion in the glenohumeral joint and motion in the scapulohumeral joint is 2:1 (Felstead and Ricketts, 2017). Therefore, the first 30° of abduction occurred entirely in the glenohumeral joint. For the remaining 120° of motion a ratio of 2:1 meant that 40° occurred in the scapulothoracic joint and 80° in the glenohumeral joint. Overall, for the 150° of abduction at the shoulder, the glenohumeral joint provided 110° and 40° was provided by the scapulothoracic joint. Due to limitations within the modelling software the 40° of scapulothoracic motion was applied throughout the whole range of glenohumeral abduction rather than initiating at 30° of glenohumeral abduction. Flexion of

100° in the sagittal plane and internal rotation of 70° were also performed separately by the model.

3.2.5 Sensitivity Study

Limitations exist within the model, particularly with regards to the inputs required to construct the bony geometry. Due to the simplistic geometries that were created within the software, locations of the origin and insertion points of the muscles had to be estimated. A sensitivity study was carried out to assess the impact of altering the origin location of the muscles. The deltoid muscle was selected as it plays a key role in all the motions simulated by the model (abduction, flexion and internal rotation). The origin location of the anterior deltoid was translated by 1mm in the x, y and z directions independently and then translated by 1mm in all three directions simultaneously. For each case the internal muscle force of the anterior deltoid was recorded throughout the range of motion.

The centre of rotation of the glenohumeral joint also had been estimated based upon the relevant geometries of the segments alongside literature. A second sensitivity study was carried out to investigate the effect of the position of the glenohumeral centre of rotation on the forces required within the whole deltoid (anterior, middle and posterior) muscle. The deltoid was selected, as with the previous study, because it provided significant force throughout all three motions. The centre of rotation was moved by 5mm in the x, y and z directions before being translated by 5mm in all directions simultaneously. Again, the internal muscle force of the deltoid was recorded for each case through the motions of abduction, flexion and internal rotation.

3.2.6 Effects of the Scapulohumeral Rhythm

Scapulohumeral rhythm refers to the coordinated motion between the glenohumeral and scapulothoracic joints (Lugo et al., 2008). It is required to maintain the contact area between the humeral head and glenoid fossa throughout abduction, to prevent impingement of the humeral head and to maintain the length and hence power output of the deltoid muscle (Lucas, 1973). In Section 1.4.3.2 it was shown that no current natural shoulder simulators account for the scapulohumeral rhythm due to the difficulty of including this motion. However, a computational study, using the AnyBody modelling system, concluded that the scapulohumeral rhythm had a significant impact on the forces within the joint due to the changing muscle moment arms and lengths through the motion (Flores-hernandez et al., 2019).

A study was conducted to determine the effect of the removal of the scapulohumeral rhythm on the internal muscle forces through the motion of abduction. The model was adapted such

that the glenohumeral joint produced the whole 150° of abduction whilst the scapulothoracic joint remained static. The internal muscle forces for each muscle was recorded through the motion.

3.3 Results

3.3.1 Overview

A model of the human shoulder was developed using the AnyBody modelling system that could calculate the internal muscle forces through the motions of abduction, flexion and internal rotation of the shoulder. The impact of translating the origin positions of the muscles was investigated alongside the impact of translating the centre of rotation of the glenohumeral joint and the removal of the scapulohumeral rhythm.

3.3.2 Abduction Model

The abduction model was used to simulate abduction from 0° to 150° with 110° of motion in the glenohumeral joint and 40° of motion in the scapulothoracic joint as detailed in Section 3.2.3. The only external force on the model was gravity. The graph of internal muscle force against the angle of abduction for each muscle group in the model is shown in Figure 3.5, the muscles which are providing the most force are labelled.

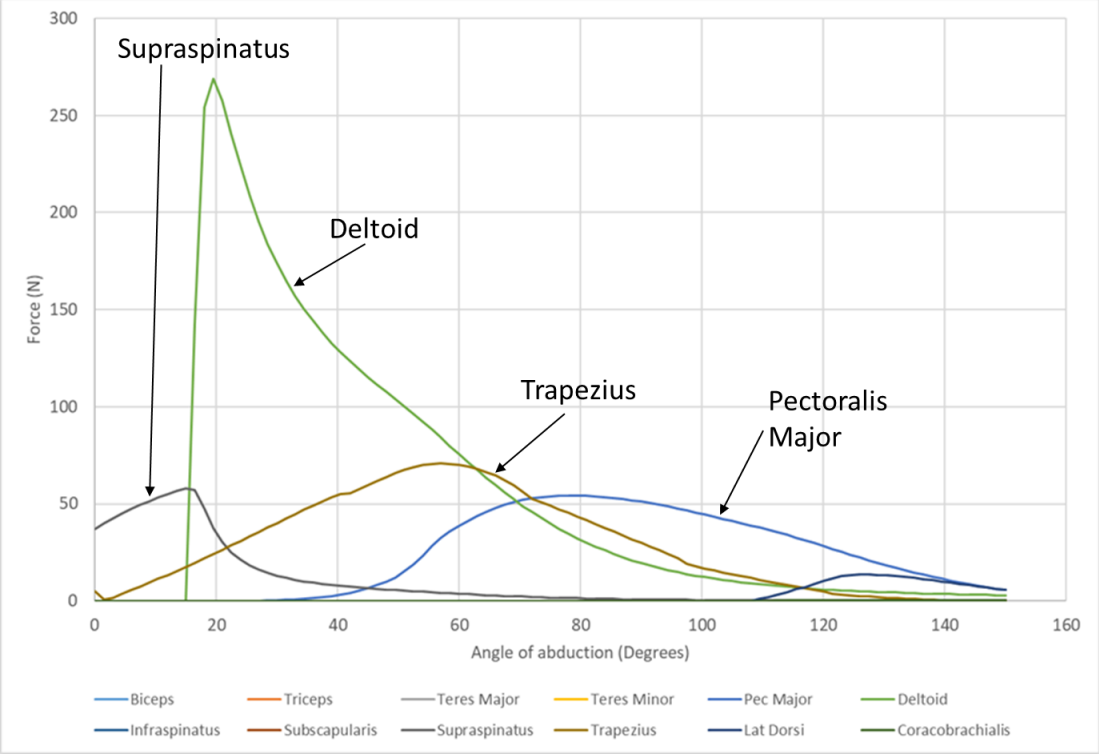

Figure 3.5 - The internal muscle forces through 150° of abduction of the shoulder joint. The key muscles are labelled.

At the beginning of the motion, the supraspinatus muscle provided 88% of all the force and so was instrumental in initiating the motion of abduction. After 16° the deltoid muscle took over producing 65% of the force required, with the supraspinatus and trapezius muscles producing the remaining force. From around 80° of abduction, the muscles producing the largest forces were the trapezius, pectoralis major and coracobrachialis which were key to the rotation of the scapulothoracic joint.

3.3.3 Flexion Model

The flexion model simulated flexion of the shoulder from 0° to 100° in the sagittal plane. No scapulothoracic motion occurred during this motion so it was completed entirely in the glenohumeral joint. The graph of the force required in each muscle against the angle of flexion is provided in Figure 3.6.

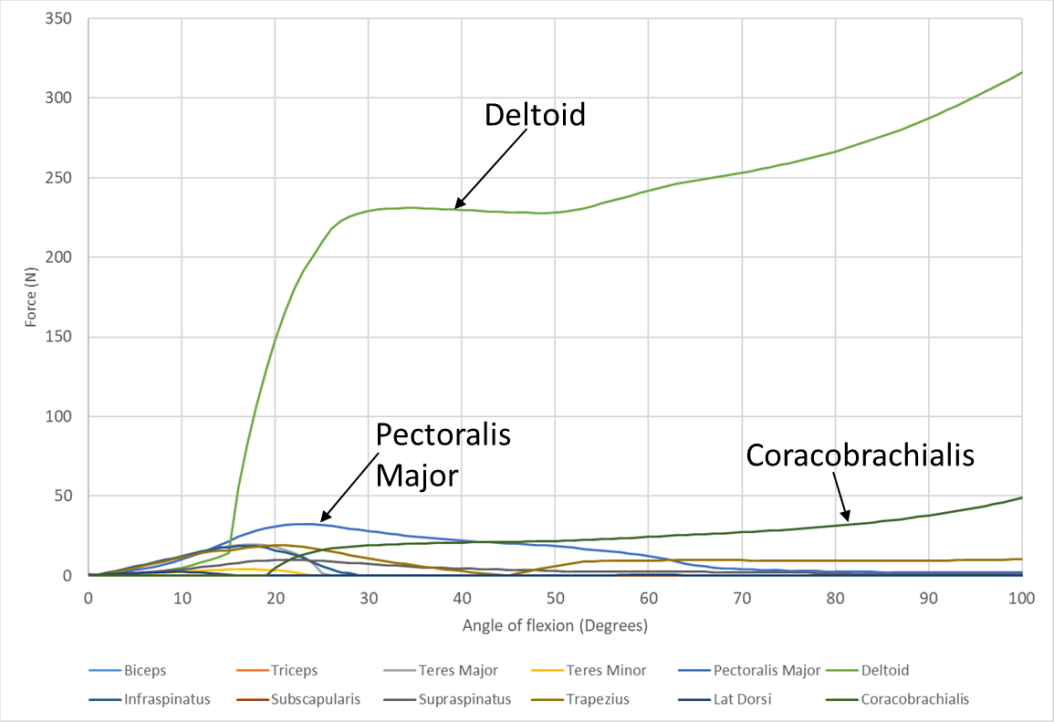

Figure 3.6 - Muscle forces through 100° of shoulder flexion. The key muscles of deltoid, pectoralis major and coracobrachialis are labelled.

The key muscles required for flexion of the shoulder joint are shown in Figure 3.6 to be the deltoid, in particular the anterior deltoid, the coracobrachialis and the pectoralis major muscles. The anterior deltoid provided the majority of the force required reaching a peak of 320 N at 100° of flexion where the deltoid produced 83% of all the force required in the joint.

3.3.4 Internal Rotation Model

The rotation model performed internal rotation of 70 ° at the glenohumeral joint. The graph of the internal force required in each muscle against the angle of internal rotation is provided in Figure 3.7. The key muscles required for internal rotation were shown, using the AnyBody model, to be the latissimus dorsi, pectoralis major, infraspinatus and subscapularis muscles. However, the force in all the muscles is considerably lower than the forces required for the abduction and flexion motions.

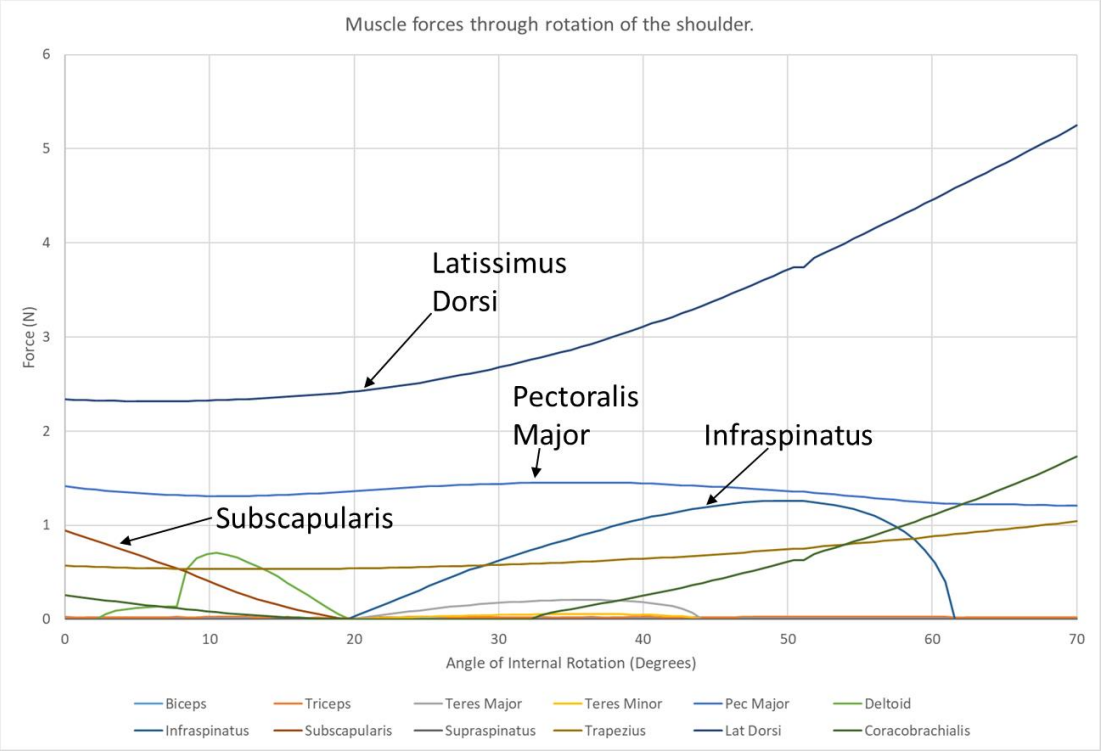

Figure 3.7 - Muscle forces through 70 ° of internal rotation of the shoulder. They key muscles of latissimus dorsi, pectoralis major, infraspinatus and subscapularis are labelled.

3.3.5 Sensitivity Study

The origin location of the anterior deltoid was moved by 1mm in the x, y and z directions before being translated by 1mm in all three directions at the same time. The percentage change in maximum anterior deltoid force is provided in Table 3.3 for abduction, flexion and internal rotation.

Table 3.3 - Percentage change in the maximum force required in the anterior deltoid though abduction, flexion and internal rotation when the origin location was translated in the x, y and z directions.

		Abduction	Flexion	Internal Rotation
Normal maximum force (N)		218	258	0.32
Percentage change in maximum force	+1mm in x	1 %	0 %	-2 %
	+1mm in y	2 %	0 %	0 %
	+1mm in z	0 %	1 %	8 %
	+1mm in x, y and z	2 %	1 %	8 %

A second sensitivity study was carried out to investigate the effect of the position of the centre of rotation of the glenohumeral joint on the deltoid muscle forces. The centre of rotation was moved by 5mm in the x, y and z directions and also all three directions simultaneously. The graph of the effect of translation of the centre of rotation on the internal deltoid force through abduction is shown in Figure 3.8.

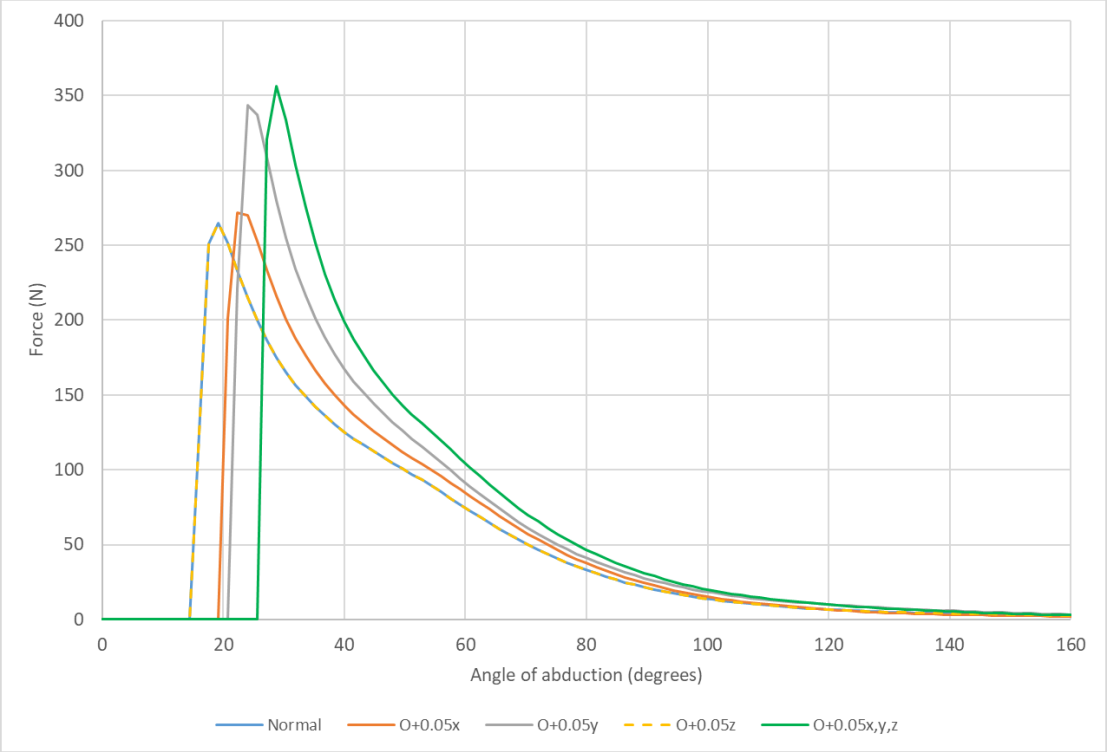

Figure 3.8 - Graph of the internal deltoid force required through 160° of abduction of the shoulder with the centre of rotation translated by 5mm in the x, y and z directions.

3.3.6 Scapulohumeral Rhythm

Scapulohumeral rhythm refers to the coordinated motion in the glenohumeral and scapulothoracic joints (Lugo et al., 2008). The impact of the removal of the scapulohumeral rhythm on the internal muscle forces at the joint was assessed to determine the importance of keeping this motion in an experimental shoulder simulator. The model was adapted such that the scapulothoracic joint remained static through the motion whilst the glenohumeral joint performed the whole 150° of abduction. The results from this model are shown in Figure 3.9 with the muscles providing the most force labelled.

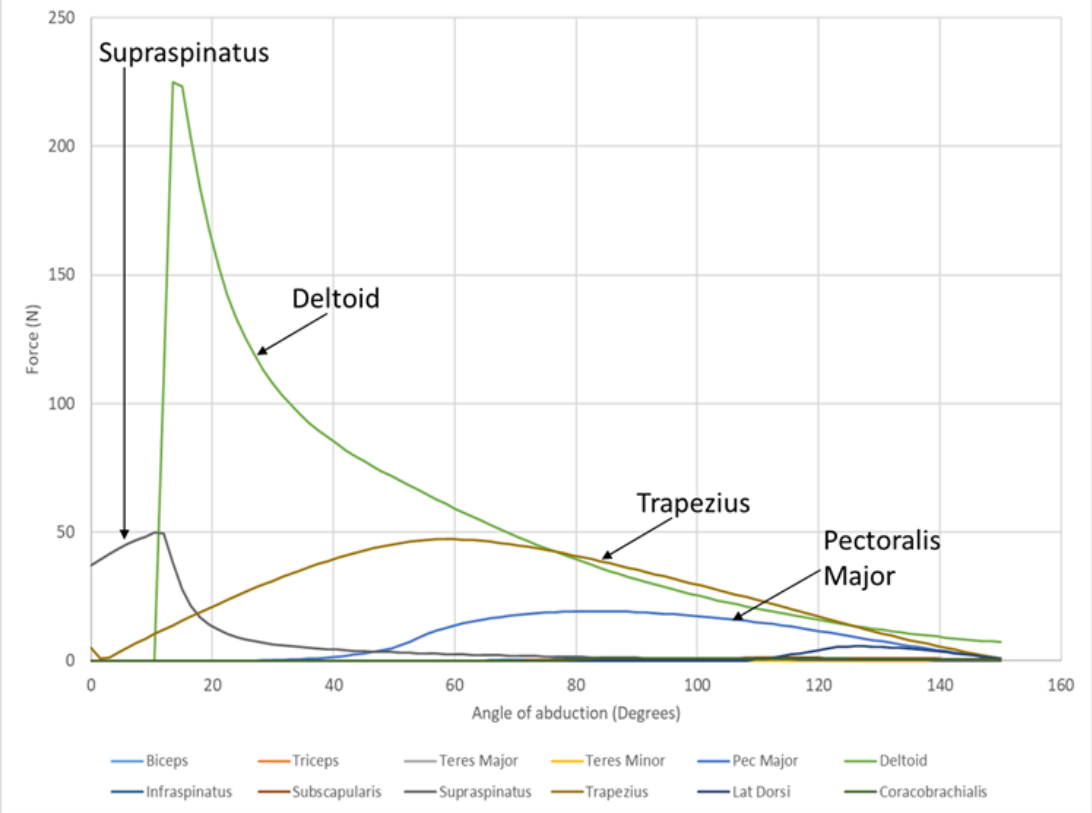

Figure 3.9 - The effect of removing the scapulohumeral rhythm on the internal muscle forces through abduction of the shoulder.

3.4 Discussion

3.4.1 Overview

The aims of this study were to determine the suitability of a computational model to provide the internal muscle forces required by an experimental natural shoulder simulator. The model was assessed using sensitivity studies looking at the effect of translating the origin locations and centre of rotation of the glenohumeral joint. The computational model was also used to determine the effect of removing the scapulohumeral rhythm during the motion of abduction.

3.4.2 Abduction Model

The results from the abduction model align well with data from literature regarding the muscles required for this motions. The graph of internal muscle force s against the angle of abduction is shown in Figure 3.4. Lam and Bordoni (2021) state that the primary muscle required for the initiation of abduction of the shoulder from 0 ° to 15 ° was the supraspinatus muscle. The deltoid then becomes primary mover until 90 ° where the motion of the scapula increases in importance (Lam and Bordoni, 2021; Maruvada et al., 2021). This supports the results obtained by the abduction model as the deltoid takes over from the supraspinatus as primary mover at 16 ° of abduction. From 80 ° of abduction, the key muscles are those which cause the rotation of the scapulothoracic joint; trapezius, pectoralis major and the coracobrachialis.

There are several computational models of the human shoulder joint through the motion of abduction in literature. A finite element model of the shoulder was made by van Der Helm (1994) which modelled abduction of the shoulder to 180°. The results from that model for the anterior and middle deltoid and the supraspinatus muscle are given in Figure 3.10. In this model the supraspinatus muscle provided very limited force throughout the whole range of motion whereas the middle deltoid produced very high levels of force throughout including during the initiation of the motion.

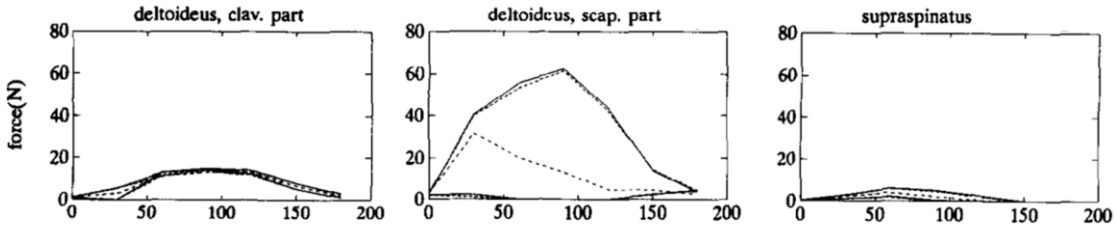

Figure 3.10 - The results from a finite element model of the shoulder which modelled abduction of the human shoulder to 180°. The results of the anterior and middle deltoid and the supraspinatus muscles are given (van der Helm, 1994a). This image is reproduced with permission

Another computational model of the human shoulder joint was made by Karlsson and Peterson (1992) which modelled the motion of abduction. The results for the anterior and middle deltoid, supraspinatus and infraspinatus are provided in Figure 3.11. The results from this model were contrasting to the model by van Der Helm (1994) as the deltoid muscle did not produce significant force until 50° of abduction. Due to issues with data presentation, it is unclear whether the infraspinatus or supraspinatus muscle produces maximum force at the beginning of the cycle however they both work to initiate the abduction motion.

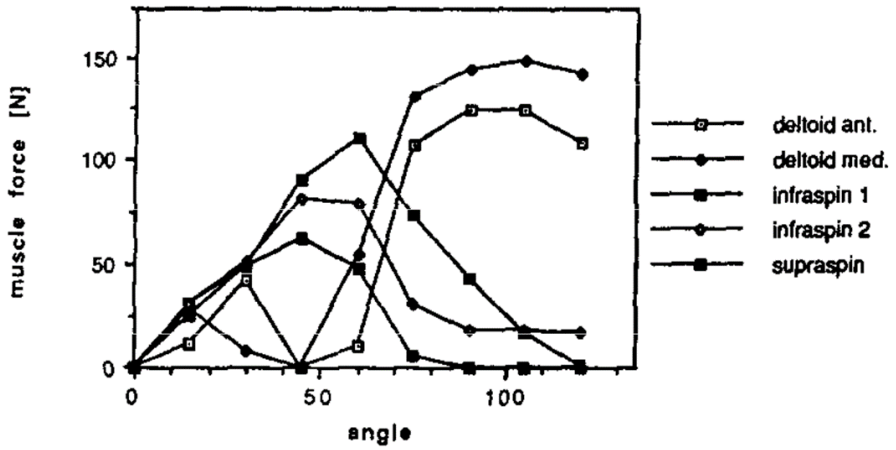

Figure 3.11 - Muscle forces in the anterior and middle deltoid, infraspinatus and supraspinatus muscles during abduction of the human shoulder in a computational model (Karlsson and Peterson, 1992). Image reproduced with permission.

The two computational models from literature presented in this section have very contrasting results regarding the initiator of abduction and the role that the supraspinatus and deltoid muscles have in the motion. The AnyBody model of the shoulder described in this Chapter provided results that agreed with literature regarding the initiating muscles of the abduction motion and the angle at which the deltoid muscle became the prime mover hence was deemed to be suitable for the development of the simulator.

3.4.3 Flexion Model

The results from the flexion model provided in Figure 3.6 are also supported by literature. The key muscles required by the AnyBody model for flexion were the anterior deltoid, coracobrachialis and the pectoralis major muscles. At 100° of flexion, the anterior deltoid provided the peak internal force reaching 320 N. Jones (2021) stated that the primary muscles required for flexion of the shoulder were the pectoralis major, coracobrachialis and anterior deltoid (Jones, 2021).

3.4.4 Internal Rotation Model

The rotation model also provided results that were supported by literature. The results from the internal rotation model were provided in Figure 3.7. The key muscles were shown, using the computational model, to be the latissimus dorsi, pectoralis major, infraspinatus and the subscapularis muscles. Jones (2021) stated that the pectoralis major, latissimus dorsi and subscapularis muscles were the key muscles required for internal rotation of the shoulder.

3.4.5 Sensitivity Study

Limitations exist within the model in regard to the inputs required to construct the bone geometries. A sensitivity study was carried out to determine the effect of moving the muscle

origin location on the internal muscle forces experienced by the muscles of the shoulder. The percentage change in the maximum anterior deltoid force were shown in Table 3.3. Through the motion of abduction, the largest percentage change in the force recorded was a change of 2% when the origin was translated by 1mm in the y direction. Similarly the maximum percentage change during the motion of flexion was 1% when the origin was translated in the z direction. A percentage change of 8% was recorded when the origin location was translated in the z direction through the motion of internal rotation however this indicates an increase of only 0.0256 N due to the low force in the muscle. Despite the inaccuracies in the estimation of the origin locations, the positions chosen were based upon anatomical diagrams and positions from literature. The error in these positions is unlikely to be over 2mm especially due to the large origins of the muscles and the natural anatomical variations between patients. Consequently, there will be a very small change in the internal muscle forces recorded if the positions of the origin locations were to change.

The centre of rotation of the glenohumeral joint had also been estimated based upon the relevant geometries of the segments alongside literature. The results from the second sensitivity study based on the motion of abduction were shown in Figure 3.8. It can be seen that there was only a small impact on the force when the centre of rotation was translated in both the z and x directions. A much larger impact on the deltoid force was recorded when it was translated in the y direction with the maximum force through abduction increased by 30%. For flexion, the maximum force required in the deltoid decreased by 8% and during rotation the maximum force in the deltoid rose by 24%. Another important impact is the delay in the angle at which the deltoid begins to produce force. The deltoid starts to produce force at 16° in the initial model however, when the centre of rotation was translated by 2mm in the y direction this angle became 25°. Lam and Bordoni (2021) stated that the deltoid muscle became the primary muscle involved with the abduction of the arm at 15°. Hence, it can be deemed that the centre of rotation is appropriately estimated as the angle at which the deltoid takes the majority of the force is close to the 15° stated in literature.

3.4.6 Scapulohumeral Rhythm

The impact of the removal of the scapulohumeral rhythm on the internal muscle forces was assessed to determine the importance of keeping this motion in an experimental shoulder simulator. The results from the original model in Figure 3.5 and the model without the scapulohumeral rhythm in Figure 3.9 are comparable between the abduction angles of 0° to 16°. As mentioned previously, due to limitations within the modelling software, the scapulothoracic motion of abduction was applied evenly throughout the whole motion instead of starting from 30° of abduction as suggested in literature (Felstead and Ricketts, 2017).

Hence the removal of the scapulohumeral rhythm altered the whole result instead of just the higher range of abduction angles. It was also noted that the maximum force required by both the deltoid and the supraspinatus muscles decreased when the scapula remained stationary. Another key point is that the deltoid force remained high throughout the whole motion as the pectoralis major muscle which had become the primary muscle in Figure 3.5 at 75° no longer produced significant force. Despite this, especially during the lower levels of abduction, the removal of the scapulohumeral rhythm caused little difference in the internal muscle forces of the primary muscles required for the abduction of the shoulder. Felstead and Ricketts (2017) stated that up to 30° of abduction the scapulohumeral rhythm played a negligible role and hence it can be assumed that the internal muscle forces would not change when the scapulohumeral rhythm was removed in this region. Scapulohumeral rhythm does not play a large role in the other motions of flexion and internal rotation and so these motions were not simulated.

3.5 Porcine Model Development

3.5.1 Overview

As previously stated in Chapter 2, the use of porcine tissue to develop the initial simulator methods reduces the ethical burden of the project by using porcine tissue from the food chain. A computational model of the porcine shoulder joint was created using the AnyBody modelling software. The model was created in order to allow for comparisons between the forces within the muscles of the human shoulder and the forces within a porcine shoulder, particularly considering the anatomical differences between the joints.

3.5.2 Input Parameters

The inputs required to model bones within the AnyBody software were mass and moment of inertia of the bones. Due to the very limited literature regarding the moment of inertia of porcine shoulder bones, steps were taken to obtain these results experimentally. Following on from a dissection of a porcine forelimb according to the methodology outlined in Chapter 2.2, the remaining soft tissues were removed such that the resulting samples were clean humerus and scapula bones. The samples were scanned using a CT scanner (XTreme CT, Scanco, Switzerland) to produce DICOM image files of the humerus and scapula geometries. The images were analysed using the segmentation software ScanIP (Synopsis, CA). A thresholding technique was used to select the outer surfaces of the bones on the scan images. The resultant models of the porcine humerus and scapula are shown in Figure 3.12.

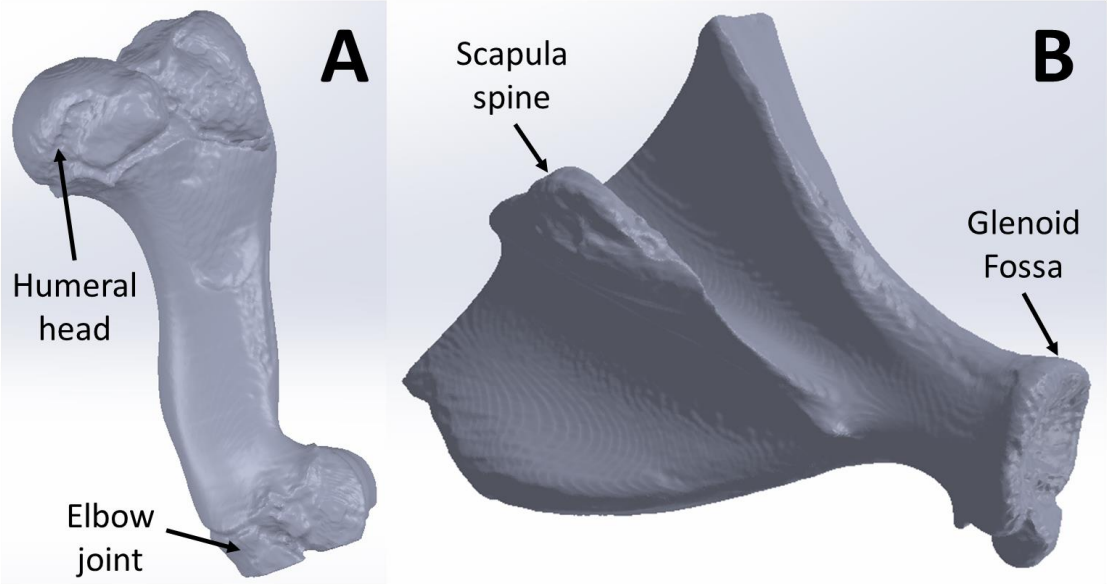

Figure 3.12 - Models of the porcine humerus and scapula following a CT scan and post processing using the ScanIP software. A: Porcine humerus. B: Porcine scapula.

The scan images were then converted to STEP files which were compatible with ABAQUS 2017 (RI, USA), a finite element software. This software allowed the properties, including moment of inertia, for the individual bones to be obtained. Therefore, both the mass and moment of inertia for the creation of the bone segments within the AnyBody model were obtained from a porcine humerus and scapula and provided in Table 3.4.

Table 3.4 - The mass and moment of inertia tensor or the porcine humerus and scapula as determined from CT scans of the bones.

	Humerus	Scapula
Mass (kg)	0.25	0.13
Moment of inertia tensor (I_{xx}, I_{yy}, I_{zz}) (kgm^2)	(0.00056, 0.000078, 0.00054)	(0.00018, 0.000081, 0.00022)

The inputs required for the modelling of the muscle segments were: maximum force (F0), muscle fibre length (Lf0) and volume of muscle fibres (Vol0). These were obtained from literature for the rotator cuff muscles of the porcine model (Mathewson et al., 2014). As with the human model, described in Section 3.2.3, several muscle strands were created with the same insertion points but several origin locations to model muscles which originate over a large area and taper towards a single insertion point. When more than one muscle was used to represent a single muscle unit, the maximum force and the volume was divided by the number of individual muscles.

The resultant model of the left porcine shoulder is shown in Figure 3.13. The bones included in the model are the spine, scapula and humerus and the initial position of the joint is at an angle of 45° of extension.

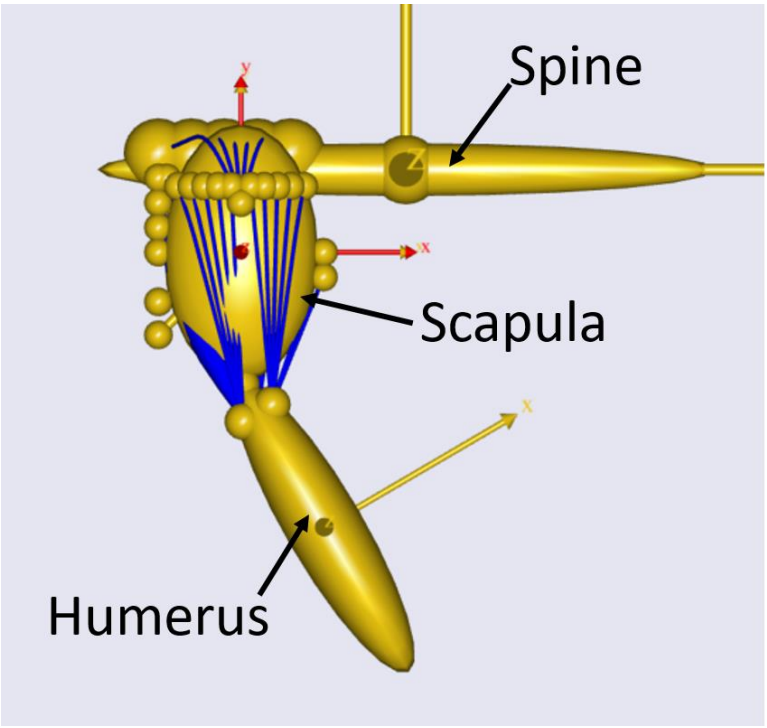

Figure 3.13 - AnyBody model of the left porcine shoulder joint including the spine, scapula and humerus bones.

A quadruped shoulder undergoes 30° of flexion and extension throughout the walking cycle (Lanovaz et al., 1999). Hence, the porcine AnyBody model was used to simulate 30° of flexion and extension from -10° to the resting position of -45° from the vertical as seen in Figure 3.10 and then returning to -10°. The resting position of -45° was measured during the dissection process detailed in Section 2.2.

A porcine shoulder joint is a weight bearing joint and is fully involved in the walking cycle of a pig. Therefore, in contrast to the human model described in Section 3.2, an additional external force had to be added to represent the weight of the pig. The reaction force of a quarter of the weight of an average pig, assuming that the pig was standing on all four limbs, was applied to the model alongside gravity (Agriculture and Horticulture Development Board, 2020).

3.5.3 Results and Discussion

The results from the porcine AnyBody model are shown in Figure 3.14. It can be seen that the muscles which produce the most force during the flexion and extension motion are the deltoid muscle and the supraspinatus muscles.

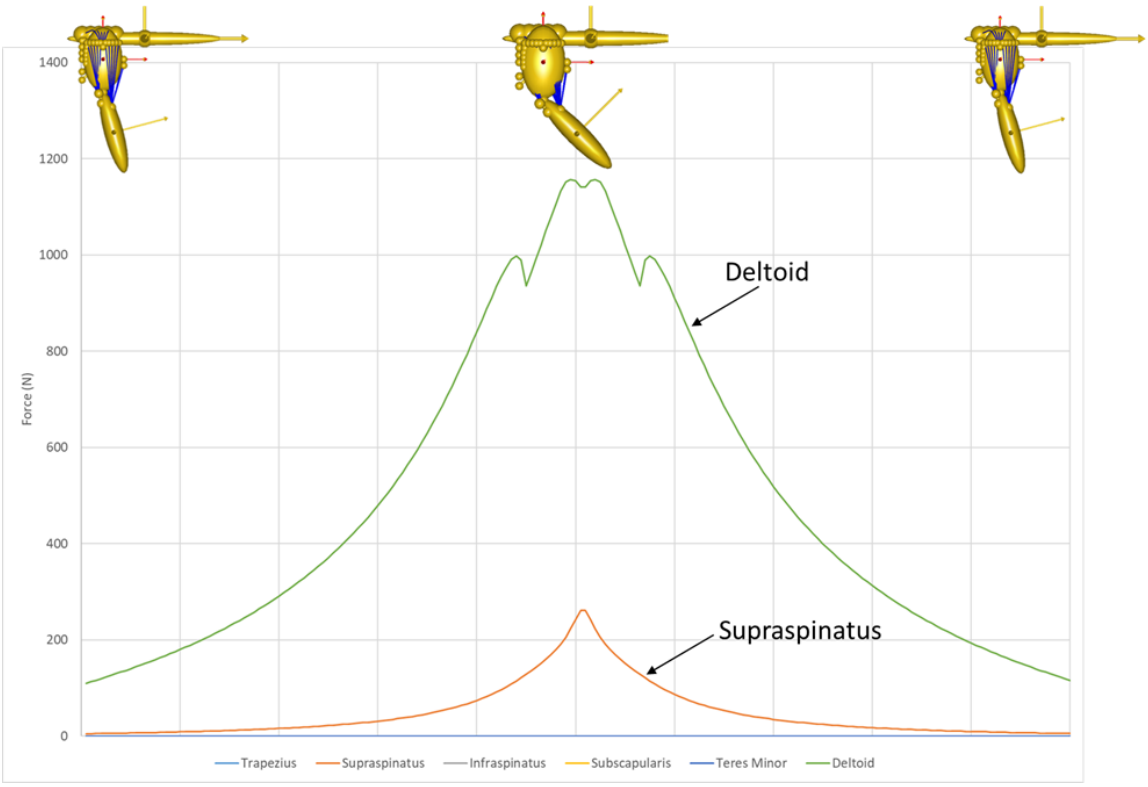

Figure 3.14 - Results for the force in each muscle during flexion and extension of the porcine joint from - 10° to - 45° and back to - 10° as indicated with the diagrams.

During the human flexion motion, shown in Figure 3.6 the maximum force was 310 N similarly in the deltoid muscle. The maximum force experienced within the porcine joint was a force of 1150 N, an increase of 271%, at peak flexion in the deltoid muscle. The porcine joint undergoes much larger forces due to the weight bearing nature of the porcine joint. Consequently, the muscles within the porcine joint are larger and can withstand much higher forces than the muscles within the human shoulder. Simulation of the human shoulder joint using a surrogate porcine model would need to have much higher forces applied in order to replicate the forces within the porcine muscle environment.

3.6 Conclusion

The computational model of the shoulder joint presented in this chapter allowed the internal muscle forces of the muscles of the shoulder complex to be calculated through a range of common motion of the shoulder joint. A multibody model of the natural shoulder joint was created using the AnyBody modelling system to simulate flexion, abduction and internal rotation of the shoulder. The open-source repository model was assessed as an option to be adapted for use within the project. However, due to results that did not align with literature for the abduction motion, it was decided that a project specific model would be made to ensure muscle force results that aligned with literature. Consequently a bespoke model was

created which included four bones (humerus, scapula, clavicle and spine) and twelve muscles of the human shoulder. Due to limitations in literature with regards to the inputs required to model the muscles, a sensitivity study was conducted to assess the impact of muscle origin and insertion locations on the outputs of the model.

The bespoke AnyBody model completed the motions of abduction, flexion and internal rotation and the key muscles were found for these motions. In particular these were the supraspinatus and deltoid muscles for 0° - 90° of abduction, the anterior deltoid and pectoralis major muscle for 0° - 100° of flexion and the latissimus dorsi, infraspinatus and subscapularis muscles for 0° - 70° of internal rotation. The removal of the scapulohumeral rhythm from the model was also assessed and found to have limited impact on the muscle forces during the lower ranges of abduction.

The final objective of this chapter of work was to develop a multibody model of the porcine joint to enable to development of a preliminary porcine shoulder joint simulator. Due to the weight bearing nature of the porcine joint and the large difference in anatomical structure of the joint the results from the porcine model were considerably different to those obtained from the human model. The maximum force within the porcine joint was much higher than those experienced within the human joint despite the range of motion achievable by the joint being much lower. The bespoke human and porcine multibody models can be used to determine inputs into the human and porcine simulators respectively.

Chapter 4 - Development of a Natural Porcine Shoulder Simulator

4.1 Introduction

Experimental simulation of a joint allows for the natural joint tissue to be tested throughout a range of loading and motion cycles. This enables the assessment of surgical interventions due to the realistic material properties and biomechanical conditions within the simulator. There is a clear clinical need for innovation in surgical interventions of the rotator cuff with failure rates of rotator cuff repairs being 25-50% at 12 months post-surgery, which increases in elderly patients with larger tears and poor quality of the remaining tissue (Greenall et al., 2018). Previous natural shoulder simulators have included experimental assessment of a very limited number of motion cycles which fails to assess the longevity of a repair method in a biomechanically accurate environment.

An in-vitro natural shoulder simulator would allow the shoulder joint to be assessed under clinically relevant biomechanical conditions with a controllable range of load and motion cycles. Further development of such simulation could allow for the assessment of rotator cuff repair methods. Significant research is needed to develop an effective simulation of the natural human shoulder joint. The natural instability of the shoulder joint has been shown to be a challenge during the simulation of the human shoulder due to the requirement of including the soft tissue surrounding the joint within a simulator. Another challenge facing experimental shoulder simulators was found to be the reliable performance of a large number of motion cycles. In order to simulate the performance of a rotator cuff repair method throughout its lifetime, cyclic motions must be achievable.

The overall aim of this chapter was to develop methodologies for experimental porcine shoulder simulation which could then be translated to a human simulator. Method development for the human shoulder simulator was undertaken using porcine tissue. This enabled method development studies to be carried out without the ethical burden and increased variability of human tissue (Bowland et al., 2018). In order to achieve the aim a series of work was planned as outlined in the flowchart in Figure 4.1. Initially a design specification was created for the porcine shoulder simulator to prioritise the features that would most benefit the translation from porcine to human and hence the development of the human shoulder simulator. A computational model of the porcine joint was previously detailed in Chapter 3 which was adapted to allow for direct comparison between the computational

and experimental set-ups. Consequently the force in each muscle would be required to be measured experimentally throughout the simulation.

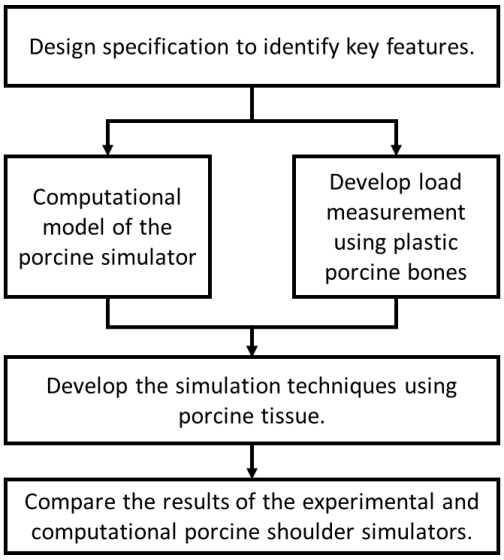

Figure 4.1 - Flowchart showing the approach to developing a porcine natural shoulder simulator.

The two main objectives of the porcine shoulder simulator were:

- To produce a repeatable flexion/extension motion cycle via the application of displacement to the intact rotator cuff muscles of the porcine specimen.
- To develop a robust and repeatable method for the measurement of loads applied to each of the four rotator cuff muscles and the deltoid muscle.

4.2 Design Specification

4.2.1 Overview

A porcine simulator was developed as the first step towards a full human shoulder simulator. Several limitations exist in terms of using porcine tissue as a surrogate for human tissue, these were discussed in Chapter 2. These limitations focus on the differences in anatomy that limit the range of motion with the porcine joint compared to the human. This limits the ability to use porcine tissue in developing a clinically relevant shoulder simulator. However, porcine tissue is readily available in the food chain from animals of similar anatomy and age; the ethical burden of using this tissue is less than using human tissue so despite the limitations it can provide valuable information in developing a natural tissue shoulder simulator. The porcine joint was therefore used to provide an indication of how the human simulator could be developed for all motions. Consequently, it was decided to push the porcine joint further than would be naturally achievable to enable a better surrogate model of the human shoulder.

A design specification specific for the porcine shoulder simulator was required in order to ensure that the simulator was suitable for use. Justification for each aspect of the design specification are provided in Sections 4.2.2 to 4.2.5 and the resultant design specification is shown in Table 4.1.

4.2.2 Determining the Range of Motion for the Porcine Shoulder Simulator

The angles for the abduction, adduction, internal rotation and external rotation were determined during the dissection of a porcine shoulder detailed in Section 2.2. During the walking cycle of a horse which, as a quadruped, is anatomically similar to the pig, approximately 0° of abduction/adduction and internal/external rotation occurs (Lanovaz et al., 1999). During the dissection, however, it was found that the porcine joint was capable of producing 5° of passive motion in all four of these directions. Consequently, to provide an indication of how the human simulator would be developed for all the motions, it would be desirable for the porcine simulator to produce the limited range of these motions. Lanovaz et al. also stated that during the equine walking cycle 30° of flexion and 10° of extension occurred. Therefore, it is essential that the simulator can produce this motion in order to simulate a quadruped walking cycle.

4.2.3 Determining Muscle Loads for the Porcine Shoulder Simulator

Using the porcine shoulder AnyBody computational model described in Chapter 3, the loads within the muscles required to produce these motions were determined. The forces within the muscles of the porcine shoulder were considerably higher than those within the human shoulder because of the weight-bearing nature of the porcine joint. The essential force values shown in Table 4.1 are taken from the maximum force required to perform 30° of flexion in the porcine shoulder when the joint is not weight bearing. If the joint is not weight bearing then the porcine shoulder acts like a pendulum with the only external force being gravity, producing much lower muscle forces. The desired values were the maximum force within the porcine muscles during weight bearing flexion of the joint.

4.2.4 Maintaining Joint Stability of the Porcine Shoulder Simulator

The supraspinatus, infraspinatus, subscapularis and teres major muscle tendons must be powered in order to retain the stability of the joint throughout simulations. During the dissections of the porcine shoulder described in Chapter 2, it was determined that the removal of the deltoid muscle would provide easier access to the remainder of the joint including the rotator cuff tendons. If the deltoid muscle must be removed, it would be essential that a wrap type feature was included to increase the stability of the joint. It would be desirable to provide

power to the four rotator cuff muscles and the deltoid muscle due to the large role that the deltoid has in motion at the joint.

4.2.5 Physical Constraints of the Porcine Shoulder Simulator

The volume of tissue which must fit inside of the simulator was measured during the dissections of the porcine joint according to the methodology in Chapter 2. The volume provided in Table 4.1 includes the scapula and humerus bones as well as the muscles to be retained. The volume did not include the extra components which were required such as pulleys, actuators and attachment materials. The length of tendon tissue that was to be retained was measured during the experiments detailed in Chapter 2. A length of 10 cm was determined to be the shortest tendon length which could still be used for a strong connection. However, a longer tendon length of 15 cm was found to improve the process of connecting the line to the tissue and hence was desired.

4.2.6 Summary of the Design Specification for the Porcine Shoulder Simulator

The design specification for the porcine shoulder simulator is provided in Table 4.1 based upon the information supplied in the previous sections.

Table 4.1 - Design specification for the porcine shoulder simulator.

	Essential	Desired
Range of Motion		
Abduction	0°	5°
Adduction	0°	5°
Flexion	30°	30°
Extension	0°	10°
Internal Rotation	0°	5°
External Rotation	0°	5°
Scapulothoracic Motion	No	No
Number of motion cycles	1	>5 (cyclic)
Load		
Maximum force through muscle	15 N	1160 N
Number of loaded muscles	4 + Deltoid wrap	5
Size		
Volume of tissue that must be included (Scapula, humerus and soft tissue)	150 x 150 x 150 mm	150 x 150 x 150 mm
Length of tendon to be retained	10cm	15cm
Control and measurement		
Force measurement	None	Measurement of force in all 5 powered muscles
Position measurement	None	Tracking of the motion throughout motion cycle

4.3 Materials and Methods

4.3.1 Sample Preparation

A porcine forelimb was dissected to the level of the glenohumeral joint following the method described in Chapter 2. Porcine tissue was obtained within 24 hours of slaughter from a local abattoir (John Penny and Sons, Leeds) from animals approximately 6 months old, weighing between 60-100 Kg. These characteristics were determined by the availability within the human food chain from where these animals were sourced. All joints were dissected and

stored at -18°C until required. The tissue was then defrosted in a refrigerator at 3°C for 24 hours prior to being prepared and tested in the simulator. The four rotator cuff tendons (supraspinatus, infraspinatus, teres minor and subscapularis) and the deltoid tendon were identified and lengths of 15 cm retained, as detailed in the design specification in Section 4.2. The side of a scalpel blade was used to remove the bulk muscle tissue from the tendon leaving thinned tendon sections as shown in Figure 4.2.

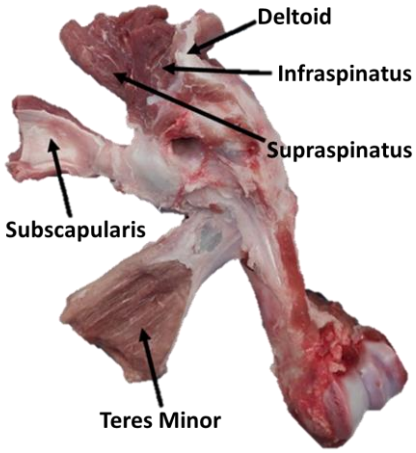

Figure 4.2 – Dissected porcine shoulder joint. The rotator cuff tendons that were retained are labelled.

Braided polyethylene thread (Dorisea extreme braid fishing line, Dorisea Fishing UK) was secured to the five thinned tendon ends via suturing using the modified finger trap stitch described in Chapter 2. Braided polyethylene thread was selected due to the high maximum load, reduced cost and ease of accessibility compared to surgical suture material. Eyelet screws were screwed into the porcine scapula at the approximate insertion locations of the five muscles to act as pulleys and maintain the line of action of the muscles. A diagram is presented in Figure 4.3 which demonstrates the positioning of the screw eyes within the insertion region of the relevant muscle.

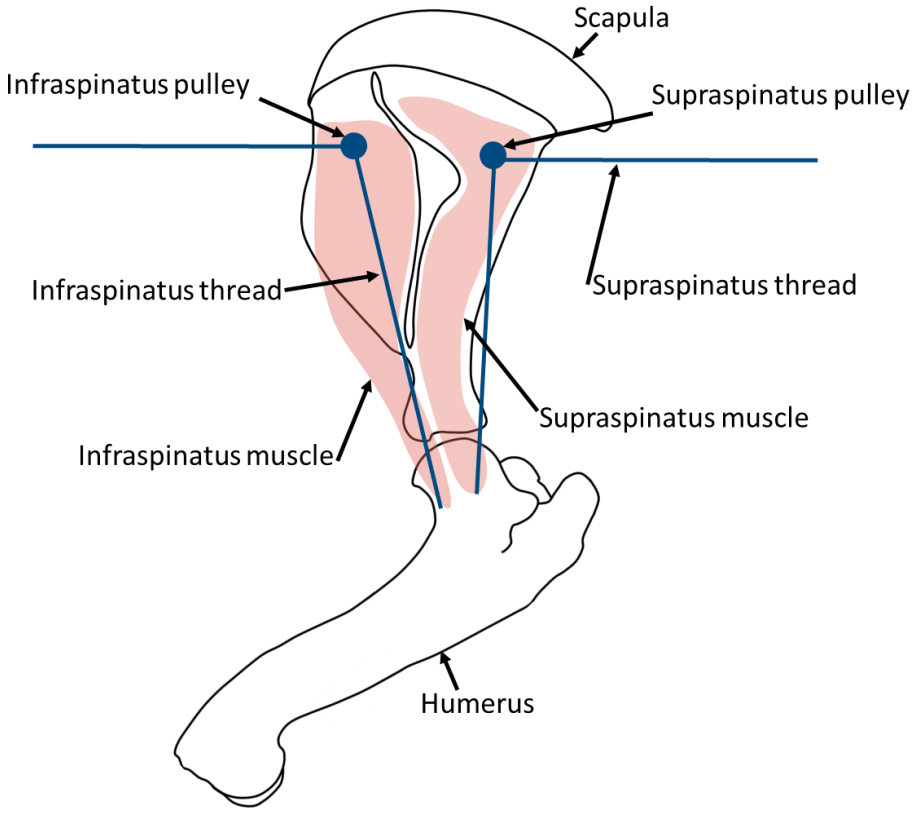

Figure 4.3 - Insertion of screw eyes to act as pulleys to maintain the line of action of the natural muscle tissues. The porcine infraspinatus and supraspinatus muscles are shown as an example of the positioning of the screw eyes.

The porcine scapula was cemented into a custom made fixture, using non-sterile Polymethylmethacrylate (PMMA) bone cement (WHW plastics, Hull, UK). A custom designed fixture was used to ensure that the scapula was cemented in the correct orientation such that the face of the glenoid fossa was parallel to the face of the fixture. The technical drawings of the fixture are provided in Appendix 2. The fixture was manufactured from Delrin (polyoxymethylene plastic) to enable cleaning of the fixture between porcine samples. The braided polyethylene thread, attached to the tendons on the humerus, was then passed through the corresponding eyelet screw on the porcine. The joint was assembled in the correct orientation on the simulator frame as demonstrated in Figure 4.4.

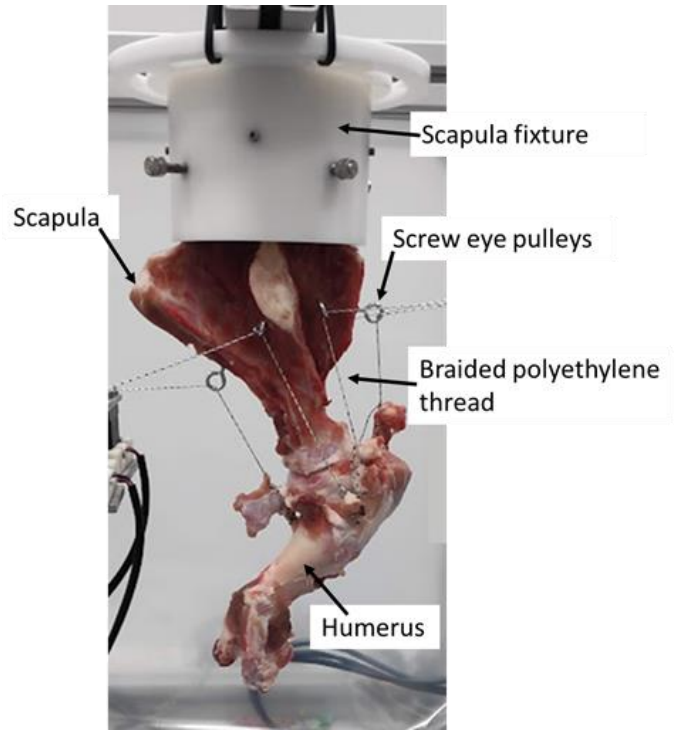

Figure 4.4 - Porcine shoulder joint mounted into the shoulder simulator.

4.3.2 Frame Design

Previously designed natural human shoulder simulators in the literature, described in Chapter 1, were analysed in order to initiate the design process for the new shoulder simulator. Due to the anatomical difference between porcine and human shoulder joints, an adaptable frame which could be configured for both joints was identified as a crucial requirement in order to reduce the cost and waste of the project. The shoulder simulator frame was designed using aluminium extrusion bars which were connected using angle brackets and T-nuts. This allowed easy repositioning of the bars to reconfigure the simulator to fit both porcine and human joints. The frame design in configuration for a porcine shoulder joint is shown in Figure 4.5.

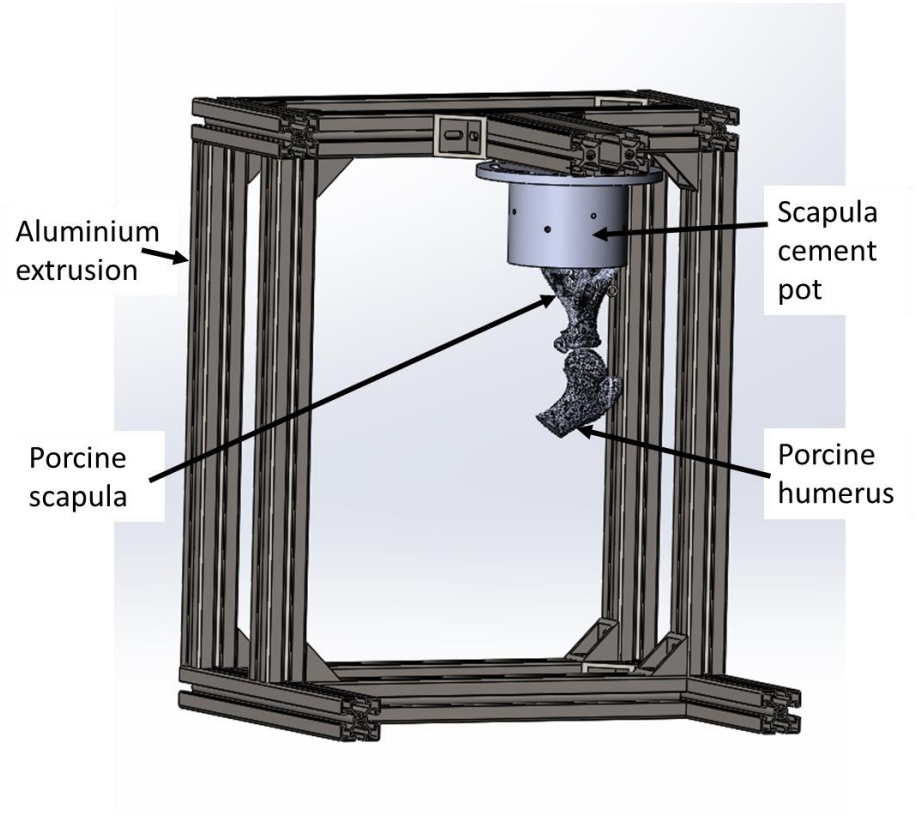

Figure 4.5 - CAD design of the porcine shoulder simulator constructed using aluminium extruded bar to allow for reconfiguration of the simulator between the human and porcine setup.

4.3.3 Actuation Methods

To meet the desired range of motion outlined in the design specification given in Section 4.2 a novel actuation system had to be developed. The system would be required to provide a cyclic actuation regime to five muscles of the shoulder joint. Other requirements for the actuation system included being able to provide enough force for use in both a porcine and human shoulder simulator and being cost effective.

Servo motors, stepper motors and linear actuators were all considered for the actuation of the shoulder simulator. The advantages and disadvantages of the actuation methods are listed in Table 4.2.

Table 4.2 - Advantages and disadvantages of the actuation methods (Klar, 2016).

Actuation method	Advantage	Disadvantage
Servo motor	• High torque at high speed • Widely available	• Higher cost and complexity
Stepper motor	• Precise motion control • High torque at low speeds • Inexpensive and widely available	• Lower torque at high speed • Can produce high vibration levels, resonance issues and heat at high speed.
Linear Pneumatic Actuator	• High peak power at high speeds	• High cost • Low positional accuracy

To control the motion of the shoulder joint in the simulator, precise control of the selected motor was required. Stepper motors were selected due to the close control that the user had over the motion produced. The selected stepper motor was able to provide high torque which would enable the same motors to be used for both the porcine and human shoulder simulators. One limitation of the stepper motors was that they were limited to low/medium speeds. This was deemed to have low impact on the simulator because of the comparatively low speed of motion that is performed at the shoulder (Rockwood and Matsen, 1998a). The shoulder simulator would produce a lower number of motion cycles than simulators of joints such as the hip and knee joints due to the limited testing life of natural tissue.

NEMA 17 (Ooznest, Essex UK) stepper motors met the required specification and were used within the shoulder simulator due to their local availability. These stepper motors had the capability of producing 3.2 Kgcm of torque (Ooznest, 2023) which was suitable for use in both the porcine and human simulator development.

The polyethylene braid which was attached to a muscle tendon and then passed through a pulley on the porcine scapula and was then secured to the corresponding stepper motor.

4.3.4 Load Sensing

4.3.4.1 Load measurement platform

The motion of the motor driving each muscle was programmed using a custom made programme to produce the motion cycle required. To compare the physical simulator to the computational models created previously, detailed in Section 3.3, the force applied to each muscle by the stepper motor was measured. The load applied to each muscle was measured using a custom load measuring platform shown in Figure 4.6. The load cell selected for use within the custom load measuring platform was required to have a capacity of over 100N for use during both the human and porcine shoulder simulators. It was also required that the load cell had high precision and accuracy over the range of forces measured so therefore it was decided that a load cell with a lower range (over 100N) would be selected to maximise the accuracy. The load cell also was required to have small dimensions to allow it to fit within the load measuring platform.

A button compression load cell (FX1901-0001-0025-L, TE Connectivity, Switzerland) was selected for use in the load platform due to its availability, low cost and load capacity of 11.34 Kg/ 111 N which was adequate for the requirements of the simulator. The accuracy of the load cells was ± 1% of the full range so hence an accuracy of ± 1.1N (TE Connectivity, 2024). The load cells were connected to a HX711 load cell amplifier (HALJIA) which amplified the signal to be read by the Arduino Uno Rev3 microcontroller board (Arduino, New York, USA).

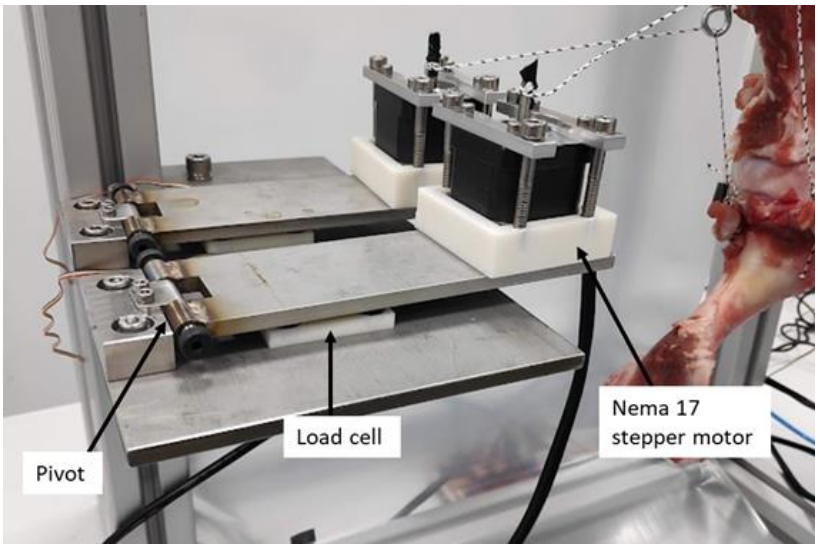

Figure 4.6 – Porcine shoulder simulator set up showing load measurement platform with the pivot, load cell and stepper motor labelled.

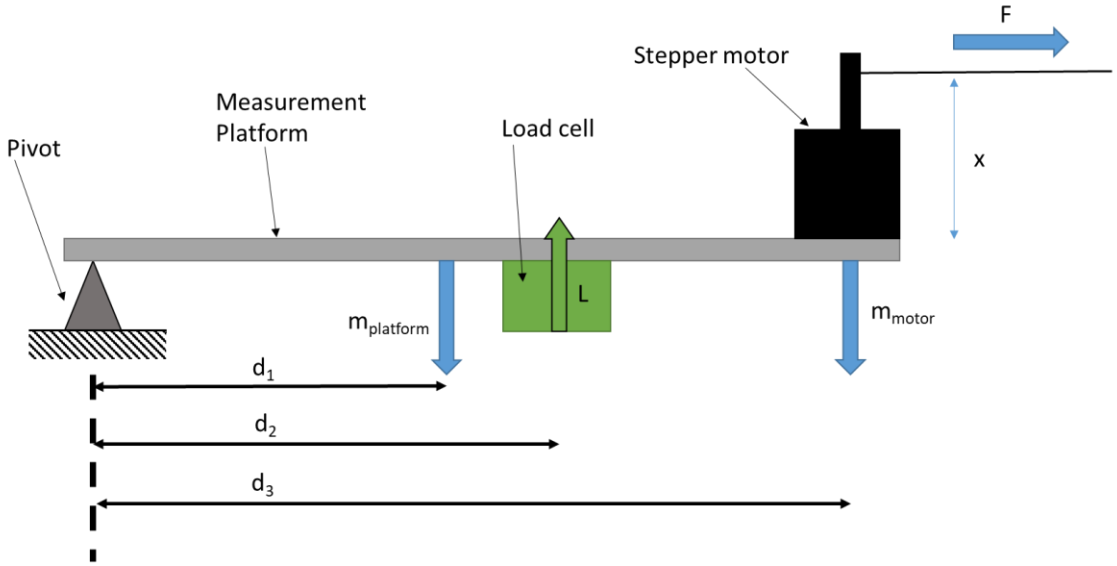

Figure 4.7 - Schematic of the load platform (shown in Figure 4.6). The pivot, measurement platform, load cell and stepper motor are labelled. F = the horizontal force in the polyethylene braided thread. X = Distance from thread to measurement platform. $M_{platform}$ = Mass of the measurement platform. M_{motor} = Mass of the stepper motor. L = Load recorded by load cell. D_1 = Distance from pivot to the centre of mass of the platform. D_2 = Distance from pivot to load cell. D_3 = Distance from pivot to stepper motor.

A schematic detailing how the horizontal force in the braided polyethylene thread was measured using the compression load cell is shown in Figure 4.7. Moments were taken around the pivot on the left hand side of the system.

$$m_{platform} g d_1 - L d_2 + m_{motor} g d_3 = F x \quad [4.1]$$

$$F = \frac{m_{platform} g d_1 - L d_2 + m_{motor} g d_3}{x} \quad [4.2]$$

Where F = the horizontal force in the polyethylene braided thread, X = Distance from thread to measurement platform, $m_{platform}$ = Mass of the measurement platform, m_{motor} = Mass of the stepper motor, L = Load recorded by load cell, d_1 = Distance from pivot to the centre of mass of the platform, d_2 = Distance from pivot to load cell and d_3 = Distance from pivot to stepper motor.

Using equations 4.1 and 4.2 the force in the horizontal braided thread, and hence the force applied to each of the tendons, was calculated from the load recorded by the compression load cell.

Due to physical space constraints within the simulator frame, it was not possible to ensure that each thread was horizontal upon leaving the stepper motor. Therefore the schematic shown in Figure 4.8 was used to calculate the angled force recorded by the load cell.

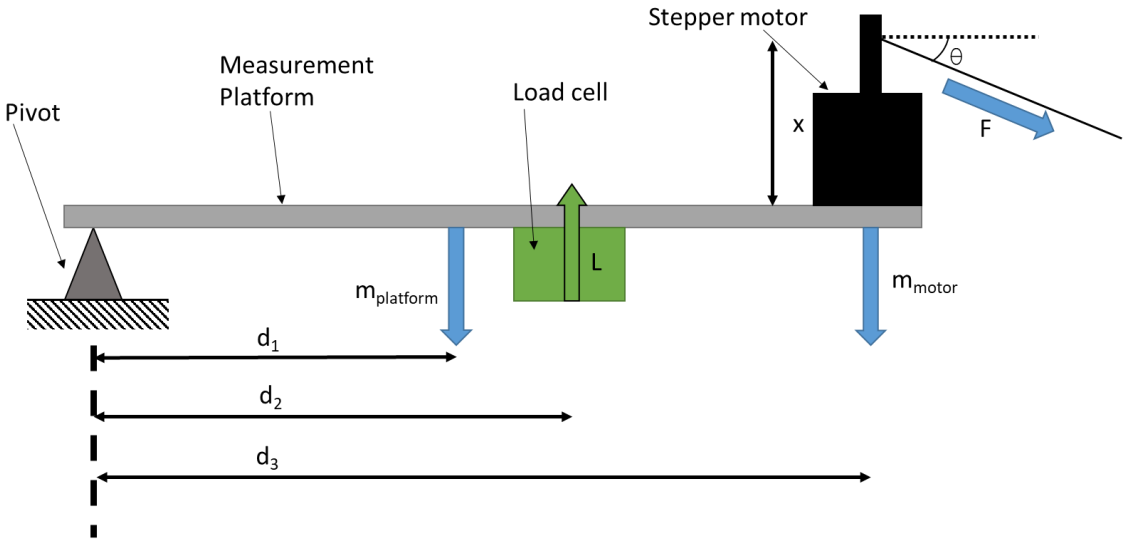

Figure 4.8 – Schematic of the load platform with an angled thread. The pivot, measurement platform, load cell and stepper motor are labelled. F = the horizontal force in the polyethylene braided thread. X = Distance from thread to measurement platform. $M_{platform}$ = Mass of the measurement platform. M_{motor} = Mass of the stepper motor. L = Load recorded by load cell. D_1 = Distance from pivot to the centre of mass of the platform. D_2 = Distance from pivot to load cell. D_3 = Distance from pivot to stepper motor. Θ = Angle from horizontal to the polyethylene thread.

Moments were again taken around the pivot on the left hand side of the schematic in Figure 4.8.

$$m_{platform} g d_1 + m_{motor} g d_3 - L d_2 + F d_3 Sin(\theta) + F x Cos(\theta) = 0 \quad [4.3]$$

$$F = \frac{L d_2 - m_{platform} g d_1 - m_{motor} g d_3}{d_3 sin(\theta) + x cos(\theta)} \quad [4.4]$$

A still image was taken from the beginning of the recording of the motion cycle. Image J software (Maryland, USA) was used to measure the angle θ which was used during the calculations.

4.3.4.2 Load cell calibration

The theoretical calculations of force assumed that there was no friction in the load measurement platforms pivot. Shoulder bolts along with precise manufacture of the parts was used to minimise the friction present however a range of preliminary tests were also completed to ensure that the purchased load cells measured the correct forces within the system. Two tests were completed with all the load cells and load cell amplifiers. Firstly force

was applied then removed from the load cells in turn to ensure that the load cells returned to 0 N force when the load was removed and measured the same value each time force was applied. The second test was to ensure that the load measurement platform allowed for the correct forces to be recorded. A 3D printed porcine scapula was used to model the porcine set up. Braided thread was passed from the load cell, through a pulley on the scapula to a load which was applied cyclically and the force in the load cells recorded. The experimental set-up for the second experiment is shown in Figure 4.9.

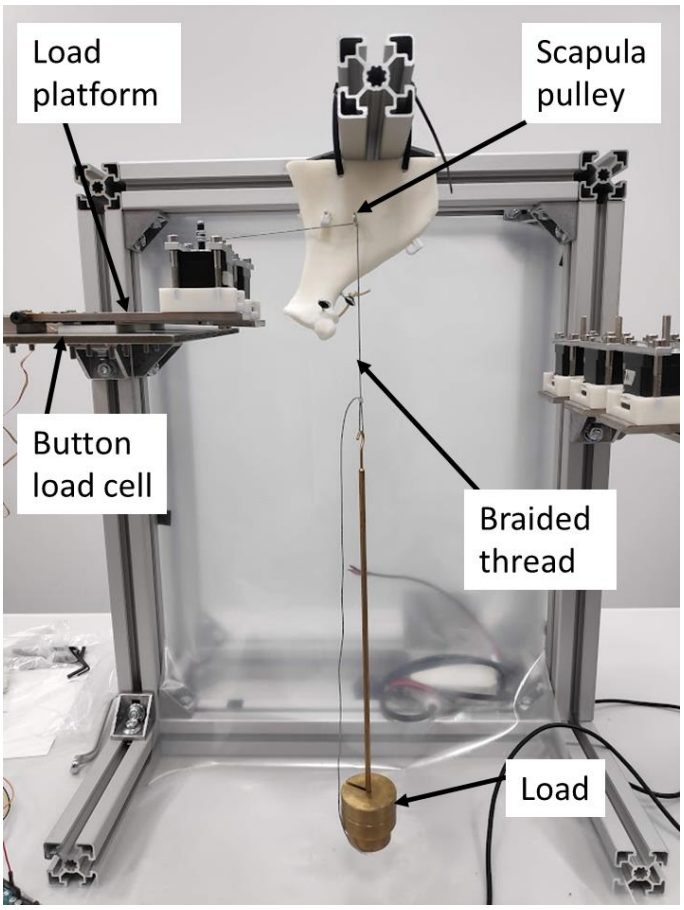

Figure 4.9 - Experimental set-up for the load cell calibration. Braided thread was passed horizontally from the load cell, through a pulley on a model porcine scapula to a weight.

In the first case, a load of 600 g was applied to the surface of the button load cells for five seconds and then removed for five seconds before being added again. In total the weight was added then removed from the load cell five times. This was then repeated three times for all six load cells. All load cells returned to the base value once the mass was removed and returned to this value after each addition of mass as shown for load cell 1 in Figure 4.10. The output value from the load cell was arbitrary as the calibration method had not been applied to the load cell. However, the output value should return to the same each time the load is applied.

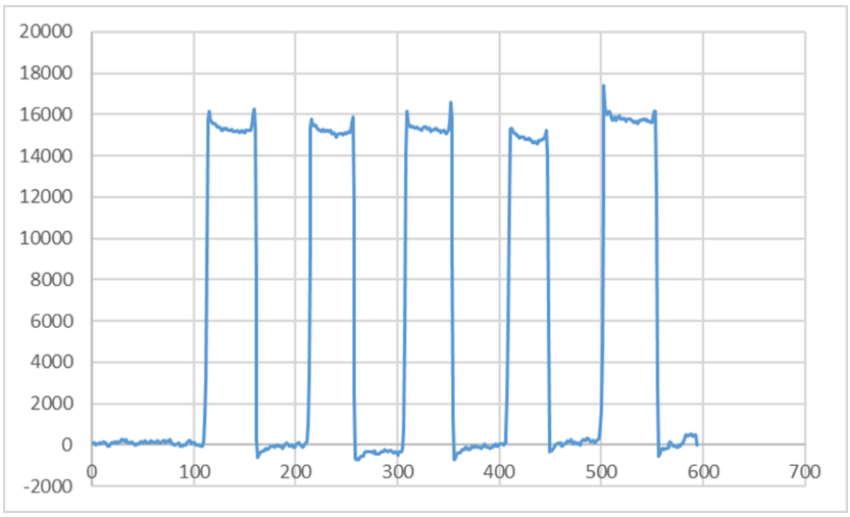

Figure 4.10 – Results for the first load cell check experiment where a 600g load was applied directly to the load cell then removed five times. The output value from the load cell (y-axis) was arbitrary as the calibration method had not been applied to the load cell.

The second experiment utilised the experimental set up shown in Figure 4.9. The load cells were in turn positioned within the load cell pivot mechanism. Polyethylene thread was then passed from the stepper motor through a pulley on the 3D printed porcine scapula to a weight. A spirit level was used to ensure that the thread was horizontal between the stepper motor and the pulley. The data outputted from the load cells was then run through a Matlab (Mathworks, Massachusetts) script containing Equation 4.2 (because the thread remained horizontal throughout). Consequently the measured force in the thread was able to be directly compared to the weight added. The same load of 600g was applied then removed from the vertical thread five times. This experiment was completed with all five load cells and the corresponding load cell amplifier boards. The results for one load cell are shown in Figure 4.11. It can be seen that the load cell recorded values of approximately 5.5 N when the load of 5.886 N (600 g) was applied to the system. All other load cells recorded forces in the range of 5 – 7 N for the same experiment.

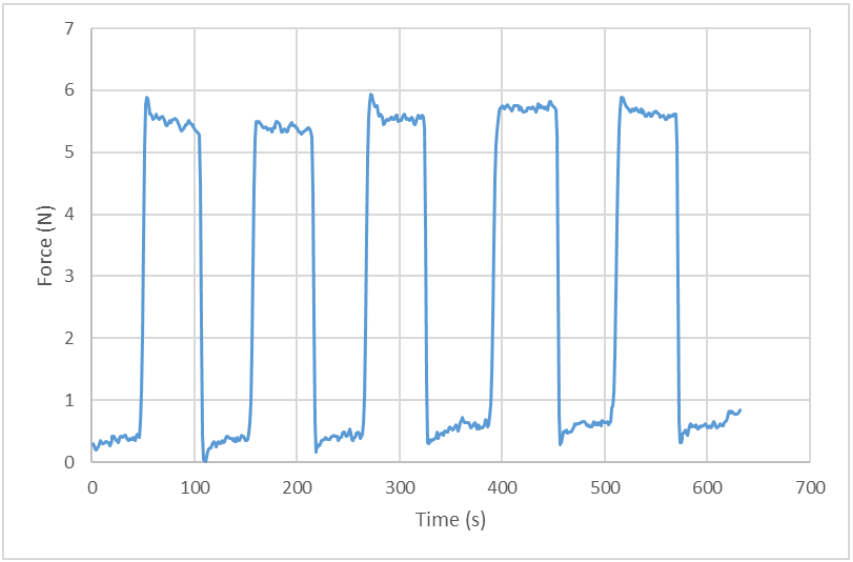

Figure 4.11 – Force results from load cell 1 after a load of 600g (5.886 N) was applied and removed five times.

An experiment was also conducted to verify the equation for the angled thread situation given in Equation 4.4. The experimental set up is shown in Figure 4.12 where the thread was at an angle of 32.5°.

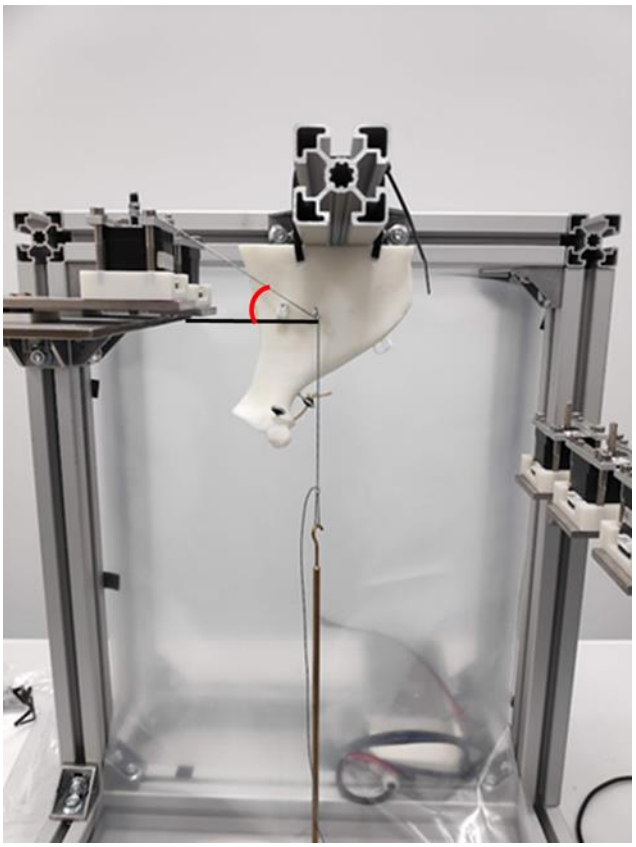

Figure 4.12 - Experimental set up with the thread entering the pulley at 32.5 degrees to the horizontal. The red line indicates the position of the 32.5 degree angle.

As with previous experiments, the data recorded from the load cell was processed by a MATLAB script which implemented Equation 4.4. The load was applied and removed five times for each load cell and load cell amplifier. The results for load cell 5 are provided in Figure 4.13, the recorded values are shown by the solid line and the expected values are indicated with the dashed line. The load cell recorded a value of approximately 5.4 N when a load of 5.886 N was applied at the angle of 32.5° which gives an average root mean square error of 1.52 across the five force peaks.

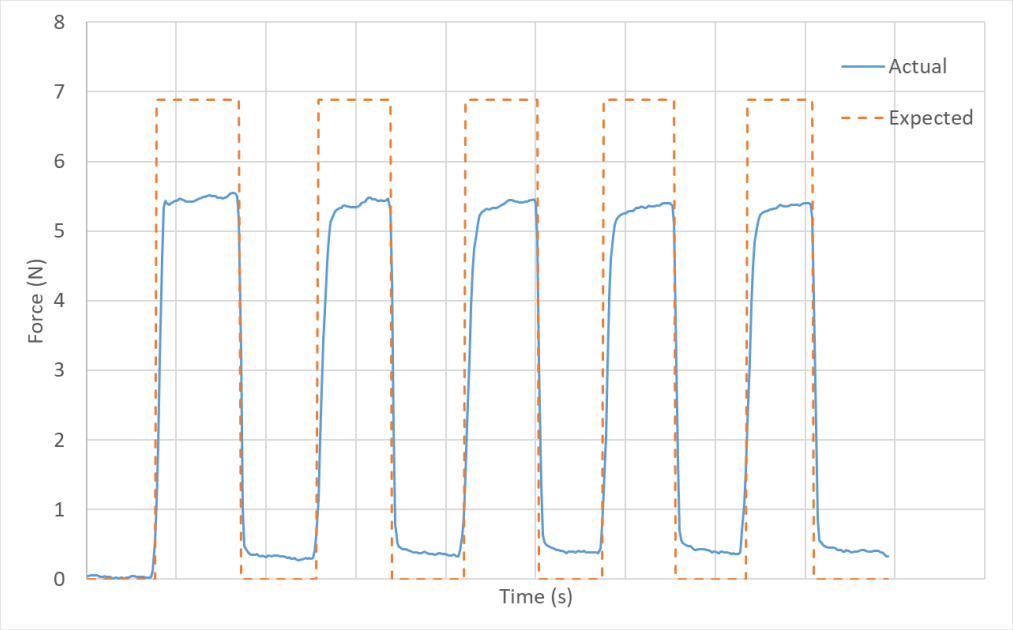

Figure 4.13 - The force results for the experiment where the thread was at an angle of 32.5 degrees to the horizontal for load cell 5. The blue line indicates the recorded values and the dashed line represents the expected values.

4.3.5 Position Sensing

The position of the porcine humerus was tracked throughout the motion cycles to allow for comparisons to be made between the expected motion and the actual performance of the simulator. Two green headed pins of 5 mm diameter were inserted into the porcine connective tissue around the humerus during the set up process of the porcine simulator. They were placed in the tissue such that both pins were at all times visible to a camera positioned directly in front of the simulator on a laboratory bench.

A Canon EOS 550d camera (Canon, Tokyo, Japan) was placed on a tripod and positioned 1 m away from the porcine simulator. The camera was used to record the porcine shoulder through a flexion/extension cycle. The captured video was post processed using a Matlab script. This was developed to track the position of the two green markers throughout the video

and plot their coordinates on a graph. From this, the average flexion and extension angles for each motion cycle were calculated.

4.3.6 Adaptation of Porcine AnyBody Model

A computational model of the porcine joint was made using the AnyBody musculoskeletal modelling software and was detailed in Chapter 3. The model was adapted in order to better reflect the physical set-up to allow for direct comparisons between the outputs from the physical simulator and the computational outputs. The differences between the two AnyBody models of the porcine joint was the addition of pulleys to the system and the range of motion for which the model produced. The model of the porcine simulator is shown in Figure 4.14 with the pulleys labelled.

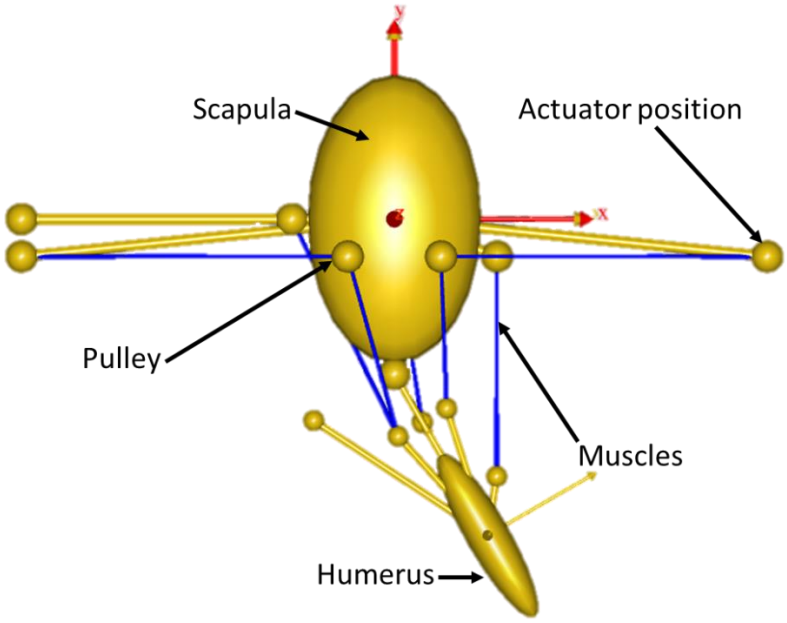

Figure 4.14 - The adapted AnyBody model of the porcine shoulder simulator. The pulley and actuator positions are labelled. These additions improve the similarity between the computational porcine model and the physical simulator set-up.

The outputs of force required in each muscle to produce 50 degrees of flexion and extension from the original and adapted models are provided in Figure 4.15.

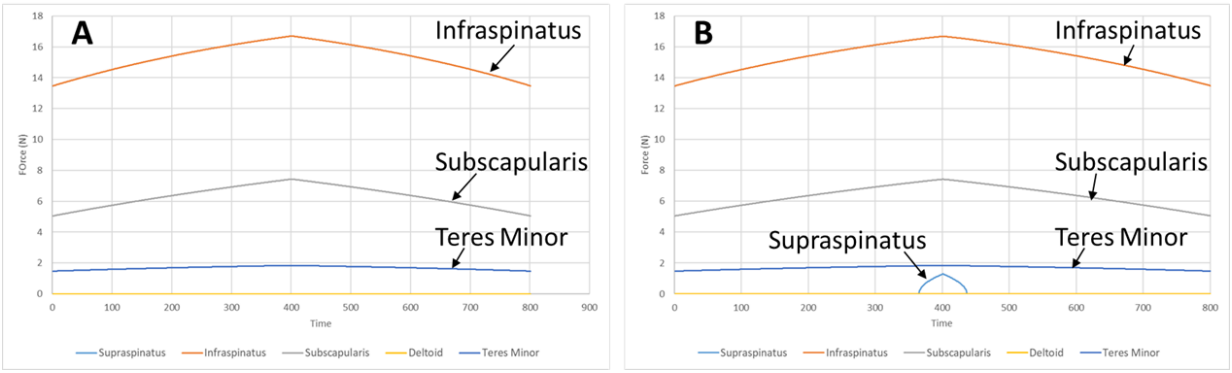

Figure 4.15 - Output from the original (A) and adapted (B) AnyBody models.

The adaptations made to the original porcine model detailed in Chapter 3 can be seen in Figure 4.15 to make little difference to the outputted force in each muscle. The magnitudes of force required in the infraspinatus, deltoid, subscapularis and teres minor muscles are identical between the two models. The only difference is the introduction of a spike of supraspinatus force at the maximum flexion position. The magnitude of this supraspinatus force is 1.2 N and hence very low in comparison to the other muscle forces occurring at that time point. Therefore the adapted porcine simulator AnyBody model has been shown to provide results comparable to the original porcine musculoskeletal model.

4.3.7 Applied Motion and Load Cycle

The motion selected for the preliminary porcine testing was a flexion and extension cycle. This was selected due to the limitations of motion within a porcine joint detailed in Section 4.2. Porcine shoulders have the maximum range of motion in the flexion/extension plane and so this was selected to ensure that the simulator could be tested throughout a large range of motion.

The rationale for the simulator development was as a prototype for a human cadaveric shoulder simulator, however the objective was not to accurately replicate the normal gait of a pig with the simulator. Therefore the maximum possible flexion achieved within the anatomical restrictions of the porcine joint was simulated, which was around 50 °.

The AnyBody computational model of the porcine shoulder simulated detailed in Section 4.3.6 was used to initially design the control cycle for the stepper motors. The ratio of forces required in each muscle to produce the flexion motion was used to calculate the ratio of motion required in each corresponding stepper motor. For example, given the data in Figure 4.15, the maximum force was produced by the infraspinatus muscle and the least by the deltoid. Therefore, the stepper motor controlling the infraspinatus muscle was coded to produce the highest displacement of the wire and the deltoid stepper motor displaced the

least. An initial Arduino (Arduino, New York, USA) programme was developed to control the five stepper motors using these calculations. The initial Arduino programme was then developed further using a trial-and-error approach to manually adjust the rotations in each stepper motor, in order to obtain the best and most visually fluid flexion and extension cycle of the joint.

The process of determining the inputs and outputs of the simulator are shown in Figure 4.16 which indicates the flow of results from literature and the computational model into the shoulder simulator. A feedback loop is also indicated, where the Arduino code is tuned in order to obtain the most appropriate and fluid motion cycle based upon the initial AnyBody model.

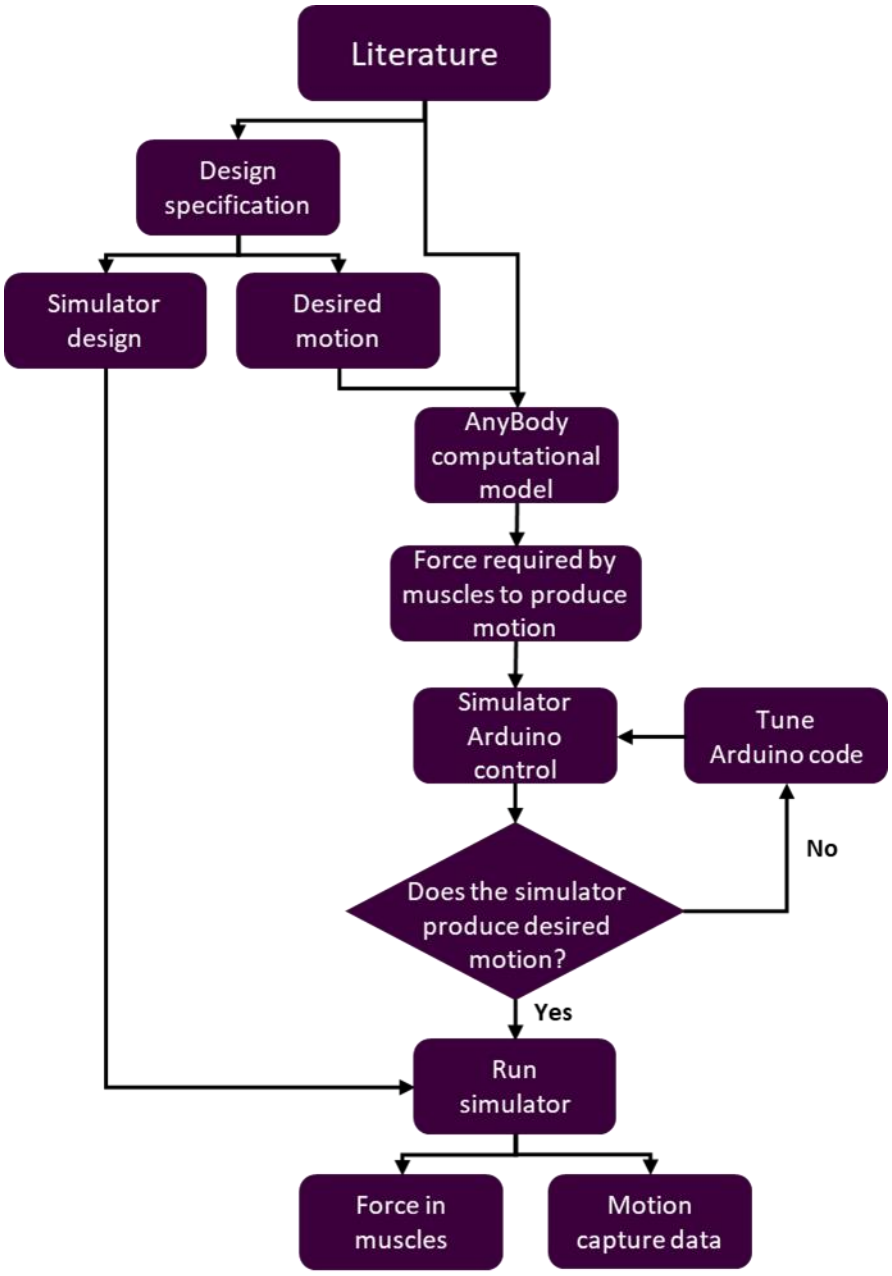

Figure 4.16 - Flowchart representing the inputs and outputs of the simulator.

4.4 Experimental Protocol

In order to refine the novel porcine shoulder simulator, a series of experiments were required. An initial test of short duration was performed to refine the Arduino program which controlled the stepper motor. An extended duration test was then completed to investigate the effect of longer cyclic motions on the simulator setup. Following this an experiment was completed which left the shoulder capsule tissue intact to assess the effect of this structure on the function of the porcine joint. The aims of each stage are detailed below.

4.4.1 Initial Pilot Test (Short Duration)

A porcine shoulder joint was manufactured via 3D printing using a Fused Deposition Modelling (FDM) approach. This enabled the motion cycle to be developed without the waste of tissue resources. The set up process for the natural tissue was followed in order to maximise the similarities between the set ups. The 3D printed joint within the simulator is shown in Figure 4.17.

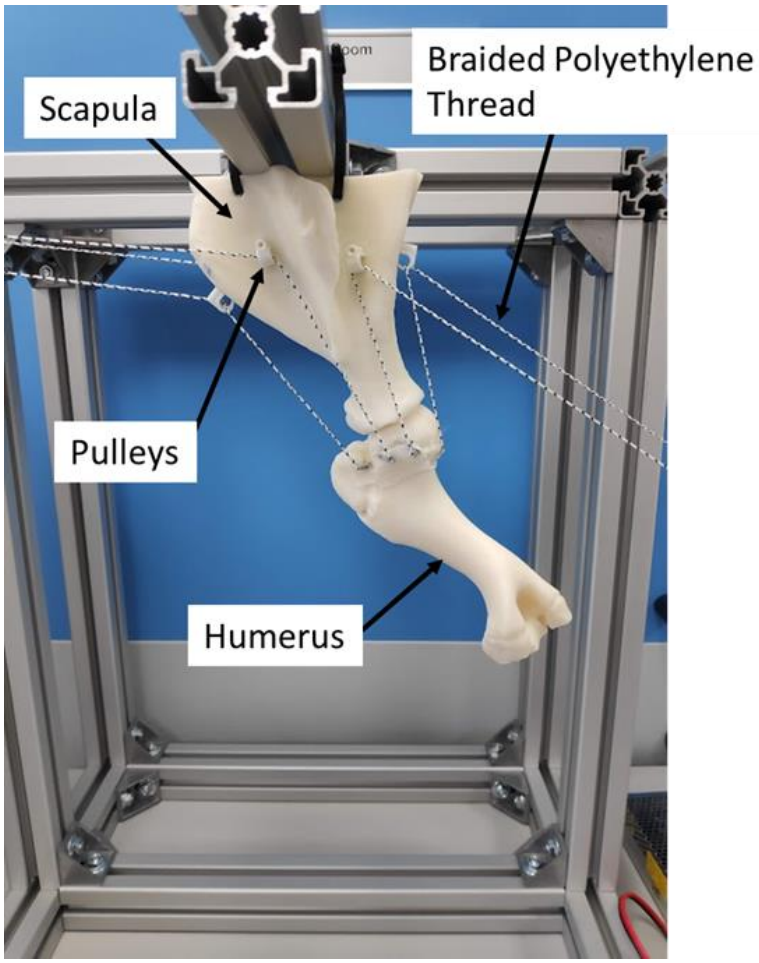

Figure 4.17 - 3D printed porcine shoulder simulator set up for the initial test of short duration.

4.4.2 Extended Duration Test

Natural tissue was then used during a longer duration test to assess the effect of the number of cycles on the results and also the repeatability of the simulator and force measurements. The porcine simulator was initially used to simulate three natural porcine shoulder joints. A single flexion and extension motion cycle comprised of the flexion and extension motions and this was repeated ten times consecutively without user input to complete a testing set. Each porcine joint underwent six runs of the testing set (i.e. six repeats of 10 cycles, totalling 60 cycles) as seen in Figure 4.18.

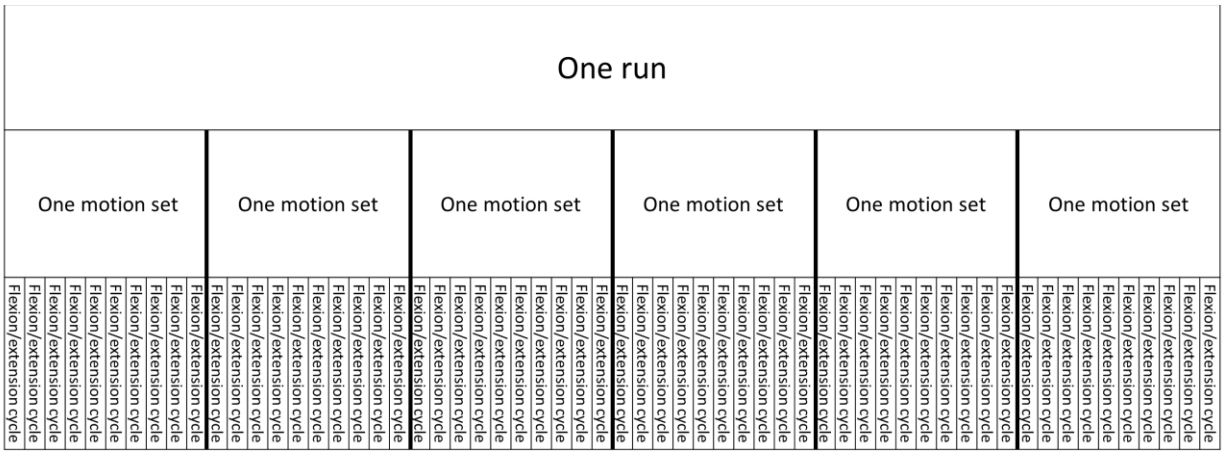

Figure 4.18 - Diagram to differentiate between the terms cycle, set and run.

The load in each load cell was recorded throughout the motion cycles as described in Section 4.3.4. Each experiment was also videoed to allow for motion tracking as described in 4.3.5.

4.4.3 Porcine Capsule Test

Firstly, a porcine capsule study was completed using the 3D printed porcine bones used in the first study to reduce the waste tissue. Four elastic bands were secured around the glenohumeral joint of the 3D printed porcine joint using screw in eyelets to replicate the role of the shoulder capsule and glenohumeral ligaments and provide constraints to the joint. The resulting plastic porcine joint is shown in Figure 4.19.

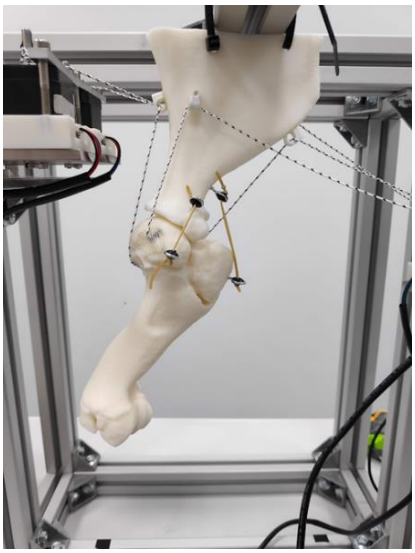

Figure 4.19 - 3D printed porcine shoulder joint with the addition of four elastic bands surrounding the joint to provide constraint

Following on from the plastic porcine capsule test, a natural porcine joint with intact capsule and glenohumeral ligaments was used in the shoulder simulator. The dissection process outlined in Chapter 2 was followed however the scapula and humerus bones were not separated and hence the capsule and glenohumeral ligaments were left intact. A cementing method was also developed to allow for the cementing of the scapula into a fixture whilst maintaining the orientation of the humerus and rotator cuff tendons. A clamp was used to support the porcine humerus in its natural position whilst the joint was placed upside down to allow for the cement to set around the scapula. The cementing configuration can be seen in Figure 4.20.

Figure 4.20 - Clamp was used in order to allow for the cementing of the scapula into the simulator fixture.

Due to the additional musculature, capsule and glenohumeral ligaments surrounding the porcine joint, the amount of flexion that the joint could achieve was severely reduced. The simulator was previously able to produce 50° flexion due to the removal of the constraining structures however when these soft tissues were left in situ the flexion achievable by the porcine joint was approximately 20°.

4.5 Results and Discussion

4.5.1 Initial Pilot Test (Short Duration)

The 3D printed porcine shoulder joint was used to refine the methods described in Section 4.3. The initial Arduino control programme was tested and then developed using a trial-and-error approach in order to obtain the best and most fluid flexion and extension cycle of the plastic porcine joint. To assess the fluidity of the cycles, the motion was tracked using the process detailed in Section 4.3.5. The Arduino code was adapted until the simulator consistently reached a flexion and extension angle of 50 degrees.

The forces recorded in each muscle during one motion set for each three porcine samples are provided in Figure 4.21A, B and C.

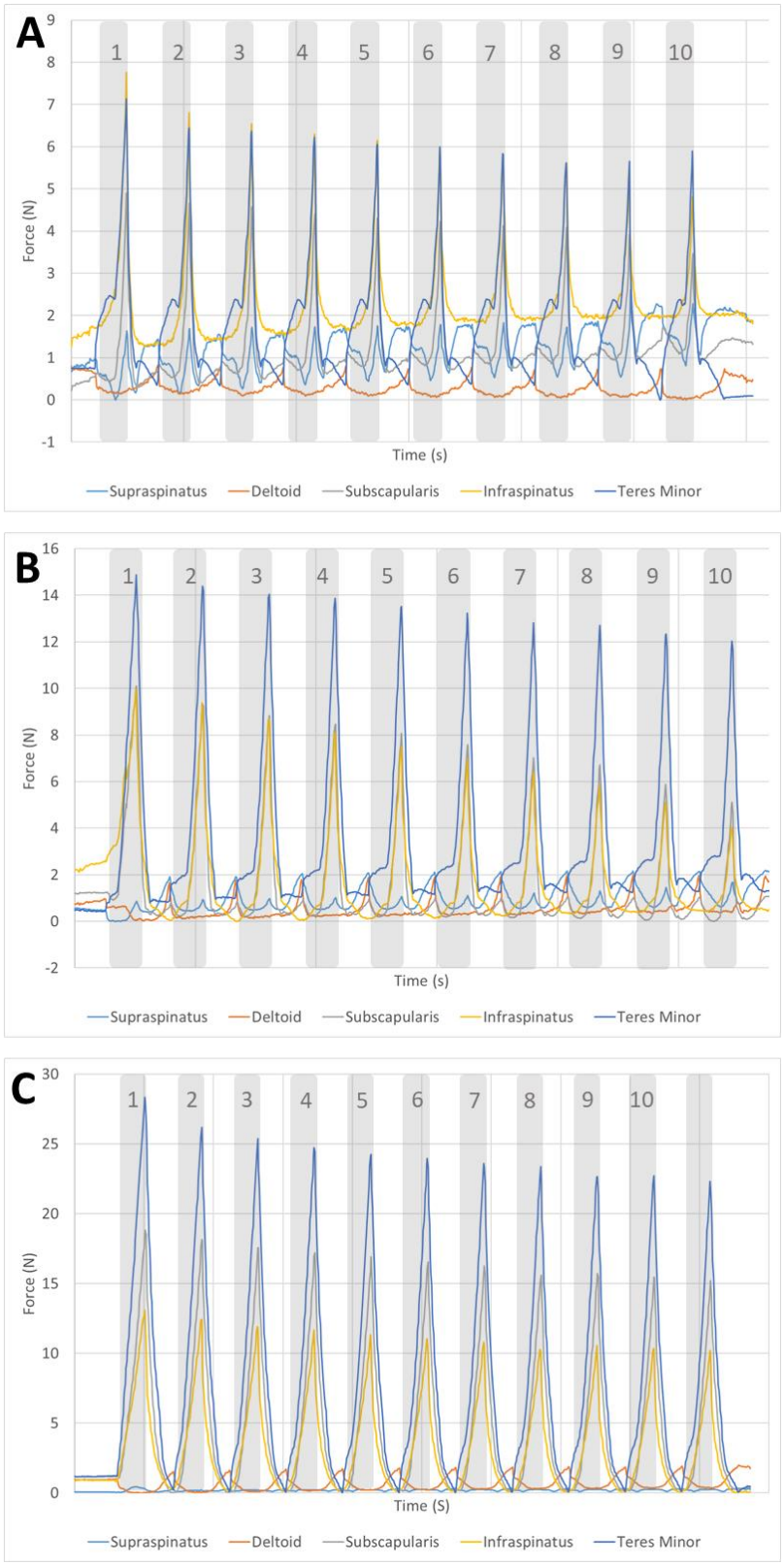

Figure 4.21 - Force required in each muscle of the porcine shoulder in order to perform a flexion and extension motion ten times. The shaded zones indicate a period of abduction and the white zones represent a period of adduction. A: Example data set from a motion set of porcine sample 1. B: Example data set from a motion set of porcine sample 2. C: Example data set from a motion set of porcine sample 3.

For each motion cycle, particularly in porcine samples 2 and 3 (shown in Figure 4.21B and C), the teres minor muscle provided the most force during the motion of flexion followed by the subscapularis and infraspinatus muscles. There was a much smaller peak of muscle force during the extension phase of the motion cycle with the majority of the muscle forces provided by the deltoid and supraspinatus muscles. Sample 1, shown in Figure 4.21A, required a peak force value of approximately 7 N in the teres minor muscle. During the same motion cycle, the maximum force required in the third sample, shown in Figure 4.21C, was approximately 30 N.

One trend that was evident from the three graphs provided in Figure 4.21A, B and C but also occurred in all other runs of the simulator is that the maximum force decreased steadily over the first 5 or 6 flexion/extension cycles to reach a plateau of the peak force. The pattern for each individual motion cycle remained consistent across the whole set of each sample.

4.5.2 Long Duration Test

The consistent decrease in peak force values during the first 5/6 motion cycles was determined to be due to difficulties in the set-up of the simulator and the positioning of the natural joint location. A considerable amount of the musculature and soft tissue surrounding the joint was removed during the dissection procedure detailed in Section 4.3.1. This led to difficulties in positioning the humeral head into the appropriate natural position within the glenoid fossa. Over the first 5 to 6 cycles the humeral head positioned itself into the natural position and hence the force in the muscles settled to a consistent pattern. In order to assess the accuracy of this hypothesis, a longer experiment was carried out which ran for thirty cycles rather than ten. The results of this test are shown in Figure 4.22.

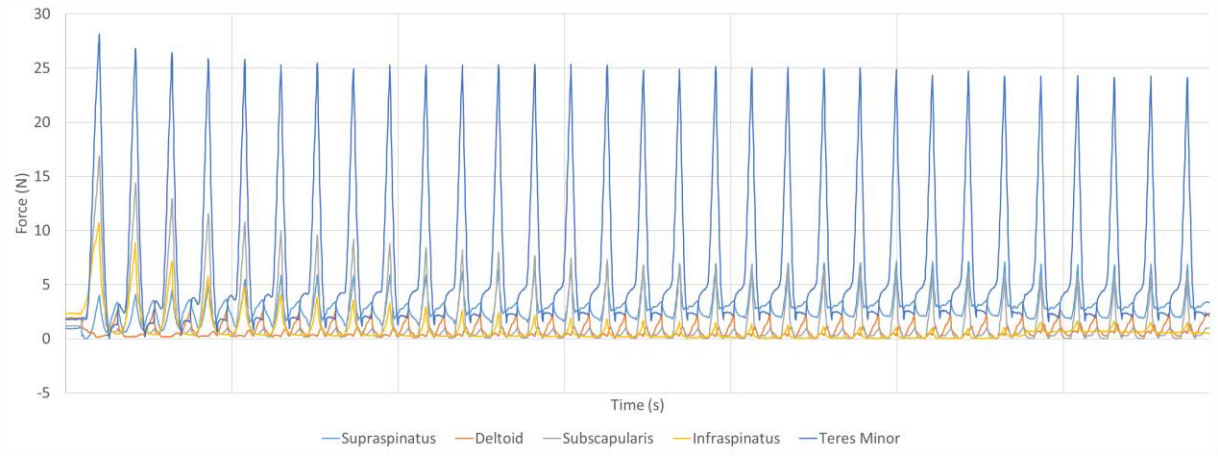

Figure 4.22 - Porcine sample undergoing the flexion and extension motion cycle thirty times.

Once again the peak force in the majority of the muscles decreased over the initial 5 motion cycles before plateauing at a constant value. The individual pattern of force required for each motion cycle was comparable throughout the set once the peak values had plateaued. In future use of the simulator, a larger number of motion cycles would be used to allow for initiation of the simulator. This is due to the results in Figure 4.22 showing that over the whole thirty cycles the force remained at the consistent value that was reached after the initial five cycles. This supported the hypothesis that these initial cycles were required in order to position the humeral head within the glenoid fossa.

During every motion cycle from all three samples, (including examples in Figure 4.21A, B and C) the teres minor muscle provided the majority of the force required for the flexion of the joint. Other muscles involved in the flexion of the joint were the infraspinatus muscle and the subscapularis. The deltoid muscle always produced force in order to extend the porcine joint. The supraspinatus muscle was inconsistently involved in both the flexion and extension motion with very low amount of force. Within the same porcine joint, the results varied between sets. This variation is shown for the infraspinatus muscle across the first sample and third sample in Figure 4.23.

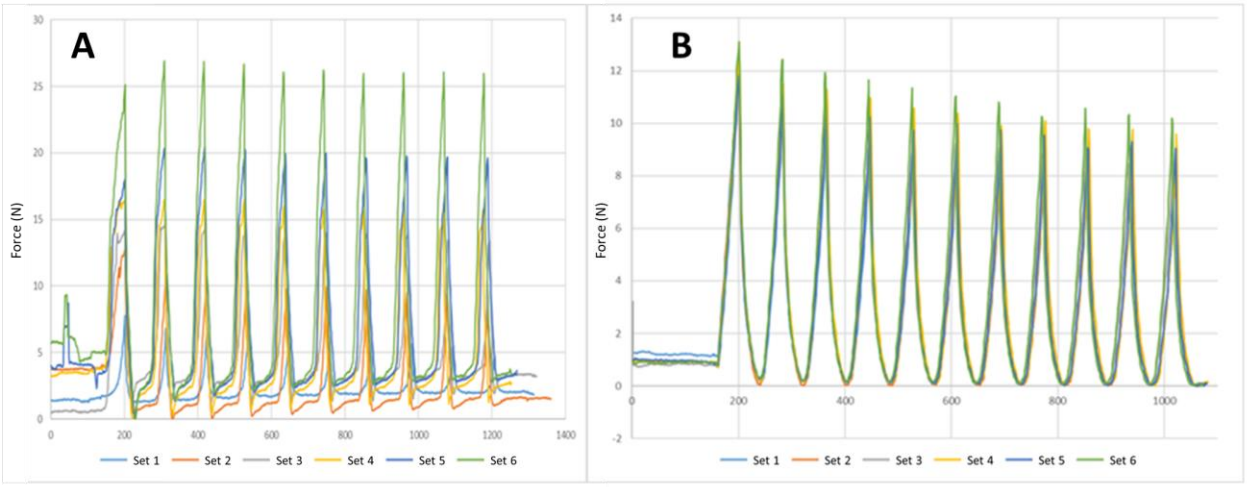

Figure 4.23- Variation across a single porcine sample for the infraspinatus muscle. Each set indicates one run through the ten flexion and extension cycles for the same sample. A - Porcine Sample 1. B - Porcine Sample 3.

There is a large variation in the results for the infraspinatus muscle across the runs of sample 1 as shown in Figure 4.23a. This variation still exists but is considerably less for the same muscle across all runs of sample 3 as shown in Figure 4.23b. The reduction of variation within the same sample was due to improvements in the set up procedure between runs of the same sample. The set up procedure was a very manual task that included the positioning of the

humeral head within the glenoid as detailed above. As the user of the simulator completed more runs with the simulator the error included in this setup procedure was decreased and hence the variation was much less for the final sample.

Section 4.3.6 detailed the development of a computational model of the porcine shoulder joint simulator using the AnyBody modelling software. The model predicted that the prime mover of flexion of the porcine joint was the infraspinatus muscle. Mathewson et al, also states that a quadruped shoulder (such as a porcine) has the infraspinatus muscle as the prime flexor (Mathewson et al., 2014). This is in contrast to the results presented above which found, using the experimental porcine shoulder simulator, that the teres minor produced greater force than the infraspinatus muscle. An alternative Arduino code was written which forced the infraspinatus motor to turn more and hence increase the force within the infraspinatus muscle throughout the flexion motion. However, that experiment found that increasing the role of the infraspinatus muscle during flexion led to a large amount of internal rotation occurring at the shoulder joint. A porcine shoulder can naturally achieve very little internal rotation (Frandson et al., 2003) due to the physical constraints provided by bony geometry and the soft tissue surrounding the shoulder joint. During both the pilot study and the long duration tests, all soft tissue was removed from the joint other than the four rotator cuff tendons and the deltoid tendon prior to use within the simulator. Therefore it was predicted that this was the reason that the joint could not perform flexion when under infraspinatus heavy control due to the lack of soft tissue constraints.

4.5.3 Porcine Capsule Test

The 3D printed porcine shoulder joint was used with the addition of an elastic band 'capsule' as detailed in Section 4.4.3. The new simulator configuration was run with the infraspinatus heavy Arduino code that previously had led to internal rotation of the joint. With the addition of the elastic band 'capsule' the shoulder performed flexion of 53° with this code. The force in the infraspinatus and teres minor muscles were recorded using the load cell platforms as described in Section 4.3.4. The force required in these two muscles throughout the flexion and extension cycle for the porcine joint with an elastic band 'capsule' is shown in Figure 4.24.

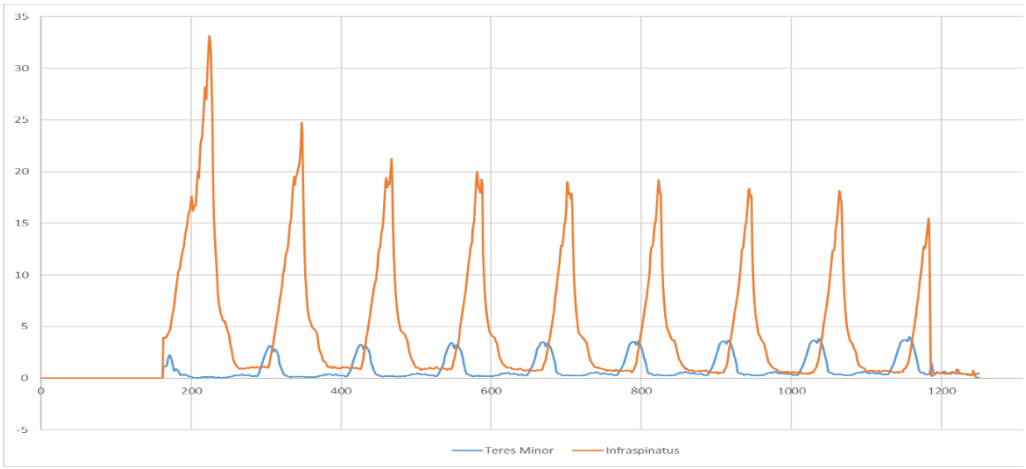

Figure 4.24- Forces in the infraspinatus and teres minor muscles during a flexion and extension cycle for a plastic porcine joint with an elastic band 'capsule'.

The results shown in Figure 4.24 indicate that the infraspinatus produced much greater force than the teres minor muscle. The decrease in peak force through the initial 5 motion cycles was still present in this test. A plateau was reached in the peak force by the fifth motion cycle.

Following on from the plastic porcine capsule test, a natural porcine joint with intact capsule and glenohumeral ligaments was used in the shoulder simulator. The flexion/extension cycle was reduced from 50° to 20° due to the presence of constraining soft tissue that surrounded the joint such as the shoulder capsule and glenohumeral ligaments.

A single porcine sample underwent the flexion and extension motion cycle six times. The force in each muscle required to perform this motion was recorded via the load cell platform system. An example set of results from one of the motion sets of the simulator is provided in Figure 4.25.

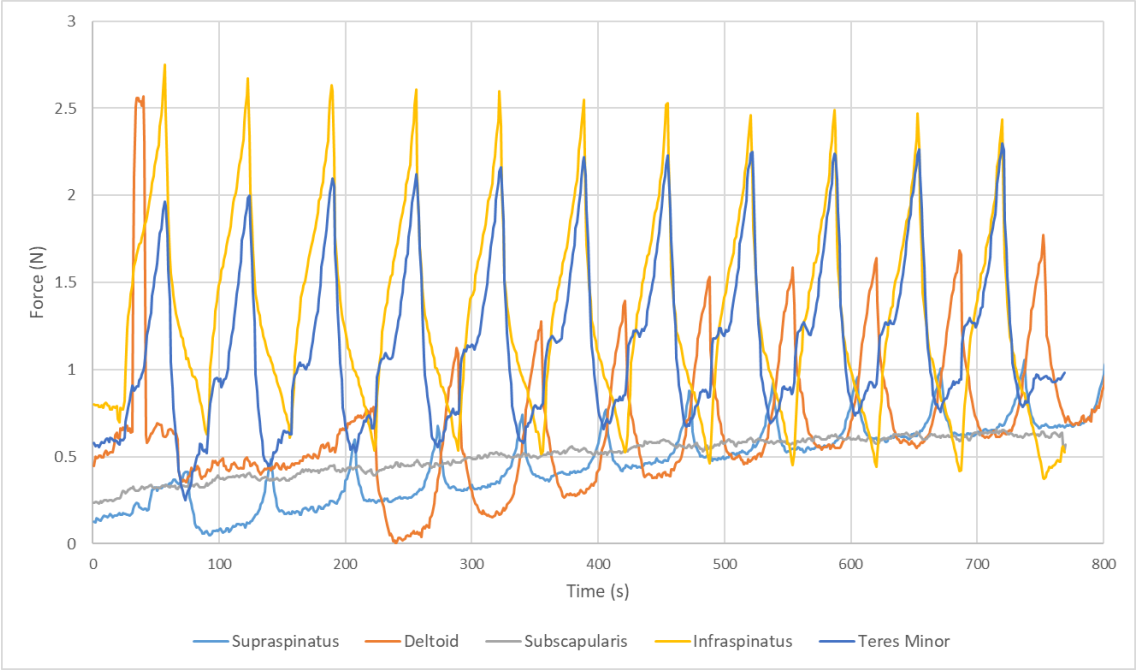

Figure 4.25- The force in each muscle required for the flexion and extension of one porcine sample that retained the shoulder capsule and glenohumeral ligaments.

Similar to previous runs of the porcine simulator, the results stabilise and become consistent after approximately 6 motion cycles. Once stabilised, the infraspinatus and teres minor muscles provide very comparable magnitudes of force and are the prime movers during the flexion phase of the motion cycle. The deltoid muscle is the prime extensor muscle however the magnitude of force required by the deltoid muscle is lower than that required by the infraspinatus and teres minor muscles during the flexion motion.

The new flexion and extension control code was assessed using a single porcine sample and the results of the force required in each muscle are provided in Figure 4.25. The primary mover in that case was the infraspinatus muscle. This aligned with the results from the AnyBody model of the same simulator configuration described in Section 4.3.6. The deltoid muscle remained as the muscle primarily required during extension of the joint.

The peak forces required for 50° of flexion when the shoulder capsule and ligaments were removed was approximately 25 N as seen in Figure 4.21. The force required when the capsule and ligaments remained, as seen in Figure 4.25, was on average 2.5 N. The large decrease in maximum muscle force was due to the much lower range of motion that the joint was capable of achieving. In the case of a removed shoulder capsule the simulator was able to achieve around 50° of flexion, however maintaining the capsule and ligaments reduced this to only 20°. Consequently the force in the system was considerably less and this was reflected across all the muscles of the joint.

Some variation between the runs of the same sample remained as shown in Figure 4.26. These were less than previously encountered due to the improvement in the user's ability at setting up the simulator in a consistent manner each time. The prime flexor in every case was the same muscle; infraspinatus, and the prime extender remained as the deltoid muscle.

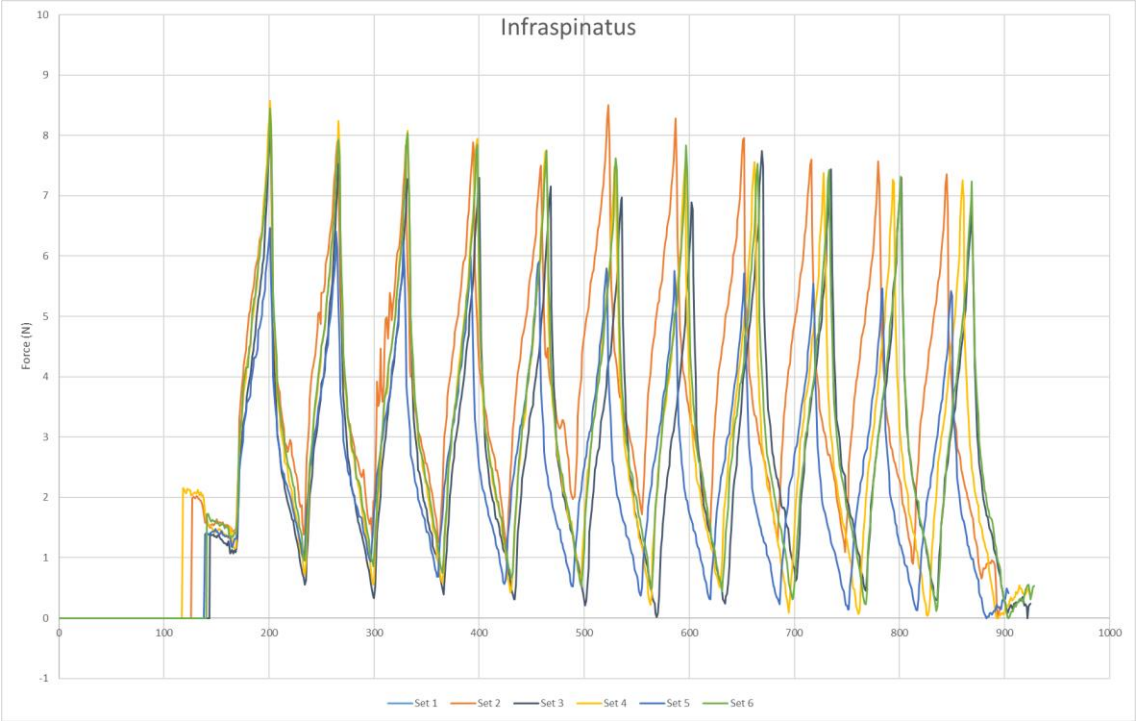

Figure 4.26- Variation in the force of the infraspinatus muscle results between the six runs of the same porcine sample that had an intact shoulder capsule and glenohumeral ligaments.

4.6 Conclusion

The shoulder simulator was designed to allow for the development of experimental methods using porcine tissue in order to make a repeatable method for the simulation of natural human shoulder joints. Variation between porcine samples was identified, particularly regarding the magnitude of force experienced by each muscle. In each case the ratio of forces between the muscles was consistent however the magnitude varied as is evident in Figure 4.21. The load measurement technique underwent considerable testing and so was not the cause for this variation. Variation between the runs of the same sample also occurred during every porcine sample however this decreased as the experimental procedure was refined. The set up between the runs of the same sample was streamlined so that minimal user involvement occurred and hence the room for error decreased. The inter-sample error was lowest for the final porcine sample which indicated that the methods were working to improve the repeatability of the simulator.

It was also found to be important that the simulator was used for at least 10 cycles. The simulator required the first 5 cycles in order to initialise and secure the humeral head into the glenoid fossa. Therefore in order to reduce the errors caused by this initiation period, a larger number of cycles was used.

The capsule and glenohumeral ligaments of the porcine joint were found to play a large role in the stability of the joint, in particular the prevention of internal rotation. By keeping these important structures within the joint, the outputs from the simulator AnyBody computational model agreed with the results from the physical simulator. The dissection process of the porcine joint with an intact joint was a more time consuming and less repeatable method than the primary method which removed all soft tissue other than the rotator cuff tendons and deltoid tendon. The results were dependant on the amount of soft tissue left surrounding the joint due to the limits this placed on the range of motion. The capsule limited the motion achievable by the joint to a more realistic porcine flexion and extension cycle which limited the use of the simulator in developing control methods for the much less constrained human joint. If the simulator was to be used to develop an accurate model of the porcine joint, then it would be imperative to keep the capsule and glenohumeral ligaments intact in order to maintain the structure of the joint. However due to the use of the simulator as a developmental tool to make a human simulator, it was determined that the range of motion of the simulator was more important than the accuracy of the porcine joint in developing the control methods.

In conclusion, a successful porcine shoulder simulator was developed which allowed for controlled motion of a natural joint. The force within each muscle/tendon unit was successfully measured throughout the motion cycles. The motion achieved was also measured by post processing of footage of the simulations. Several considerations have been identified when moving onto human tissue, particularly the importance of a capsule and ligaments and the importance of a consistent set-up procedure both between samples and within samples.

Chapter 5 – Translation from a Porcine to a Human Natural Shoulder Simulator

5.1 Introduction

A human shoulder simulator would allow for the natural shoulder joint tissue to be tested throughout a range of loading and motion cycles. In previous Chapters, the methodologies for a porcine shoulder simulator were developed. The use of porcine tissue allowed for method development studies to be conducted without the ethical burden and increased variability of human cadaveric tissue. The porcine shoulder simulator, developed in Chapter 4, enabled for repeatable cyclic testing of the shoulder through actuation of the rotator cuff muscles and deltoid. However, this highlighted some limitations arising from the use of porcine tissue such as the altered anatomy of the porcine joint and the limited motion that could be achieved with the joint. Therefore, in order to achieve a shoulder simulator to better represent the biomechanics of a human shoulder joint, human cadaveric tissue must be used.

Previous human shoulder simulators were discussed in Section 1.4.3.2 which informed some of the approach for the human shoulder simulator detailed in this Chapter. To translate the methods for a shoulder simulator from the porcine model to a human cadaveric sample, a design specification for the human shoulder simulator was created. A computational model of the human shoulder, which was previously detailed in Chapter 3, was adapted to better represent the simulator set up and hence allow for direct comparisons between the computational and experimental set-ups. Methodologies were also developed regarding the dissection and preparation of the human tissue samples.

The human shoulder simulator used cadaveric tissue preserved following the saturated salt solution method. Data was not available in the literature that could inform degradation of this type of tissue over time in terms of the effects on mechanical properties of the tissues. Therefore, a pilot study was carried out to assess the effect of time out of the saturated salt solution on the mechanical properties of the tissue to determine appropriate durations of further studies.

The main objectives of this Chapter were:

- To develop a design specification for a novel human shoulder simulator.
- To adapt the AnyBody model of the human shoulder in order to inform the design of the simulator.
- To translate the methodology of a porcine shoulder simulator to a cadaveric human shoulder simulator and demonstrate the efficacy of the simulator.

- To study the effect of time out of solution on the biomechanical changes in the tissue treated with the saturated salt solution preservation method.

5.2 Design Specification

Several limitations existed with the porcine shoulder simulator, detailed in Chapter 4, due to the restrictions related to the anatomy of the porcine joint. Consequently the porcine simulator produced very limited ranges of motion, particularly in terms of abduction/adduction. The loads within the muscles of the porcine shoulder were also limited by the orientation of the porcine joint within the simulator.

The human simulator developed needed to better re present the motions and loads that the human shoulder is subjected to in vivo to ensure clinical relevance. The design specification for the human shoulder simulator is presented in Table 5.1. The essential and desired values for each criteria are provided in the table and the rationale for each value is described in the following text.

Table 5.1 - Design specification for the creation of a human shoulder simulator (Terry and Chopp, 2000; Doriot and Wang, 2006; Felstead and Ricketts, 2017).

	Essential	**Desired**
Range of motion		
Abduction	30°	90°
Adduction	0°	20°
Flexion	60°	90°
Extension	0°	20°
Internal Rotation	30°	90°
External Rotation	10°	30°
Scapulothoracic Motion	None	None
Number of motion cycles	10	>30
Load		
Maximum force through muscle	160N	160N
Number of loaded muscles	5	6
Size		
Volume of tissue that must be included	50 x 30 cm	50 x 30 cm
Length of tendon to be retained	15cm	15cm
Control and Measurement		
Force measurement	Measurement of force in all 5 powered muscles.	Measurement of force in all 6 powered muscles.
Position measurement	2D tracking of the humerus throughout the motion cycle.	Tracking of the humerus throughout the motion cycle in 3D.

The angles for the range of motion were based upon the range of motion for an average 75 year old male subject with no shoulder pathology provided in Table 1.1 (Doriot and Wang, 2006). The rotator cuff muscles predominately have a role in the lower angles of motion before the remaining shoulder muscles (in particular the deltoid muscle) take over (Terry and Chopp, 2000). Due to the use of the simulator to understand the role of the rotator cuff muscles in the motion at the shoulder, it was deemed that producing the higher ranges of

motion through the use of the scapulothoracic joint was unnecessary. There is limited scapulothoracic motion during the first 30° of abduction and 60° of flexion at the shoulder however, beyond this the role of the scapulothoracic motion increases (Felstead and Ricketts, 2017). Due to the removal of the scapulothoracic motion, the values for abduction/adduction and flexion/extension motion were limited. Hence the minimum required values for flexion and abduction were 60° and 30° respectively. Ideally a greater range of abduction will be achieved until the impingement of the humeral head on the coracoid process of the scapula which is approximately at 90° of abduction (Felstead and Ricketts, 2017). Future adaptations of the simulator could take the additional joint motion into account in order to simulate the higher ranges of motion.

The four rotator cuff muscles (infraspinatus, supraspinatus, teres minor and subscapularis) and the middle deltoid tendon must be actuated by the simulator in order to achieve the range of motion required. Actuation of the anterior deltoid is also desirable, particularly during the flexion motion in order to achieve the higher ranges of flexion. The maximum force to be experienced in the muscles was determined using the AnyBody modelling of the natural human shoulder joint detailed in Section 3.2.

The force and position measurements were undertaken using the same methodologies as explained in Chapter 4 to obtain the force in each muscle throughout the motion and the tracking of the humerus to ensure the correct motion is achieved. A greater volume of tissue was required within the simulator due to the larger nature of the human joint compared to the porcine shoulder. However, the simulator was designed to be interchangeable from the porcine to the human samples and so this did not impact the functioning of the simulator.

5.3 Adaption of the Human AnyBody Shoulder Model

The development of the AnyBody model of the human shoulder joint was detailed in Chapter 3. Adaptions were made to the model to align it with the physical simulator to allow for comparisons to be made between the outputs of the computational model and the physical simulator. It was important for direct comparisons to be made as the computational model was used to inform design choices in the physical simulator. The muscles of the shoulder complex that were not included in the simulator were removed from the model and the pulley locations were added. The spine and clavicle were also removed from the computational model as these were not included in the simulator.

The computational model of the original natural human shoulder complex is provided in Figure 5.1A. The model of the shoulder simulator is shown in Figure 5.1B, the pulley locations and actuator location are labelled.

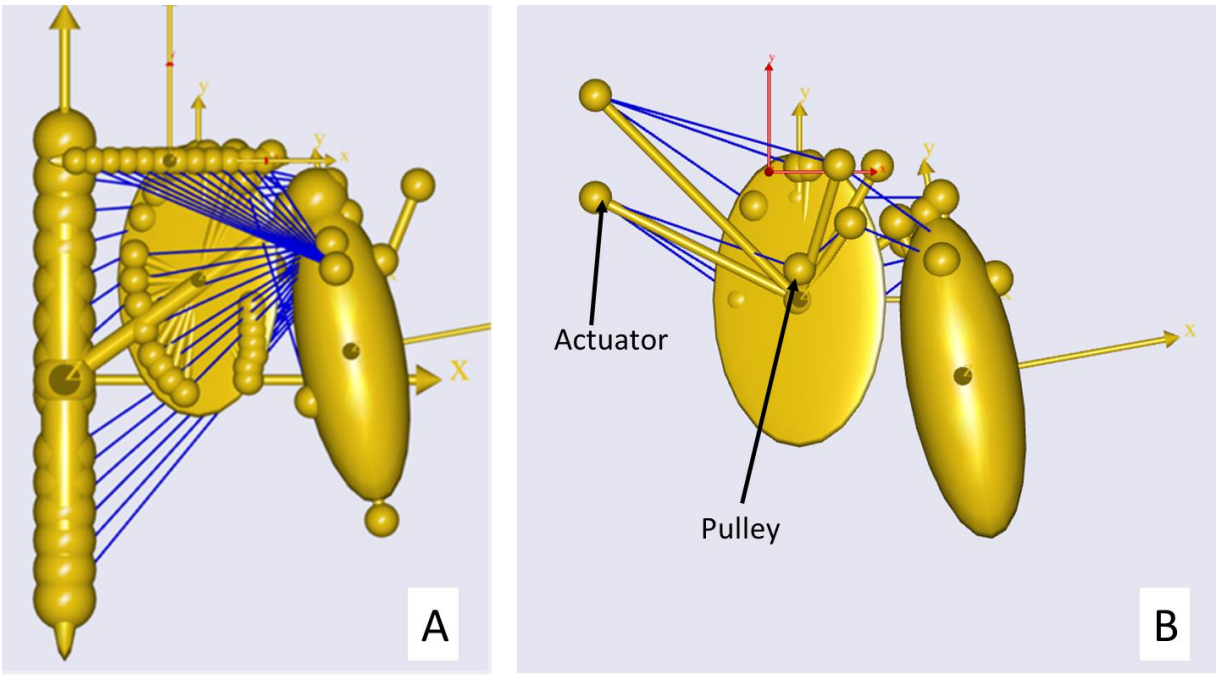

Figure 5.1 - The AnyBody computational model of the human shoulder simulator. A: The original AnyBody model of the whole shoulder complex. B: The adapted model for the physical human shoulder simulator.

The force required in each of the muscles during 100 ° of abduction derived by the simulator model are provided in Figure 5.2A and the original shoulder model in Figure 5.2B.

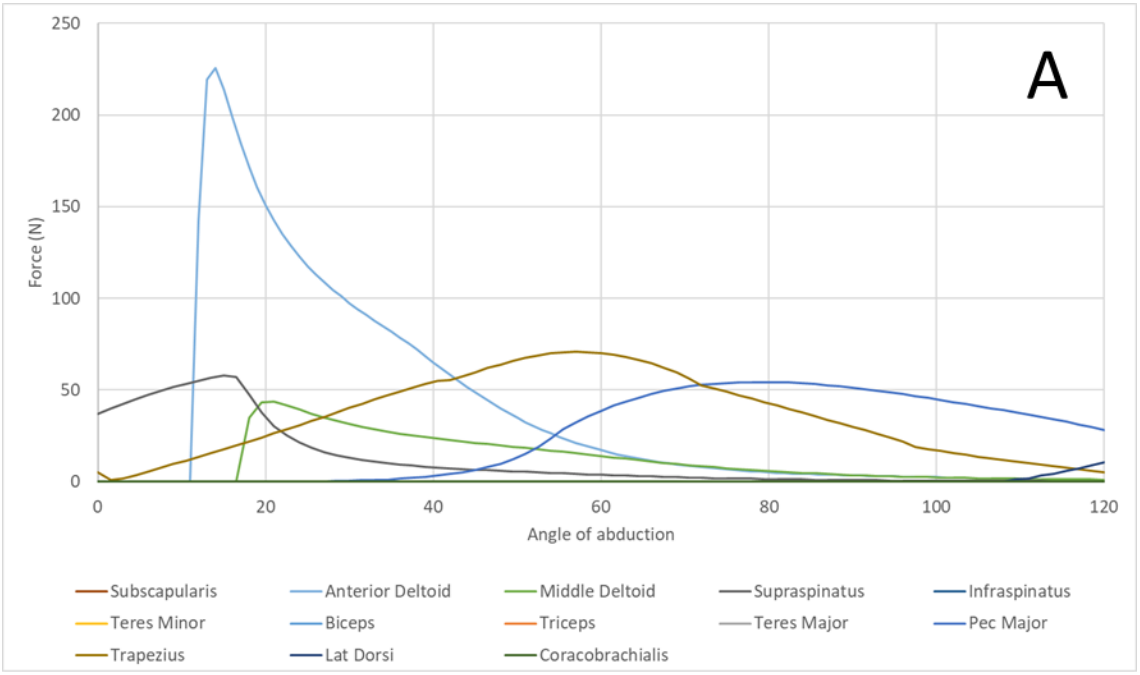

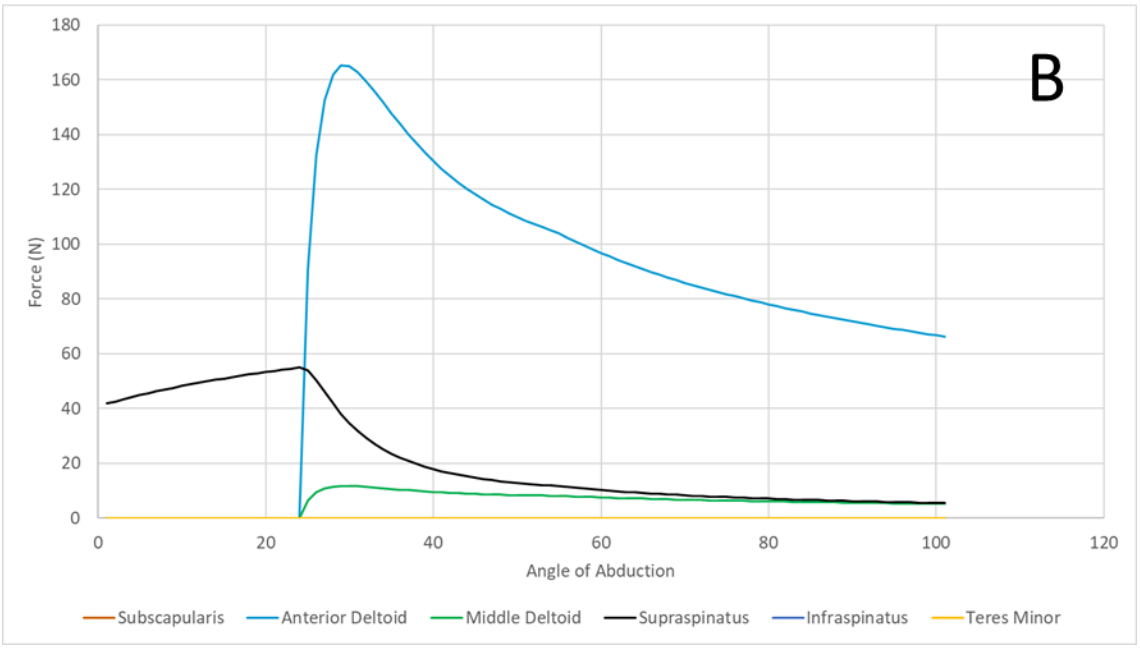

Figure 5.2 - Output of muscle forces for the adapted human simulator AnyBody model (A) and the original shoulder model (B).

The adapted simulator model had comparable results to the original full shoulder model especially during the first 60° of motion. In the original model the role of the trapezius muscle increased during the first half of the motion. This was due to the scapulothoracic motion that was programmed into the original shoulder model. The simulator holds the scapula stationary and so no scapula motion was included in the simulator computational model. For the first 30° of motion very little scapula motion occurs (Felstead and Ricketts, 2017), hence the two

models produce similar force outputs during this range. For the higher range of motion, scapulothoracic motion plays a more important role and hence the two models results deviate.

The magnitude of force is different between the two models. The peak deltoid force is 165 N for the adapted model however is 260 N in the original model. The change in load is likely to be due to the exclusion of the lower arm during the adapted human simulator model. Despite the magnitude of force being different, the ratios of forces across the different muscle groups is comparable. As the simulation will always be performed without a lower arm, the ratio of forces will be more comparable than the total magnitude of force.

The muscle forces required for abduction of the shoulder from a computational model by Karlsson and Peterson (1991) are given in Figure 5.3. The quality of the figure presentation is limited however it can be seen that the supraspinatus muscle provides force initially before decreasing as the deltoid (anterior and middle) take over as prime movers. The muscles which initiate and provide maximum force are the same in the AnyBody model of the human simulator presented in Figure 5.2 and the results from this study (Karlsson and Peterson, 1992).

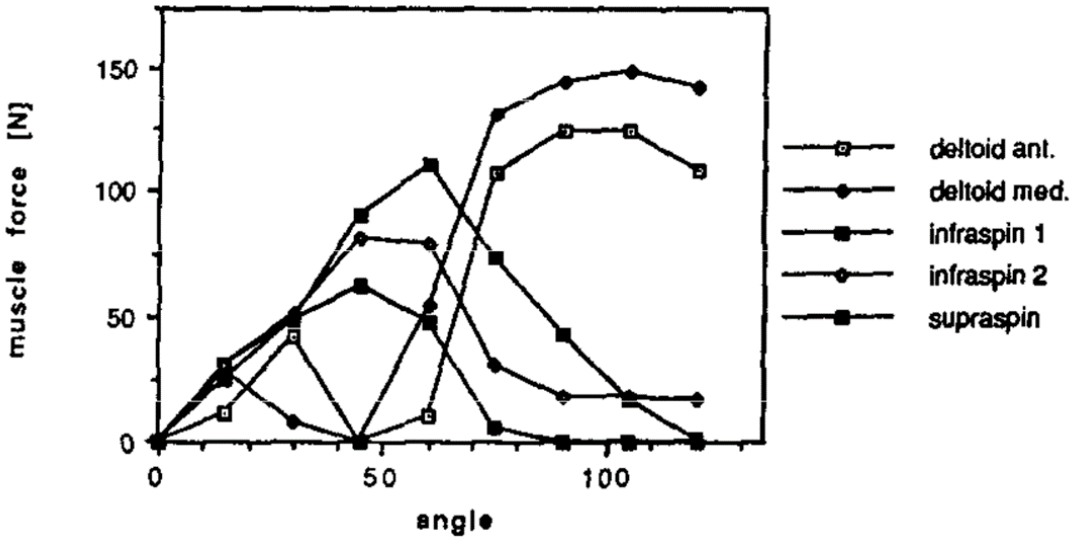

Figure 5.3 - Muscle forces required for abduction of the shoulder from a computational model by Karlsson and Peterson (1991). Image reproduced with permission (Karlsson and Peterson, 1992).

5.4 Human Tissue Methods

5.4.1 Tissue Selection

Cadaveric human tissue treated using the saturated salt solution method was used for this study due to the accessibility of the tissue within the University of Leeds. Fresh frozen human tissue is often used during biomechanical testing of joints due to the similarity to living tissue

in terms of appearance and properties. However, some limitations of this tissue type are that the tissue begins the decomposition process immediately after thawing and the effect of freeze thaw cycles on the tissue requires further investigations. Hence there is a restricte d time period in which to work with the tissue before mechanical properties and flexibility of the tissue change (Beger et al., 2020).

Human tissue preserved with the saturated salt solution method are used for orthopaedic surgical skills training (Bissonnette et al., 2019). The range of motion achievable at the preserved shoulder joint is comparable to that of the natural joint and surpasses the range of motion of a joint treated with the traditional formaldehyde method. The average values of range of motion of the shoulder are provided in Table 5.2 (Burns et al., 2018).

Table 5.2 -Range of motion (°) at the shoulder joint for a natural joint, a joint treated with formaldehyde and a joint treated with the saturated salt solution technique (Burns et al., 2018).

	Natural Living Joint	Formaldehyde	Saturated Salt Solution
Flexion	193	120	158
Abduction	132	125	160
Internal Rotation	96	89	104
External Rotation	31	94	111

The range of motion of the joint treated with the saturated salt solution technique is larger than that of the formaldehyde treated tissue for all motion types. For abduction, internal and external rotation the saturated salt solution tissue was more flexible than the natural joint. However the values for the preserved tissues range of motion are during passive motion (the tissue is moved as far as possible) which contrasts to the values for the natural tissue during active motion (relying on the muscles). The saturated salt solution tissue is able to perform the limited range of motion required by the shoulder simulator and was therefore deemed to be a suitable tissue type for use within the simulator.

5.4.2 Dissection Protocol

Experience exists within the University of Leeds regarding the dissection of human tissue, specifically the hip, knee, ankle and spine joints. The methodology for the dissection of the human shoulder was developed based upon that experience and under the guidance of the School of Anatomy faculty members and consultant upper limb orthopaedic surgeons.

The human tissue treated with saturated salt solution was obtained from the School of Anatomy after the conclusion of surgical skills training courses using the specimens. No surgical training had been conducted on the shoulders of the specimens and so the tissue had not been altered prior to dissection. The personal data of the specimens (age and gender) was collected and recorded. The recorded personal data of each sample is given in Appendix 3. Ethical approval for the use of the tissue for research was granted prior to the commencement of the study under the HTA license 12279 in the School of Anatomy and local ethics under the license LTMECH-10.

The upper limbs were firstly removed from the cadaveric torso by separating the scapula from the posterior of the ribcage. The acromioclavicular joint was disarticulated which allowed for the removal of the clavicle. The lower arm was removed at the elbow joint to leave the scapula and humerus bones alongside the soft tissue of the shoulder as shown in Figure 5.4.

Figure 5.4 – The left humerus, scapula and surrounding soft tissue following the primary removal of the clavicle, ribcage and lower arm of the human left arm (sample 1).

The outer muscles and fat of the shoulder complex were removed including the trapezius, latissimus dorsi and biceps muscles until the four rotator cuff muscles (supraspinatus, infraspinatus, teres minor and subscapularis) and the middle and anterior deltoid were identified. These muscles were dissected from the scapula leaving the humeral attachments intact. The insertions of the muscles onto the scapula were marked to ensure that they could be identified later in the set up process. The anterior, posterior and superior views of the dissected human shoulder are provided in Figure 5.5A, B and C respectively with the rotator cuff tendons and anterior and middle deltoid tendons labelled.

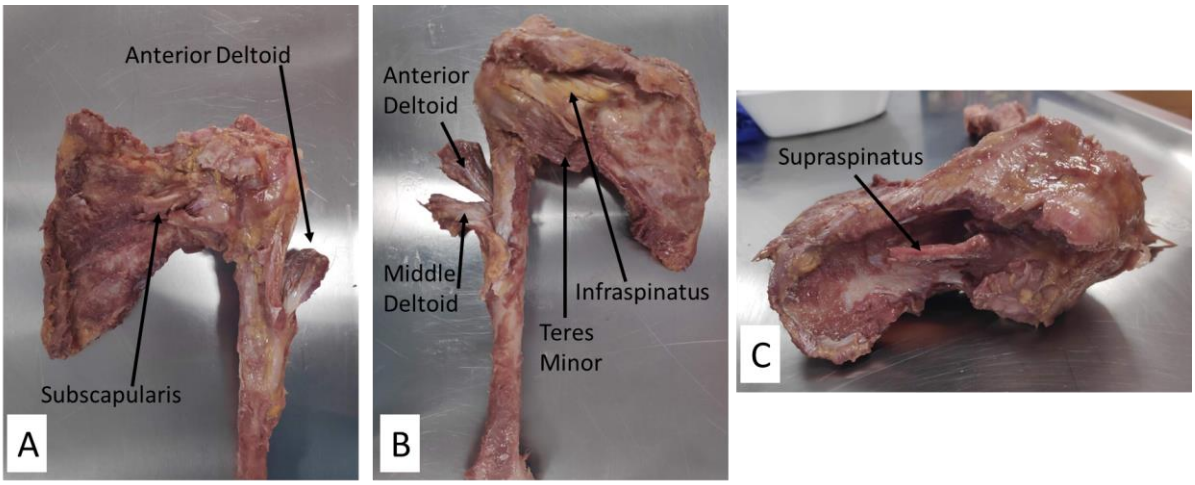

Figure 5.5 – Dissected human shoulder joint with the four rotator cuff tendons (infraspinatus, supraspinatus, teres minor and subscapularis), middle and anterior deltoid tendons labelled. A: Anterior view of the human shoulder. B: Posterior view of the human shoulder. C: Superior view of the human shoulder. All images of sample 1.

5.5 Model Development of the Human Simulator from the Porcine Natural Shoulder Simulator

5.5.1 Human Sample Preparation

The set up procedure for the human shoulder sample was developed by adapting the procedure for porcine tissue which was detailed in Section 4.3. Braided polyethylene thread (Dorisea extreme braid fishing line, Dorisea Fishing UK) was secured to the six tendon ends via the modified finger trap suture technique detailed in Chapter 2. The resultant sample is shown in Figure 5.6A. The approximate insertion location of the six tendons onto the scapula were identified during the dissection process. Eyelet screws were screwed into the human scapula at these points to act as pulleys and maintain the lines of action of the muscles and are shown in Figure 5.6B. A small bead of a two part epoxy glue (Araldite, Basel, Switzerland) was applied to the exposed screw tip to ensure that the force would not retract the screw out of the scapula.

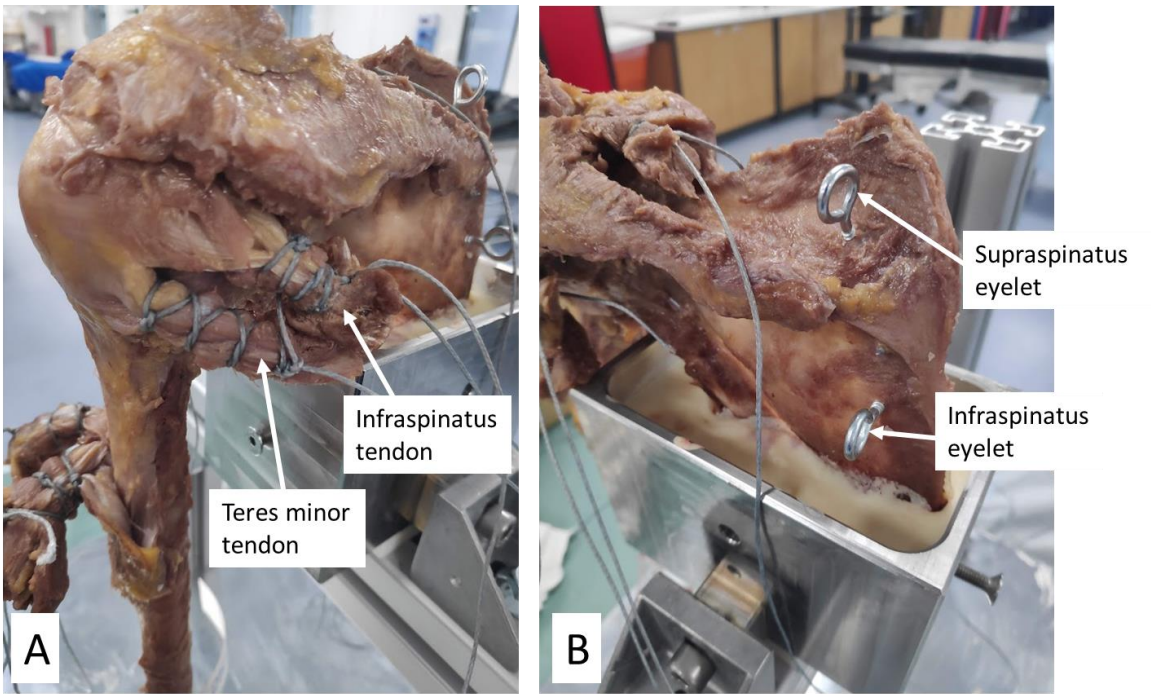

Figure 5.6 - The set-up of the human shoulder sample (sample 1). A: Posterior view of the modified finger trap suture used to connect the tendon ends to the actuation system. B: Posterior view of the eyelets screwed into the scapula at the approximate muscle insertion locations.

A fixture was designed to allow for the cementing of the human scapula whilst the joint was held in a natural position with the joint capsule intact. The fixture is shown in Figure 5.7 during the cementing process and the technical drawings are provided in Appendix 4. The human scapula was cemented into a custom made fixture using non sterile Polymethylmethacrylate (PMMA) bone cement (WHW plastics, Hull, UK).

Figure 5.7 - The custom made cementing fixture during the cementing process.

5.5.2 Human Frame Adaptions

The simulator frame was designed for the porcine shoulder simulator such that it could be repositioned to hold a human shoulder joint. Certain elements of the frame could be altered depending on if the sample was a right or left shoulder. All the positions are marked so that the components were placed in consistent locations on the frame. The addition of a screen between the human tissue sample and the electronic components of the simulator allowed for the electronics to be better protected from any liquid that may be sprayed. The frame in the set up for testing a human cadaveric sample is shown in Figure 5.8.

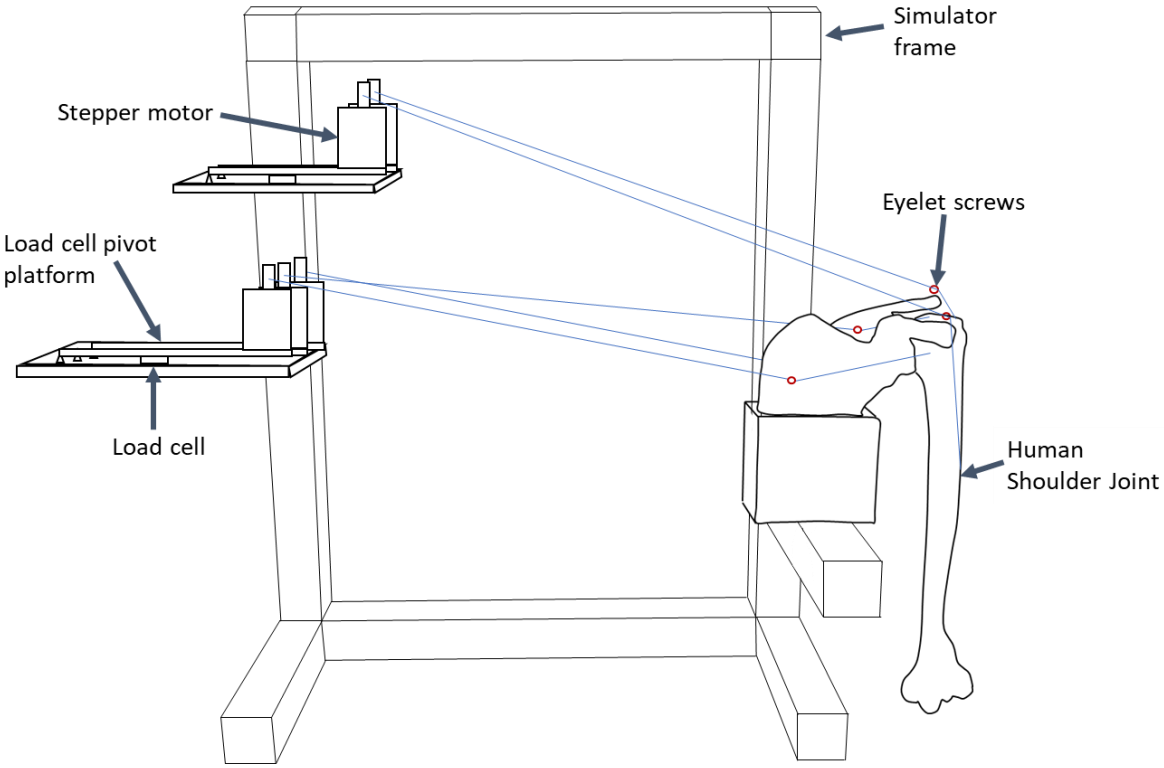

Figure 5.8 – Schematic of the frame set up for the human cadaveric shoulder, showing key parts.

5.5.3 Actuation and Sensing Methods

The actuation method is based upon that used in the porcine shoulder simulator and described in Section 4.3.3. In the human simulator, six tendons were required to be actuated. The addition of the anterior deltoid tendon was required due to its important role in the flexion of the human shoulder as discussed in Section 3.4. Due to the limitations of using an Arduino Mega control board (Arduino, New York USA), only five stepper motors could be independently controlled at any one time. Hence the infraspinatus and teres minor muscles were actuated using the same stepper motor. This pair of muscles were selected as the force s produced by these muscles during simulations of abduction/adduction and flexion/extension using the AnyBody model described in Chapter 2 were very similar.

The load and position sensing methods used were the same as the methods developed using the porcine tissue. Button load cells, FX1901-0001-0025-L (TE Connectivity, Schaffhausen, Switzerland), were used in a pivoted load measurement platform. Equation 4.4 was used to calculate the loads experienced by each muscle throughout the motion cycle. A still image was taken from the beginning of the recording of the motion cycle. Image J (Image J, Maryland, USA) was used to measure the angle (θ) from horizontal to the polyethylene thread for each muscle.

The position of the humerus was tracked throughout the motion cycle to allow comparisons to be made between the expected motion and the actual performance of the simulator. A Canon EOS 550d camera (Canon, Tokyo, Japan) was placed on a tripod which was positioned 1 m away from the human shoulder simulator. The camera was used to record each motion set and the resultant video was post processed using a custom Matlab script as described in Section 4.3.5. This tracked the position of two markers throughout the video to calculate the maximum and minimum angle of each motion.

5.5.4 Applied Motion and Load Cycle

The motion selected for the preliminary human testing was a flexion/extension motion cycle and an abduction/adduction motion cycle. These motions were selected due to the frequency of the motions within the activities of daily living. The scapulothoracic motion was not to be modelled in order to prevent additional complexity of the design as detailed in Section 5.2. Consequently, the maximum abduction and flexion angle that the simulator could reach was limited due to the impingement of the humeral head onto the acromion of the scapula (Lugo et al., 2008).

The AnyBody computational model of the human shoulder simulator detailed in Section 5.3 was used to initially design the control cycle for the stepper motors. The ratio of forces required in each muscle to produce the abduction/adduction and flexion/extension motions during the computational model was used to calculate the ratio of motion required in each corresponding stepper motor. An initial Arduino (Arduino, New York, USA) programme was developed to control the five stepper motors using these calculations. The initial Arduino programme was then developed further using a trial-and-error approach to adjust the rotations in each stepper motor, in order to achieve the best and most fluid motion cycles.

From the Anybody computational model detailed in Section 5.3 it was deemed that the deltoid muscle must be separated into two bundles in order to achieve the full range of motion of the shoulder. In the porcine model the anterior, middle and posterior portions of the deltoid muscle were able to be approximated to a single insertion location on the scapula due to the small role that this played in the motion. However, the anterior and middle/posterior bundles of the deltoid muscle in the human shoulder play two separate roles in the actuation of the shoulder due to the different lines of actuation of the muscle. The middle/posterior deltoid is required more in abduction/adduction motions however the anterior deltoid is necessary for the flexion of the shoulder due to its insertion on the much more anterior portion of the acromion. Consequently the muscles required to be powered in the human shoulder simulator were the four rotator cuff muscles (supraspinatus, subscapularis, infraspinatus and teres

minor) along with the anterior and middle/posterior deltoid. Due to restrictions with the control methodology, only five independent muscle controls could be performed at any time. Therefore, due to the results shown in Figure 5.2 and discussions with orthopaedic surgeons, it was decided to control the infraspinatus and teres minor muscles together due to their similar roles within the abduction/adduction and flexion/extension motions of the shoulder.

5.6 Final Human Shoulder Simulator Design

The final design for the human shoulder simulator is provided in Figure 5.9. The key components of the simulator are labelled including the stepper motors which allowed for active control of the retained tendons. The active control of five muscles was required in the design specification detailed in Table 5.1. It was desired to be able to provide active control of the six retained muscles of the shoulder joint (anterior deltoid, middle deltoid, infraspinatus, supraspinatus, subscapularis and teres minor) however due to the limitations with the control board this was not possible as detailed in Section 5.5.4. Consequently the teres minor and infraspinatus tendons were controlled together due to their similar roles in the abduction and flexion motions as demonstrated using the computational AnyBody model.

The load cell and load measurement platforms were also labelled in Figure 5.9. The methodology for the calculation of total force in the tendons based upon the load cell readings were provided in Section 4.3.4. The forces recorded for the infraspinatus and teres minor muscles were the same as they were controlled together using the same stepper motor. Force measurements were recorded for all muscles throughout all motion cycles of both abduction/adduction and flexion/extension.

Motion tracking markers were applied to the tissue and the motion was tracked using the methodologies developed with the porcine simulator detailed in Section 4.3.5. The cycles were recorded which enabled the maximum abduction and flexion angles to be determined.

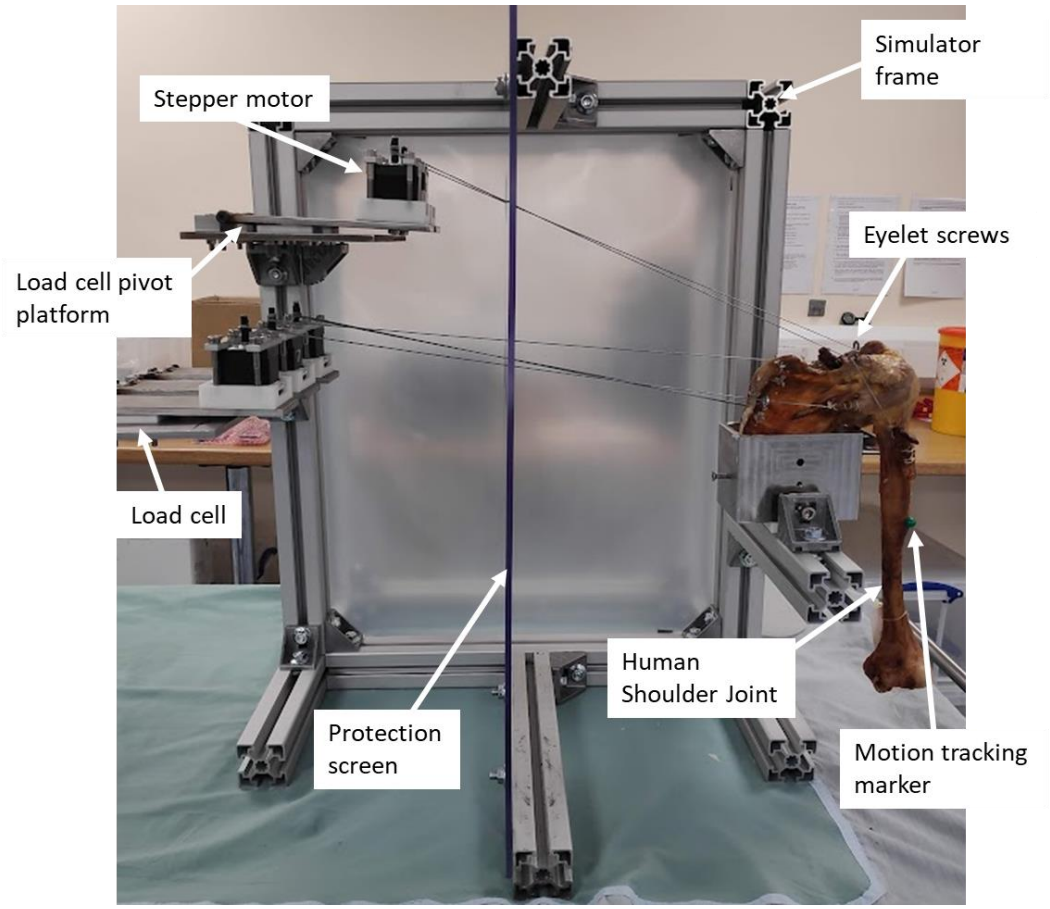

Figure 5.9 - Photograph of the human shoulder simulator with key components of the design labelled (sample 1).

5.7 Preliminary Human Shoulder Simulator Study

5.7.1 Overview

The human shoulder simulator discussed in this Chapter translated the methodology from a porcine simulator to enable human cadaveric shoulder joints to be tested. The aim of the preliminary human tissue study was to ensure that the human tissue was suitable for use within the shoulder simulator and that the force measurement system developed with the porcine model was appropriate for the human simulator.

5.7.2 Methods

A single sample treated with the saturated salt solution method was used in the simulator. The sample was dissected and the simulator set up as described in Section 5.5. The motion selected to be performed by the simulator was a flexion/extension motion cycle and an

abduction/adduction motion cycle. These motions were selected due to the frequency of the motions within the activities of daily living. As specified in the design specification in Section 5.2, the scapulothoracic motion was not to be modelled in order to prevent additional complexity of the design. Due to this limitation, and the role of the rotator cuff muscles in the lower ranges of motion, the angles of flexion/extension and abduction/adduction to be performed by the simulator were 60° and 30° respectively. The Arduino code used to control the motors was tuned in order to achieve the full ranges of motion using the same method as for the porcine simulator which is detailed in the flowchart in Figure 4.16.

The tissue was removed from the saturated salt solution, dissected, set up and was subjected to a testing regime of three repeats of 10 cycles of the flexion/extension motion and the abduction/adduction motion. This testing regime was the same protocol as was developed for the porcine tissue and shown in Figure 4.18.

The resultant forces from each muscle during the simulation process were recorded for every cycle and repeat of motion cycle. A uniform weight of 0.6 kg was applied axially to each load cell prior to the simulation regime commencing in order to enable calibration of each of the load cells for each cycle. The calibration value was applied to each reading for each load cell through the cycle. A Matlab (Mathworks, Massachusetts) script then used the equation provided in Section 4.3.4.1 to calculate the force in the braided thread based upon the reading from the compression load cell and the angle of the corresponding cord into the motor as measured using imageJ (Maryland, USA) as detailed in Section 4.3.4.1. Each motion cycle was repeated three times which resulted in three repeats of force data for each muscle through the motion cycle. This then enabled a mean of all the measurements at each time point to be found resulting in a mean motion cycle for the sample. In order to ensure that the cycles were in phase prior to the mean calculations, the first supraspinatus peak was aligned in all repeats.

5.7.3 Results and Discussion

The simulation was successfully completed for the cadaveric human sample. An example of a single repeat of an abduction/adduction motion cycle is provided in Figure 5.10. Each line represents the force in a muscle during the ten cycles of the abduction/adduction motion.

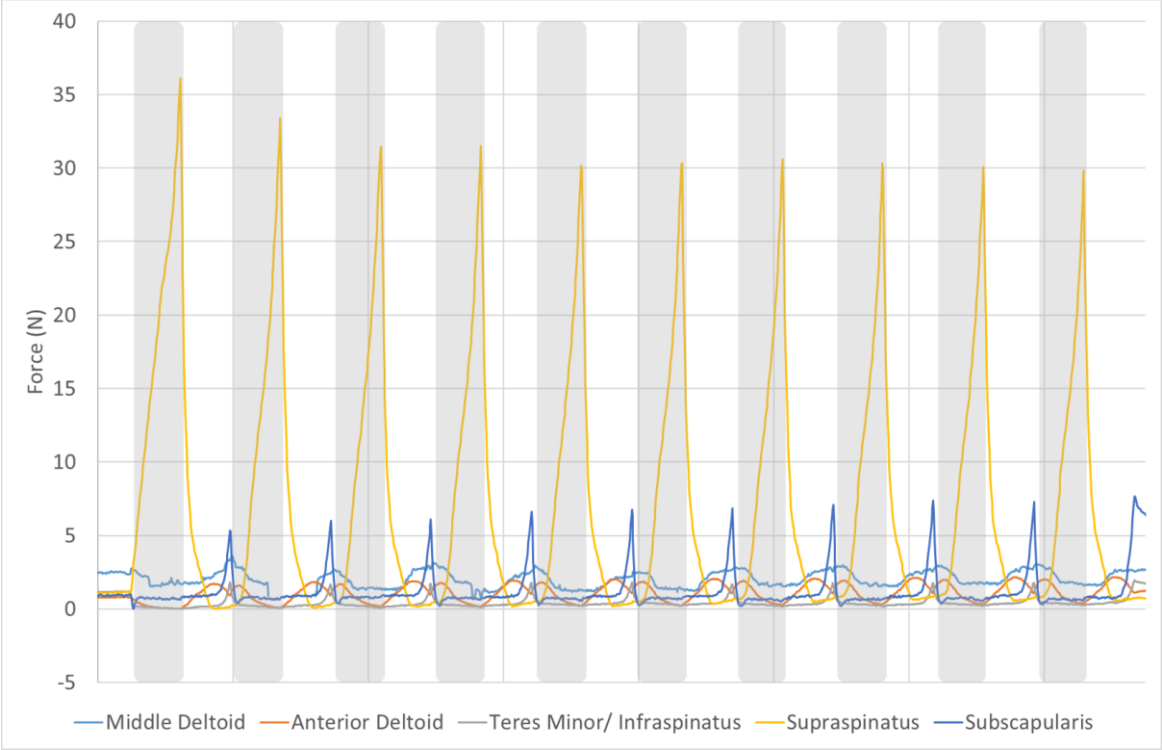

Figure 5.10 - An example of a force graph for a single repeat of the abduction/adduction motion with sample 1. The grey zones highlighted are the periods of abduction and the white zones refer to periods of adduction.

The maximum force in all the muscles, decreased over the first five cycles to reach a plateau of the peak force. This was also found in the porcine studies conducted in Chapter 4. This was postulated to be a result of repositioning of the shoulder joint at the start of movement. The supraspinatus muscle contributed the most force to the abduction motion which corresponds to literature which states that the supraspinatus muscle was responsible for the initiation of the abduction motion (Lam and Bordoni, 2021; Mancuso et al., 2021; Abdelwahab et al., 2021).

The mean peak supraspinatus force for cycles 6-10 of the three repeats of the abduction/adduction motion are given in Figure 5.11. Each repeat has consistent peak supraspinatus force between the cycles 6-10 as seen by the small ranges given for each repeat in Figure 5.11.

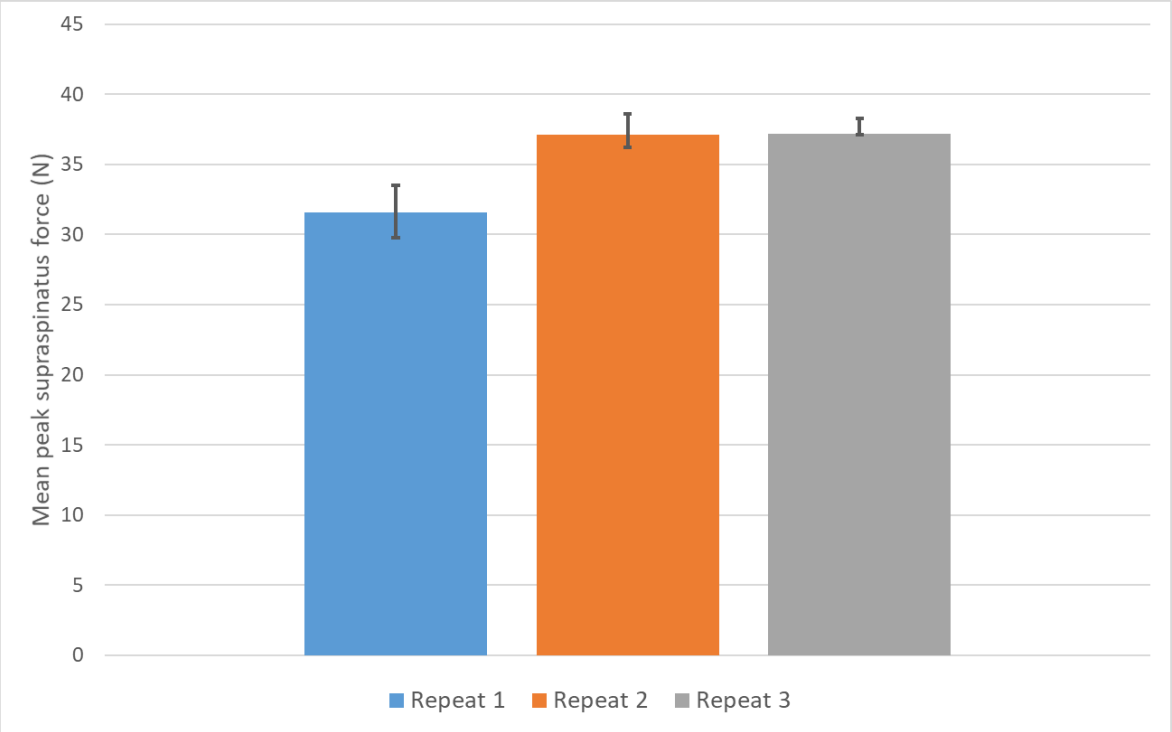

Figure 5.11 - Mean peak supraspinatus force for cycles 6-10 of the three repeats of the abduction/adduction motion cycles. The range for each repeat are given.

The mean of the supraspinatus force for each repeat for the cycles 6-10 of the abduction/adduction motion was determined to produce a mean cycle of the supraspinatus force. The ranges across the whole of the 6-10 cycles are plotted alongside the mean cycle and given in Figure 5.12. The ranges were smallest during the increase and decrease of the supraspinatus force. However, during the point of minimum abduction, when the supraspinatus force was minimal, the ranges were largest suggesting inconsistencies between the repeats at these low values.

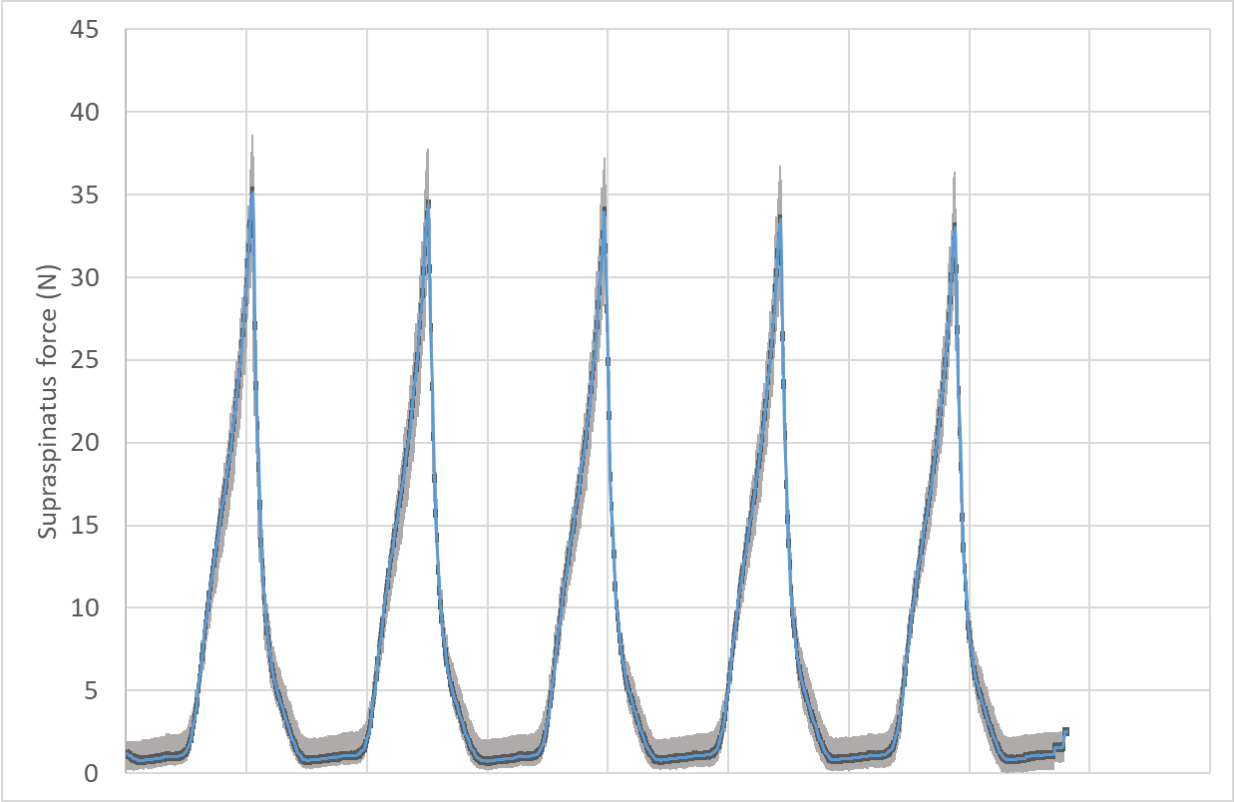

Figure 5.12 - Mean of the force against time for each repeat for the cycles 6-10 of the abduction/adduction motion. The range for each data point are also plotted (grey).

5.8 Pilot Study: Effect of Time on Tissue Properties

5.8.1 Overview

The aim of the study was to assess the effect of time following removal from the saturated solution on the biomechanical properties of the cadaveric shoulder tissue. The range of motion of the embalmed tissue was comparable to that of the natural joint (Section 5.4). Preserved tissue prevents the decrease in tissue properties due to the rapid putrefaction of fresh frozen samples (Hayashi et al., 2014). The tissue can be stored in the embalming fluid for 18 months without showing any signs of degradation (Lombardero et al., 2017), however, once removed the tissue will start to degrade. Burns et al. found that there was little difference in the appearance, odour, feel and suitability of the tissue after 15 days out of the solution (Burns et al., 2018). To inform future cadaveric shoulder studies using this tissue type, an investigation on the degradation and resultant change in properties of saturated salt solution tissue over time was conducted.

5.8.2 Methods

Due to limited overall availability of human shoulder tissue, this study used the same sample as utilised in the preliminary study. The tissue was prepared, dissected and set up within the simulator in the same was as described in Section 5.5. After conclusion of the preliminary test,

the tissue was stored out of the embalming fluid at room temperature for 14 days and retested. This was continued for 4 time points, each 14 days apart, over a total time period of 6 weeks (0/2/4/6 weeks). The resultant force in each muscle during the simulation process were recorded for every cycle and repeat of motion cycle.

5.8.3 Results and Discussion

The simulation was completed at each of the time points over a 6 week period and th e muscle forces were recorded for the motion sets and repeats described previously. Force graphs (Figure 5.10) were recorded for each of the three repeats at each time point. In order to provide a consistent point within the cycle to compare the behaviour of the tissue, the maximum point of abduction (30°) and minimum point of abduction (0°) were taken. The mean contribution of the total force being applied to each muscle at each minimum and maximum abduction across the four time points are given in Figure 5.13. The 95% confidence interval for each percentage contribution for the five muscles are also given in Table 5.3.

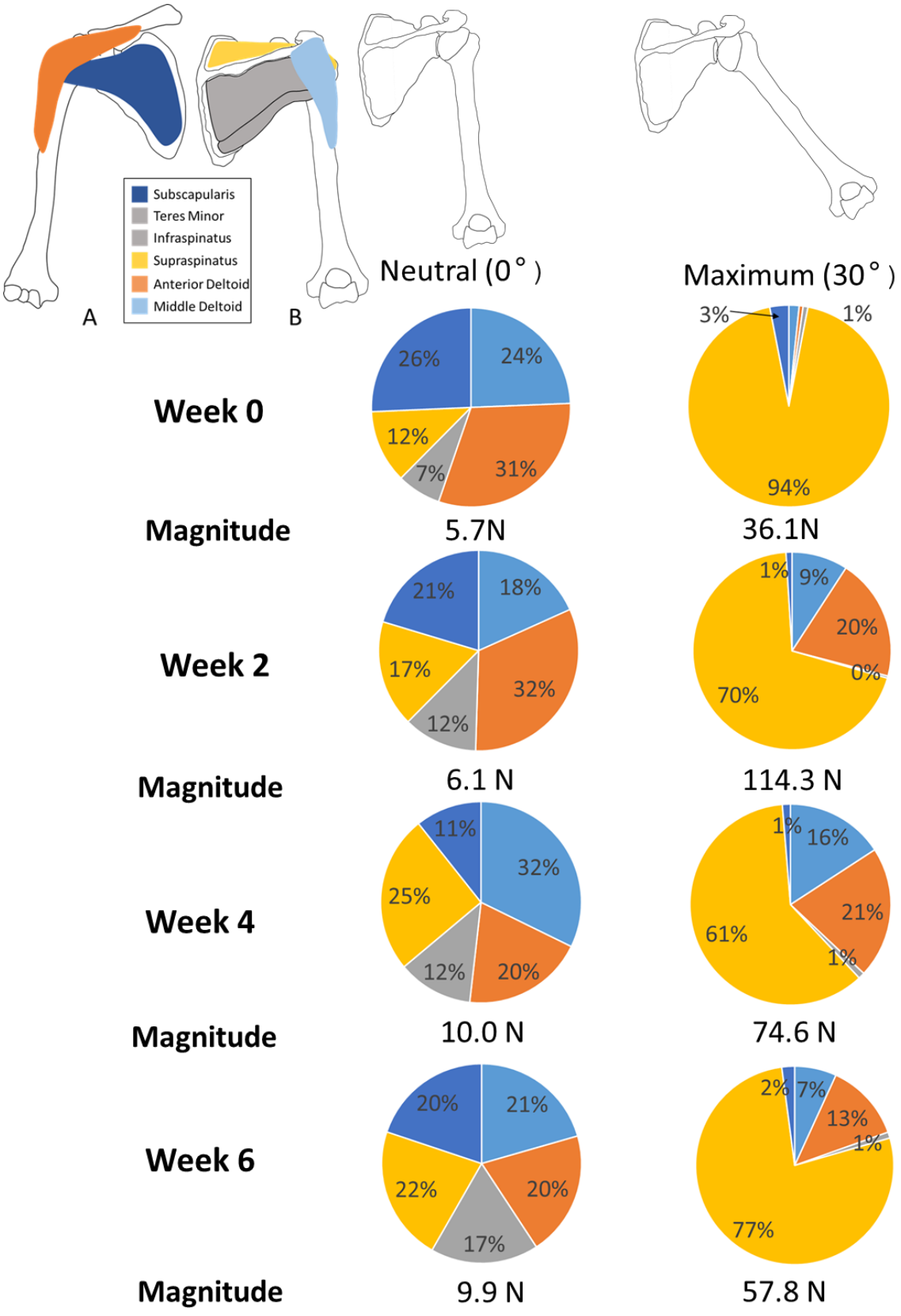

Figure 5.13 - The mean contributions of the total force by each muscle at minimum and maximum abduction for the four time points (week 0, 2, 4 and 6).

Table 5.3 - Percentage contribution of each muscle during the repeats of the abduction motion through the four time points with the 95% confidence interval. The shaded cells are consistent with the colour of the respective segment in the pie charts displayed in Figure 5.13

Week	Middle Deltoid	Anterior Deltoid	Teres Minor/ Infraspinatus	Supraspinatus	Subscapularis
	Neutral (0°)				
0	24 ± 4.0%	31 ± 1.6%	7 ± 0.8%	12 ± 4.4%	26 ± 4.6%
2	18 ± 0.9%	32 ± 2.0%	12 ± 1.6%	17 ± 2.6%	21 ± 3.7%
4	32 ± 2.6%	20 ± 2.8%	12 ± 1.1%	25 ± 5.5%	11 ± 1.5%
6	21 ± 2.7%	20 ± 1.4%	17 ± 5.5%	22 ± 7.4%	20 ± 4.9%
	Maximum (30°)				
0	1 ± 0.8%	1 ± 0.1%	1 ± 0.1%	94 ± 0.9%	3 ± 0.6%
2	9 ± 2.3%	20 ± 3.7%	0 ± 0.1%	70 ± 5.9%	1 ± 0.2%
4	16 ± 3.0%	21 ± 1.6%	1 ± 0.1%	61 ± 4.3%	1 ± 0.2%
6	7 ± 1.1%	13 ± 0.5%	1 ± 0.1%	77 ± 1.2%	2 ± 0.6%

Some similar trends were observed across all time points at which the tissue was assessed. The ratio of the forces between the different muscles at specific angular positions during the cyclic is shown in Figure 5.13. In all cases, at 30° abduction, the supraspinatus muscle provided the most force followed by the anterior and middle deltoid muscles. However, the proportion and magnitude of force that was provided by the supraspinatus muscle varied greatly between time points. At week 0, 94% of the force was provided by the supraspinatus muscle, this decreased to 70%, 61% and 77% in weeks 2, 4 and 6 respectively. As well as the contribution of supraspinatus force changing through the time points, the magnitude of total force also changed. At week 0 the total force was 36.1 N, this increased greatly to 114.3 N at week 2 before decreasing through weeks 4 and 6 to 74.6 N and 57.8 N respectively. The initial large increase in force was predicted to be due to the drying out of the tissue following removal of the tissue from the embalming fluid. The tissue visibly started to degrade past week 2, becoming more flexible leading to the lower forces required for the same angle of motion. The confidence intervals at the maximum angle of abduction do not increase through the time period suggesting that the results from the simulator remained consistent within repeats and within the cycles at a specific time point.

At 0° of abduction, the split of force is different at each time point and the 95% confidence intervals are larger than at 30° abduction as seen in Figure 5.13. Each muscle contributes in each case, indicating the force required to hold the shoulder in place and prevent dislocation however the ratio is not consistent between time points. The shoulder capsule plays an

important role in maintaining the structure of the joint at the neutral position and so changes in the stiffness and mechanical properties of the capsule would affect the force that each muscle must undergo to prevent dislocation. The magnitude of force in each muscle is also considerably lower at 0° abduction and so a smaller change in magnitude of each muscle force would lead to a larger effect on the percentage alongside the measurement error of the load cells.

5.8.4 Summary

Through the completion of this study it was shown that there was an important effect caused by the tissue degradation over time. In order to minimise the effect, all testing should be aimed to be completed within 14 days of removal of the tissue from the embalming fluid and if suitable the tissue should be stored in the fluid between testing days. Throughout the experimental protocol, the tissue should be sprayed with water to maintain hydration and lower the effect of the tissue drying out on the results. It was also concluded that longer motions, of at least 20 cycles should be conducted in order to allow for the tissue settling period that occurs during the first five cycles of the motion.

5.9 Conclusion

The porcine shoulder simulator detailed in Chapter 4 was modified to be compatible with a human shoulder joint. Human cadaveric tissue treated with the saturated salt solution method was selected for use within the simulator due to the accessibility of the tissue and the appropriate functional characteristics of the tissue. The tissue was dissected by consultant shoulder surgeons to ensure an accurate and repeatable methodology was created.

The human shoulder simulator actuates tendons (infraspinatus, supraspinatus, teres minor, subscapularis anterior deltoid and posterior/middle deltoid) of the shoulder joint to produce flexion/extension and abduction/adduction motions. A computational model (AnyBody) of the shoulder was adapted to reflect the simulator constraints and set up. The results from the computational model informed the inputs into the control of the simulator in order to produce the desired motions.

The simulator was used with cadaveric tissue preserved using the saturated salt solution method. The preliminary tests suggested that repeatable results for the force in each muscle through the motion of abduction could be obtained through the use of the simulator with human tissue. The preserved tissue underwent a degradation process when the tissue was left out of the solution over a period of weeks. Consequently, all future testing with this tissue type will be conducted within 14 days of the removal of the tissue from the fluid and if suitable, the tissue will be stored in the fluid between testing days.

Chapter 6 – Application of the Human Shoulder Simulator

6.1 Introduction

The methods developed for a porcine shoulder simulator were translated to a human cadaveric simulator and the efficacy of the simulator demonstrated (Chapter 5). Additionally a study was carried out to assess the effects of time following the removal of the cadaveric tissue from saturated salt solution on the mechanical properties, and information used to determine durations of future studies.

Clinically, the double row repair method is the current standard surgical technique for the repair of the supraspinatus tendon, however there is limited functional preclinical testing of this method (Pandey and Jaap Willems, 2015). Most biomechanical studies looking at the strength of the double row repair method used a tensile testing machine with cyclic loading of the repair (Meier and Meier, 2006; Kingdom, 2006; Kulwicki et al., 2010). This does not assess the strength of the fixation during multidirectional functional movements of the shoulder. There is also not the ability to determine the change in muscle forces from the intact state through the tearing process to a repaired rotator cuff due to the single point of testing performed in these studies. Therefore, the aim of this study was to assess the impact on muscle forces of a rotator cuff tear and a double row repair of the rotator cuff using the human shoulder simulator to apply functional loading to the tendons of the shoulder joint.

The main objectives for this Chapter were:

- To use the human shoulder simulator to assess the repeatability of the simulator at producing cyclic motion over 50° abduction and 70° flexion.
- To study the change in muscle forces between the intact rotator cuff, a rotator cuff tear and a double row repair of the rotator cuff.

Overall four cadaveric samples were available for the studies detailed in Chapter 5 and in this Chapter. Sample 1 was used in the first study to investigate the effect of time following removal from the saturated salt solution on tissue biomechanics detailed in Chapter 5. The remaining samples (2, 3 and 4) were used for the second study to look at the effect of rotator cuff tears and repairs on the internal muscle forces of the joint.

6.2 Study Design

6.2.1 Range of Motion

Three cadaveric shoulder samples were available for this study (samples 2, 3 and 4). Following the conclusion of the previous study (Chapter 5), the angle of motion applied was reviewed. In

Chapter 5, a limited range of motion had been used due to the role of the scapulothoracic joint at the higher ranges of motion. However, if an abduction motion to the point of impingement of the humeral head onto the acromion is used, then this enables a wider range of motion to be achieved, thus providing additional understanding of the biomechanics of the shoulder joint throughout the abduction and flexion motions. Consequently a larger range of motion of 50° abduction and 70° flexion was selected for testing in this Chapter. To enable comparisons to be made between sample 1 (Chapter 5) and the samples in this study (Chapter 6), an initial objective was to compare the effects of the limited (detailed in Section 5.7) and extended range of motion (detailed above). The remaining samples (3 and 4) were tested under the extended motion cycles only. All motion sets included 20 motion (abduction/adduction or flexion/extension) cycles to account for the initial bedding in process that occurred during the first 5 cycles described in Section 5.7.

6.2.2 Incorporating Rotator Cuff Tears into the Shoulder Simulation

The effect of a tear of the supraspinatus, the most commonly torn rotator cuff muscle (Kim et al., 2010), on the muscle forces of the shoulder was studied. The intact shoulder would undergo the extended motion cycles. Following intact tests, with guidance from an orthopaedic upper limb surgeon, a 50% anterior artificial tear of the supraspinatus was made at the insertion of supraspinatus onto the humeral head. The supraspinatus muscle was measured between the anterior edge and the infraspinatus tendon, a scalpel was used to cut the supraspinatus 50% from the anterior edge as shown in Figure 6.1. The shoulder was then tested using the same extended motion cycles protocol.

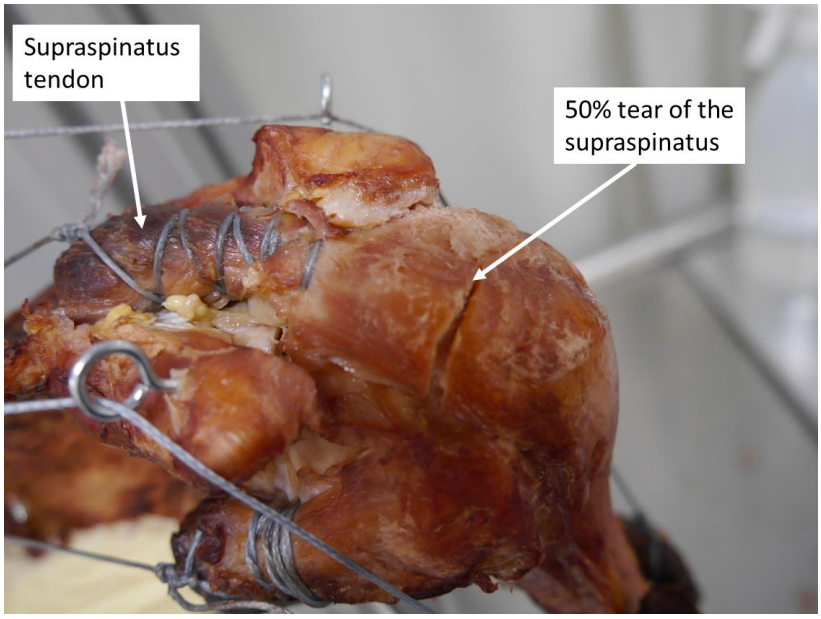

Figure 6.1 - Cadaveric shoulder (sample 2), photograph showing a 50% anterior artificial tear (created via a scalpel incision) of the supraspinatus tendon.

The tear was then extended to a full artificial tear of the supraspinatus muscle which detached the tendon from its insertion site as shown in Figure 6.2. A full extended motion cycle protocol was again performed on the sample.

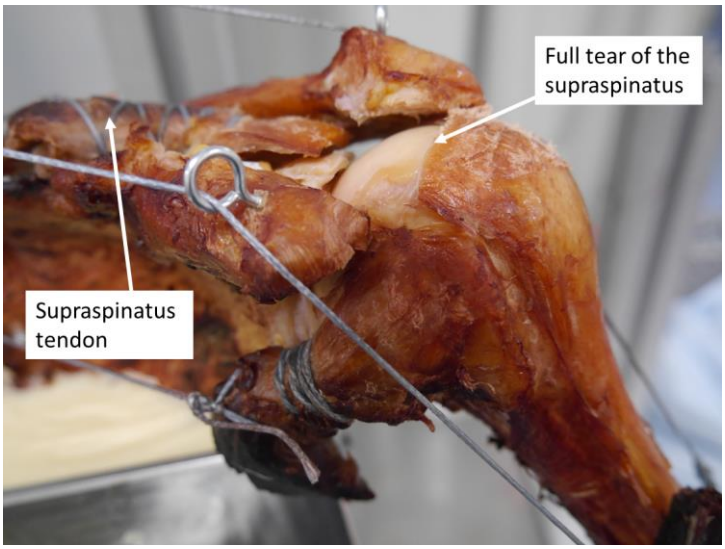

Figure 6.2 – Cadaveric shoulder (sample 2), photograph showing a full artificial tear (created via scalpel incision) of the supraspinatus which detached the tendon from its insertion site on the humerus.

Finally, a double row repair of the supraspinatus was performed by the orthopaedic surgeon and the sample underwent the same motion protocol. The double row repair method was selected as it is a very widely used method of surgical repair that offers some of the best outcomes for tears of the supraspinatus (Matthews et al., 2006). The double row repair of the fully torn supraspinatus muscle is shown in Figure 6.3.

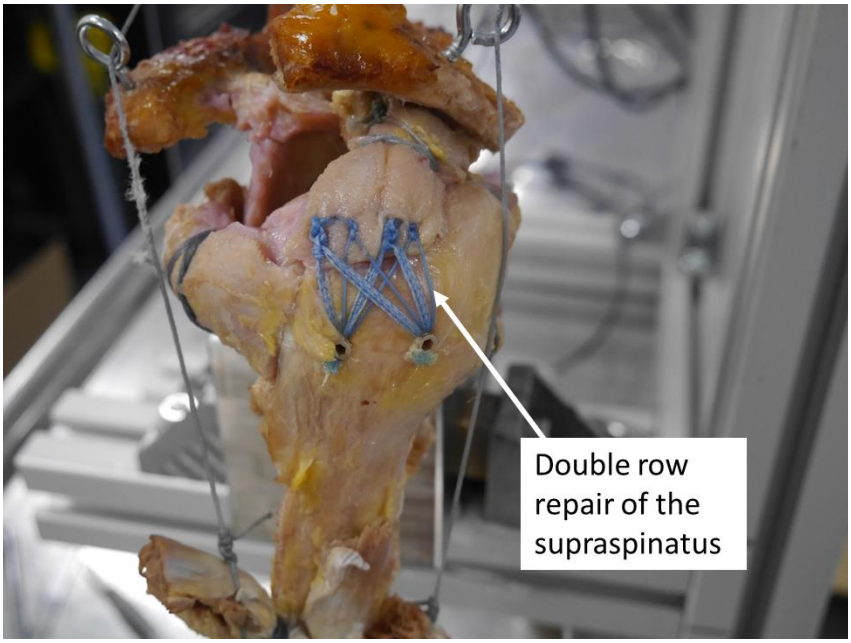

Figure 6.3 – Cadaveric shoulder (sample 4), photograph showing a double row repair of the supraspinatus tendon as carried out by an upper limb surgeon.

6.2.3 Available Cadaveric Samples

The overall design of the studies and available samples is provided in Figure 6.4. The samples are listed across the top with the test protocols each sample was planned to undergo listed beneath. Lines are drawn between test conditions where direct comparisons can be made between samples.

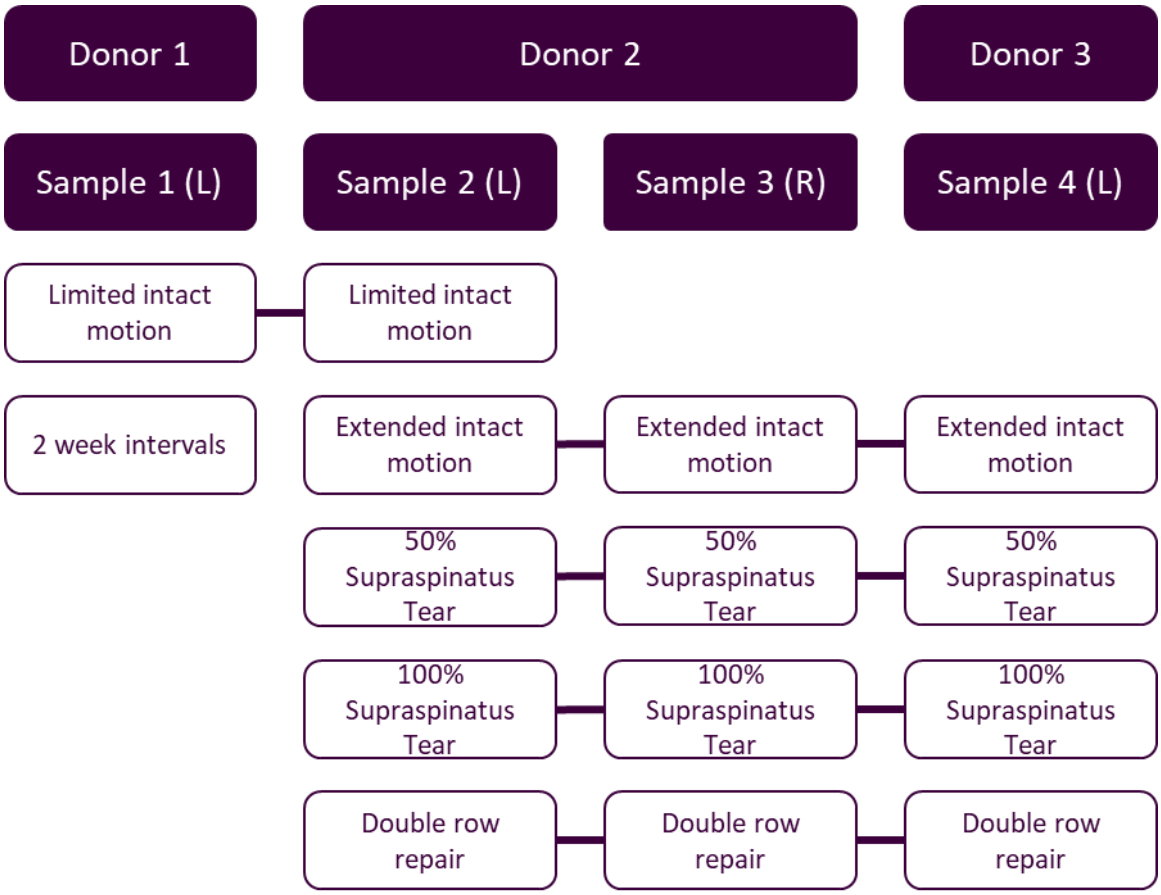

Figure 6.4 - Design of study - Effects of rotator cuff tear and repairs, showing available shoulder samples. The lines indicate where comparisons can be made between samples (NB sample 1 was tested in Chapter 5).

Three cadaveric shoulder samples were available for this study (samples 2, 3 and 4). Samples 2 and 3 were the left and right shoulders from the same donor and sample 4 was a left shoulder from a separate donor. Each sample was dissected by an orthopaedic upper-limb surgeon in order to maintain consistency throughout the dissection process. During the dissection process, a visual inspection was made regarding the quality of the rotator cuff tendons and the presence of any shoulder pathology. Samples 2 and 4 had good quality, intact rotator cuffs as assessed by the orthopaedic surgeon. Sample 4 was a much larger sample than sample 2 with a greater amount of soft tissue and fat surrounding the glenohumeral joint however both samples had good quality soft tissue. Sample 3 however, had a very large degenerative bucket handle tear of the supraspinatus muscle (Figure 6.5). The anterior and posterior portion of the supraspinatus were still attached to the humeral head however this was mainly tough scar tissue in place of tendinous tissue. The tendon had retracted considerably due to the degenerative nature of the tear. In consultation with the orthopaedic surgeons, it was deemed that if seen clinically, this tear would not be repaired due to the retraction of the remaining tissue and the degeneration of the surrounding tissues.

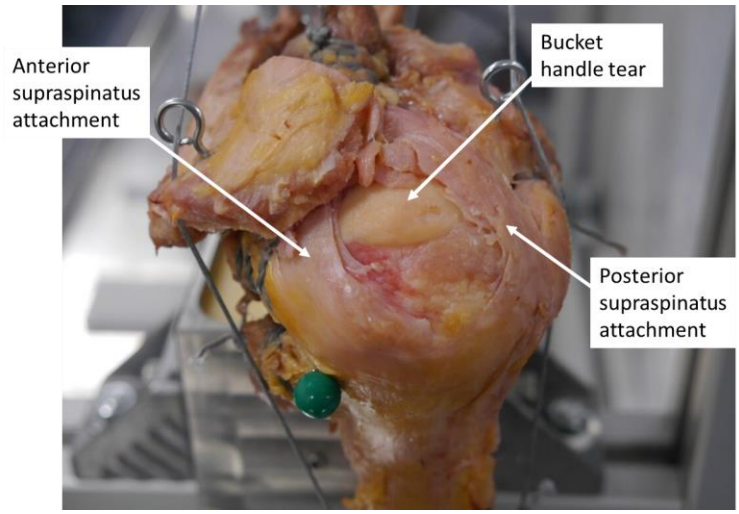

Figure 6.5 – Cadaveric shoulder sample 3. The anterior and posterior portion of the supraspinatus attachment is labelled along with the bucket handle tear.

Due to the tear identified in sample 3, the study design was altered to reflect this and is provided in Figure 6.6. Sample 3 underwent the same extended motion cycle to investigate the range of motion of the joint with such a large tear. Comparisons were then to be made between an artificial 50% tear of the supraspinatus and the natural tear found in sample 3.

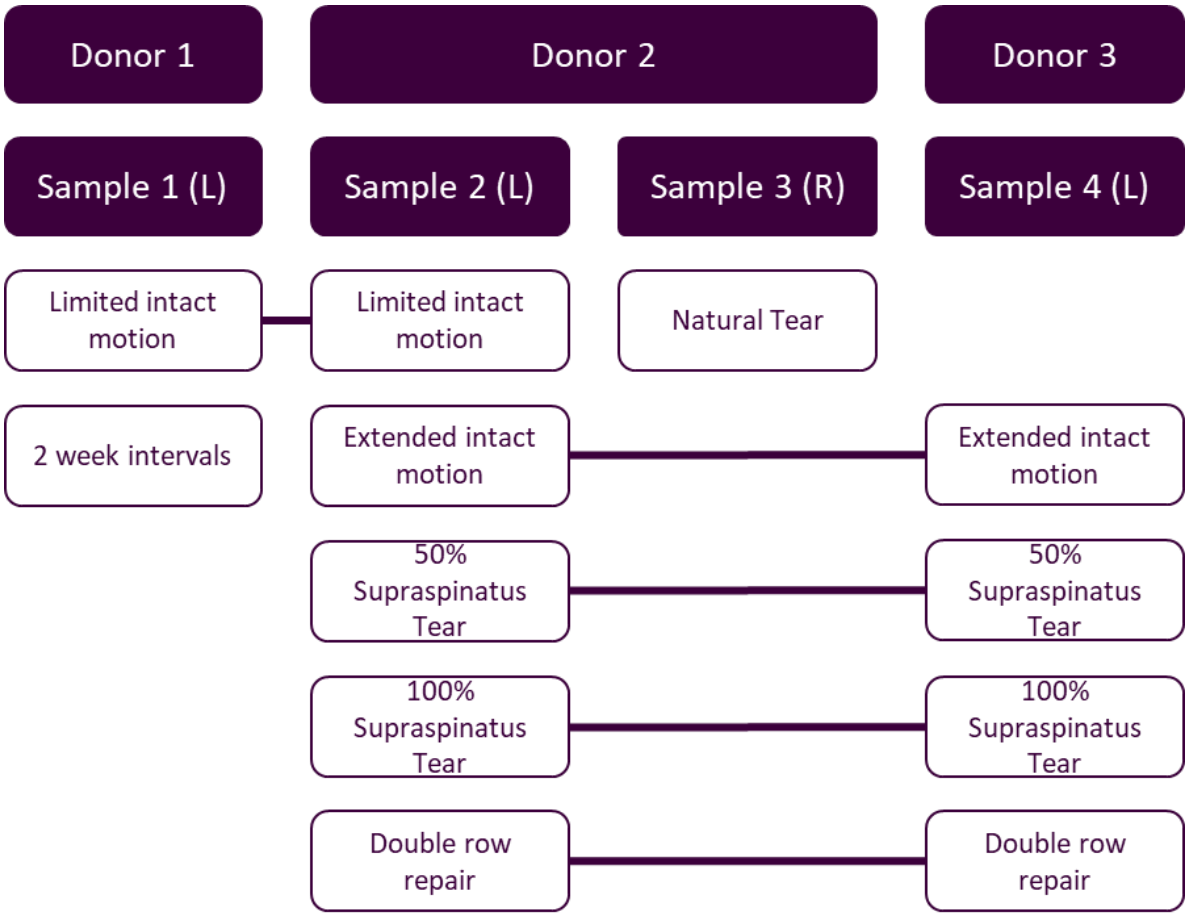

Figure 6.6 - Final study design (adapted from Figure 6.4) due to large natural tear in sample 3.

6.2.4 Sub Study Comparisons

This section describes the sub-study comparisons that were made. Due to limited availability of the samples, and two shoulders from one donor and some tissue degeneration, samples were selected to be compared in different ways to answer specific questions, these groupings are shown in Figure 6.7. The sub studies were:

A – The effect of increased angle of motion on the muscle forces.

B – The repeatability of the human shoulder simulator when performing the same motion with different samples.

C – The effect of a 50% artificial tear of the supraspinatus on the muscle forces within the joint.

D – The effect of a 100% artificial supraspinatus tear on the muscle forces within the joint.

E – The effect of a double row repair of the supraspinatus muscle on the muscle forces.

F – The difference between an artificial tear and a natural tear of the supraspinatus muscle.

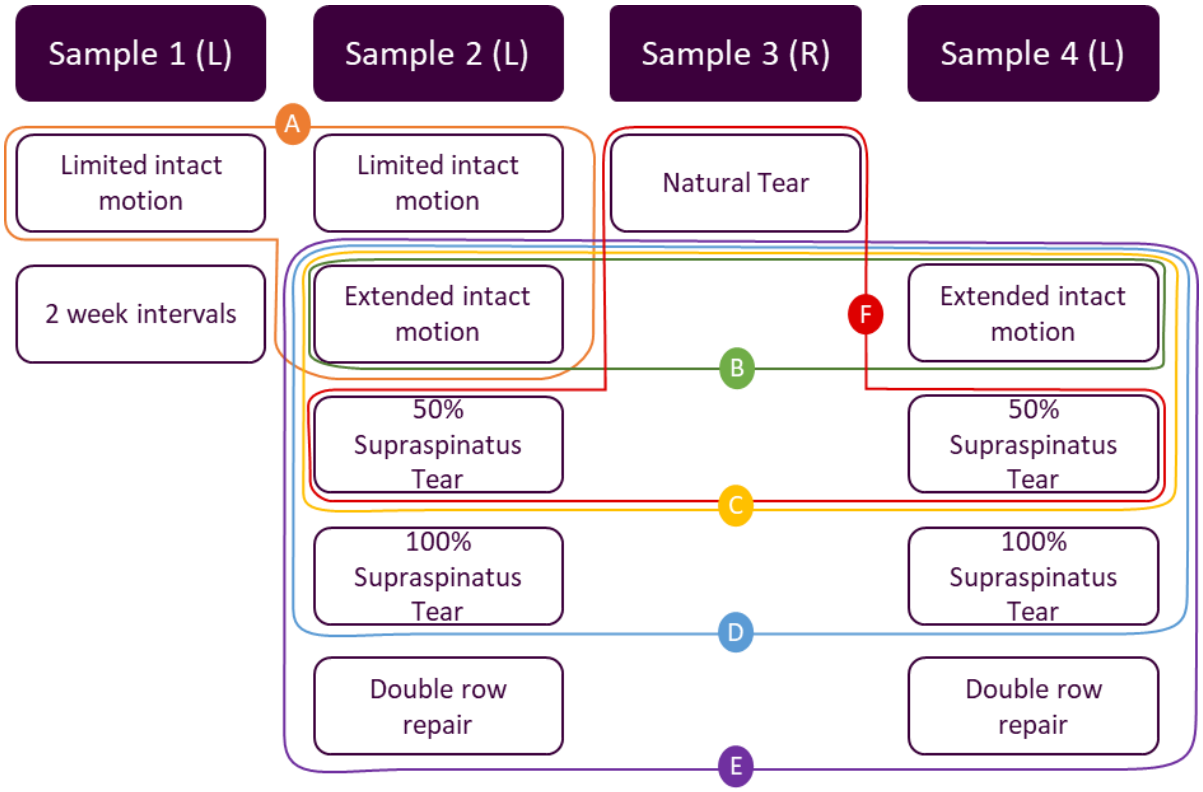

Figure 6.7 - The study design updated to show the sub studies (A - F) which will answer individual research questions. A: The effect of increased angle of motion on the muscle forces. B: The repeatability of the simulator when performing motion with different samples. C: The effect of a 50% artificial tear of the supraspinatus. D: The effect of a 100% artificial tear of the supraspinatus. E: The effect of a double row repair of the supraspinatus. F: The difference between an artificial tear and the natural tear of the supraspinatus.

6.3 Flexion motion cycles

Three repeats of the flexion motion cycle were conducted for each sample through every test case detailed in Figure 6.7. Flexion of the shoulder is predominantly conducted through the use of the anterior deltoid, coracobrachialis and pectoralis major muscles with limited impact of the rotator cuff tendons other than in their role of maintaining joint stability (Chang et al., 2023). Both the coracobrachialis muscle and the pectoralis major muscle were removed during the dissection process to allow for access to the rotator cuff muscles lying below. The flexion motion was performed in all cases (intact, torn and repaired) due to the reliance on the anterior deltoid for the motion.

A single motion cycle of the flexion motion performed with sample 2 is shown in Figure 6.8. The primary flexor was the anterior deltoid, and the rotator cuff muscles (supraspinatus, infraspinatus, teres minor and subscapularis) provided limited force.

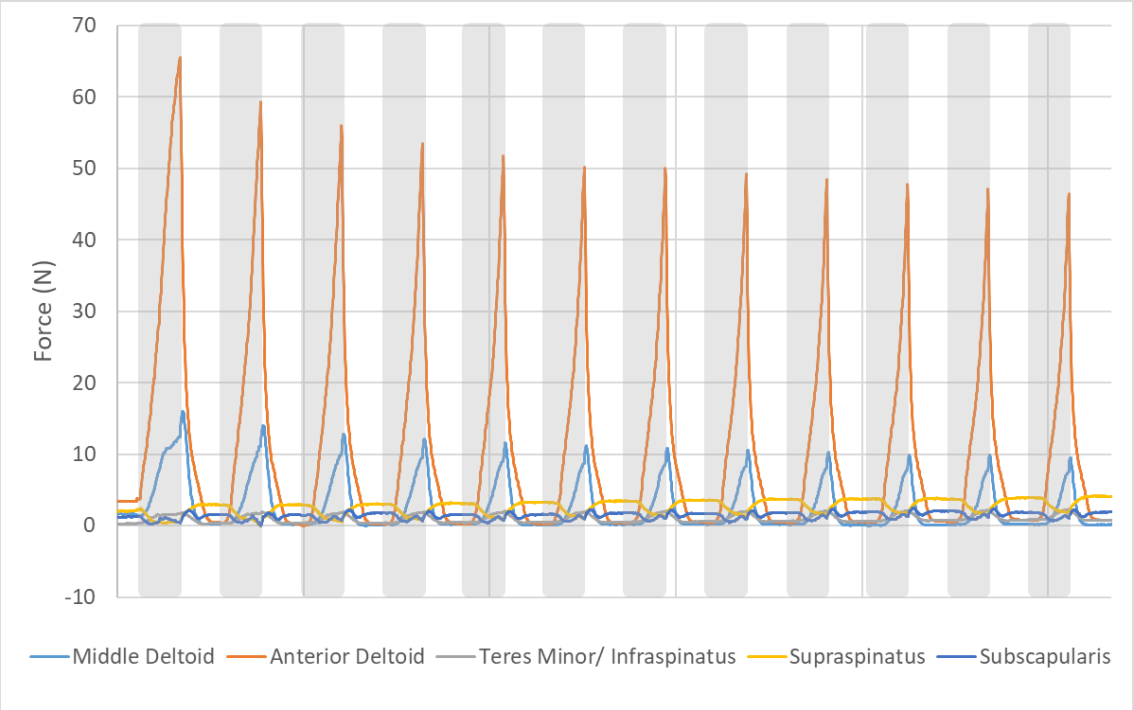

Figure 6.8 - The muscle force values for a single repeat of the flexion motion with sample 2. The grey zones represent periods of flexion and the white zones show periods of extension.

The mean ratios of force across the three flexion repeats with an intact and artificial 50% supraspinatus tear in sample 2 are shown in Figure 6.9. At maximum flexion in the intact case, the anterior deltoid is providing 80% of the total force within the joint with the rotator cuff as a whole providing only 6%. After an artificial 50% tear of the supraspinatus tendon, the anterior deltoid provides 84% of the force. Due to the very limited changes within the force distributions between the test cases at all angles of flexion, the remainder of the studies focus on the effect of the test cases on muscle forces through the abduction motions.

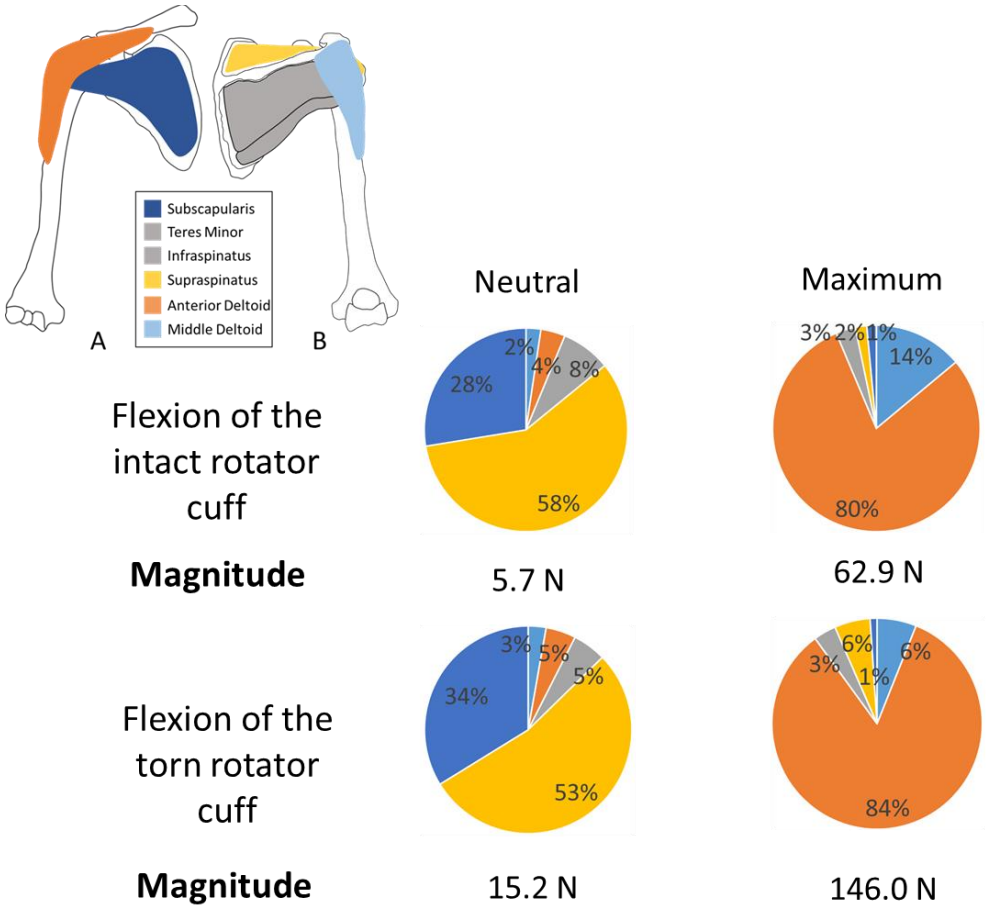

Figure 6.9 - The mean distributions of the force required in flexion for the three repeats of the intact and 50% artificial supraspinatus tear in sample 2.

6.4 Sub Study A: Effect of increased angle of motion on the muscle forces

The cadaveric shoulder sample in this study (sample 2) underwent both the limited and extended motion protocols. Three repeats of the motion cycle were conducted as stated in the protocol described in Section 5.7 for both the limited and extended motion cycles. The limited abduction cycles were performed appropriately by the simulator and force data was obtained from all load cells throughout. All three repeats of the extended abduction were conducted successfully and the motion was visually consistent. The force data obtained from the load cell was appropriate for the first motion cycle however for repeats 2 and 3, the anterior deltoid load cell produced very sporadic and low values throughout the extended motion. Due to the post-processing of the data occurring after all repeats were conducted, it was not possible for additional repeats of the extended abduction cycle to be conducted. Consequently, the data presented for the extended motion cycle in sample 2 is based solely on the first repeat of the abduction motion.

The force in each muscle throughout the 20 motion cycles for the first repeat of the limited and extended abduction motion are given in Figure 6.10A and B respectively. The distribution

of the total force between the muscles of the shoulder during cycles 6-10 of the limited and extended motion cycles are shown in Figure 6.11. The distribution values are the mean of the three limited abduction repeats however are the first repeat of the extended abduction run.

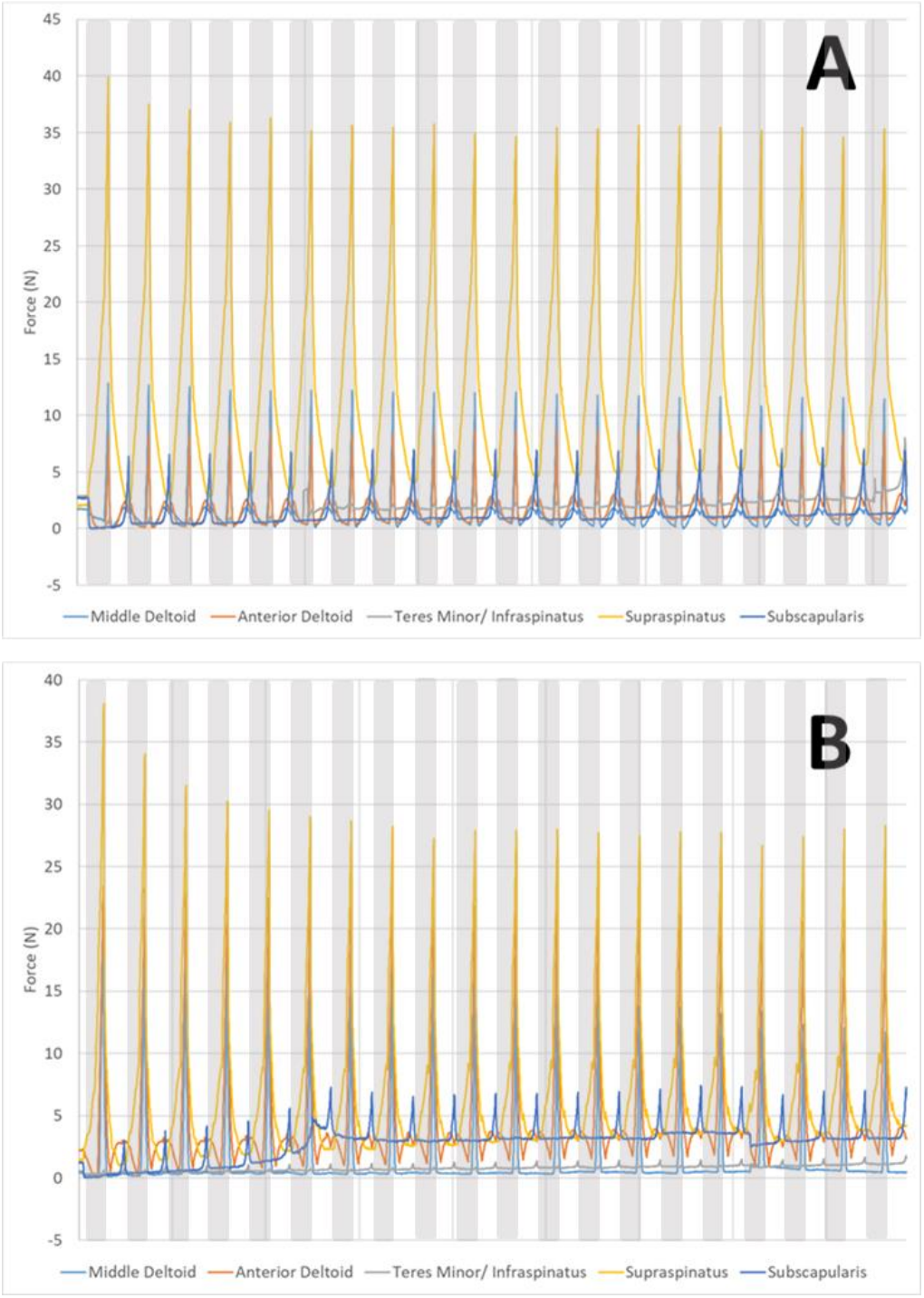

Figure 6.10 - Force in each muscle during abduction against time of sample 2. A: Limited abduction of 30 degrees. B: Extended abduction of 50 degrees. The grey zones indicate periods of abduction and the white zones indicate periods of adduction.

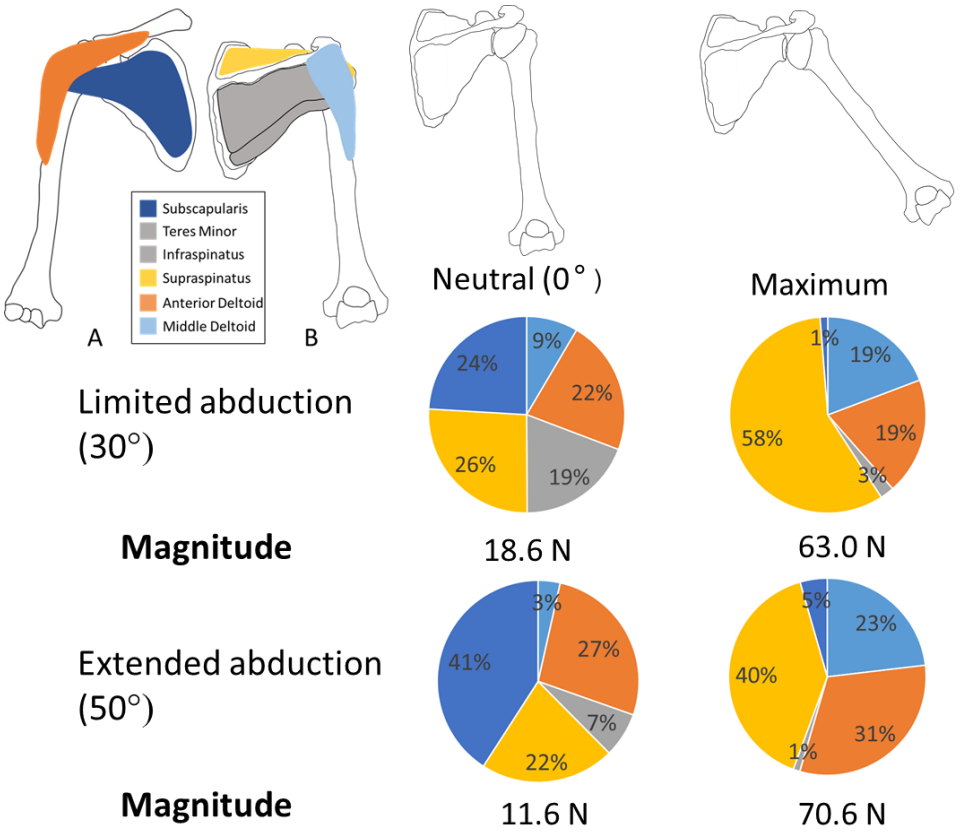

Figure 6.11 - The mean distribution of force between the rotator cuff muscles at mean neutral position and mean maximum abduction position during the limited and extended motion protocols. The distribution for the extended cycle is based solely on repeat 1 due to errors with the anterior deltoid load cell.

The limited abduction cycle that was used with sample 1 in the previous study (Chapter 5) was also repeated with sample 2 alongside the extended motion protocol. An example for a single repeat of the graph of the forces required for the limited motion cycles for sample 2 is given in Figure 6.10A. As with sample 1, the supraspinatus muscle provided the majority of the force at maximum abduction. However, if the magnitude of the force in the supraspinatus muscle is compared with Figure 5.9 and Figure 5.12 for sample 1, this is lower in sample 2 than sample 1 and the proportion of the total force that the supraspinatus muscle contributed was also lower. This was however consistent across all the repeats with sample 2 indicating that this may be related to inter-sample variation.

The mean distribution of the total force between the muscles during cycles 6-10 of both the limited and extended motions (sample 2) is given in Figure 6.11. It can be seen that the total magnitude of force was higher when a higher angle of abduction was reached due to the increased effect of gravity on the joint. The ratio of the force between the different muscles at the maximum abduction also changed between the two motion cycles. The anterior and middle deltoid were contributing a higher proportion of the force at the maximum abduction

angle (50°) compared to the supraspinatus. This corresponds to Lam and Bordoni (2021) who stated that the primary muscle during the initiation of abduction was the supraspinatus muscle, then the deltoid muscle took over as primary mover up until 90° (Lam and Bordoni, 2021). In this study at a higher angle of abduction, the deltoid muscles contributed a higher percentage of force once the abduction motion had been initiated by the supraspinatus muscle (Figure 6.11).

A single abduction to 50° performed by the simulator was plotted against the angle of abduction and compared to the initial AnyBody model of the human shoulder simulator, described in Section 5.3, and shown in Figure 6.12. In both cases the supraspinatus muscle is the force producing the maximum force between 0° and 23° abduction. In the computational model of the simulator set up the anterior deltoid then takes over as prime mover however in the physical simulator this is a more gradual increase in force in both the anterior and middle deltoid muscles which continue increasing through to 50° abduction. The forces in the computational model given in Figure 6.12A are considerably higher (maximum of 163 N) than those in the physical simulator (maximum 27 N). The lower arm weight was removed in the computational model however the full weight of the upper arm was left intact. During the physical experiments, all musculature and surrounding tissue was removed from the upper arm other than the required tendons, hence the simulated weight of the upper arm was considerable less than that modelled computationally.

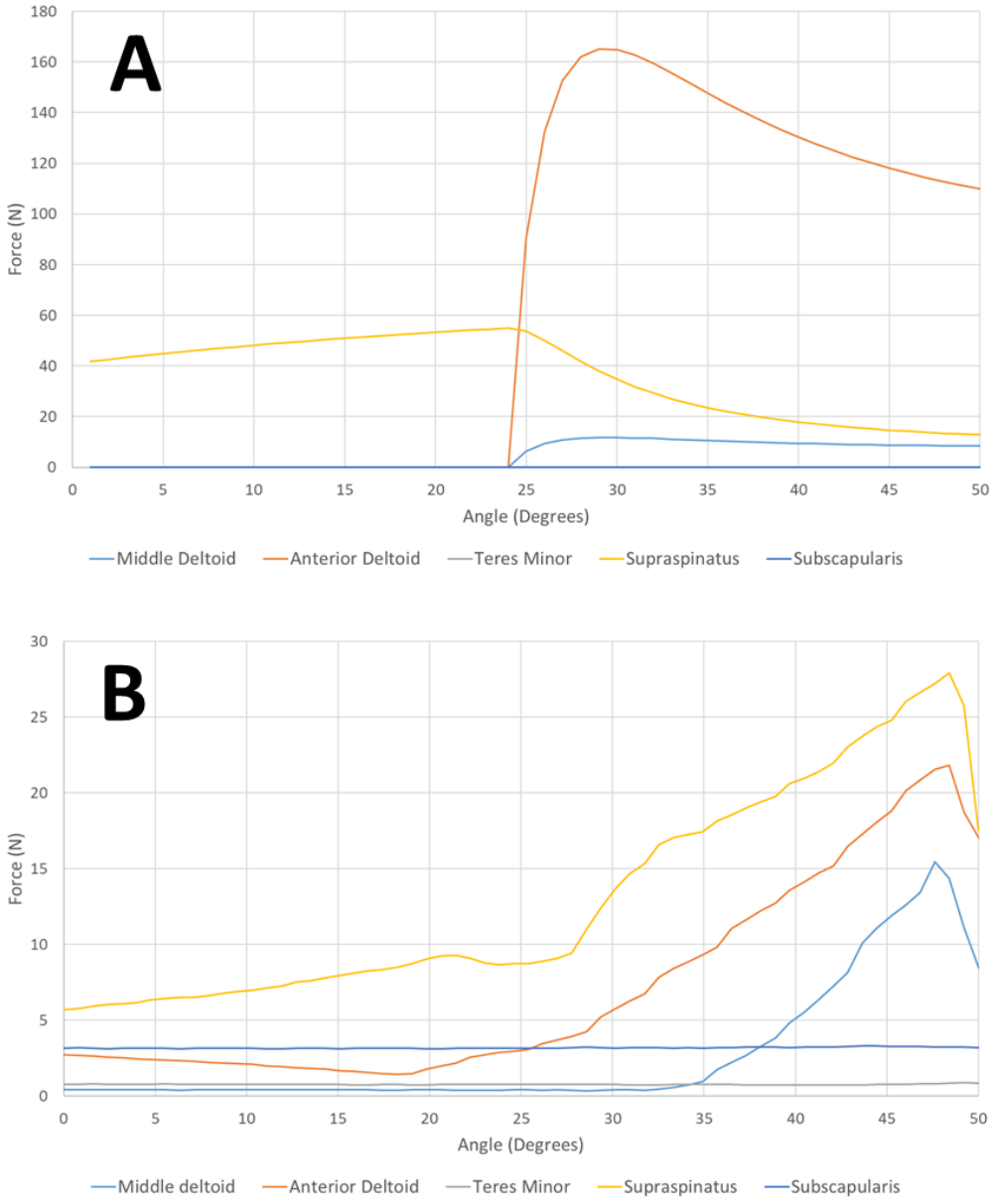

Figure 6.12 - A single cycle of abduction from 0° - 50° performed by the computational AnyBody simulator model (A) and the human shoulder simulator (B).

6.5 Sub Study B: Repeatability of the human shoulder simulator when performing the same motion with different samples.

The extended motion protocol was performed using both sample 2 and sample 4 as detailed in Figure 6.6. Forces measured during the first repeat of the extended motion cycle for sample 2 are provided in Figure 6.10B and an example of the forces measured during the extended motion cycle in sample 4 are given in Figure 6.13. The mean distribution of the total force between the muscles of the shoulder joint at the maximum and minimum abduction values for all repeats and cycles 6-10 are shown in Figure 6.14 for the forces measured during the extended motion cycle in sample 2 and sample 4. Due to the inconsistencies in the anterior

deltoid load cell readings during the repeats of the extended motion cycle, the data is based purely on the first repeat of this motion.

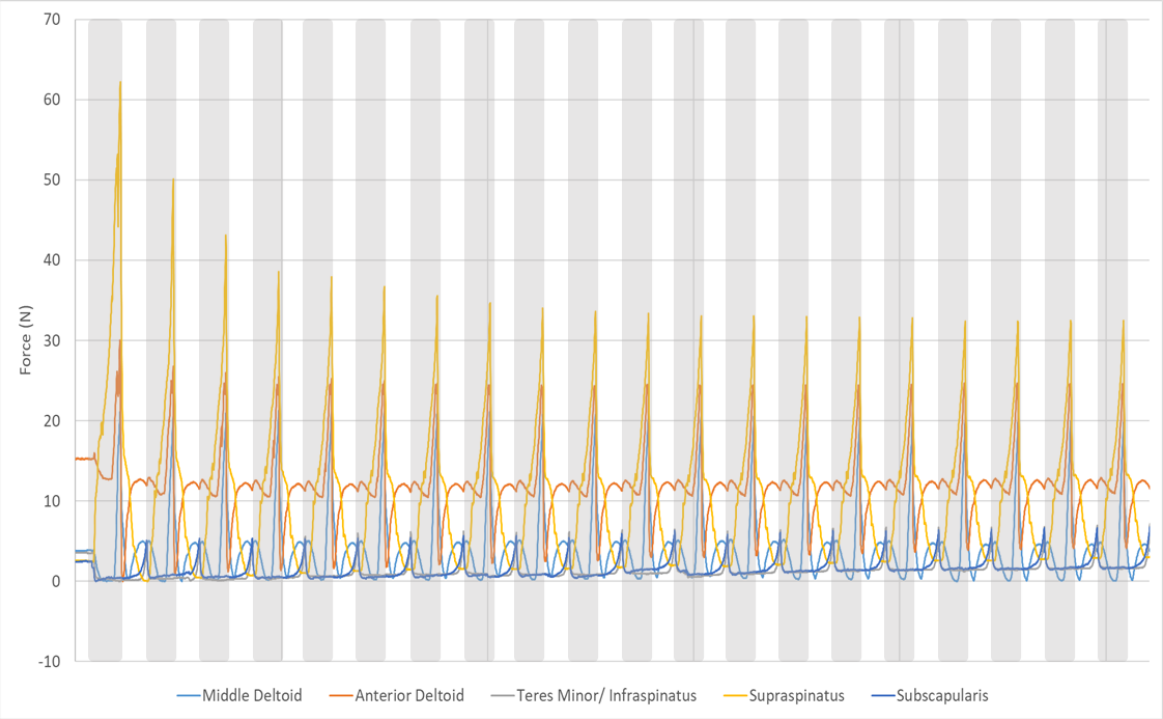

Figure 6.13 - An example of the typical force in each muscle during the extended motion cycle (sample 4). The grey zones indicate periods of abduction and white shows adduction.

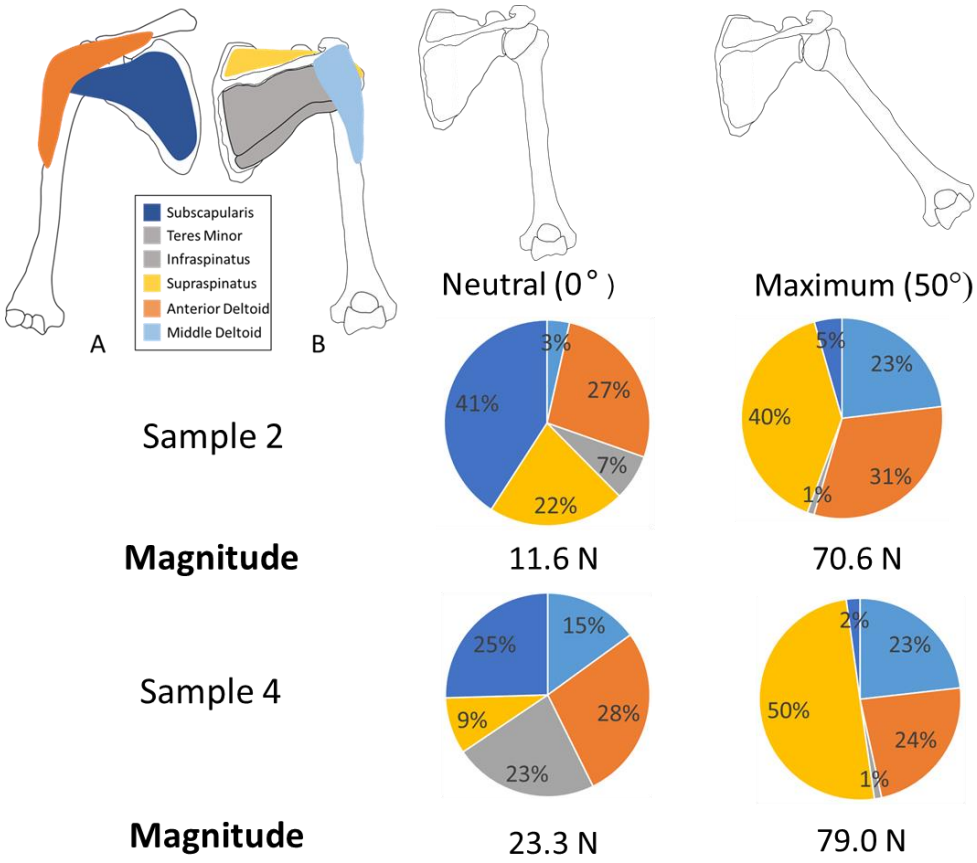

Figure 6.14 - The mean distribution of the total force between the muscles of the shoulder joint at the maximum and minimum abduction values for sample 2 and sample 4.

The last 11 cycles of the extended motion conducted in sample 2 were then plotted on top of each other starting at 0° abduction to investigate the repeatability of the results from the simulator. The graphs for each individual muscle are shown in Figure 6.15 along with the original force graph of a single repeat of sample 2 with the investigated section highlighted in blue.

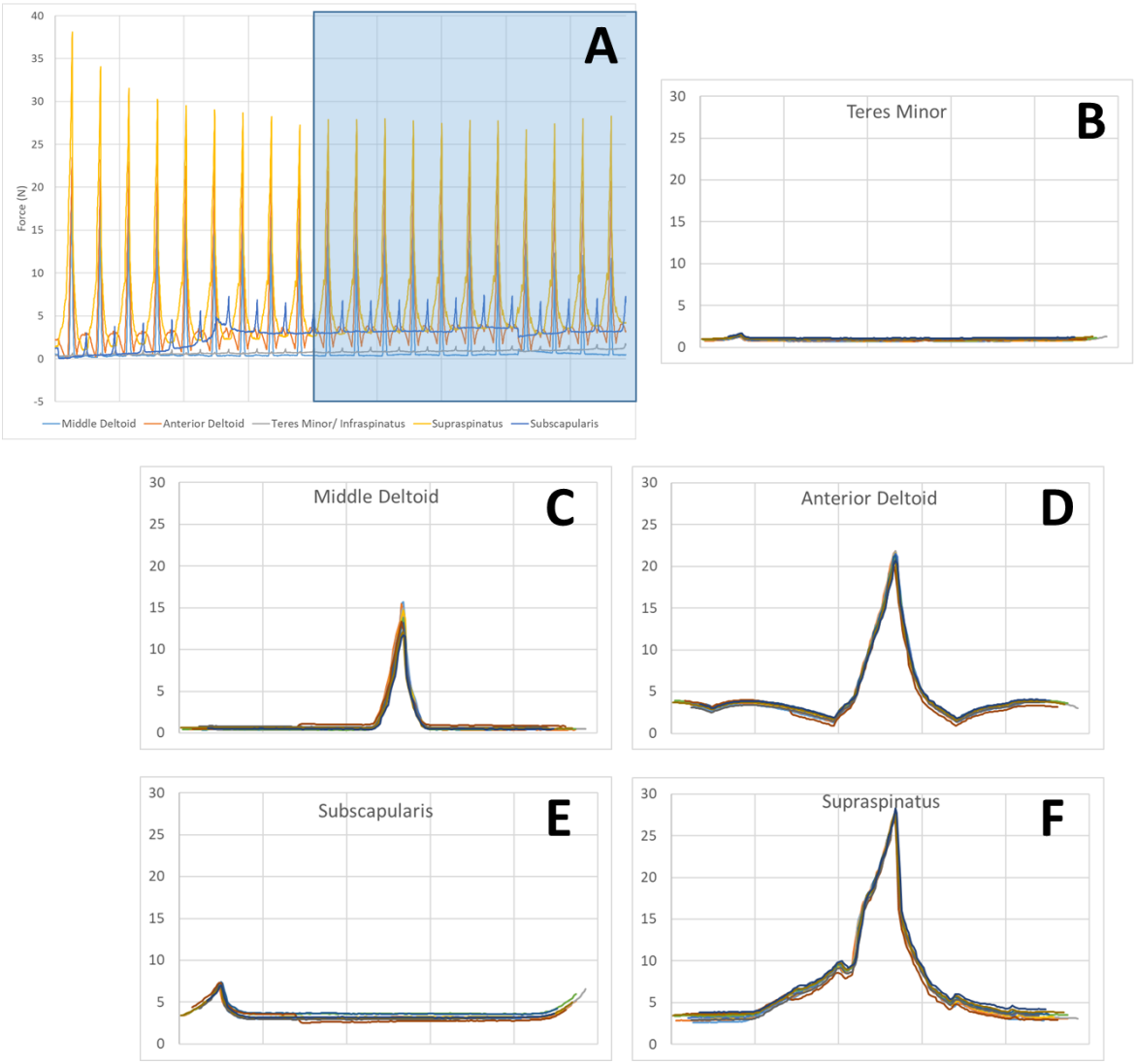

Figure 6.15 - The repeatability of the abduction motion cycle for sample 2. Each individual cycle (10 – 20) is plotted on the same axes for each motion, the plotted cycles are indicated by the blue area on image A. A: Repeated cycles for all muscles in cycles 0 - 20. B: Forces in teres minor for cycles 10 - 20. C: Forces in the middle deltoid for cycles 10 – 20. D: Forces in the anterior deltoid for cycles 10 – 20. E: Forces in the subscapularis for cycles 10 – 20. F: Forces in the supraspinatus for cycles 10 – 20.

The extended motion protocol was performed with both sample 2 and sample 4 as detailed in Section 6.2. An example of a single repeat of forces required in sample 2 for the extended motion was provided in Figure 6.10 and for sample 4 in Figure 6.13. As with the previous experiments, the force decreases over the initial 5 cycles as the joint repositions into its natural joint position (Figure 6.15A). For sample 2, the decrease in force is approximately a maximum of 10N for the supraspinatus muscle. However, in sample 4, the supraspinatus muscle decreases by over 30 N over the first five cycles.

The comparison between the distributions of the force across the two samples is provided in Figure 6.14. At maximum abduction of 50°, the distribution of force between the muscles is very similar for samples 2 and 4. In both cases, the supraspinatus muscle provides the majority of the force closely followed by the middle and anterior deltoids. The magnitude of force is higher in sample 4 however that was expected as it was predicted that the larger sample size would result in a higher moment around the joint. As also found with the previous experiments discussed in Section 6.4, the distribution of force at 0° abduction was less consistent. The distribution is consistent within a sample because the muscles return to a very similar value each time the zero degrees is achieved as seen in Figure 6.15. However, when comparing the two samples, the distribution of force and magnitude of force is inconsistent. The subscapularis muscle plays a much larger role during the neutral position in sample 2 whereas the middle and anterior deltoid provide more force in the neutral position of sample 4.

6.6 Sub Study C: Effect of a 50% artificial tear of the supraspinatus on the muscle forces within the joint.

A 50% artificial tear of the supraspinatus was performed on samples 2 and 4. The breakdown of the force required by each muscle at minimum and maximum abduction with an intact rotator cuff and a 50% tear of the supraspinatus muscle in sample 2 and sample 4 are given in Figure 6.16 and Figure 6.17 respectively. The results for the intact rotator cuff are the same as given in Section 6.5 and are provided in this section for comparisons to be made between the two tear states.

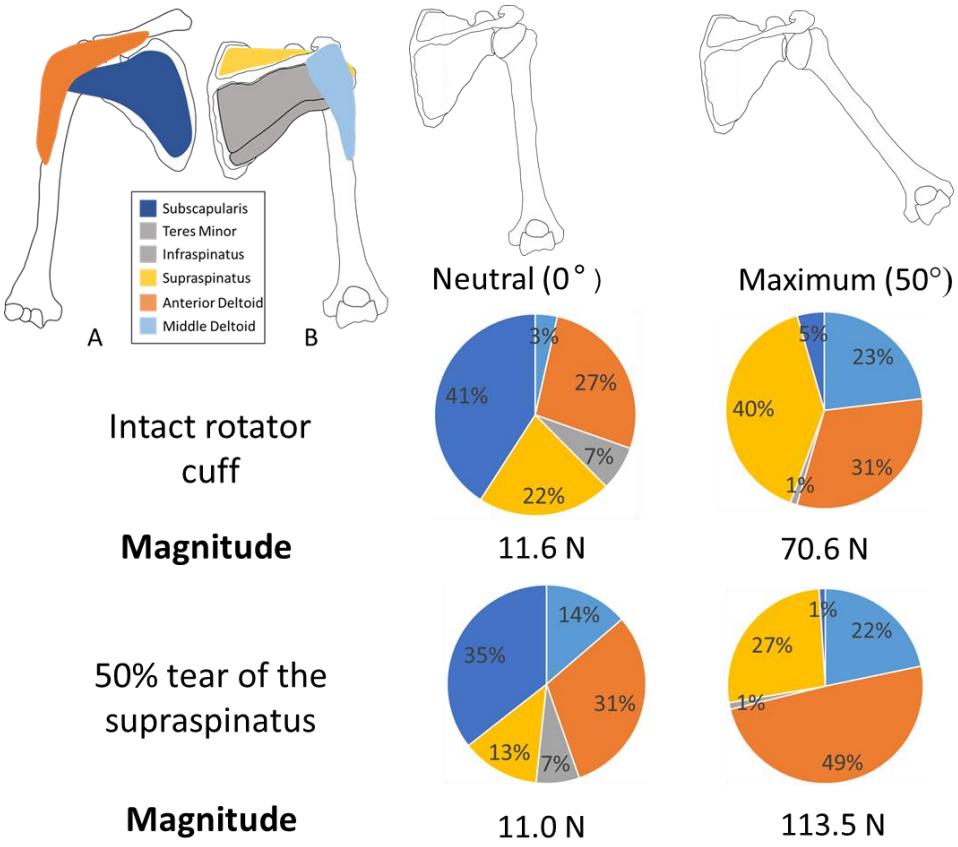

Figure 6.16 - Percentage of force required by each muscle at minimum and maximum abduction with an intact rotator cuff and a 50% artificial tear of the supraspinatus muscle in sample 2.

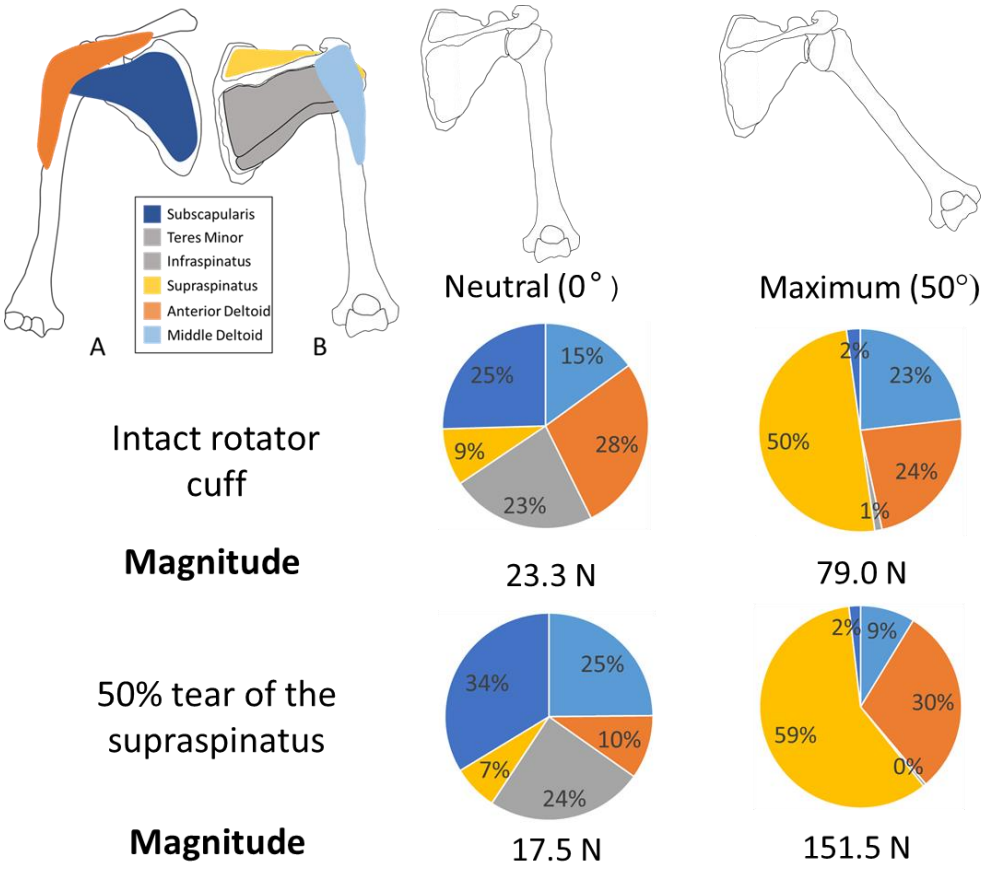

Figure 6.17 - Percentage of force required by each muscle at minimum and maximum abduction with an intact rotator cuff and a 50% artificial tear of the supraspinatus muscle in sample 4.

For sample 2, at maximum abduction, the supraspinatus contributed a lower proportion of force when it is torn (27%) compared to the intact state (40%). The anterior muscle becomes the primary muscle providing force at 50° abduction. As anterior tears of the supraspinatus progress, it has been reported that the force within the deltoid muscle increases to compensate for the decrease in force within the supraspinatus muscle (Oh et al., 2011; Dyrna et al., 2018; Mancuso et al., 2021). The supraspinatus muscle also provides a lower amount of force at 0° abduction, however force in both the subscapularis and middle deltoid muscles increases.

This is in contrast to the results from sample 4 given in Figure 6.17. The proportion of force required in the supraspinatus muscle at maximum abduction increased from 50% to 59% when a 50% artificial tear was performed on the supraspinatus muscle. The proportion of force in the middle deltoid decreased and in the infraspinatus/teres minor the proportion increased as a result of the tear at maximum abduction. This is in contrast to the literature where it is reported that the deltoid muscle increases to compensate the lower force produced by the

supraspinatus muscle (Mancuso et al., 2021). Sample 4 was anatomically larger sample than sample 2 with a larger humerus, scapula, rotator cuff and deltoid and a greater amount of fat surrounding the joint. The method to produce the 50% artificial tear was identical for both samples in that the supraspinatus tendon was measured then cut halfway from the anterior edge. Oh et al (2011) suggested that there was a critical length of a rotator cuff tear after which the joint biomechanics altered. It is possible that due to the larger joint in sample 4, this critical length was not reached and hence the biomechanics had not considerably changed.

The magnitude of force within all the muscles at minimum and maximum abduction was higher in the torn state than when the supraspinatus was intact for both samples 2 and 4. This suggests that a greater quantity of force is required to maintain the stability of the joint throughout motion. The rotator cuff plays a very important role in the compression of the humeral head into the glenoid fossa (Lugo et al., 2008; Abdelwahab et al., 2021). Therefore, if one part of the rotator cuff is torn, the other muscles must apply more force in order to keep the joint stable and to prevent dislocation of the shoulder.

6.7 Sub Study D: Effect of a 100% supraspinatus artificial tear on the muscle forces within the joint

The 50% tear of the supraspinatus tendon as discussed in Section 6.6 was continued using a scalpel incision to the whole width of the supraspinatus tendon on both sample 2 and 4. The full artificial tear of the supraspinatus muscle is shown in Figure 6.2 which resulted in the supraspinatus tendon being completely removed from the humeral head. The samples were then used in the simulator with the extended abduction protocol.

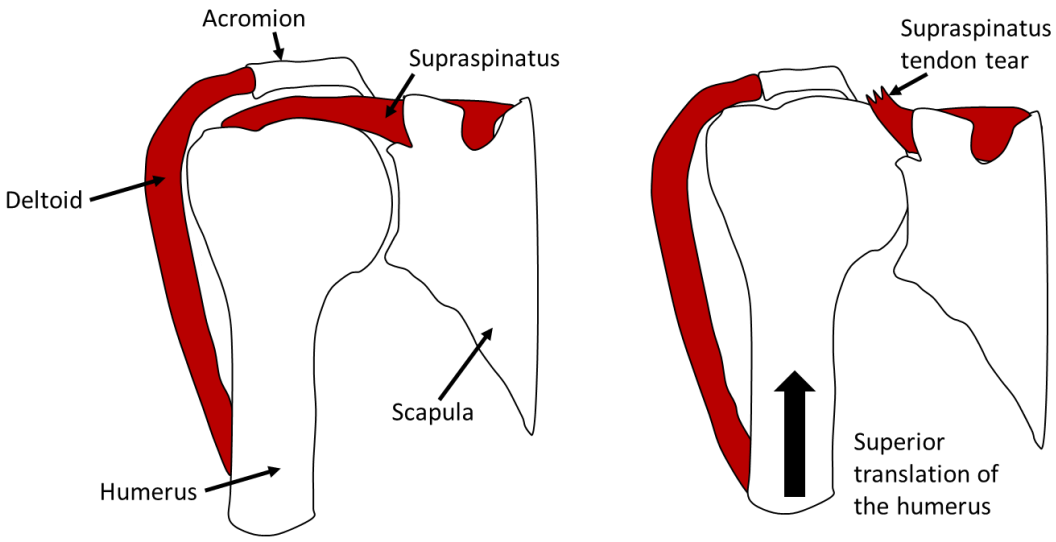

Figure 6.18 – Schematic showing superior translation of the humerus when the supraspinatus tendon is fully torn.

The rotator cuff muscles have a large role in the compression of the humeral head into the glenoid fossa, therefore superior migration of the humeral head occurred with a tear of the supraspinatus (Lugo et al., 2008; Oh et al., 2011) as shown in Figure 6.18. When the extended motion protocol was run with the fully torn supraspinatus tendon, for both samples 2 and 4, the humeral head translated superiorly until there was impingement on the acromion of the scapula with very little abduction occurring. It was determined that it was impossible to initiate the abduction motion without the supraspinatus tendon intact and that abduction could only begin if the humerus was to start from an angle of 15° as shown in Figure 6.19. This is supported by Lam and Bordoni (2021) who reported that the primary muscle required for the abduction of the shoulder from 0-15° was the supraspinatus muscle. When the supraspinatus muscle was then removed the abduction protocol struggled to initiate motion unless the humerus started from an angle of 15°.

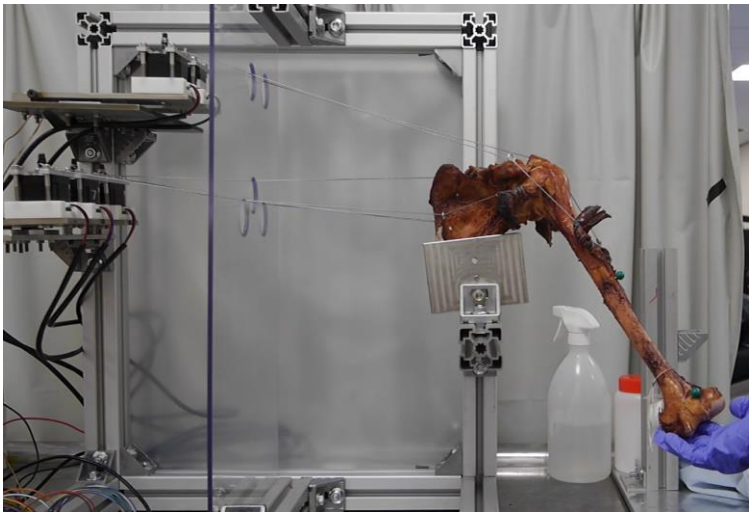

Figure 6.19 – Photograph of the humerus being held at 15 degrees abduction in the shoulder simulator to allow for the abduction of the shoulder to occur (sample 2).

The force required in each muscle in order to produce abduction from 15° to 50° are shown in Figure 6.20. The humerus was prevented from adducting all the way to the neutral position in order to allow for the next cycle of abduction to occur. The middle and anterior deltoid produced the majority of the force required to abduct the shoulder. The teres minor and infraspinatus muscles also produced a much higher amount of force. This force was required to keep the humeral head in the glenoid socket and prevent anterior translation of the head.

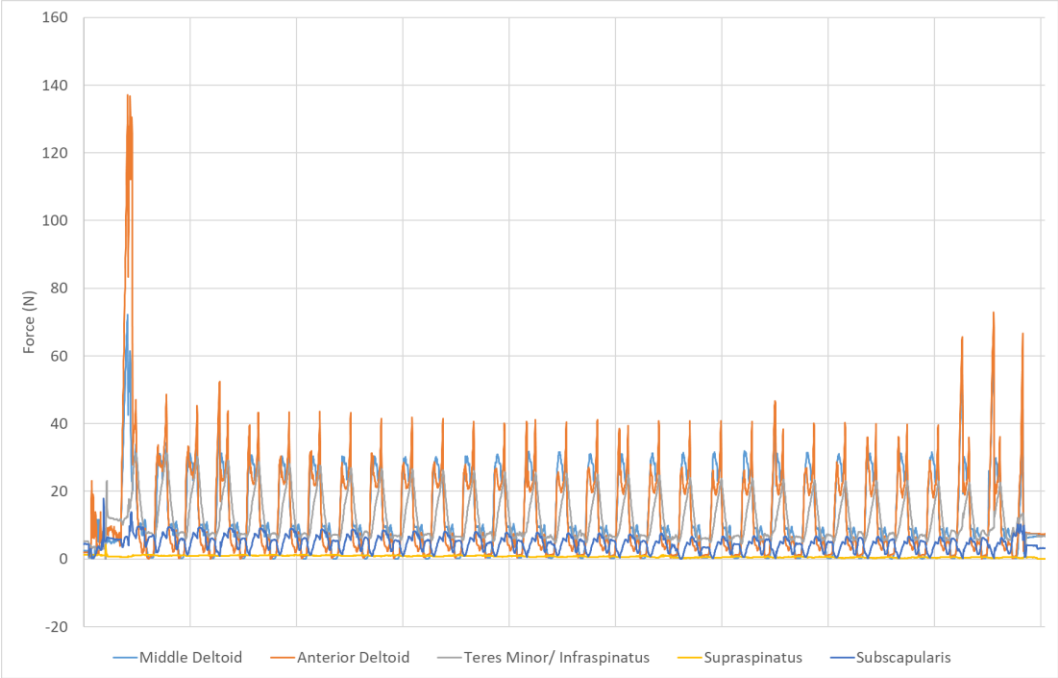

Figure 6.20 - The forces recorded in each muscle in order to produce abduction when a 100% artificial tear of the supraspinatus had occurred. The humerus was held at a starting position of 15 degrees of abduction and prevented from reaching the neutral position following each cycle.

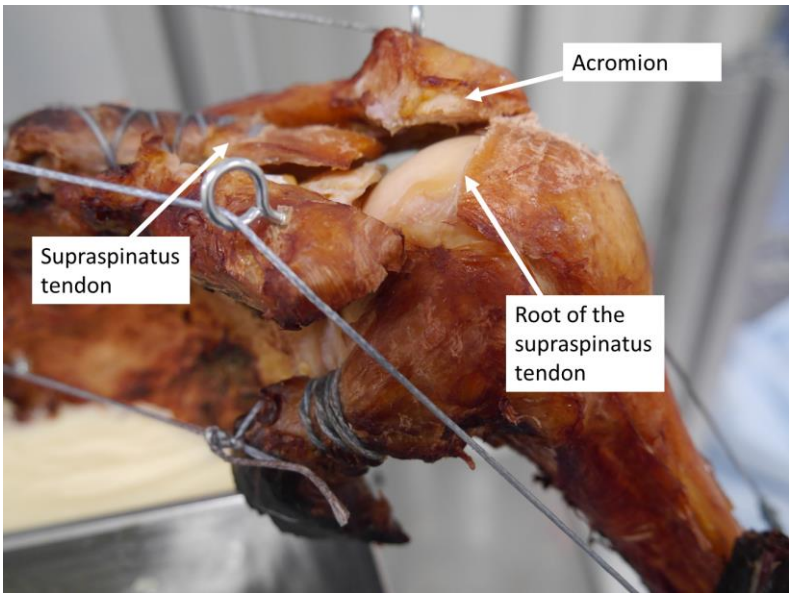

Figure 6.21 - The 100% artificial tear of the supraspinatus tendon with the root of the tendon indicated along with the detached tendon and the acromion of the scapula (sample 2).

Due to the methodologies used to perform the 100% supraspinatus tear, which are described in Section 6.2.2, there was a ridge in the remaining root of the supraspinatus tear as indicated in Figure 6.21. The supraspinatus tendon root would catch on the posterior portion of the acromion due to the ridge. This was another reason that the humerus was held at an angle of

15° and prevented from adducting to the neutral position in order to prevent the catching of this ridge.

6.8 Sub Study E: Effect of a double row repair of the supraspinatus muscle on the muscle forces.

After the supraspinatus tendon had been fully torn, an upper limb surgeon performed a double row repair of the tendon using clinically available bone anchors and suture tape. The resultant double row repair is shown in Figure 6.3. The extended motion protocol was applied to the repaired samples (sample 2 and 4). The percentage of force required by each muscle at the minimum and maximum abduction with an intact rotator cuff, 50% artificial tear and a double row repair in sample 2 and sample 4 are given in Figure 6.22 and Figure 6.23 respectively. The results for the intact rotator cuff and the 50% tear are the same as provided in Section 6.6 and are provided again in this section for comparative purposes.

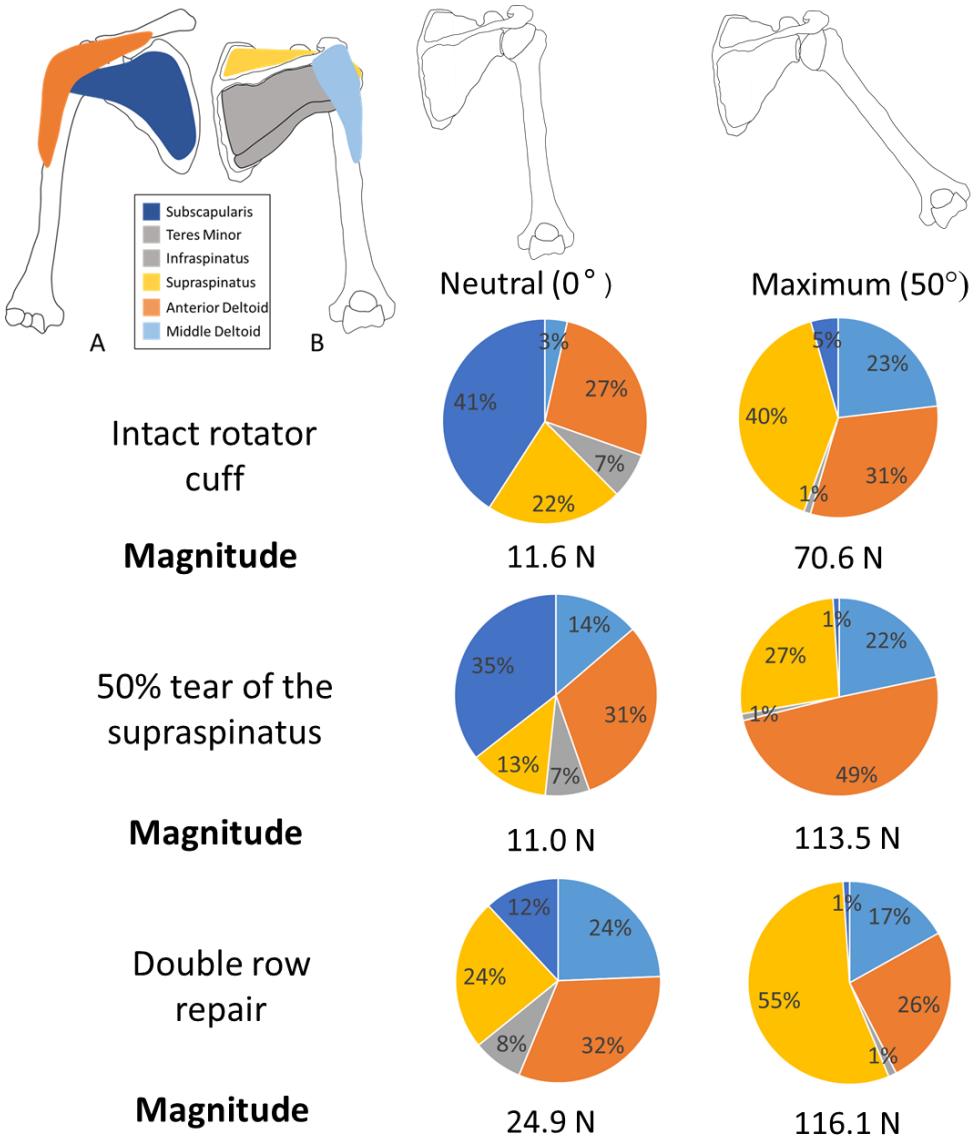

Figure 6.22 - The mean percentage of force between the muscles at maximum and minimum abduction for sample 2 with an intact cuff, an artificial 50% tear of the supraspinatus and a double row repair of the supraspinatus.

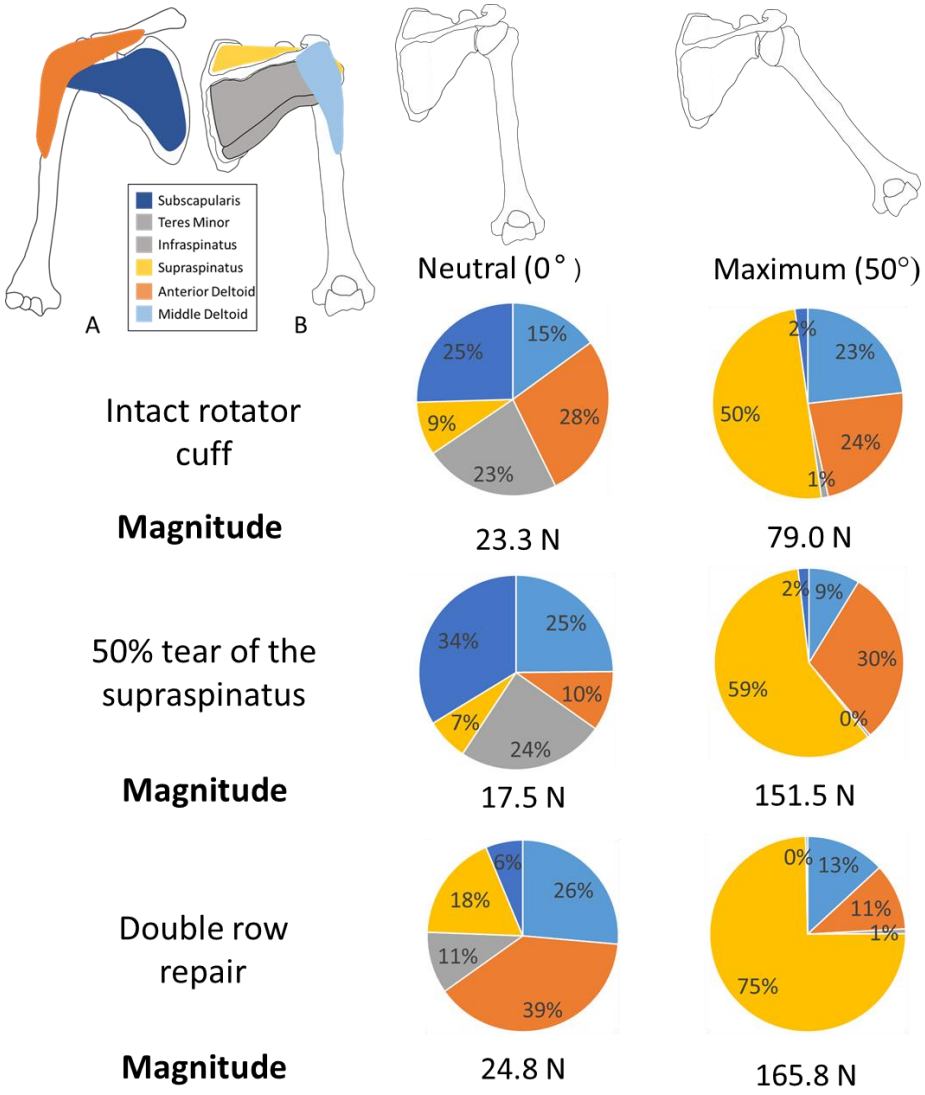

Figure 6.23 - The mean percentage of force between the muscles at maximum and minimum abduction for sample 4 with an intact cuff, an artificial 50% tear and a double row repair of the supraspinatus.

At maximum abduction the force in the supraspinatus muscle decreased when a 50% tear of the supraspinatus muscle was present. The force then increased from 27% to 55% of the total force when the muscle was repaired. The proportion of force contributed by the supraspinatus muscle was higher in the repaired state than in the intact state. Similarly, the results for sample 4 show that the proportion of force required in the supraspinatus muscle was higher when the supraspinatus muscle was repaired compared to the intact rotator cuff (Figure 6.23). In sample 4 the proportion of force between the intact and repaired state increased from 50% to 75% which was an increase of 84.9 N in the supraspinatus muscle.

The double row repair method involved the addition of bone anchors to the humeral head from which suture tape was passed through the tendon to anchor it down to the humerus as

shown in Figure 6.3. This increased the stiffness of the tendon-bone interface compared to the natural tendon-bone interface. A cadaveric study performed by Hatta et al (2016) found that stiffness increased with a double row repair of the supraspinatus compared to the intact rotator cuff. This increase in stiffness could have led to altered biomechanics within the joint which may influence the success rate of the repair method (Hatta et al., 2016). The double row repair method allowed for the line of action of the supraspinatus muscle to return to its original angle because the tendon was returned to the original footprint of the tendon (Akhtar et al., 2021). This is in contrast to the torn scenario when only the posterior 50% of the tendon was still attached which caused the line of action of the muscle to shift posteriorly causing external rotation of the joint.

The saturated salt solution tissue preservation method likely impacted the interaction between the natural tissue and the repair. Bissonnette et al. 2019, stated that the cadavers preserved with the saturated salt solution were deemed as overall suitable for surgical skills training (Bissonnette et al., 2019) and hence the method was selected for this study. However, the difference in mechanical properties of the tissue between living tissue and preserved cadaveric tissue would lead to different interactions between the tissue and the surgical repair method. Each cadaver was treated the same way prior to the study and therefore comparisons between the samples are able to be undertaken.

The magnitude of total force was also considerably higher in the repaired supraspinatus than with the intact rotator cuff. In sample 2 the total force magnitude increased by 64% between the intact and repaired state, for sample 4 this increase was 72%. This suggests that the repair method did not restore the initial rotator cuff biomechanics. It is possible that the stiffening of the supraspinatus tendon led to an overcompensation in the compression of the humeral head into the glenoid fossa. Therefore the magnitude of force across all muscles increased in order to keep the humerus in a neutral position against the pull of the supraspinatus tendon.

6.9 Sub Study F: Difference between an artificial tear and a natural tear of the supraspinatus muscle.

Sample 3 was found to have a large degenerative tear following the dissection procedure as outlined in Section 6.2.3. The originally planned study could not be conducted with this sample, however the opportunity to compare the forces required in the muscle to perform abduction with the naturally torn supraspinatus and an artificial tear of the supraspinatus arose. Both samples underwent the same extended abduction process, sample 2 had an artificial 50% tear of the supraspinatus muscle and sample 3 with the naturally degraded tear.

The mean breakdown of the total force between the muscles for both of these samples is given in Figure 6.24.

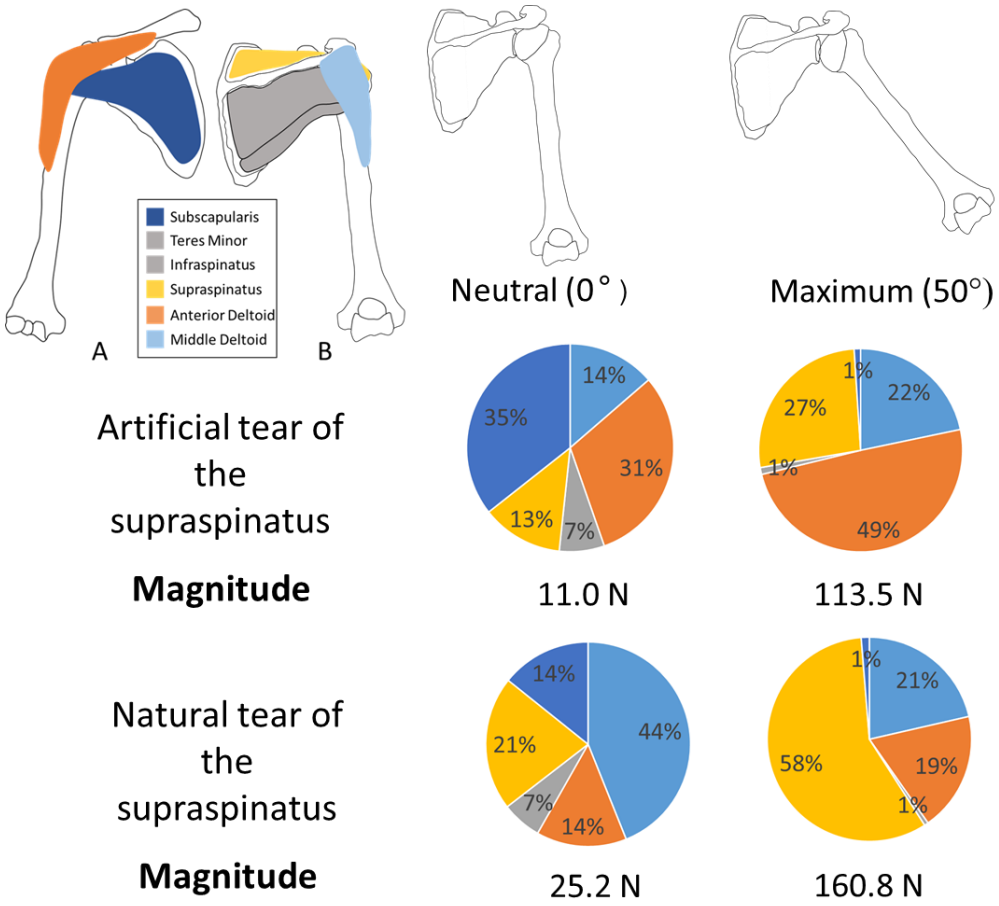

Figure 6.24 - The mean distribution of the total force required at maximum and minimum abduction for the artificial tear of the supraspinatus muscle in sample 2 and the natural tear of the supraspinatus in sample 3.

The difference between a naturally occurring tear of the supraspinatus as found following the dissection of sample 3 and an artificial tear such as that produced in sample 2 was compared. The two types of tears were different. The naturally occurring tear in sample 3 was a bucket handle tear where the anterior and posterior edges of the tendon were intact whereas the middle portion was torn. In contrast, the artificial tear was a 50% tear from the anterior edge of the tendon. The difference in the two tear types are shown in Figure 6.25. The line of action of the supraspinatus muscle in each case is displayed as an arrow on the Figure. It can be seen that when the supraspinatus tendon is torn from the anterior edge, the line of action translates posteriorly due to the location of the remaining bone-tendon connection. However, in the case of a bucket handle tear, the line of action is largely unaffected as both the anterior and posterior portions of the tendon are still intact. Consequently, the artificial and natural

tears are not directly comparable however some conclusions can be drawn from the comparison between the two types.

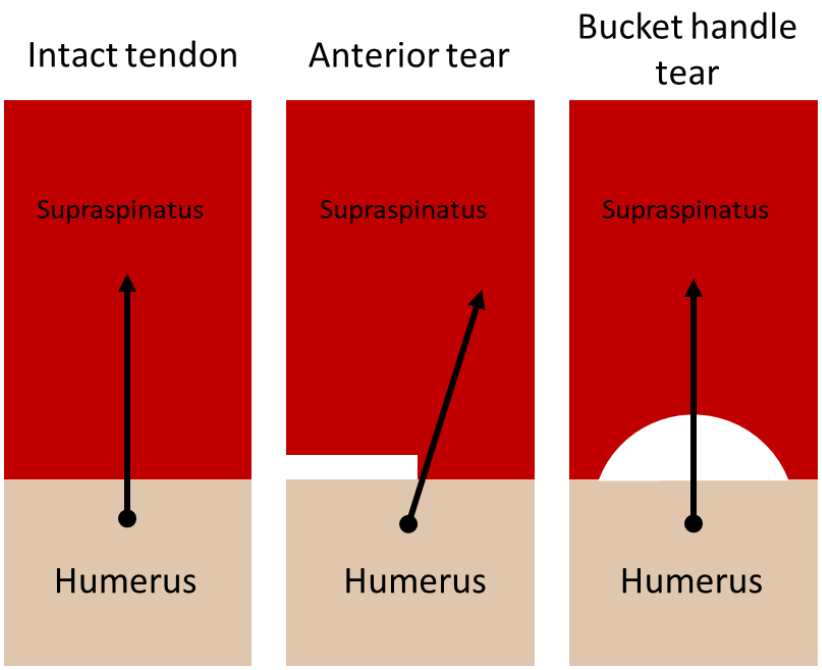

Figure 6.25 – Schematic to show the difference between an intact supraspinatus, an anterior tear and a bucket handle tear of the supraspinatus. The simplified line of action of the muscle is shown by the arrow.

The mean distribution of the total force between the muscles of the shoulder at minimum and maximum abduction for the artificial and natural tear cases were provided in Figure 6.24. The contribution of the supraspinatus muscle decreased with the artificial tear with the anterior deltoid compensating as discussed in Section 6.6. However, in the natural tear sample, the supraspinatus muscle provided 58% of the force. This suggests that the impact of the natural tear on the supraspinatus tendon is low due to the considerable force that is still produced by the tendon. The unaltered line of action of the muscle may impact the force producing capacity of the tendon compared to the anterior tendon tear.

The magnitude of total force required in all the muscles at maximum abduction is higher for natural tear cases than during the artificial tear. This supports the theory that the tear causes the shoulder to become less stable due to the role of the supraspinatus muscle in maintaining stability of the humeral head into the glenoid fossa. Due to the decrease in stability of the joint, the remaining rotator cuff tendons and the tendons of the deltoid must apply a greater magnitude of force to prevent the joint from dislocating.

6.10 Overall Discussion

The aim of this chapter of work was to assess at the effectiveness of the human shoulder simulator through the testing of four cadaveric samples. The first objective outlined in Section 6.1 was to use the human shoulder simulator to assess the repeatability of the simulator at producing cyclic motion. The output from the simulator was the force in each muscl e over the movement cycles, as shown for example in Figure 6.10. For all cases of this force over-time graph, the magnitude of force in all muscles decreased over the first 7 cycles to reach a plateau. From that point onwards, the force in each muscle was very repeatable throughout the remaining cycles. This is shown in Figure 6.15, where the cycles (10-20) are plotted on top of each other starting at 0° abduction. The point at which each muscle initiates to perform the abduction motion is repeatable throughout the 11 cycles as is the magnitude of force produced by each muscle. Consequently the simulator is able to perform repeatable cycles. There is some difference observed in the results between samples a s shown in the difference between the results for samples 2 and 4 shown in Figure 6.22 and Figure 6.23. The results are comparable for the intact states of the two samples however considerable difference exist between the 50% artificial tear results of the two samples. The difference in results between these samples was likely to be due to the inherent differences between human tissue samples and within a single sample the simulator has been shown to be consistent.

The second objective was to use the simulator to assess the effect that a rotator cuff tear and repair had on the muscle forces within the joint. Three samples were available for the study however due to a large rotator cuff tear in one of the samples only two samples were suitable for the full range of testing. In order to maximise the testing possible with two samples, a study design was created (Figure 6.7) with a series of six sub studies. Each sub study was designed to compare two samples which underwent the same motion cycle and same test conditions. Following the conclusion of sub study A it was shown that the simulator was able to accurately model a larger range of motion. Originally the motion was limited to 30° abduction due to the increasing effect of scapulothoracic motion past this abduction angle. The deltoid muscle provides a larger quantity of force at the middle range of abduction, therefore by increasing the abduction angle to 50° the deltoid muscle was able to take a more active role in the motion whilst also preventing the impingement of the humeral head on the acromion of the scapula. The results were compared between samples of which none contained scapulothoracic motion hence the extended motion cycle allowed for a better understanding of the joint biomechanics. The results from this sub study showed that the deltoid muscle played a more active role during the 50° abduction compared to the limited 30° motion which was predominantly created by the supras pinatus muscle.

Sub studies B to E looked at the comparison in results between samples 2 and 4 for varying levels of rotator cuff tears and repairs. Initially the samples were tested in an intact natural state using the extended motion cycles. A 50% tear of the supraspinatus muscle was then performed by an upper limb surgeon to replicate an anterior rotator cuff tear, which were then tested with the extended motion cycles. The 50% tear was extended to a full artificial supraspinatus tear which resulted in the supraspinatus tendon being fully detached from the humeral head. The extended motion cycle was performed by the joint however due to instabilities within the shoulder it was unable to perform the motion from the 0° position. However, if the joint motion started from an angle of 15° the deltoid muscle could abduct the shoulder effectively. This finding was supported by another study which found that the supraspinatus initiated the first 15° of abduction before the deltoid muscle played more of a role in the motion (Lam and Bordoni, 2021). Finally a double row repair of the tendon was performed by an upper limb surgeon which was tested using the extended motion cycle.

The forces required for the extended motion cycle for both samples were comparable with the supraspinatus muscle providing the majority of the force along with the anterior and middle deltoids at maximum abduction. The 50% tear in sample 2 resulted in a decrease in supraspinatus force compensated for by an increase in the anterior deltoid force. This was not seen in the same test scenario in sample 4 as the contribution of the supraspinatus muscle did not decrease. It was predicted that this was possibly due to the difference in size between the two samples and that a critical tear size had not been reached to alter the biomechanics of the joint as discussed in Section 6.6. Further samples would be required to evaluate this further and to assess the impact of different sized tears on the biomechanics of the joint. The tear was then extended on both samples to form a full supraspinatus artificial tear which detached the tendon from the humeral head. A double row repair was carried out on the torn tendon by an upper limb surgeon in both sample 2 and 4. In both cases the results showed that the supraspinatus contributed a higher percentage of force than during the intact natural case. This suggests that the stiffness of the repair is greater than the natural intact tendon which impacts the forces undergone by the tendon which could be a reason for the very high failure rates of the surgical repair of the rotator cuff tendon. A common failure mechanism for repairs is the tendon pulling through sutures suggesting a weakness at the tendon-suture interface (Cummins and Murrell, 2003). This could be due to the much higher forces passing through the supraspinatus tendon than during an intact scenario. Further human tissue samples would enable testing to continue to support the trends identified with the samples presented through this Chapter. This would be particularly the case for the 50% tear scenario which has conflicting results in the two samples.

6.11 Conclusion

The human shoulder simulator detailed in Chapter 5 was used with human cadaveric samples in order to assess the repeatability of the simulator, the effect of time on tissue quality and the effect of rotator cuff tear and repairs on the muscle forces within the joint. The testing indicated that cyclic testing of cadaveric samples could be successfully achieved using the novel shoulder simulator and this resulted in repeatable muscle force data during abduction and flexion motions. The difference in muscle forces and contributions during the abduction motion for an intact rotator cuff, an artificial tear of the supraspinatus and a double row repair was also studied in two independent samples. Further work to continue these studies for additional human tissue samples would enable a clearer picture to be formed regarding the results.

Chapter 7 – Overall Discussion, Conclusions and Future Work

7.1 Introduction

The rotator cuff tendons encircle the glenohumeral joint to prevent dislocation of the shoulder by compressing the humeral head into the glenoid fossa. The rotator cuff muscles also provide an important role in the initiation of the wide range of movement at the shoulder joint (Hess, 2000). Over half of all major injuries to the shoulder joint are tears of the rotator cuff tendons which can cause stiffness, instability, weakness and pain which limit the function of the joint (Rockwood and Matsen, 1998; May and Garmel, 2020). There is a high incidence of rotator cuff tears which increases with age. Approximately 30% of adults aged over 60 years have a rotator cuff tear, rising to 62% of adults over the age of 80 years (May and Garmel, 2020). Conservative treatment for tears of the rotator cuff including physiotherapy can be successful particularly for small tears. However in over 40% of cases continuing pain and weakness lead to the requirement for surgical intervention (Greenall et al., 2018). Failure rates of surgical repairs of rotator cuff tears are variable (17% to 94%) depending on the size and depth of the tear alongside the age of the patient (Zheng et al., 2008; Greenall et al., 2018). Assessment of current surgical treatments and development of new treatments are limited by a lack of appropriate functional pre-clinical testing. This is currently mainly limited to biomechanical static cadaveric testing which does not assess the efficacy of a treatment over an extended number of cycles or the functional ability of the repair method.

The aim of this research was to develop an experimental simulator that would test a natural shoulder joint through a wide range of repeatable motions through the application of appropriate loads. Additionally, the aim was for this simulation method to be used to test the efficacy of rotator cuff repair methods and assess the effects on the joint biomechanics. The objectives included the evaluation of surrogate animal (porcine) tissue, the development of a computational model of the human and porcine shoulder joints, the development of a porcine shoulder simulator followed by the translation to a natural human shoulder simulator using cadaveric tissue. The aims were decided through collaboration with consultant orthopaedic surgeons in order to maximise the clinical relevance of the research. This collaboration was maintained throughout the research to understand the problem and then to assess the value of the human shoulder simulator with the inclusion of the rotator cuff tears.

7.2 Project Overview

Initially a surrogate animal model of the shoulder joint was sought to reduce the ethical burden and cost of using human cadaveric tissue. Animal models provide the opportunity to use healthy tissue with more consistent biomechanical properties (Derwin et al., 2010; Hast et al., 2014; Lebaschi et al., 2016). However, the difference between animal and human anatomy led to challenges in finding a suitable surrogate model for the human shoulder joint. Most accessible animal tissue is sourced from quadruped animals where the shoulder joint is a weight bearing joint and hence the function of the joint is very different from the highly mobile joint of the human (Hast et al., 2014). One of the objectives of the project was to determine if a suitable surrogate animal model of the shoulder joint was available. The objective was met through the dissection of porcine shoulder joints and a review of the literature regarding the difference between porcine and human shoulder anatomy described in Chapter 2. Consequently, the suitability of a surrogate animal model for the development of a natural shoulder simulator was investigated. The porcine shoulder was found to not be suitable for use as a replica of the human joint in a natural shoulder simulator due to the anatomical differences between the two joints. Therefore, the porcine joint was to be used for the development of the methodologies required for the simulation of the shoulder joint which would then be translated to the human shoulder joint in order to provide relevant clinical outcomes.

A computational model of the shoulder complex was created (Chapter 3) in order to inform the loading and motion regimes in the natural joint simulator. Computational models of joints allow for further understanding into the role of muscles in producing motion around the joint (Veeger et al., 1991; Maurel et al., 1996). The outputs from the computational model informed the requirements of motion and force which were inputs into the design specification for the shoulder simulator. The differences between a porcine surrogate model of the shoulder and the human shoulder joint were also investigated using bespoke computational models of the two joints.

Design specifications for both the porcine shoulder simulator and the human shoulder simulator were then made using outputs from the two computational models as well as other research regarding the two joints. The porcine design specification is described in Chapter 4 and the human design specification is given in Chapter 5. This identified that the porcine joint simulator could be used to develop the methodologies for the human shoulder joint including the proof of concept of using stepper motors to induce displacement of the rotator cuff tendons and the methodology developed for force measurement. However, a simulator using human cadaveric tissue would be required to enable testing of the human rotator cuff due to

the differences between the human and porcine joints as found through the design specifications and dissections of the porcine joint.

The fourth objective included the development of a natural shoulder simulator capable of cyclic shoulder motions. A porcine shoulder simulator was made initially which enabled cyclic testing of the porcine joint through the motions of flexion and extension. The four rotator cuff tendons and the deltoid tendon were actively powered using stepper motors to control the displacement of the tendons. The force in each muscle required to perform the motion was measured throughout the cycle. The methodology developed using the porcine tissue was then translated to a human cadaveric sample which was able to produce higher values of flexion/extension and abduction/adduction motions.

The human shoulder simulator was used to assess the impact of rotator cuff tears and their subsequent surgical repair on the biomechanics of the joint as outlined in the fifth objective of the project. Failure rates of surgical repairs of rotator cuff tears were found to be variable (17% to 94%) depending on the size and depth of the tear alongside the age of the patient (Zheng et al., 2008; Greenall et al., 2018). The main cause for failure of surgical repair strategies were reported to be mechanical failure at the repair site of the tendon-bone interface (Zheng et al., 2008). Quantifying the change in loads through the tendon-bone region between the natural intact rotator cuff, the torn supraspinatus and the repaired supraspinatus gave an indication on the effect of the repair strategies at returning the joint to the natural intact biomechanics.

The human shoulder simulator was used with three cadaveric shoulder samples to investigate the effect of a double row repair method on the muscle forces within the joint (Chapter 6). The overall force within all the muscles of the shoulder model increased with the presence of a tear of the rotator cuff then increased further with a double row repair of the supraspinatus tendon. The force specifically in the supraspinatus tendon decreased in the presence of a tear as the deltoid muscle contributed a higher proportion of load in order to achieve the abduction motion. The force in the supraspinatus increased considerably, to a higher contribution than in the intact scenario, when the supraspinatus tendon was repaired using the double row repair method. These results suggested that the current gold standard repair method (double row repair) causes an increase in force within the supraspinatus tendon and generally within the shoulder muscles possibly due to the increase of stiffness of the tendon-bone interface. This could indicate the reason for high failure rates because the forces within the tendon are higher which would encourage suture pull out and mechanical failure of the repair method.

7.3 Novelty of the Human Shoulder Simulator

Natural shoulder simulators previously reported in the literature have been described in Chapter 1 in order to inform the design of this project and to identify the gaps in the capability of these devices. A comparison of the most notable shoulder simulators is given in Table 1.4, this showed that cyclic motion (i.e. repeated cycles) using the natural joint had currently not been investigated.

All the simulators discussed in Section 1.4.3.2 used linear pneumatic actuators to control the muscles of the shoulder through the motion cycles. It was decided for this simulator to use stepper motors due to the close control that the user had over the motion produced. Table 4.2 gives the advantages and disadvantages of a variety of actuation methods including pneumatic actuators and the stepper motors. Pneumatic actuators have higher power than the stepper motors at high speeds however have lower positional accuracy. The speed of motion of the simulator was not considered to be of high importance due to the low speed of motion that is performed at the shoulder (Rockwood and Matsen, 1998a). The shoulder simulator would perform a limited number of cycles (<50) due to the constraints associated with the cadaveric tissue during prolonged testing. Hence, it was concluded that the positional accuracy of the stepper motors were more beneficial to the simulator design than the high power of the pneumatic actuators.

Inputs to the simulator in order to determine the displacements to be applied to each muscle were calculated using different techniques in each of the simulators analysed in Section 1.4.3.2. The Aachen shoulder simulator used a teach-in method where the user passively moved the humerus in the desired motion to determine the length of muscles and hence actuation needed to produce the motion (Verjans et al., 2016). This method allowed for a wide range of motions to be modelled however it did not account for the natural distribution of force between the muscles seen in vivo. The simulator made by Guo et al (2023) used input data from the cross sectional area of the individual muscles and EMG data from literature (Guo et al., 2023). Kedgley et al (2007) tested four different regimes of muscle loading alongside a passive system: (1) equal loads applied to each muscle, (2) the cross sectional area of each muscle was relative to the applied loads, (3) loads were applied based upon the average force from an EMG study, and (4) loads from the EMG study changes as a function of abduction angle. It was deemed that none of these methods gave a true representation of the loading due to the assumptions made in each method. The cross sectional area of the muscles was found to change constantly throughout the motion cycles and so picking a single ratio based upon a snapshot of the motion led to inconsistences. The difficulty in obtaining accurate EMG data for the muscles of the shoulder, in particular the rotator cuff muscles was also noted.

However, it was found that all the active muscle controlled methods provided more repeatable motion than the passive scenario (Kedgley et al., 2007). The simulator developed during this project used input data from a bespoke biomechanics computational model described in Chapter 3. A model of the human shoulder simulator was developed which applied the desired motion to the joint. Inverse kinematics were then used to calculate the force required in each muscle to produce the desired motion. This information was used to inform the motion cycle, a process of tuning the code was used in order to ensure that the correct motion was performed.

The other simulators studied performed very limited number of cycles (<3) except from the Baumgartner simulator which did not use the natural shoulder joint. The novelty of the developed simulator was the ability to perform long cycles of both abduction/adduction and flexion/extension. Increasing the number of cycles performed by the simulator would allow for its use to assess the efficacy of a rotator cuff repair method over a longer period. During the experiments detailed in Chapter 6, the force in each muscle of the joint was shown to decrease over the first 6 cycles before reaching a plateau which then remained constant for the remainder of the motion cycle. This was deemed to be due to the bedding in of the humeral head into the glenoid fossa at the beginning of the motion. In the case of a very limited number of motion cycles being performed (<3), as with other simulator, the plateau of muscle forces would not have been reached and so hence the muscle forces recorded by the simulator would be skewed higher.

In summary the key areas of novelty of the human shoulder simulator developed through this project were the ability to perform cyclic motion, the calculation of the input displacements and the control of the rotator cuff muscles. This shoulder simulator was the first simulator which used a bespoke computational model to develop the trajectories for the physical cadaveric simulator instead of relying on estimations of muscle force from literature. The other key novelty was the ability of the simulator to perform cyclic motions (>3 cycles of each motion) to allow the assessment of rotator cuff biomechanics over a longer time period.

7.4 Limitations

Several limitations with the human shoulder simulator developed through this project were identified which should be considered in future studies involving the use of this simulator. Decisions were made in the design process to limit the complexity of the initial design however, these impacted the accuracy of the human shoulder simulator. Firstly, during the dissection process the arm inferior to the elbow joint and the surrounding muscles, fat and skin were removed to allow for easy access to the glenohumeral joint and the rotator cuff

tendons. The lower arm weighs approximately 1.5% of body weight (Dempster and Gaughran, 1967). For an average weight male of 85 Kg the lower arm therefore weighs approximately 13 Kg (NHS Digital, 2023). The lower arm increases the contact forces within the joint and hence the muscle forces during the abduction and flexion motions due to the higher loads that must be moved. The weight distribution of the arm is moved further away from the centre of rotation and hence the moments around the joint are increased (Pria, 2022).Some previously reported shoulder simulators included a weight on a rod extending from the base of the humerus in order to replicate the weight of the lower arm (Kedgley et al., 2007; Verjans et al., 2016; Guo et al., 2023). The bespoke AnyBody model of the human shoulder joint and the human simulator was used to assess the impact of removing the lower arm on the muscle forces in the shoulder joint. It was determined that the magnitude of the loads decreased however the distribution of force between the muscles remained constant with the removal of the lower arm. Consequently, during the development of this simulator, there was no replacement for the lower arm. Due to the difference in mechanical properties of living human tissue and saturated salt solution treated cadavers, the magnitude of force in each joint was deemed not to be an accurate output from the simulator. The comparisons between forces contributed by each muscle would be a more appropriate measure to allow for comparisons between each repeat and the different test scenarios.

The number of muscles that could be independently controlled was limited to five due to the control board that was selected for use of controlling the stepper motors. Consequently, the infraspinatus and teres minor tendons were controlled through the same stepper motor in order to allow for independent control of both the anterior and middle portions of the deltoid as described in Chapter 5. Both of these muscles do not play a large role in the motion of the shoulder however are key to stabilising the humeral head into the glenoid fossa, hence it was decided that they could be actuated together. The other muscles that were removed from the model including the posterior deltoid, latissimus dorsi and pectoralis major may play a more important role in the function of the shoulder joint. These muscles were removed following the decision to remove the scapulothoracic motion from the simulator. The pectoralis major and latissimus dorsi muscles have an important role in rotating the scapula throughout the abduction motion. The muscles also had to be removed in order to allow for access during the dissection process to reach the rotator cuff muscles which lie beneath these muscles. The pattern of required forces at the higher degrees of abduction was likely to be different if the scapulothoracic motion was included due to the role of the scapulothoracic joint at higher degrees of abduction. As the scapula was held stationary for all testing with the simulator, comparisons between samples and test scenarios could be made and assessed.

Porcine tissue was selected to be explored as a suitable surrogate tissue due to its availability within the food chain and the consistent age of slaughter leading to uniform tissue quality and mechanical properties (Derwin et al., 2010). Through the dissection of porcine shoulder joints, the anatomy and functionality of the porcine shoulder was assessed to determine the suitability of the porcine model to mimic the human shoulder joint. It was concluded that due to several anatomical differences between the two joints, the porcine shoulder could not be used to replicate the biomechanics and motion of the human shoulder joint. Therefore, only the method development process could be achieved using the porcine tissue and all further studies required the use of human cadaveric tissue. There is a very high prevalence of rotator cuff tears among the older population, 62% of adults over the age of 80 years have a rotator cuff tear (May and Garmel, 2020). Consequently, a high proportion of the cadaveric samples were likely to have some rotator cuff pathologies which was seen through this study where 25% of the samples had a tear of the key rotator cuff muscles. As a result of the inconsistencies between samples, a higher number of samples would be required for use within a study to allow for conclusions to be drawn between samples however this was difficult to achieve due to the availability and cost of the samples. Hence, the study design was completed in a way to maximise the use of the samples based upon the condition of the natural joint. In the final study of this project, a single sample underwent all test conditions of natural joint, 50% tear of the supraspinatus, 100% tear of the supraspinatus and double row repair. This allowed comparisons to be made within a sample as well as between samples maximising the data that could be obtained from a single sample. The biological healing process was not studied in the repair cases due to the nature of the cadaveric tissue however, the mechanical function of the repair strategy immediately post-surgery was instead studied.

7.5 Research Value and Impact

This thesis has provided a methodology for preclinical functional simulation of the natural shoulder joint through cyclic motion of the joint. The lack of functional preclinical testing is likely to be a factor in the very high failure rates of surgical repairs of the rotator cuff tendons; 17% to 94% depending on the size and depth of the tear alongside the age of the patient (Zheng et al., 2008; Greenall et al., 2018). Through the development of a novel shoulder simulator that could subject the natural shoulder joint and rotator cuff tendons to appropriate forces and motions through multiple motion cycles, the aim of the project was met. The simulator adds value to the simulation techniques currently available by allowing for cyclic testing to enable assessment of how a repair behaves beyond the initial motion. The cadaveric joints were tested in several scenarios from intact, partially torn, fully torn and repaired which

enabled the change in biomechanics within a sample to be assessed to determine the effect a rotator cuff tear and repair have on the joint biomechanics.

The data obtained through the project, in particular the study discussed in Chapter 6 on rotator cuff repair methods, showed that the successful cyclic testing of cadaveric samples could be achieved using the novel shoulder simulator in order to obtain repeatable force data through the abduction and flexion motions. The difference in muscle forces and contributions during the abduction motion for an intact rotator cuff, a tear of the supraspinatus and a double row repair was also studied in two independent samples.

The ability to collect baseline force data of the natural joint biomechanics allowed for the muscle forces and contributions after a double row repair of the supraspinatus to be compared to the natural state. The ability of the repair method at restoring the natural biomechanics of the joint could also be assessed. This ensures that the variability of cadaveric tissue does not limit the outcomes of the simulator as the results from each sample can be compared to the baseline for the specific sample.

A successful cadaveric shoulder simulator would allow for more informed surgical decision making to take place regarding the impact of tear types and the requirement for surgical intervention and the type of repair to provide maximum biomechanical repair for a tear type. The type of tear on the sample was shown, in Section 6.6, to have a large effect on the muscle forces within the joint and to also impact the ability of the joint to perform normal abduction movement. If the size at which a tear begins to overly impact the surrounding muscles of the shoulder could be determined through more cadaveric testing then informed decisions regarding the point at which surgical interventions are required could be made.

Current testing methodologies for assessment of the efficacy of rotator cuff repairs predominantly use static testing followed by in vivo animal testing which has large ethical considerations and costs associated (Waltrip et al., 2003; Kim et al., 2006; Smith et al., 2006). The development of a cadaveric shoulder simulator which enables active control of the muscles through a range of motions reduces the need for in vivo animal testing to determine the mechanical efficacy of a repair method. Reducing, replacing and refining the use of animal models is a key target within the scientific community (Home Office et al., 2014), hence the use of a cadaveric shoulder simulator would add value with the reduction of the need for in vivo animal testing.

7.6 Future Work

The human shoulder simulator was developed and shown to allow for cyclic testing of cadaveric shoulder samples to obtain repeatable force data through the abduction and flexion motions. The difference in muscle forces and contributions during the abduction motion for an intact rotator cuff, a tear of the supraspinatus and a double row repair was also studied in two independent samples. Additional human tissue samples would need to be used to gain more data on the repeatability of the simulator particularly between samples. The sample size discussed in Chapter 6 was low, particularly due to the variability in the tissue received. Therefore the completion of additional samples would provide additional results of force in the muscles for different test conditions in order to compare to the current results and provide a clearer picture to be formed regarding the trends of these results.

It was shown in Section 1.4.3.2 that all current natural shoulder simulator hold the scapula stationary during abduction and prevent any scapulothoracic motion from occurring. Future work could look at including the scapulohumeral rhythm within the novel natural shoulder simulator through the use of additional stepper motors controlling the scapula position.

The method of determining the input code required to produce the required motion within the simulator was detailed in Figure 4.16 and contained a tuning stage which was a manual process. Future work could turn this stage into an automated process using a PID controller to drive the muscles until the force measured using the load cells meets a required level obtained from the AnyBody model.

It was found in Section 6.9 that there was a considerable difference in the force results between a natural tear of the supraspinatus and the manmade tear of the supraspinatus. The tears were in different positions on the supraspinatus tendons which altered the biomechanics in different ways as seen in Figure 6.25. It was also noted in Section 6.9 that the methodologies used to create the manmade tear of the supraspinatus resulted in a ridge being formed at the remaining root of the tendon. The ridge in the supraspinatus tendon would then catch on the posterior portion of the acromion causing irregularities in the results. Due to the predominately chronic nature of natural rotator cuff tears, the tendon normally thins before tearing (Rockwood and Matsen, 1998). However, in the case of the manmade tear a cut was made through otherwise healthy tendon tissue resulting in the ridge. Consequently, a study to determine the best way to accurately recreate a natural tear of the supraspinatus tendon would allow for more accurate testing of this injury state to be performed.

From the human shoulder testing conducted in Chapter 6, it was also determined that the size of rotator cuff tear would affect the impact on the muscle forces and the existence of a critical

size at which the biomechanics are considerably altered might exist. Further testing should be conducted which incrementally increases the size of the rotator cuff tears in order to determine if a critical size does exist. If the point at which the biomechanics of the rest of the muscles of the shoulder are considerably altered could be determined then this would further inform surgical decision making regarding the size of tear and the impact of surgical repair for a specific tendon tear.

Due to the very high failure rates of rotator cuff repairs the use of augmentation devices has been increasing. The aim of an augmentation device is to mechanically support the tendon to allow for tissue growth and rotator cuff repair by reducing the force going through the tendon (Cobb et al., 2022). Several clinical studies have taken place regarding the clinical outcomes of using synthetic and biological patches to augment rotator cuff repairs (Ranebo et al., 2018; Cowling et al., 2020; Smolen et al., 2020; de Andrade et al., 2022) however biomechanical studies to look at the effect of a patch on the underlying muscle forces are lacking. Consequently, a study to assess the impact of different augmentation devices on the biomechanics and muscle forces within the joint would allow for further understanding on the biomechanical effect of the device.

7.7 Conclusions

The overall aim of the project was met through the design and development of a natural shoulder simulator which allows for functional cyclic testing of the natural shoulder through common motions. The human cadaveric testing completed with the simulator indicated that successful cyclic testing of cadaveric samples could be achieved using the novel shoulder simulator in order to obtain repeatable force data through the abduction and flexion motions. The shoulders were able to be tested in the natural state (intact and torn) followed by a manmade tear of the supraspinatus tendon and a surgical double row repair. The change in force distribution between these states was recorded and assessed to determine the change in biomechanics between these states. The double row repair of the supraspinatus tendon caused a higher force to be experienced by the supraspinatus during the abduction motion than in the intact state. This could be an indication for the high mechanical failure rate of the surgical repair strategies however further research is required before concrete conclusions can be made.

Overall, the work detailed in this thesis shows the value and potential for using a cadaveric human shoulder simulator to investigate the effect of rotator cuff tears and repairs on the biomechanics of the natural shoulder joint. There is also potential for the shoulder simulator

to be used to assess other variables in rotator cuff repair including alternative surgical repair methods and augmentation devices.

Chapter 8 References

Abdelwahab, A., Ahuja, N., Iyengar, K.P., Jain, V.K., Bakti, N. and Singh, B. 2021. Traumatic rotator cuff tears - Current concepts in diagnosis and management. *Journal of Clinical Orthopaedics and Trauma*. **18**, pp.51–55.

Agriculture and Horticulture Development Board 2020. GB Average Carcase Weight. [Accessed 12 July 2021]. Available from: https://ahdb.org.uk/pork/gb-average-carcase-weight.

Ahmad, Z., Al-Wattar, Z. and Rushton, N. 2020. Tissue Engineering for the Ovine Rotator Cuff: Surgical Anatomy, Approach, Implantation and Histology Technique, along with Review of Literature. *Journal of Investigative Surgery*. **33**(2), pp.147–158.

Akhtar, A., Richards, J. and Monga, P. 2021. The biomechanics of the rotator cuff in health and disease – A narrative review. *Journal of Clinical Orthopaedics and Trauma*. **18**, pp.150–156.

de Andrade, A.L.L., Garcia, T.A., Brandão, H. de S., Sardeli, A.V., Mouraria, G.G. and Belangero, W.D. 2022. Benefits of Patch Augmentation on Rotator Cuff Repair: A Systematic Review and Meta-analysis. *Orthopaedic Journal of Sports Medicine*. **10**(3), pp.1–12.

Anspach, D. 2020. What are the activities of daily living? [Accessed 3 December 2020]. Available from: https://www.thebalance.com/what-are-the-activities-of-daily-living-2388730.

AnyBody 2024. The AnyBody Managed Model Repository. [Accessed 25 April 2024]. Available from: https://www.anybodytech.com/software/ammr/.

AnyBody Technology 2024. Introduction to Muscle Modeling. Available from: https://anyscript.org/tutorials/Muscle_modeling/intro.html.

AnyBody Technology 2021. The AnyScript Reference Manual : AnyMuscleModel. [Accessed 20 April 2021]. Available from: file:///C:/Program Files/AnyBody Technology/AnyBody.7.3/Documentation/AnyScriptReference/reference/classes/AnyMuscleModel.html?highlight=muscles.

Athwal, G. and Armstrong, A. 2017. Rotator Cuff Tears. [Accessed 25 November 2020]. Available from: https://orthoinfo.aaos.org/en/diseases--conditions/rotator-cuff-tears/.

Barnes, C.J., Van Steyn, S.J. and Fischer, R.A. 2001. The effects of age, sex, and shoulder dominance on range of motion of the shoulder. *Journal of Shoulder and Elbow Surgery*. **10**(3), pp.242–246.

Baumgartner, D., Tomas, D., Gossweiler, L., Siegl, W., Osterhoff, G. and Heinlein, B. 2014. Towards the development of a novel experimental shoulder simulator with rotating scapula and individually controlled muscle forces simulating the rotator cuff. *Medical and Biological Engineering and Computing*. **52**(3), pp.293–299.

Beger, O., Karagül, M.İ., Koç, T., Kayan, G., Cengiz, A., Yılmaz, Ş.N. and Olgunus, Z.K. 2020. Effects of different cadaver preservation methods on muscles and tendons: a morphometric, biomechanical and histological study. *Anatomical Science International*. **95**(2), pp.174–189.

Bergmann, G., Graichen, F., Bender, A., Kääb, M., Rohlmann, A. and Westerhoff, P. 2007. In vivo glenohumeral contact forces-Measurements in the first patient 7 months postoperatively. *Journal of Biomechanics*. **40**(10), pp.2139–2149.

Bisbinas, I., Magnissalis, E., Gigis, I., Beslikas, T., Hatzokos, I. and Christoforidis, I. 2013. Rotator cuff repair: A biomechanical ex vivo ovine study. *Proceedings of the Institution of Mechanical Engineers, Part H: Journal of Engineering in Medicine*. **227**(5), pp.560–570.

Bolsterlee, B., Veeger, H.E.J. and Chadwick, E.K.J. 2013. Clinical applications of musculoskeletal modelling for the shoulder and upper limb. *Medical and Biological Engineering and Computing*. **51**(9), pp.953–963.

Bowland, P., Ingham, E., Fisher, J. and Jennings, L.M. 2018. Development of a preclinical natural porcine knee simulation model for the tribological assessment of osteochondral grafts in vitro. *Journal of Biomechanics*. **77**, pp.91–98.

Burns, D.M., Bell, I., Katchky, R., Dwyer, T., Toor, J., Whyne, C. and Safir, O. 2018. Saturated Salt Solution Cadaver-Embalming Method Improves Orthopaedic Surgical Skills Training. *Journal of Bone and Joint Surgery*. **18**(September), pp.1–10.

Cadova, M. 2013. Use of OpenSim and AnyBody modelling software for dynamic simulation of the human masticatory system. , pp.5–6.

Cartner, J., Hartsell, Z., Ricci, W. and Tornetta, P. 2011. Can we trust ex vivo mechanical testing of fresh-frozen cadaveric specimens? The effect of postfreezing delays. *Journal of Orthopaedic Trauma*. **25**(8), pp.459–461.

Chang, L.-R., Anand, P. and Varacallo, M. 2023. *Anatomy, Shoulder and Upper Limb, Glenohumeral Joing* [Online]. StatPearls Publishing. Available from: https://www.ncbi.nlm.nih.gov/books/NBK537018/.

Clavert, P. 2015. Glenoid labrum pathology. *Orthopaedics and Traumatology: Surgery and Research*. **101**(1), pp.S19–S24.

Cobb, T.E., Dimock, R.A.C., Memon, S.D., Consigliere, P., Ajami, S., Imam, M. and Ali Narvani, A. 2022. Rotator Cuff Repair With Patch Augmentation: What Do We Know? *Archives of Bone and Joint Surgery*. **10**(10), pp.833–846.

Coley, B., Jolles, B.M., Farron, A. and Aminian, K. 2008. Arm position during daily activity. *Gait and Posture*. **28**, pp.581–587.

Cone, S.G., Warren, P.B. and Fisher, M.B. 2017. Rise of the Pigs: Utilization of the Porcine Model to Study Musculoskeletal Biomechanics and Tissue Engineering During Skeletal Growth. *Tissue Engineering - Part C: Methods*. **23**(11), pp.763–780.

TE Connectivity 2024. *FX1901-0001-0025-L datasheet*.

Cowling, P., Hackney, R., Dube, B., Grainger, A.J., Biglands, J.D., Stanley, M., Song, D., Conaghan, P.G. and Kingsbury, S.R. 2020. The use of a synthetic shoulder patch for large and massive rotator cuff tears - A feasibility study. *BMC Musculoskeletal Disorders*. **21**(1), pp.1–12.

Cummins, C. and Murrell, G.A.C. 2003. Mode of Failure for Rotator Cuff Repair with Suture Anchors Identified at Revision Surgery. *Journal of Shoulder and Elbow Surgery*., pp.128–133.

Debski, R.E., McMahon, P.J., Thompson, W.O., Woo, S., Warner, J. and Fu, F.H. 1995. A new dynamic testing apparatus to study glenohumeral joint motion. *Journal of Biomechanics*. **28**(7), pp.869–874.

Delp, S., Anderson, F., Arnold, A., Loan, P., Habib, A., John, C., Guendelman, E. and Thelen, D. 2007. OpenSim: open-source software to create and analyze dynamic simulations of movement. *IEEE Transactions on Biomedical Engineering*. **54**(11), pp.1940–1950.

Dempster, W. 1955. Space requirements of the seated operator: Geometrical, kinematic and mechanical aspects of the body with special reference to the limbs.

Dempster, W.T. and Gaughran, G.R.L. 1967. Properties of body segments based on size and weight. *American Journal of Anatomy*. **120**(1), pp.33–54.

Derwin, K.A., Baker, A.R., Iannotti, J.P. and McCarron, J.A. 2010. Preclinical models for translating regenerative medicine therapies for rotator cuff repair. *Tissue Engineering - Part B: Reviews*. **16**(1), pp.21–30.

Doriot, N. and Wang, X. 2006. Effects of age and gender on maximum voluntary range of motion of the upper body joints. *Ergonomics*. **49**(3), pp.269–281.

Dorisea 2017. Dorisea Extreme Braid 100% Pe 100m Briaded Fishing Line. [Accessed 21 June 2021]. Available from: https://www.amazon.co.uk/109Yards-String-Abrasion-Resistant-Incredible-Superline/dp/B077P77V2W/ref=sr_1_4?dchild=1&keywords=Dorisea%252BExtreme%252BBraid%252B100%2525%252BPe%252BYellow%252BBraided%252BFishing%252BLine%252B109Yards-2187Yards%252B6-550Lb%252BTest%252BFishing%252BWire%25.

Dowson, D. and Unsworth, A. 2016. Physical Joint Simulators *In*: *Proceedings of the Institution of Mechanical Engineers, Part H: Journal of Engineering in Medicine*., pp.345–346.

Dyrna, F., Kumar, N.S., Obopilwe, E., Scheiderer, B., Comer, B., Nowak, M., Romeo, A.A., Mazzocca, A.D. and Beitzel, K. 2018. Relationship Between Deltoid and Rotator Cuff Muscles During Dynamic Shoulder Abduction: A Biomechanical Study of Rotator Cuff Tear Progression. *American Journal of Sports Medicine*. **46**(8), pp.1919–1926.

Edemekong, P., Bomgaars, D., Sukumaran, S. and Levy, S. 2020. Activities of Daily Living.

Favre, P., Sheikh, R., Fucentese, S.F. and Jacob, H.A.C. 2005. An algorithm for estimation of shoulder muscle forces for clinical use. *Clinical Biomechanics*. **20**(8), pp.822–833.

Felstead, A.J. and Ricketts, D. 2017. Biomechanics of the shoulder and elbow. *Orthopaedics and Trauma*. **31**(5), pp.300–305.

Ferreira, L.M., Johnson, J.A. and King, G.J.W. 2010. Development of an active elbow flexion simulator to evaluate joint kinematics with the humerus in the horizontal position. *Journal of Biomechanics*. **43**(11), pp.2114–2119.

Flores-hernandez, C., Eskinazi, I., Hoenecke, H.R. and Lima, D.D.D. 2019. Scapulothoracic rhythm affects glenohumeral joint force. *JSES Open Access*. **3**(2), pp.77–82.

Frandson, R., Wilke, W. and Fails, A. 2009. *Anatomy and physiology of farm animals* 7th Edition. Wiley-Blackwell.

Frandson, R., Wilke, W.L. and Fails, A.D. 2003. *Anatomy and Physiology of Farm Animals* Sixth Edit. Philadelphia, Pennsylvania: Lippincott Williams & Wilkins.

Funk, L. 2005. Rotator cuff biomechanics. [Accessed 3 December 2020]. Available from: https://www.shoulderdoc.co.uk/article/384%0A.

Giles, J.W., Boons, H.W., Ferreira, L.M., Johnson, J.A. and Athwal, G.S. 2011. The effect of the conjoined tendon of the short head of the biceps and coracobrachialis on shoulder stability and kinematics during in-vitro simulation. *Journal of Biomechanics*. **44**(6), pp.1192–1195.

Giles, J.W., Ferreira, L.M., Athwal, G.S. and Johnson, J.A. 2014. Development and Performance Evaluation of a Multi-PID Muscle Loading Driven In Vitro Active-Motion Shoulder Simulator and Application to Assessing Reverse Total Shoulder Arthroplasty. *Journal of Biomechanical Engineering*. **136**(December), pp.1–10.

Goetti, P., Denard, P.J., Collin, P., Ibrahim, M., Hoffmeyer, P. and Lädermann, A. 2020. Shoulder & Elbow Shoulder biomechanics in normal and selected pathological conditions. . **5**(August).

Greenall, G., Carr, A., Beard, D., Rees, J., Rangan, A., Merritt, N., Dritsaki, M., Nagra, N.S., Baldwin, M., Hopewell, S. and Cook, J.A. 2018. Systematic review of the surgical management of rotator cuff repair with an augmentative patch: A feasibility study protocol 11 Medical and Health Sciences 1103 Clinical Sciences 11 Medical and Health Sciences 1117 Public Health and Health Services. *Systematic Reviews*. **7**(1).

Groves, D. 2015. Geometric Variances in Hip Osteoarthritis and Tribology of the Natural Hip. . (June).

Guo, R., Ferle, M., Nebel, D. and Hurschler, C. 2023. The development and evaluation of an in-vitro shoulder simulator with active muscle simulation. *Scientific Reports*. **13**(1), pp.1–11.

Hast, M.W., Zuskov, A. and Soslowsky, L.J. 2014. The role of animal models in tendon research. *Bone and Joint Research*. **3**(6), pp.193–202.

Hatta, T., Giambini, H., Hooke, A.W., Zhao, C., Sperling, J.W., Steinmann, S.P., Yamamoto, N., Itoi, E. and An, K.N. 2016. Comparison of Passive Stiffness Changes in the Supraspinatus Muscle After Double-Row and Knotless Transosseous-Equivalent Rotator Cuff Repair Techniques: A Cadaveric Study. *Arthroscopy - Journal of Arthroscopic and Related Surgery*. **32**(10), pp.1973–1981.

Hayashi, S., Homma, H., Naito, M. and Oda, J. 2014. Saturated Salt Solution Method : A Useful Cadaver Embalming for Surgical Skills Training. . **93**(27), pp.1–10.

Heinrichs, C., Knierzinger, D., Stofferin, H. and Schmoelz, W. 2018. Validation of a novel biomechanical test bench for the knee joint with six degrees of freedom. *Biomedical Engineering*. **63**(6), pp.709–717.

van der Helm, F.C.T. 1994a. A finite element musculoskeletal model of the shoulder mechanism. *Journal of Biomechanics*. **27**(5).

van der Helm, F.C.T. 1997. A three-dimensional model of the shoulder and elbow *In*: *1st International Conference of the International Shoulder Group*. Delft, Netherlands: Shaker Publishing BV, pp.65–70.

van der Helm, F.C.T. 1994b. Analysis of the kinematic and dynamic behaviour of the shoulder mechanism. *Journal of Biomechanical Engineering*. **27**(5), pp.527–550.

Hess, S.A. 2000. Functional stability of the glenohumeral joint. *Manual Therapy*. **5**(2), pp.63–71.

Home Office, Department for Business Innovation and Skills and Department of Health 2014. *Working to reduce the use of animals in scientific research*.

Jiang, M., Lawson, Z.T., Erel, V., Pervere, S., Nan, T., Robbins, A.B., Feed, A.D. and Moreno, M.R. 2020. Clamping soft biologic tissues for uniaxial tensile testing: A brief survey of current methods and development of a novel clamping mechanism. *Journal of the Mechanical Behavior of Biomedical Materials*. **103**(July 2019), p.103503.

Jimenez-Cruz, D., Dubey, M., Board, T. and Williams, S. 2022. An in vitro methodology for experimental simulation on the natural hip joint. *PLoS ONE*. **17**(8 August), pp.1–12.

Jones, O. 2021. TeachMe Anatomy: The Shoulder Joint. [Accessed 15 April 2021]. Available from: https://teachmeanatomy.info/upper-limb/joints/shoulder/.

Karlsson, D. and Peterson, B. 1992. Towards a model for force predictions in the human shoulder. *Journal of Biomechanics*. **25**(2), pp.189–199.

Keating, J., Waterworth, P., Shaw-Dunn, J. and Crossan, J. 1992. Relative Strengths of the Rotator Cuff Muscles: A Cadaver Study. *Bone and Joint Surgery*. **75**(1), pp.137–140.

Kedgley, A.E., Mackenzie, G.A., Ferreira, L.M., Drosdowech, D.S., King, G.J.W., Faber, K.J. and Johnson, J.A. 2007. The effect of muscle loading on the kinematics of in vitro glenohumeral abduction. *Journal of Biomechanics*. **40**(13), pp.2953–2960.

Kessel, L. and Bayley, I. 1986. *Clinical Disorders of the Shoulder*. Churchill Livingstone.

Kim, D.H., Elattrache, N.S., Tibone, J.E., Jun, B., Delamora, S.N., Kvitne, R.S. and Lee, T.Q. 2006. Biomechanical Comparison of a Single-Row Versus Double-Row Suture Anchor Technique for Rotator Cuff Repair. *The American Journal of Sports Medicine*. **34**(3), pp.407–414.

Kim, H.M., Dahiya, N., Teefey, S.A., Middleton, W.D., Stobbs, G., Steger-May, K., Yamaguchi, K. and Keener, J.D. 2010. Location and initiation of degenerative rotator cuff tears: An analysis of three hundred and sixty shoulders. *Journal of Bone and Joint Surgery*. **92**(5), pp.1088–1096.

Kingdom, U. 2006. Comparison of Single and Double-Row Fixation in Arthroscopic Rotator Cuff Repair. , pp.2425–2431.

Klar, S. 2016. Choosing Stepper- or servo- Driven Actuators to Replace Air Cylinders. *Tech Briefs*. [Online]. [Accessed 3 June 2024]. Available from: https://www.techbriefs.com/component/content/article/26067-choosing-stepper-or-servo-driven-actuators-to-replace-air-cylinders#:~:text=Electric actuators with stepper motors,and in force-sensitive applications.

Kulwicki, K.J., Kwon, Y.W. and Kummer, F.J. 2010. Suture anchor loading after rotator cuff repair: Effects of an additional lateral row. *Journal of Shoulder and Elbow Surgery*. (19), pp.81–85.

Lafosse, L., Lanz, U., Saintmard, B. and Campens, C. 2010. Arthroscopic repair of subscapularis tear: Surgical technique and results. *Orthopaedics and Traumatology: Surgery and Research*. **96**(8).

Lam, J. and Bordoni, B. 2021. *Anatomy, Shoulder and Upper Limb, Arm Abductor Muscles* [Online]. Treasure Island, FL: StatPearls Publishing. Available from: https://www.ncbi.nlm.nih.gov/books/NBK537148/?report=reader#_NBK537148_pubdet_.

Langohr, G.D.G. 2015. Fundamentals of the Biomechanical Characteristics Related to the Loading of Reverse Total Shoulder Arthroplasty Implants and the Development of a Wear Simulation Strategy.

Lanovaz, J.L., Clayton, H.M., Colborne, G.R. and Schamhardt, H.C. 1999. Forelimb kinematics and net joint moments during the swing phase of the trot. *Equine veterinary journal. Supplement*. **30**, pp.235–239.

Lebaschi, A., Deng, X.-H., Zong, J., Cong, G.-T., Carballo, C., Album, Z.M., Camp, C. and Rodeo, S.A. 2016. Animal Models for Rotator Cuff Repair. *Annals of the New York Academy of Sciences*. **1383**(1), pp.1–15.

Lemieux, P.O., Hagemeister, N., Tétreault, P. and Nuño, N. 2013. Influence of the medial offset of the proximal humerus on the glenohumeral destabilising forces during arm elevation : a numerical sensitivity study. *Computer Methods in Biomechanics and Biomedical Engineering*. **16**(1), pp.103–111.

Lemieux, P.O., Nuño, N., Hagemeister, N. and Tétreault, P. 2012. Mechanical analysis of cuff tear arthropathy during multiplanar elevation with the AnyBody shoulder model. *Clinical Biomechanics*. **27**(8), pp.801–806.

Liu, A., Jennings, L.M., Ingham, E. and Fisher, J. 2015. Tribology studies of the natural knee using an animal model in a new whole joint natural knee simulator. *Journal of Biomechanics*. **48**(12), pp.3004–3011.

Lombardero, M., Yllera, M.M., Costa-e-Silva, A., Oliveira, M.J. and Ferreira, P.G. 2017. Saturated salt solution: a further step to a formaldehyde-free embalming method for veterinary gross anatomy. *Journal of Anatomy*. **231**(2), pp.309–317.

Longo, U.G., Carnevale, A., Piergentili, I., Berton, A., Candela, V., Schena, E. and Denaro, V. 2021. Retear rates after rotator cuff surgery: a systematic review and meta-analysis. *BMC Musculoskeletal Disorders*. **22**(1), pp.1–14.

Lucas, D. 1973. Biomechanics of the Shoulder Joint. *Archives of Surgery*. **107**, pp.425–432.

Lugo, R., Kung, P. and Ma, C.B. 2008. Shoulder biomechanics. *European Journal of Radiology*. (68), pp.16–24.

Lumen Learning 2024. Skeletal Muscle - Anatomy and Physiology 1. [Accessed 12 November 2024]. Available from: https://courses.lumenlearning.com/suny-ap1/chapter/skeletal-muscle/#:~:text=This fascicular organization is common,or fascicle of the muscle.

Mancuso, F., Benedetto, P. Di, Tosolini, L., Buttironi, M.M., Causero, A., Ortopedica, C., Sanitaria, A., Integrata, U. and Maria, P.S. 2021. Treatment options for massive rotator cuff tears : a narrative review. *Acta Biomedica*. **92**(3).

Manske, R. 2018. Rotator Cuff Repair *In*: *Clinical Orthopaedic Rehabilitation: A Team Approach*., pp.117–129.

Martini, F., Nath, J. and Bartholomew, E. 2017. *Fundamentals of anatomy and physiology*. Pearson Education Limited.

Maruvada, S., Madrazo-Ibarra, A. and Varacallo, M. 2021. *Anatomy, Rotator Cuff* [Online]. Treasure Uskand (FL): StatPearls Publishing. Available from: https://www.ncbi.nlm.nih.gov/books/NBK441844/.

Mathewson, M.A., Kwan, A., Eng, C.M., Lieber, R.L. and Ward, S.R. 2014. Comparison of rotator cuff muscle architecture between humans and other selected vertebrate species. *Journal of Experimental Biology*. **217**(2), pp.261–273.

Matthews, T.J.W., Hand, G.C., Rees, J.L., Athanasou, N.A., Carr, A.J., Carr, P.A.J. and Surgery, O. 2006. Pathology of the torn rotator cuff tendon - Reduction in potential for repair as tear size increases. . **88**(4).

Maurel, W., Thalmann, D., Hoffmeyer, P., Beyloe, P., Gingins, P., Kalra, P. and Thalmann, N.M. 1996. *A Biomechanical Musculoskeletal Model of Human Upper Limb for Dynamic Simulation*.

May, T. and Garmel, G. 2020. *Rotator cuff injury* [Online]. Available from: https://www.ncbi.nlm.nih.gov/books/NBK547664/.

McCormick, F., Wilson, H., Gupta, A., Bruce, B., Harris, J., Abrams, G., Hussey, K. and Cole, B. 2014. Single-row, double-row, and transosseous equivalent techniques for isolated supraspinatus tendon tears with minimal atrophy: A retrospective comparative outcome and radiographic analysis at minimum 2-year followup. *International Journal of Shoulder Surgery*. **8**(1).

Meier, S.W. and Meier, J.D. 2006. The effect of souble-row fixation on initial repair strength in rotator cuff repair: A biomechanical study. *Arthroscopy - Journal of Arthroscopic and Related Surgery*. **22**(11), pp.1168–1173.

Milano, G., Grasso, A., Zarelli, D., Deriu, L., Cillo, M. and Fabbriciani, C. 2008. Comparison between single-row and double-row rotator cuff repair: A biomechanical study. *Knee Surgery, Sports Traumatology, Arthroscopy*. **16**(1), pp.75–80.

Minagawa, H., Yamamoto, N., Abe, H., Fukuda, M., Seki, N., Kikuchi, K., Kijima, H. and Itoi, E. 2013. Prevalence of symptomatic and asymptomatic rotator cuff tears in the general population: From mass-screening in one village. *Journal of Orthopaedics*. **10**(1), pp.8–12.

Murrell, G. and Walton, J. 2001. Diagnosis of Rotator Cuff Tears. *The Lancet*. **357**(9258), pp.769–770.

Najibi, S., Banglmeier, R., Matta, J. and Tannast, M. 2010. Material properties of common suture materials in orthopaedic surgery. *The Iowa Orthopaedic Journal*. **30**, pp.84–88.

NHS Digital 2023. Health Survey for England, 2021 part 2, Adults' health: Hypertension. , pp.1–27.

Nikooyan, A.A., Veeger, H.E.J., Chadwick, E.K.J., Praagman, M. and Helm, F.C.T. Van Der 2011. Development of a comprehensive musculoskeletal model of the shoulder and elbow. *Medical and Biological Engineering and Computing*. **49**, pp.1425–1435.

Oh, J.H., Jun, B.J., McGarry, M.H. and Lee, T.Q. 2011. Does a Critical Rotator Cuff Tear Stage Exist? *Journal of Bone and Joint Surgery*. **93**(22), pp.2100–2109.

Oh, J.H., Mcgarry, M.H., Jun, B.J., Gupta, A., Chung, K.C., Hwang, J. and Lee, T.Q. 2012. Restoration of Shoulder Biomechanics According to Degree of Repair Completion in a

Cadaveric Model of Massive Rotator Cuff Tear Importance of Margin Convergence and Posterior Cuff Fixation. *The American Journal of Sports Medicine*. **40**(11), pp.2448–2453.

Oosterwijk, A.M., Nieuwenhuis, M.K., van der Schans, C.P. and Mouton, L.J. 2018. Shoulder and elbow range of motion for the performance of activities of daily living: A systematic review. *Physiotherapy Theory and Practice*. **34**(7), pp.505–528.

Ooznest 2023. Technical Specification: NEMA17 Stepper Motors. [Accessed 10 July 2023]. Available from: https://ooznest.co.uk/product/nema17-stepper-motors/.

Pallan, R.L. 2016. Characterisation and in vitro simulation of the natural hip. *PQDT - UK & Ireland*. (September).

Pandey, V. and Jaap Willems, W. 2015. Rotator cuff tear: A detailed update. *Asia-Pacific Journal of Sports Medicine, Arthroscopy, Rehabilitation and Technology*. **2**(1), pp.1–14.

Pandy, M.G. 2001. *Computer Modeling and Simulation of Human Movement* [Online]. Available from: www.annualreviews.org.

Paul, G. 2011. Interfacing Jack and AnyBody: Towards anthropometric musculoskeletal digital human modelling *In*: *1st International Symposium on Digital Human Modelling*.

Paul, S., Yadav, A.K. and Goyal, T. 2022. Comparison of tear characteristics, outcome parameters and healing in traumatic and non-traumatic rotator cuff tear: a prospective cohort study. *Musculoskeletal Surgery*. **106**(4), pp.433–440.

Peterson, S.L. and Rayan, G.M. 2011. Shoulder and upper arm muscle architecture. *Journal of Hand Surgery*. **36**(5), pp.881–889.

Plausinis, D., Jazrawi, L., Zuckerman, J. and Rokito, A. 2006. Anatomy and Biomechanics of the Shoulder *In*: *Sports Medicine*. Lippincott Williams and Wilkins.

Pria, P.D. 2022. Biomechanics of the shoulder joint. *Human Orthopaedic Biomechanics: Fundamentals, Devices and Applications*., pp.285–303.

Ranebo, M.C., Björnsson Hallgren, H.C., Norlin, R. and Adolfsson, L.E. 2018. Long-term clinical and radiographic outcome of rotator cuff repair with a synthetic interposition graft: a consecutive case series with 17 to 20 years of follow-up. *Journal of Shoulder and Elbow Surgery*. **27**(9), pp.1622–1628.

Rasmussen, J. 2003. *AnyBody-a software system for ergonomic optimization MovAiD: Movement Assisting Devices View project Passive Orthosis for Upper Extremity Assistance (Patient@Home) View project* [Online]. Available from: https://www.researchgate.net/publication/233782872.

Rasmussen, J., Vondrak, V., Damsgaard, M., De Zee, M., Christensen, S.T. and Dostal, Z. 2002. *THE ANYBODY PROJECT-COMPUTER ANALYSIS OF THE HUMAN BODY*.

Rau, G., Disselhorst-Klug, C. and Schmidt, R. 2000. Movement biomechanics goes upwards: From the leg to the arm. *Journal of Biomechanics*. **33**(10), pp.1207–1216.

Rockwood, C. and Matsen, F. 1998a. *The Shoulder Volume 1* 2nd ed. Philadelphia, Pennsylvania: W.B. Saunders Company.

Rockwood, C. and Matsen, F. 1998b. *The Shoulder Volume 2* 2nd ed. Philadelphia, Pennsylvania: W.B. Saunders Company.

Sambandam, S.N., Khanna, V., Gul, A. and Mounasamy, V. 2015. Rotator cuff tears: An evidence based approach. *World Journal of Orthopaedics*. **6**(11), pp.902–918.

Schall, F., Seitz, A.M., Hacker, S., Drongelen, S. Van, Wolf, S.I., Ignatius, A. and Dürselen, L. 2019. German Society of Biomechanics (DGfB) Young Investigator Award 2019 : Proof-of-Concept of a Novel Knee Joint Simulator Allowing Rapid Motions at Physiological Muscle and Ground Reaction Forces. . **7**(September), pp.1–10.

Sharkey, N., Marder, R. and Hanson, P. 1994. The entire rotator cuff contributes to elevation of the arm. *Journal of Orthopaedic Research*. **12**(5), pp.699–708.

Sharkey, N.A., Smith, T.S. and Lundmark, D.C. 1995. Freeze clamping musculo-tendinous junctions for in vitro simulation of joint mechanics. *Journal of Biomechanics*. **28**(5), pp.631–635.

Shen, G., Zhang, J.F. and Fang, F.Z. 2019. In vitro evaluation of artificial joints: a comprehensive review. *Advances in Manufacturing*. **7**(1), pp.1–14.

Sherman, S.L. 2018. Editorial Commentary: The Krackow Stitch: More Than 30 Years of Tendon Repair and Still Holding Strong. *Arthroscopy - Journal of Arthroscopic and Related Surgery*. **34**(3), pp.669–670.

Smith, C., Alexander, S., Hill, A., Huijsmans, P., Bull, A.M.J., Amis, A., De Beer, J. and Wallace, A. 2006. A Biomechanical Comparison of Single and Double-Row Fixation in Arthroscopic Rotator Cuff Repair. *The Journal of Bone and Joint Surgery*. **88**(11), pp.2425–2431.

Smith, G.C.S., Bouwmeester, T.M. and Lam, P.H. 2017. Knotless double-row SutureBridge rotator cuff repairs have improved self-reinforcement compared with double-row SutureBridge repairs with tied medial knots: a biomechanical study using an ovine model. *Journal of Shoulder and Elbow Surgery*. **26**(12), pp.2206–2212.

Smolen, D., Haffner, N., Mittermayr, R., Hess, F., Sternberg, C. and Leuzinger, J. 2020. Application of a new polyester patch in arthroscopic massive rotator cuff repair — a prospective cohort study. *Journal of Shoulder and Elbow Surgery*. **29**(1), pp.e11–e21.

Sonnabend, D.H. and Young, A.A. 2009. Comparative anatomy of the rotator cuff. *Journal of Bone and Joint Surgery - Series B*. **91**(12), pp.1631–1637.

Steenbrink, F., Groot, J.H. De, Veeger, H.E.J., Helm, F.C.T. Van Der and Rozing, P.M. 2009. Glenohumeral stability in simulated rotator cuff tears. *Journal of Biomechanics*. **42**, pp.1740–1745.

Steinbrück, A., Schröder, C., Woiczinski, M., Fottner, A., Müller, P.E. and Jansson, V. 2013. Patellofemoral contact patterns before and after total knee arthroplasty : an in vitro measurement. . (June).

Su, W., Chu, C., Lin, Cheng-li, Lin, Chii-jen, Ph, D., Jou, I., Ph, D. and Chang, C. 2012. The Modified Finger-Trap Suture Technique : A Biomechanical Comparison of a Novel Suture Technique for Graft Fixation. *Arthroscopy: The Journal of Arthroscopic and Related Surgery*. **28**(5), pp.702–710.

Sward, L., Hughes, J.S., Amis, A. and Wallace, W.A. 1992. the Strength the of Surgical Cuff Repairs of. *Surgery*. **74**(4), pp.2–5.

Tashjian, R.Z. 2012. Epidemiology, Natural History and Indications for Treatment of Rotator Cuff Tears. *Clinics in sports medicine*. **31**, pp.589–604.

Terry, G.C. and Chopp, T.M. 2000. *C) by the National Athletic Trainers* [Online]. Association, Inc. Available from: www.journalofathletictraining.org.

Thorup, V.M., Tøgersen, F.A., Jørgensen, B. and Jensen, B.R. 2007. Biomechanical gait analysis of pigs walking on solid concrete floor. *Animal*. **1**(5), pp.708–715.

Tortora, G. and Nielson, M. 2012. *Principles of Human Anatomy* 12th ed. John Wiley and Sons.

Turner, A.S. 2007. Experiences with sheep as an animal model for shoulder surgery: Strengths and shortcomings. *Journal of Shoulder and Elbow Surgery*. **16**(5 SUPPL.), pp.158–163.

Veeger, H.E.J. and van der Helm, F.C.T. 2007. Shoulder function: The perfect compromise between mobility and stability. *Journal of Biomechanics*. **40**(10), pp.2119–2129.

Veeger, H.E.J., Van Der Helm, F.C.T., Van Der Woude, L.H. V, Pronk, G.M. and Rozendal, R.H. 1991. *Inertia and Muscle Contraction Parameters for Musculoskeletal Modelling of the Shoulder Mechanism.*

Verjans, M., Siroros, N., Eschweiler, J. and Radermacher, K. 2016. Technical concept and evaluation of a novel shoulder simulator with adaptive muscle force generation and free motion. *Current Directions in Biomedical Engineering*. **2**(1), pp.61–65.

Waltrip, R.L., Zheng, N., Dugas, J.R. and Andrews, J.R. 2003. Rotator Cuff Repair A Biomechanical Comparison of Three Techniques. *The American Journal of Sports Medicine*. **31**(4), pp.493–497.

Weber, T., Lazarev, I., Englert, C., Dendorfer, S. and Thomas, H. 2016. Influence of Rotator Cuff Tears on Glenohumeral Stability During Abduction Tasks. *Journal of Orthopaedic Research*. **34**(9), pp.1628–1635.

Williams, G.R., Rockwood, C., Bigliani, L.U., Iannotti, J.P. and Stanwood, W. 2004. Rotator Cuff Tears : Why Do We Repair Them ? *The Journal of Bone and Joint Surgery*. **86-A**(12), pp.25–27.

Wishart, J.M., Need, A.G., Horowitz, M., Morris, H.A. and Nordin, B.E.C. 1995. Effect of age on bone density and bone turnover in men. *Clinical Endocrinology*. **42**(2), pp.141–146.

Zheng, N., Harris, H.W. and Andrews, J.R. 2008. Failure analysis of rotator cuff repair: A comparison of three double-row techniques. *Journal of Bone and Joint Surgery*. **90**(5), pp.1034–1042.

Appendix 1

Drawing of the fixture required for the fixation method study conducted in Chapter 2.

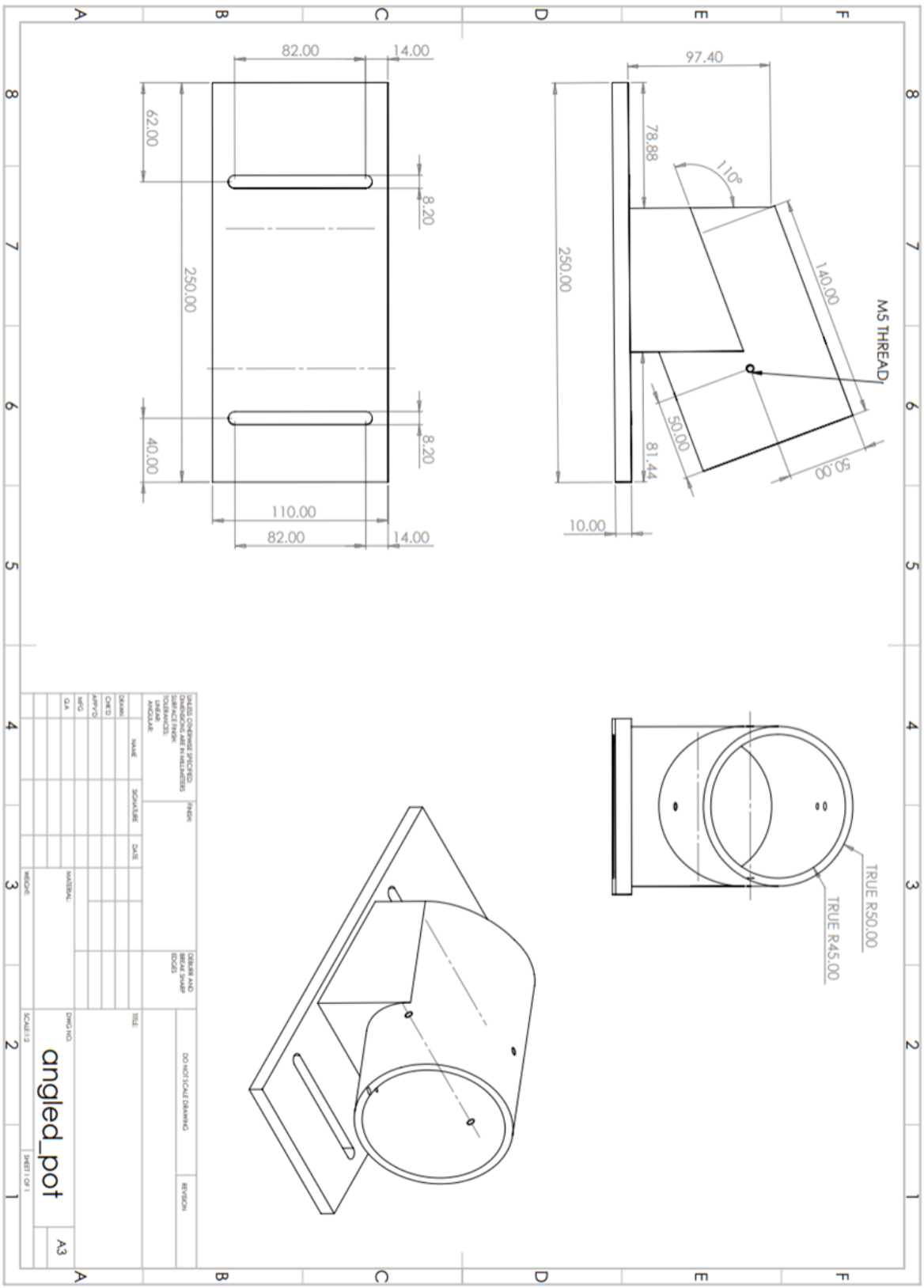

Appendix 2

Drawing of the porcine scapula fixture for the porcine shoulder simulator described in Chapter 4.

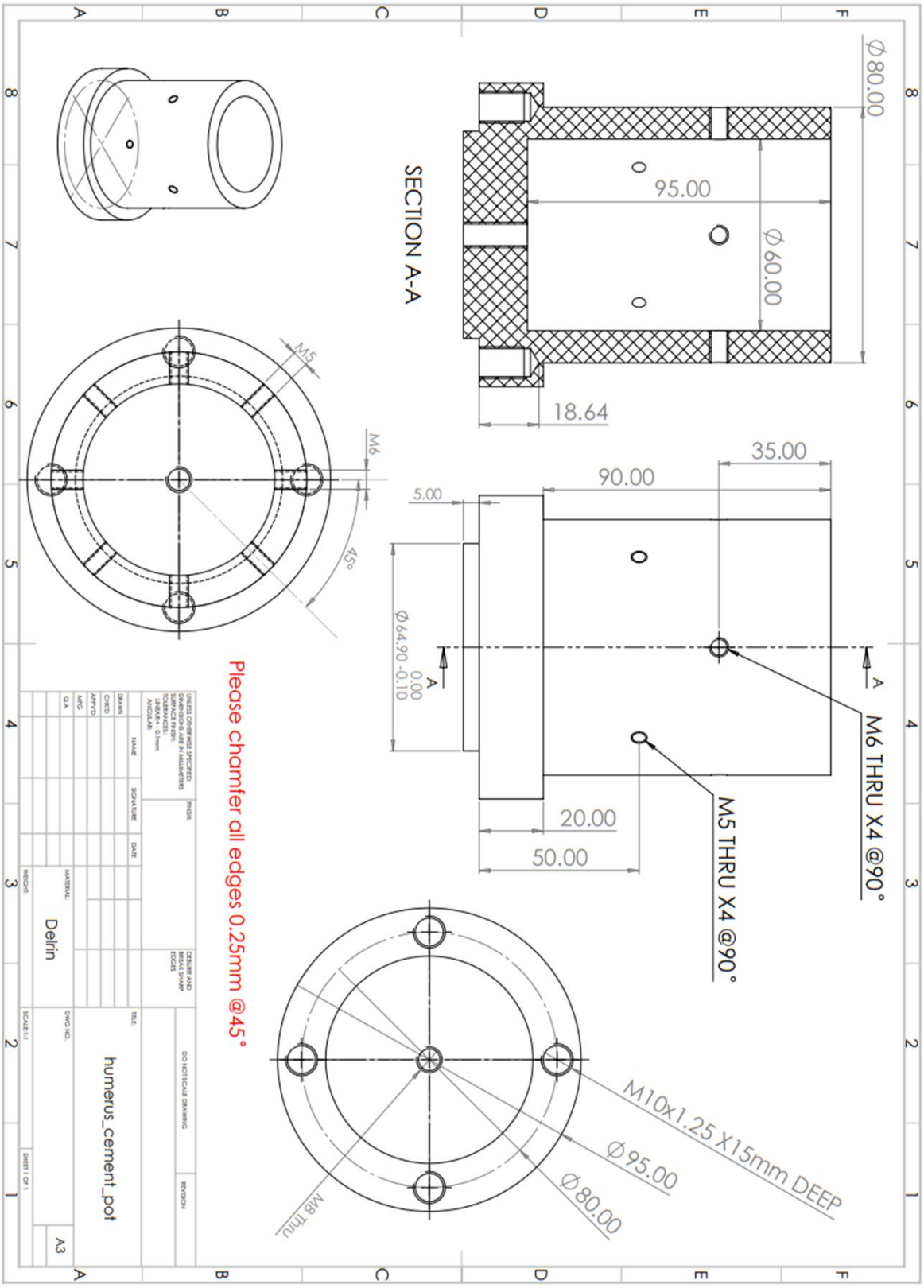

Appendix 3

Human tissue samples detailing the donor ID, gender and age.

Donor ID	Anatomy ID #	Sample	Sub Studies	Gender	Age
1L		1	A	Female	87
2L	43/23	2	A,B,C,D,E,F	Male	94
2R		3	F		
3L	48/23	4	A,B,C,D,E,F	Male	91

Appendix 4

Human scapula fixture required for the cementing process of the human scapula detailed in Chapter 5.